



City Research Online

City, University of London Institutional Repository

Citation: Cowley, A. (2004). Hot ductility and its relationship to transverse cracking in steels. (Unpublished Doctoral thesis, City University London)

This is the accepted version of the paper.

This version of the publication may differ from the final published version.

Permanent repository link: <https://openaccess.city.ac.uk/id/eprint/8416/>

Link to published version:

Copyright: City Research Online aims to make research outputs of City, University of London available to a wider audience. Copyright and Moral Rights remain with the author(s) and/or copyright holders. URLs from City Research Online may be freely distributed and linked to.

Reuse: Copies of full items can be used for personal research or study, educational, or not-for-profit purposes without prior permission or charge. Provided that the authors, title and full bibliographic details are credited, a hyperlink and/or URL is given for the original metadata page and the content is not changed in any way.

*Doctor of Philosophy
(PhD) Degree*

**HOT DUCTILITY AND ITS RELATIONSHIP
TO TRANSVERSE CRACKING IN STEELS**

by

Andrew Cowley – June 2004

*Department of Mechanical Engineering and Aeronautics
City University, London, UK*

'Look to the LORD and his strength; ...'
Psalm 105:4

'... all things are possible with God'
Mark 10:27

Contents

Declaration	i
List of Symbols and Abbreviations	ii
List of Figures	iii
List of Tables	xi
Acknowledgements	xii
Abstract	xiii
1 Introduction	1-1
2 Literature Review	2-1
2.1 The Continuous Casting Process	2-2
2.1.1 Transverse Cracking	2-5
2.1.2 Mechanics of the Slab Straightening Process	2-6
2.2 Hot Ductility	2-8
2.2.1 The Ductility Trough	2-9
2.2.2 Thin Ferrite Films	2-10
2.2.3 Precipitate Free Zones	2-13
2.2.4 High Ductility High Temperature Region (HDHT)	2-15
2.2.5 High Ductility Low Temperature Region (HDHT)	2-18
2.2.6 Measurement of Hot Ductility	2-18
2.3 High Temperature Cracking and Softening Processes	2-21
2.3.1 Dynamic Recovery	2-23
2.3.2 Dynamic Recrystallisation	2-24
2.4 Influence of Processing Conditions and Composition	2-27
2.4.1 Influence of Process Variables on Hot Ductility	2-27
2.4.2 Influence of Microstructure on Hot Ductility	2-31
2.4.3 Influence of Chemical Composition on Hot Ductility	2-34

3	Experimental Method	3-1
3.1	Measurement of Hot Ductility	3-1
3.1.1	Measurement of Reduction of Area (R of A)	3-3
3.1.2	The Induction Test	3-4
3.1.3	The Instron Test	3-7
3.2	Microscope Examination	3-11
3.3	Grain Size and Type Measurements	3-12
4	Low Temperature Straightening	4-1
4.1	Introduction	4-1
4.2	Experimental Details.....	4-3
4.2	Results and Discussion	4-4
4.3.1	Low Temperature End of the Trough	4-7
4.3.2	High Temperature End of the Trough	4-11
4.3.3	Depth of the Trough	4-12
4.4	Conclusions	4-17
5	Influence of Cooling Rate and Sulphides on Hot Ductility.....	5-1
5.1	Introduction	5-1
5.2	Experimental Details.....	5-2
5.3	Results and Discussion.....	5-3
5.3.1	Analysis of Flow Curves.....	5-11
5.3.2	Conditions Required for Obtaining a Narrow Trough.....	5-16
5.3.3	Influence of S and Sulphides.....	5-18
5.3.4	Influence of Cooling Rate.....	5-19
5.3.5	As-Cast Samples	5-21
5.4	Conclusions	5-22
6	Mathematical Modelling.....	6-1
6.1	Introduction	6-1
6.2	Experimental Details.....	6-3
6.3	Results and Discussion.....	6-5
6.3.1	Simple C-Mn Steels.....	6-5
6.3.2	Grain Boundary Sliding in Austenitic Stainless Steel	6-13
6.3.3	Relevance of the Hot Ductility Curve to Transverse Cracking ...	6-20
6.4	Conclusions	6-21

7	Influence of Columnar Grains	7-1
7.1	Introduction	7-1
7.2	Experimental Details.....	7-2
7.3	Results and Discussion	7-3
	7.3.1 Chromium Carbides	7-7
	7.3.2 Analysis of Flow Curves.....	7-8
	7.3.3 Interpretation of the Hot Ductility Curves	7-10
7.4	Conclusions	7-14
8	Influence of Residual Copper.....	8-1
8.1	Introduction	8-1
8.2	Experimental Details.....	8-3
8.3	Results and Discussion	8-4
8.4	Conclusions	8-5
9	Summary of Results	9-1
9.1	Low Temperature Straightening	9-1
9.2	Influence of Cooling Rate and Sulphides on Hot Ductility.....	9-3
9.3	Mathematical Modelling	9-5
9.4	Influence of Columnar Grains	9-6
9.5	Influence of Residual Copper	9-7
10	Future Work	10-1
11	Publications	11-1
12	References	12-1

Declaration

I grant powers of discretion to the University Librarian to allow this thesis to be available for photocopying and for inter-library loan, and for the title and summary to be made available for outside organisations. This permission covers only single copies made for study purposes, subject to the normal conditions of acknowledgement.

Signed: (Candidate)

Date:

List of Symbols and Abbreviations

A	- Temperature independent constant.
Ae ₃	- The 'upper critical' temperature marking the upper limit of the $\alpha + \gamma$ two-phase region under equilibrium conditions as shown on phase diagrams.
Ar ₃	- The 'upper critical' temperature marking the start of the austenite (γ) to ferrite (α) phase transformation of a steel under non-equilibrium cooling conditions.
AlN	- Aluminium Nitride.
DIF	- Deformation induced ferrite.
DRX	- Dynamic recrystallisation.
GBS	- Grain boundary sliding.
L	- Gauge length.
MnS	- Manganese Sulphide.
N	- Temperature independent constant.
Nb(CN)	- Niobium carbonitride.
Q	- Activation energy for deformation, J mol ⁻¹ .
R	- Universal molar gas constant, 8.314 510(70) J K ⁻¹ mol ⁻¹ .
r	- Radius of curvature of the slab ('R'-bending radius).
R of A	- Reduction of area.
SFE	- Stacking fault energy.
t	- Slab thickness.
T	- Absolute temperature, Kelvin (K).
T _m	- Melting point temperature, K.
TiN	- Titanium Nitride.
V	- Casting speed, typically 0.9 m min ⁻¹ .
VN	- Vanadium nitride.
α	- Ferrite. Body centred cubic form of iron and solid solutions based on it; it is stable up to 1183 K.
α	- Temperature independent constant.
δ	- Delta ferrite. Body centred cubic form of iron similar to α ; it is stable between 1673 K and the melting point, 1808 K.
δ	- Skin thickness of the solidifying slab.
Δ	- Distance from a tangent point to the first bending rolls.
γ	- Austenite. Face centred cubic form of iron and solid solutions based on it; it is stable between 1183 K and 1766 K.
$\dot{\epsilon}$	- The overall bending strain rate in the slab during straightening.
ϵ_s	- The bending strain at the slab surface during straightening.
σ	- Stress (either peak or steady state).

List of Figures

- Figure 2.1:** Schematic illustration of continuous casting methods in use.¹³
- Figure 2.2:** (a) Continuously cast sections, sizes are in millimetres (adapted from ref. 14) and (b) the range of products available from the Corus large structural mill at Teeside.¹⁵
- Figure 2.3:** Schematic diagrams of (a) a continuous caster with a straight mould and (b) slab casting phenomenon (longitudinal section).¹³
- Figure 2.4:** (a) Cold machine scarfed slab showing transverse cracking and (b) a partially rolled slab showing severe edge cracking.¹⁸
- Figure 2.5:** Surface strain and overall strain rate resulting from bending.²³
- Figure 2.6:** A schematic diagram of a typical hot ductility curve.
- Figure 2.7:** Schematic diagram of reduced ductility in the high temperature, low ductility region.²⁵
- Figure 2.8:** (a) C-Mn-Al steel showing flat facets on fracture surface; (b) enlarged view of a showing lack of voiding around MnS inclusions;² (c) intergranular microvoid coalescence type fracture in C-Mn-Al steel²⁶ and (d) ductile dimples showing voiding around inclusions within the thin film of ferrite.²⁷
- Figure 2.9:** (a) schematic diagram showing mechanism for transformation induced intergranular failure;² (b) thin ferrite films at the boundaries of austenite grains in a C-Mn-Al steel tested at 1023K with $A_{e3}=1085K$ and $A_{r3}=973K$ ($60Kmin^{-1}$).²⁶
- Figure 2.10:** Effect of percentage ferrite phase present on hot ductility.³⁵
- Figure 2.11:** (a) A typical wedge type crack formed in a Nb containing steel⁴¹ and (b) enlarged view showing microvoid nucleation at inclusions.²
- Figure 2.12:** Precipitate free zone around the grain boundary in a Nb-containing steel, fractured at 950K. The grain boundary contains fine precipitates of Nb(CN) and coarse MnS inclusions.⁴²
- Figure 2.13:** Schematic illustrations showing intergranular microvoid coalescence of Nb-bearing steels by deformation in (a)-(c) the low temperature region and (d)-(f) the duplex phase region.⁴³

Figure 2.14: Schematic illustration showing the ductility levels that can be achieved with and without dynamic recrystallisation at the high temperature end of the trough.⁹

Figure 2.15: Typical high temperature ductile rupture failure observed in the HDHT region.⁴⁵

Figure 2.16: (a) Experimental arrangement for measuring hot ductility in the as-cast condition,⁵⁴ (b) Hot tensile test using as-cast notched specimen,⁵⁵ (c) hot tensile test employing resistance heating for solution treatment of specimen⁵⁶ and (d) using radiant heating for solution treatment.¹⁸

Figure 2.17: Schematic diagram showing (a) how the width of the ductility trough could be controlled by the dynamic recrystallisation (DRX); (b) how increasing the strain rate reduces the depth and width of the trough, ϵ_{c1} , ϵ_{f1} and T_{D1} refer to the lower strain rate and ϵ_{c2} , ϵ_{f2} and T_{D2} refer to the higher strain rate and (c) how refining the grain size reduces the depth and width of the trough, ϵ_{c1} , ϵ_{f1} and T_{D1} refer to the coarser grain size and ϵ_{c2} , ϵ_{f2} and T_{D2} refer to the finer grain size.⁶⁸

Figure 2.18: Stress-elongation curves for a C-Mn-Al-Nb steel, solution treated and tested in air, the arrow indicates that dynamic recrystallisation is occurring.⁶⁹

Figure 2.19: A typical temperature profile observed at a Scunthorpe continuous caster.

Figure 2.20: Fracture surfaces of a low Al steel tested at 1073K showing refinement of dimples and particles as cooling rate increases from (a) 25Kmin⁻¹ to (b), 100Kmin⁻¹. With the increase in cooling rate there is a corresponding drop in R of A from 52% to 24%.⁷² The influence of cooling rate on hot ductility for a C-Mn-Al steel with Ti addition and Ti:N ratio of 3.4:1 is shown in (c), data taken from ref. 72.

Figure 2.21: Effect of grain size on % R of A.⁷⁵

Figure 2.22: Schematic illustration showing austenite structure in the solidified shell.⁸⁴

Figure 3.1: Illustration of difficulty measuring total uniform elongation when necking occur.⁸¹

Figure 3.2: Schematic drawing of induction test specimen.

Figure 3.3: Schematic drawing of the induction hot-tensile apparatus.

Figure 3.4: Calibration chart developed to select motor frequency required to give specified strain rate.

Figure 3.5: Temperature gradient along the central axis of sample heated to a constant temperature within the induction coil.

Figure 3.6: Photographs of the Instron test apparatus, with (a) the furnace chamber closed and (b) open, (c) the furnace control unit and (d) a schematic diagram showing the construction of the Isoheat 'Rapid Cool' furnace attached to the Instron machine.

Figure 3.7: Instron Sample Dimensions.

Figure 3.8: A chart showing how temperatures recorded at the top and bottom of the sample compared to the programme running on the Eurotherm measured using the inner and outer thermocouples.

Figure 4.1: Hot ductility curves for steels 1 to 4, showing A_{e3} , A_{r3} and T_D temperatures.

Figure 4.2: TEM Micrographs of (a) high Mn high C steel tested at 1173K, showing sparse precipitation of Nb(CN) and (b) typical Nb(CN) precipitation in a steel similar to (a) but containing 0.011% P, this steel has been cast and cooled to the test temperature of 1173K at 100Kmin^{-1} .⁹⁹

Figure 4.3: Micrographs of (a) steel 1 tested at 1148K, showing evidence of intergranular ductile failure by microvoid coalescence (SEM), (b) steel 3 tested at 1098K, showing mechanism of intergranular failure by microvoid coalescence within the softer ferrite film (x60), (c) a Nb containing steel tested at 1198K, showing flat facets indicating intergranular failure by grain boundary sliding and (d) steel 3 tested at 1198K, showing grain boundary sliding as the failure mechanism (x60).

Figure 4.4: Micrographs of steel 1 (mag. x60) tested at (a) 1148K, thin films of ferrite surround austenite grain boundaries, 10% ferrite, 36% R of A, (b) 1123K, films have now developed, 27% ferrite, 48% R of A, (c) 1098K, marked substructure is apparent in ferrite, ~50% ferrite, 63% R of A and (d) 1073K, mostly ferrite with heavy substructure, 74% ferrite, 88% R of A.

Figure 4.5: Micrographs of steel 2 (mag. x60) tested at (a) 1073K, showing very thin ferrite films at boundaries ($A_{e3} = 1085K$), (b) 1023K, showing growth of ferrite film, (c) 973K, the A_{r3} temperature, showing ferrite within the matrix and (d) 923K, showing much ferrite within the matrix.

Figure 4.6: Micrographs of steel 3 (mag. x60) tested at (a) 1123K, showing ferrite in very thin film at temperatures of minimum ductility, <0.5% ferrite, 43% R of A (b) 1098K, showing growth of ferrite film, 24% ferrite, 47% R of A (c) 1073K, 45% ferrite, 72% R of A and (d) 1048K, 75% ferrite, 77% R of A.

Figure 4.7: Calculated percentage ferrite present in the four steels.

Figure 4.8: Influence of test temperature on observed and calculated % ferrite for (a) high Mn, high C steels 2 and 4 and (b) low Mn, low C steels 1 and 3. The relevant sections of the hot ductility curves are also included: EF – equilibrium ferrite, OF – observed ferrite.

Figure 4.9: Austenitic grain structures (mag. x60) seen in (a) steel 2 (high Mn, high C, Al), showing dynamically recrystallised grains, tested at 1173K and (b) steel 3 (low Mn, low C, Nb), showing the as-cast austenitic structure and evidence of wedge cracking, also tested at 1173K.

Figure 4.10: Stress strain curves for steel 1, showing onset of dynamic recrystallisation.

Figure 4.11: Stress strain curves for steel 2, showing onset of dynamic recrystallisation.

Figure 4.12: Stress strain curves for steel 3, showing no evidence of dynamic recrystallisation.

Figure 4.13: Stress strain curves for steel 4, showing evidence of dynamic recrystallisation.

Figure 5.1: Calculated equilibrium %S in solution versus temperature for the two Mn levels.

Figure 5.2: Hot ductility curves for steels 5 to 8.

Figure 5.3: Digital micrographs (mag. x60) of steel 5 at (a) 1148K, fully austenitic (b) 1123K, thin ferrite film (c) 1098K, thickened films + ferrite in matrix, and (d) 1073K, structure nearly fully ferritic.

- Figure 5.4:** Digital micrographs (mag. x60) of steel 6 at (a) 1173K, fully austenitic (b) 1123K, thin ferrite film (c) 1098K, thickened films + ferrite in matrix, and (d) 1073K, structure nearly fully ferritic.
- Figure 5.5:** Digital micrographs of steel 7 (mag. x60) at (a) 1073K, fully austenitic (b) 1048K, thin ferrite films, (c) 1023K, thickened films + ferrite in matrix, and (d) 973K, nearly fully ferritic.
- Figure 5.6:** Digital micrographs (mag. x60) of steel 8 at (a) 1123K, fully austenitic (b) 1073K, thin ferrite film (c) 1023K, thickened films + ferrite in matrix, and (d) 998K, structure nearly fully ferritic.
- Figure 5.7:** Stress strain curves for steel 5, showing onset of dynamic recrystallisation.
- Figure 5.8:** Stress strain curves for steel 6, showing onset of dynamic recrystallisation.
- Figure 5.9:** Stress strain curves for steel 7, showing no evidence of dynamic recrystallisation.
- Figure 5.10:** Stress strain curves for steel 8, showing evidence of dynamic recrystallisation.
- Figure 5.11:** Curves of the strain to the peak stress against temperature for steels 5 to 8.
- Figure 5.12:** Curves of peak stress against temperature for steels 5 to 8.
- Figure 5.13:** Curves of a) strain to the peak stress and b) peak stress against temperature for steels 1 and 3.
- Figure 5.14:** Curves of a) strain to the peak stress and b) peak stress against temperature for steels 2 and 4.
- Figure 5.15:** Curves of equilibrium (dashed) and observed (solid) percentage ferrite for steels 5 to 8.
- Figure 5.16:** Elongated MnS inclusions encouraging the formation of DIF in steel 8. Steel tested at 1098K (mag x800).
- Figure 5.17:** Hot ductility curves for a typical as-cast C-Mn-Nb-Al steel, given different cooling rates to the test temperature.¹⁰⁷
- Figure 5.18:** Schematic diagram showing the effect of cooling rate on hot ductility (based on Figure 2.21⁷⁵ showing grain size having a similar effect on the hot ductility curve).
- Figure 5.19:** Hot ductility curves for as-cast steels, showing little change with percentage sulphur present.

- Figure 6.1:** Schematic diagram showing how depth of the trough controls the temperature for onset of DRX, T_d .
- Figure 6.2:** Hot ductility curves and ε_c against temperature for the C-Mn-Al steels 9 and 10, having high and low sulphur respectively. Arrows indicate the point at which the projected base of the trough intersects the curve of ε_c against temperature and therefore when ductility will start to improve.
- Figure 6.3:** Spherical MnS precipitates found in C-Mn steel with a high S level. Tested at 1123K, $3 \times 10^{-4} \text{ s}^{-1}$ with a cooling rate of 10 Kmin^{-1} and giving R of A=55%. (mag x1150)
- Figure 6.4:** Calculated R of A values from Table 6.2 plotted against those observed experimentally.
- Figure 6.5:** (a) Equilibrium percentage ferrite at temperatures below the A_{e3} for typical 0.1C-0.6Mn steel calculated using the 'Thermocalc' program⁹⁸ and (b) the influence of percentage ferrite on hot ductility.¹¹⁷
- Figure 6.6:** Elongated MnS inclusions favouring ferrite nucleation, high S steel tested at 1123 K. (mag x482)
- Figure 6.7:** Calculated curves and experimentally determined values of ε_p against temperature for (a) coarse grain size, $240 \mu\text{m}$ (after Ref. 108) and (b) fine grain size, $40 \mu\text{m}$.
- Figure 6.8:** Hot ductility curves obtained from tensile tests and calculated ε_p converted to R of A values against temperature for the coarse grained samples, T_d for each strain rate is marked by an arrow (after Ref. 108).
- Figure 6.9:** Hot ductility curves and calculated peak strain, ε_p , converted to R of A values against temperature.
- Figure 6.10:** The influence of $\dot{\varepsilon}$ on the length of cracks formed by grain boundary sliding, (a) $3 \times 10^{-1} \text{ s}^{-1}$ and (b) $3 \times 10^{-4} \text{ s}^{-1}$, both samples being tested at the minimum ductility temperature of 1123 K (mag x120).
- Figure 6.11:** Influence of temperature on amount of carbides precipitated at γ grain boundaries, (a) 1123 K, boundaries saturated with precipitation and (b) 1273 K, considerable reduction in precipitation. (SEM x1200)

Figure 6.12: (a) Irregular serrated boundaries showing the early stages of DRX, 1123 K, $3 \times 10^{-4} \text{ s}^{-1}$. The cracks are sufficiently long enough to cause poor ductility even when DRX is well advanced at higher temperatures (b) Substantial DRX present at 1173 K, $3 \times 10^{-3} \text{ s}^{-1}$. (mag x120)

Figure 6.13: Coarse grained sample with good ductility and no evidence of DRX, 1223 K, $3 \times 10^{-1} \text{ s}^{-1}$. (mag x120)

Figure 6.14: Schematic diagram highlighting the parts of the ductility curve that are relevant to the problem of transverse cracking.

Figure 7.1: Influence of initial undeformed grain size after heat treatment, D_0 , on minimum R of A value.²

Figure 7.2: Sample directions.

Figure 7.3: Hot ductility curves for the four sample directions studied; **A** - transverse direction, **B** - casting direction, **C** - through thickness direction and **D** - through thickness at 45° to casting direction.

Figure 7.4: Stress - strain curves for samples taken transverse to the casting direction (A).

Figure 7.5: Stress – strain curves for samples taken parallel to the cast direction (B).

Figure 7.6: Stress – strain curves for samples taken in the through thickness direction (C).

Figure 7.7: Stress – strain curves for samples taken through thickness, 45° to the casting direction (D).

Figure 7.8: Failed samples (a) in the through thickness direction, C, showing excellent ductility and (b) parallel to the casting direction, B, showing poor ductility and numerous cracks.

Figure 7.9: Chromium carbides at γ grain boundaries at (a) 1273K and (b) 973K (SEM, mag. x300).

Figure 7.10: Optical micrograph (mag. x60) of (a) serrated boundaries present in through thickness sample, C, tested at $>1173\text{K}$, and (b) absence of serrated boundaries in sample parallel to casting direction, B, at 1173K.

Figure 7.11: Curves showing variation of peak stress with temperature for the four sample directions.

Figure 7.12: Curves of the strain to the peak stress against temperature for the four sample directions.

Figure 7.13: Schematic diagram of columnar grain structure in the four sample directions.

Figure 7.14: Micrographs of sample sections taken in (a) through thickness direction, C, showing long columnar grains (mag. x3), (b) cross-section of through thickness sample, showing cigar shape of columnar grains – the dendritic nature of grains can also be discerned (mag. x6) and (c) cross-section of casting direction sample A, showing presence of very long columnar grains traversing across the entire gauge diameter (mag. x6).

Figure 7.15: Tensile sample taken in the casting direction, B, and strained to failure at 1273K, showing cracks (a) forming at 45° to tensile axis and (b) subsequently being opened by normal stress (scale in b is mm).

Figure 7.16: Failed sample taken from direction D, showing very poor ductility resulting from enhanced grain boundary sliding due to the long columnar boundaries lying at 45° to the tensile axis.

Figure 8.1: Influence of copper on the hot ductility of C-Mn-Al steels.⁸⁷

Figure 8.2: Hot ductility curves for a, b solution treated and c, d as cast C-Mn-Al-Nb steels, tested in various atmospheres (steel 1 was only tested as cast in 'air').⁷⁰

Figure 8.3: Hot ductility curves showing the effect of residual copper. Steels 10 and 11 were cooled at 200 Kmin⁻¹, 12 and 13 at 60 Kmin⁻¹.

List of Tables

Table 2.1: Possible softening processes occurring on hot deformation.⁵⁹

Table 3.1: An example Isoheat Furnace heating programme.

Table 4.1: Analysis of steels studied in this section, wt. %.

Table 4.2: Transformation temperatures of steels examined, K (at 60Kmin⁻¹).

Table 4.3: Temperatures for onset of dynamic recrystallisation, T_D.

Table 4.4: Calculated and observed R of A values for the four steels.

Table 5.1: Analysis of steels studied in this section, wt. %.

Table 5.2: Transformation temperatures of steels examined, K (at 60Kmin⁻¹). The Ae temperatures were calculated using the Thermocalc program and the Ar temperatures by dilatometry.

Table 5.3: Amount of S in solution at 1633K and the quantity of MnS able to precipitate out on cooling to the test temperature.

Table 5.4: Percentage S in solution at 1603K and the volume fraction of MnS present in the steels after both hot rolling and solution treatment.

Table 5.5: Ar₃ transformation temperatures for steels 5 to 8 at cooling rates of 25, 60 and 200 Kmin⁻¹.

Table 6.1: Analysis of steels studied in this section, wt. %.

Table 6.2: Calculated and observed R of A values for a selection of C-Mn-Al steels.

Table 7.1: Compositions of the steel studied in this section, wt. %.

Table 8.1: Analysis of steels studied in this section, wt. %. * Studied in previous work using oxidising atmosphere.⁷⁰

Acknowledgements

I would like to express my immense gratitude to Professor Barrie Mintz for his help, guidance, encouragement, phenomenal patience and knowledge that he has imparted to me on the subject of Hot Ductility. Furthermore, I thank both Professor Mintz and Mrs Jenny Mintz for their friendship, kindness and hospitality during my time of study – I will always be indebted to them both and am unable to thank them enough for helping me all through this.

Thanks are also due to a very long list of people and institutions that help helped me with this work; Professor A.R.D. Thorley for the provision of the laboratory facilities during my time at City University, Professor D. Arcoumanis for continued support and allowing my to submit this thesis, Corus and EPSRC for funding the work, Corus and TWI for supplying the steel used, in particular Dr. D.N. Crowther (Swinden Technology Centre) for arranging all machining and dilatometry, Dr M. Pope (Scunthorpe Works) for supplying the stainless steel and Dr. J. Wei of Timken Research for carrying Thermocalc calculations of transformation temperatures and equilibrium ferrite volume fractions against temperature.

I am also extremely grateful to Dr Rouckaya Abushosha, Tom Rose, Iain Wright, Dr. Osvaldo Cominelli, Dr Brett McKinley, Roy Vipond, Eric Skinner, Chris Barber, Brian Burns, Ferdinand Carty, Laurie Frampton, Brian, Alan and Paul. I am indebted to many of these people for their assistance with the laboratory equipment and all for their friendship, support and encouragement during my time in the School of Engineering. Special thanks are also due to Adrian Hall, Maria Suchacki, Professor Axel Johne, Donal Walsh and all my other friends at the CASS Business School for my time in the Computing Services Department, helping me get to where I am today and encouragement to finish this thesis.

Finally, I would like to thank my wife and best friend, Lorraine, both of our parents and my grandparents for their love, patience, help, support and encouragement, especially during the preparation of this thesis. And last, but absolutely by no means least, my God and saviour who makes all things possible ... even completion of a thesis!

Abstract

The influence of the A_{r3} on the hot ductility of steels was examined. Tensile samples were heated to 1603K, cooled at 60Kmin^{-1} and tested in the temperature range 1323-873K at a strain rate of $3 \times 10^{-3}\text{s}^{-1}$. The A_{r3} was altered by variations in C, (0.1 to 0.15%C), Mn, (0.6 to 1.4%Mn), Si (0.1 to 0.5%Si) and P, (0.001 to 0.025%P). Elements that raise the A_{r3} e.g. Si and P were found to lead to recovery in ductility at slightly higher temperatures at the low temperature end of the trough. However, reducing C levels to $<0.1\text{C}$ had the most pronounced influence on hot ductility since ductility was then observed to recover just below the A_{e3} and the trough was very narrow. The lower C level allowed large amounts of deformation-induced ferrite (equilibrium amounts) to form, ferrite having excellent ductility.

The influence of both S in solution and elongated sulphides on hot ductility was also examined. Although elongated sulphides encouraged ferrite formation, this was a relatively minor improvement. In these steels, low C levels ($<0.1\%$) i.e. high A_{e3} temperatures, ensured ductility recovered rapidly just below the A_{e3} obscuring the effect of S. Similar behaviour was noted with as-cast steel, increasing the S level from 0.004 to 0.019% had little influence on the hot ductility. Increasing the cooling rate after solidification, from conventional continuous casting to that pertaining to thin slab casting, results in worse ductility. This can be ascribed to finer precipitation and/or a finer inclusion distribution at the γ grain boundaries.

A model was devised for predicting the hot ductility curve for simple plain C-Mn steels. However, this model has limited application and further development is needed to take into account the influence of grain boundary sliding on the reduction of area values.

Columnar grains were found to be very detrimental to hot ductility and to avoid transverse cracking, it is suggested magnetic stirring be used in the mould to break up the columnar structure.

A Cu addition was found not to influence hot ductility at a cooling rate of 25Kmin^{-1} , but ductility was worse at 200Kmin^{-1} . Oxidising conditions are required to properly show the effect of residuals; unfortunately time was not available for undertaking this.

1. Introduction

The discovery and development of new materials and processes to manufacture them has always been a crucial factor in the prosperity and technical development of the world's nations. Steels have been an essential part of this development since the Industrial Revolution of the late 1800's. Production of iron and steel accounted for around ninety percent of all metals consumed during the decade 1980-90, where annual production had risen to around 750 million tonnes. A range of published forecasts during this period predicted world steel production would exceed 1000 million tonnes by the year 2000. This level of annual production consumes about three billion tonnes of raw materials and accounts for approximately six percent of the world's total primary energy use¹. The dominance of steels is due to their versatility in production and processing; the wide spectrum of applications in which their properties can be exploited; their ease of fabrication and with environmental issues becoming ever more important, ease of recycling. However, steel now faces strong competition from other materials such as aluminium, polymers, ceramics and composites. Therefore, its properties need to be continually improved, production costs reduced and innovative new applications sought.

The hot ductility of steels has become a subject of great importance ever since continuous casting was introduced commercially, around 1960, and transverse cracking was found to occur particularly in the niobium grades of steels for oil platform and line pipe. In the continuous casting operation, molten steel is poured from a ladle via a tundish into an oscillating, water-cooled mould, which is often curved. Crack propagation occurs when the cast strand is straightened which puts the top surface and edges into tension. Such cracks are found to be intergranular, meandering along the austenite boundaries and their ability to

¹ B. Wilshire, D. Homer and N.L. Cooke: *Technological and Economic Trends in the Steel Industries*, Pineridge Press, 1983, ISBN 0-906674-21-4.

form is highly dependent on composition as this controls precipitation, which is known to exacerbate the problem. Nb as a micro-alloying element has been found to be particularly deleterious as it precipitates dynamically during straining as Nb(CN) both within the matrix and at the austenite boundaries.

The straightening operation is carried out in the temperature range from around 1273 down to 973K, and coincides with the interval in which steel exhibits a ductility minimum in laboratory hot tensile tests. This apparently clear correlation between transverse cracking and tensile hot ductility has led to extensive laboratory studies during the last 25 years. Considerable work has been carried out into reducing the deleterious influence of the micro-alloying additions, and it is common to restrict additions to the minimum required to give the required properties in the finished product and to adjust cooling conditions so that the temperature at the straightener is as high as possible so as to reduce precipitation. However, even when these precautions are taken it is common to have to scarf the surface and roll wide and trim off the cracked edges leading to considerable scrap losses. As supply of suitable grades of iron ore are becoming scarce, scrap is increasingly being used, resulting in increased residual levels. This has led to a deterioration in the surface quality of slabs. Furthermore, scrap will have high levels of copper and sulphur, which are known to reduce ductility.

City University has been developing the hot ductility test over a number of years to make it more and more useful as a simulative test to both help understand and, more important commercially, predict the likelihood of transverse cracking occurring. Cooling rates to the test temperature and strain rate are chosen to correspond with those undergone during the straightening operation and tensile samples can be cast in-situ prior to testing. The work that has been done^{2,3,4,5,6} in examining the influence of composition (Nb, V, S, Ti

² B. Mintz, S. Yue and J. J. Jonas: *Int. Materials Reviews* 1991, Vol. 36, No. 5, pp. 187-217.

and Ca) on hot ductility has been of great benefit to the steel industry in controlling transverse cracking. It has also very much increased our fundamental understanding of the microstructural factors which influence hot ductility. The present programme is aimed at continuing this work in both developing our understanding of the ductility trough as well as furthering our knowledge on the relationship of the hot tensile test to the problem of transverse cracking.

The work will also concentrate on thin slab casting, as this is likely to revolutionise steel production in the next decade. As a thinner strand would result in a much larger throughput requirement for the reheating furnace, direct rolling immediately after straightening is a necessity. As the strand is not reheated, considerable savings will be made and a thinner slab requires less rolling reduction. A defect free surface is then vital for the economic production of slabs. Whereas problems have been overcome for the thin slab casting of strip, this is not the case for plate. Presently, it has not been possible to thin slab cast steels in the peritectic carbon range 0.1 to 0.16%, which virtually precludes a large slice of the plate market.

³ B. Mintz and R. Abushosha: *Ironmaking and Steelmaking*, 1993, 20, 6, pp. 445-452.

⁴ R. Abushosha, R. Vipond and B. Mintz: *Materials Science and Technology*, 1991, 7, pp. 1101-1107.

⁵ B. Mintz, Z. Mohamed and R. Abushosha: *Materials Science and Technology*, 1989, 5, pp. 682-688.

⁶ R. Abushosha, R. Vipond and B. Mintz: *Materials Science and Technology*, 1991, 7, pp. 613-621

2. Literature Review

The hot ductility of steels has been the subject of many investigations since the continuous casting of steel was introduced commercially and cracking was observed during the straightening operation. Considerable progress has been made over the past 25 years towards understanding this phenomenon. More recent work at City University ^{7,8,9,10} has gone far into interpreting the hot ductility curve and it has been possible to separate the contributions of deformation induced ferrite, grain boundary sliding and dynamic recrystallisation to hot ductility.

There have been two major reviews ^{2,11} on this subject and this work will be summarised in this chapter; it is important to discuss the relevance of the hot ductility tensile test to the problem of transverse cracking. This test is used to simulate the conditions experienced during the straightening operation, where temperatures range from 1273K down to 973K and strain rates are in the range 10^{-3} to 10^{-4}s^{-1} . Information obtained using these conditions has been found very useful in assessing the probability that a steel will suffer from transverse cracking at the straightener,¹² but great care has to be taken in interpreting the results so that they can be used to improve commercial practice. The reduction of area values (R of A) is taken as a measure of the ductility and the value required to prevent transverse cracking occurring is dependent on the exact test conditions.

⁷ B. Mintz and J. J. Jonas: Mat. Sci. and Technol., 1994, Vol. 10, pp. 721-727.

⁸ G. S. I. L. Cardoso, S. Yue and B. Mintz: submitted to Mat. Sci. and Technol., 1995.

⁹ B. Mintz: Mat. Sci. and Technol., 1996, 12, pp. 132-138.

¹⁰ B. Mintz, R. Abushosha and M. Shaker: Mat. Sci. and Technol., 1989, 5, pp. 682-688.

¹¹ B. Mintz: ISIJ Int., 1999, 39, No. 9, pp. 833-855.

¹² B. Mintz and J.M. Arrowsmith: Met. Technol., 1979, 6, pp. 24-32.

2.1 The Continuous Casting Process

Continuous casting was introduced commercially in the 1960's and is a very efficient way to produce steel, offering great advantages over other methods of steel production. As well as the economic benefits and improved yield, continuous casting processes were developed to overcome a number of the traditional ingot-related difficulties, such as piping, entrapped slag and structure variation throughout the length of the solidified product. Continuous casting virtually eliminates these problems and in addition, steels produced by this route generally have an improved surface quality, fewer oxide inclusions and a more uniform chemical composition. From the production point of view, not having to pour into moulds, then strip, handle and reheat the ingots before rolling allows enormous cost savings to be made. Although there are many different methods of the continuous casting process in use commercially, they can be broadly grouped into the categories shown in Figure 2.1.

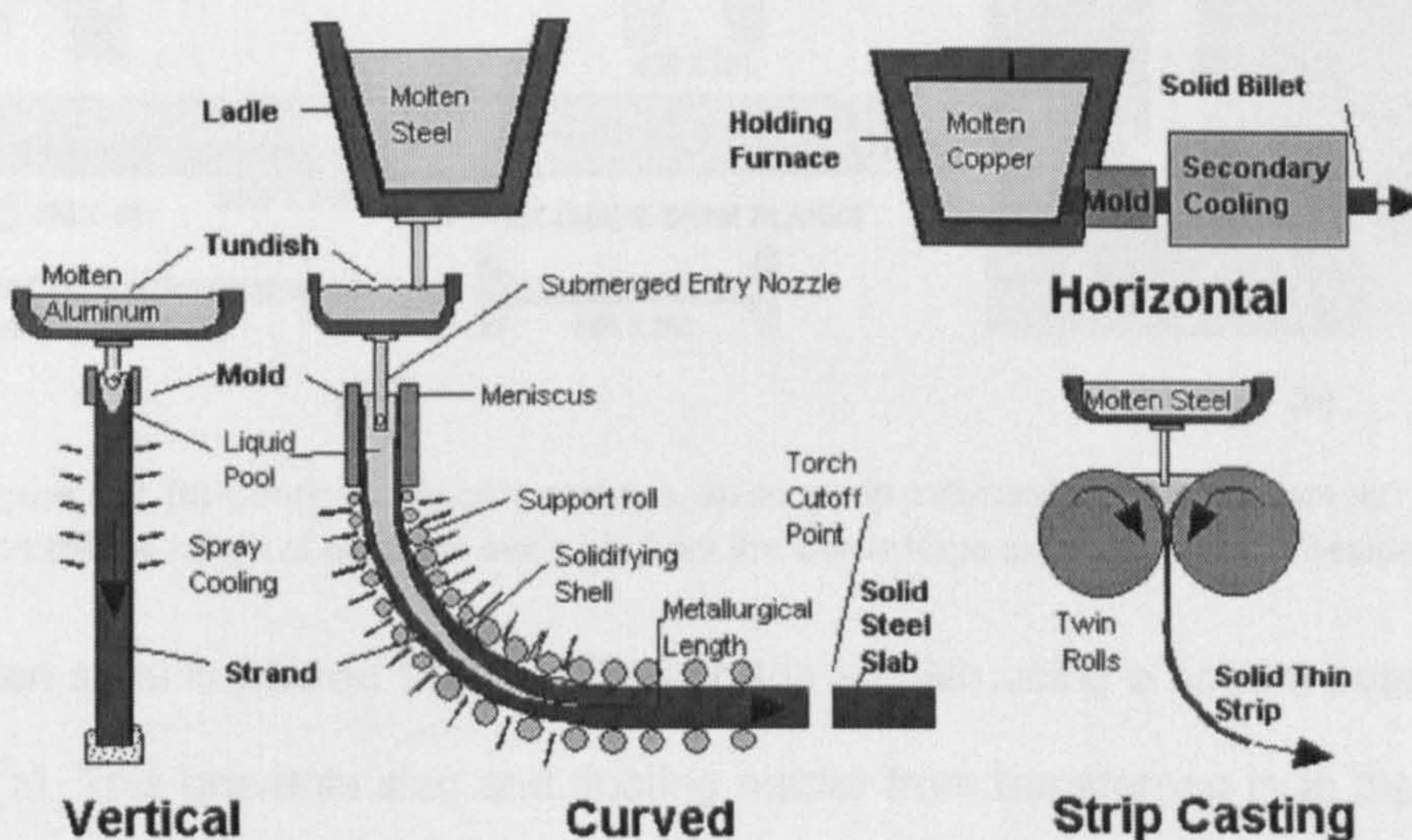


Figure 2.1: Schematic illustration of continuous casting methods in use.¹³

The vast majority of continuously cast steel is produced using the curved method employing a curved mould so that the strand only needs to be straightened once solidified. The vertical continuous caster is generally only used to cast aluminium and a few other

¹³ B.G. Thomas: Introduction to Continuous Slab Casting, Continuous Casting Consortium, 2003, <http://bgtsunsparc.me.uiuc.edu/introduction/overview.html>.

metals; it is not commonly used to cast steel since the machine/building height limits the maximum length of strip that can be cast. The horizontal method is used occasionally for steel and other non-ferrous alloys.

Depending on the application of the final product, steel sections can be continuously cast in many different shapes and sizes. Figure 2.2 (a) shows the types of section available and their sizes, whilst Figure 2.2 (b) shows examples of final products available from the Corus large structural mill at Teeside. Direct strip casting is now being pioneered at many sites worldwide and steel is being produced with thicknesses around 1.5 to 5mm.

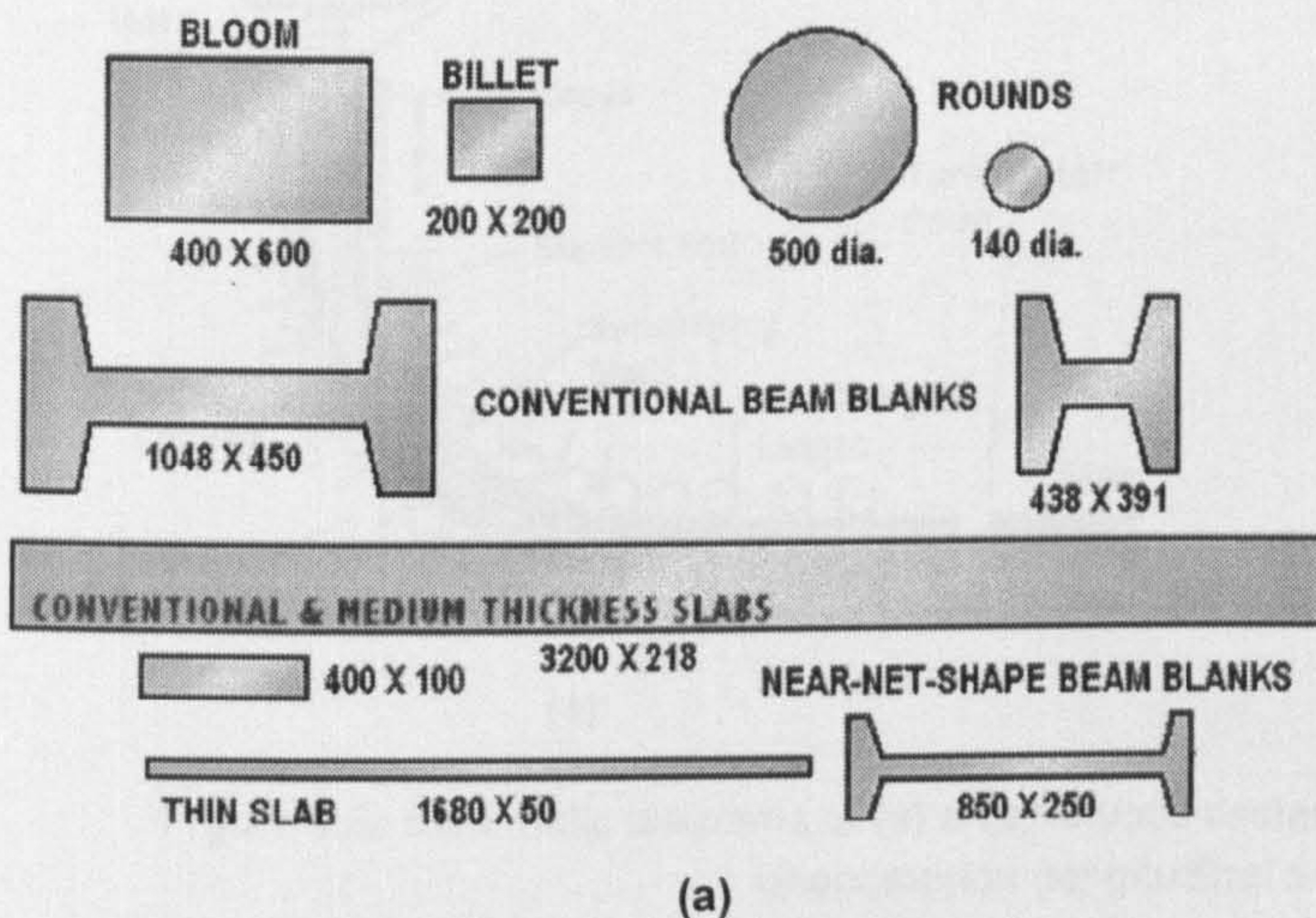


Figure 2.2: (a) Continuously cast sections, sizes are in millimetres (adapted from ref. 14) and (b) the range of products available from the Corus large structural mill at Teeside.¹⁵

Molten steel is poured from a ladle into the tundish using a bottom pouring process, Figure 2.3 (a). This prevents slag and floating matter from transferring in to the subsequent castings and results in a cleaner product being obtained. From the tundish, the molten steel enters a water-cooled curved copper mould through a submerged entry nozzle; this method of pouring avoids possible splashing and oxidation. The mould oscillates at between 60 and 120Hz² to prevent sticking; mould fluxes, or lubricants such as rapeseed oil, are also used

¹⁴ B. Kozak and J. Dzierzawski: AISI Learning Centre, 2002, <http://www.steel.org/learning/howmade/concast.htm>.

¹⁵ M. Pettifor: 49th Hatfield Lecture, Technology: driving steel forward, Steel World, 2002, Vol. 7, pp. 11-19.

to further prevent the solidifying steel from sticking to the mould wall. However, the oscillation causes transverse ripples (or oscillation marks) to be formed on the surface of the strand,¹⁶ Figure 2.3 (b). Solidification of the steel below the mould is accelerated by direct water sprays, but up to ten metres may have to emerge before the steel becomes solid to the core, this is known as the metallurgical length, see Figure 2.3 (a).

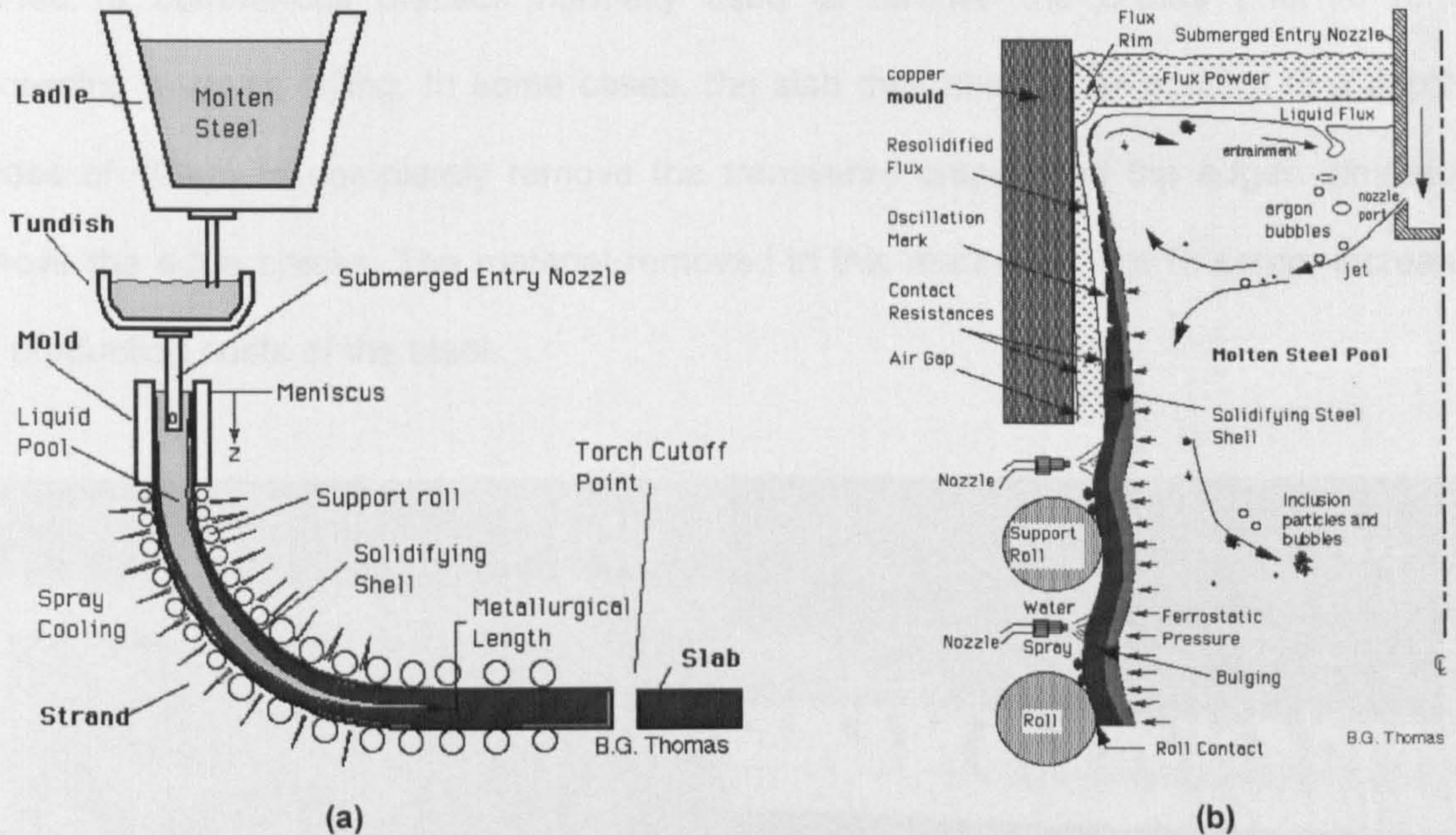


Figure 2.3: Schematic diagrams of (a) a continuous caster with a straight mould and (b) slab casting phenomenon (longitudinal section).¹³

When the strand is sufficiently solidified, and no breakout of the molten steel at the centre of the strand is likely to occur, the strand is straightened. This operation is usually carried out in the temperature range of 1273K down to 973K, which coincides with the low ductility region observed when the steels are tensile tested in the laboratory (discussed in section 2.2.1). The strain rates experienced at the top surface of the strand are normally in the range 10^{-4} to 10^{-3}s^{-1} . Slabs are constantly cut from the end of the strand using gas cutters, ready for further processing into sheets, rod and other sections.

¹⁶ E.T. Turkdogan: AIME Steelmaking Conf. Proc., 1987, 70, p. 399

2.1.1 Transverse Cracking

During the process of straightening the vertically cast curved strand, the top surface is put into tension and transverse and edge cracking can occur. The cracks are generally fine and difficult to see and can be 0.2mm wide and from 1 to 15mm in depth.¹⁷ As shown in Figure 2.4, the transverse and edge cracks can be readily observed when the slab is scarfed, a commercial practice normally used to remove the cracks prior to further processing such as rolling. In some cases, the slab may need to be scarfed to a depth in excess of 10mm to completely remove the transverse cracks and the edges trimmed to remove the edge cracks. The material removed in this manner is lost to scrap, increasing the production costs of the steel.

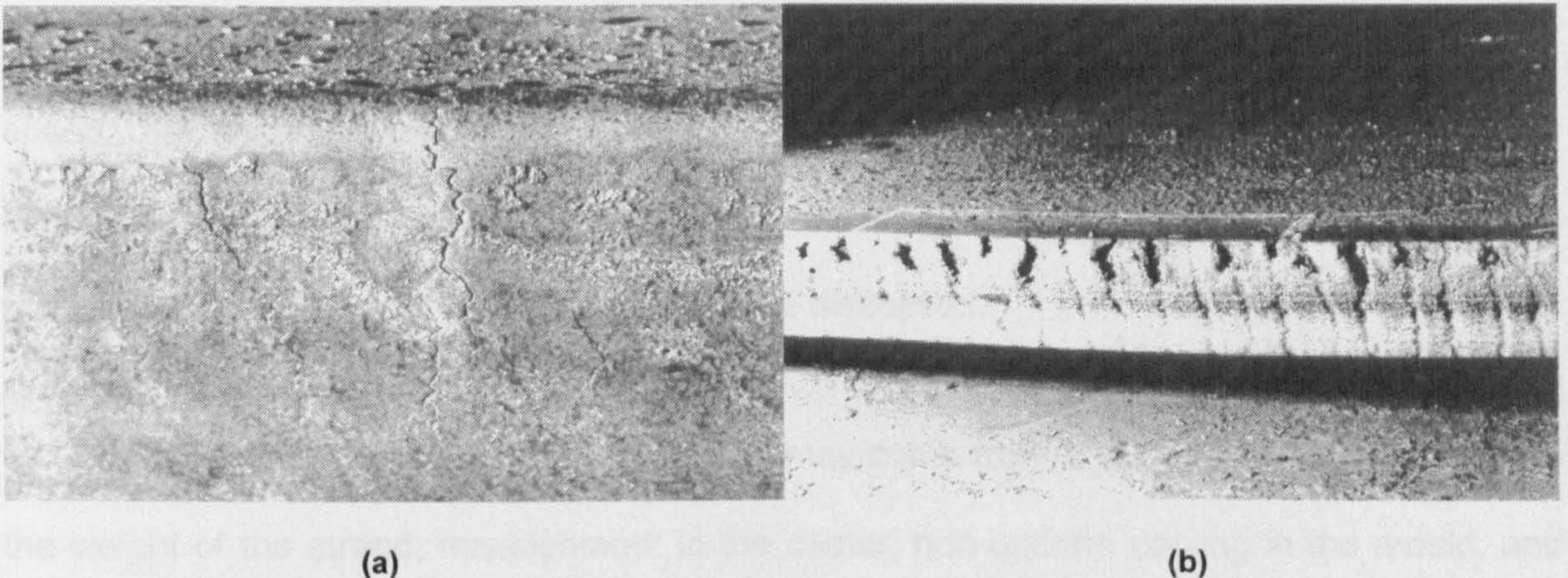


Figure 2.4: (a) Cold machine scarfed slab showing transverse cracking and (b) a partially rolled slab showing severe edge cracking.¹⁸

The base of the oscillation marks formed in the mould are thought to act as stress concentrators which promote crack formation and growth during the straightening process.¹⁹ The cracks have been shown to be intergranular in nature and meander along the prior austenite grain boundaries, with coarse grained regions being particularly susceptible to

¹⁷ J.K. Brimacombe and K. Sorimachi: Metall. Trans., 1977, 8B, p. 489.

¹⁸ D.N. Crowther: The Hot Ductility of Steels, PhD Thesis, 1986, City University London, UK.

¹⁹ L. Schmidt and A. Josefsson: 1974, Scan. J. Met., 3, p. 193.

cracking.¹⁹ Precipitates of AlN,²⁰ MnS and Nb(CN) and various oxides²¹ have been shown to be present on the crack surfaces. Niobium grades for oil platform and line pipe have been found to be particularly susceptible to transverse cracking due to Nb(CN) precipitating dynamically during straining, both within the matrix and at the austenite (γ) boundaries.²²

2.1.2 *Mechanics of the Slab Straightening Process*

Transverse cracking always occurs on the top surface of the strand which is put into tension during straightening, not the underside which is put into compression. Generally, transverse cracking will occur if the stress on the top surface during straightening exceeds the fracture strength of the solidifying, or solidified, strand. The amount of strain that the top surface of the strand is subjected to depends on factors relating to the continuous caster in question. These factors include the geometry of the mould (e.g. radius of curvature), casting speed, rate of cooling and strand temperature at the straightener. These factors have been explained in detail by Lankford²³ and some will be covered briefly in section 2.4 of this review, where their effect on hot ductility will be discussed.

Stresses on the strand during casting may come from a number of sources such as the weight of the strand, misalignment in the caster, non-uniform cooling in the mould, and the straightening operation. However, the surface strain and strain rate experienced at the straightener may be the largest the slab is subjected to in the continuous casting process. The bending strain at the slab surface, ϵ_s , is given approximately by the following equation:

$$\epsilon_s = \frac{t}{2R} \quad (2.1)$$

²⁰ H. Mori: Tetsu To Hagane, 60, 784.

²¹ R.C. Cochrane: 1982, unpublished work referenced by D.N. Crowther.¹⁶

²² B. Mintz: 1995, EPSRC Research proposal GR/K61692, Hot Ductility and its Relationship to Transverse Cracking during continuous casting.

²³ W.T. Lankford: 1972, Metall. Trans., 3, p. 1331.

Where t is the slab thickness and R is the radius of curvature of the strand before straightening (dictated by the mould curvature). A surface strain of 1.15% is expected for typical process values of $t = 0.23\text{m}$ and $R = 10\text{m}$. Lankford proposed three values for the gauge length (L) involved when bending a slab; the distance from a tangent point to the first bending rolls (Δ), the skin thickness (δ) and the slab thickness (t); this gives rise to uncertainties in the value of the gauge length. The surface strain and overall strain rate experienced by the slab during bending are shown in Figure 2.5. The strain rate ($\dot{\epsilon}$) can be calculated using the following equation:

$$\dot{\epsilon} = \epsilon_s \frac{V}{L} \quad (2.2)$$

Where V is the casting speed and L is the gauge length. Bernard *et al*²⁴ obtained similar results to Lankford; for a typical casting speed of 0.9 m/min and L between 6 and 10m, the strain rate at the surface of the strand was found to be in the range 1.7×10^{-3} to $2.9 \times 10^{-3} \text{ s}^{-1}$. Unfortunately, these results are only approximate and apply to the slab as a whole; locally, i.e. the base of the oscillation marks, the values of ϵ_s and $\dot{\epsilon}$ may be markedly different. In commercial continuous casters the strain rates experienced at the straightener are between 3×10^{-3} and $3 \times 10^{-4} \text{ s}^{-1}$.

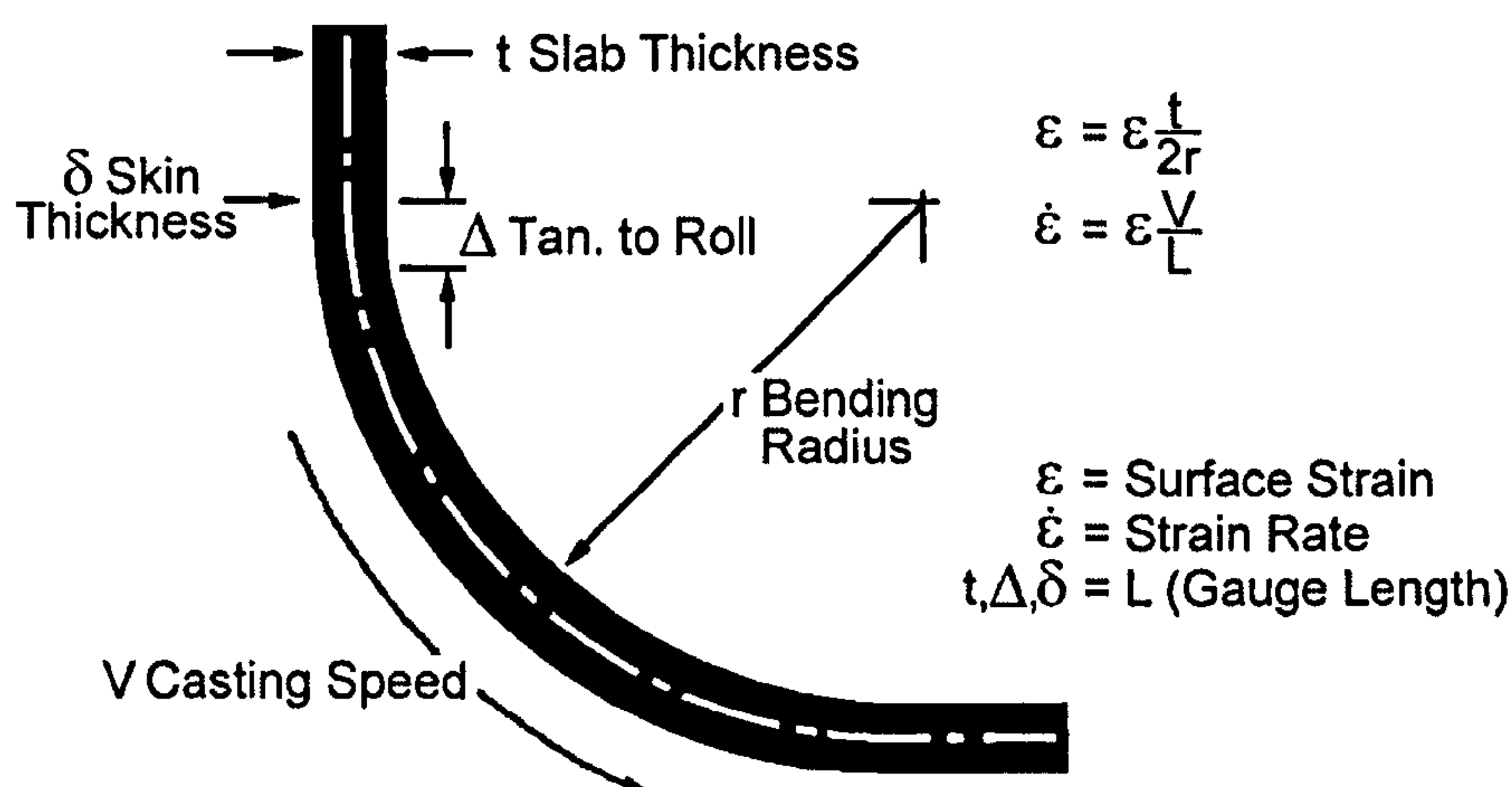


Figure 2.5: Surface strain and overall strain rate resulting from bending.²³

²⁴ G. Bernard, J.P. Birat, B. Conseil and J.C. Humbert: Rev. Métall., 1978, 75, p. 467.

2.2 Hot Ductility

As previously mentioned, 1273 to 973K is the temperature range in which the straightening operation is carried out in continuous casting and the serious commercial problem of transverse cracking can occur. Much study has been undertaken over the past 25 years to increase the understanding of the factors that influence hot ductility of steel in this temperature range. One of the ways in which this poor hot ductility can be measured is by reduction of area (R of A) values obtained from hot tensile testing. The trough observed in the hot ductility curve using reduction of area values is shown in Figure 2.6; this shows the hot ductility curve (solid lines) to be made up of three distinct regions, two having high ductility separated by a region of low ductility or embrittlement.

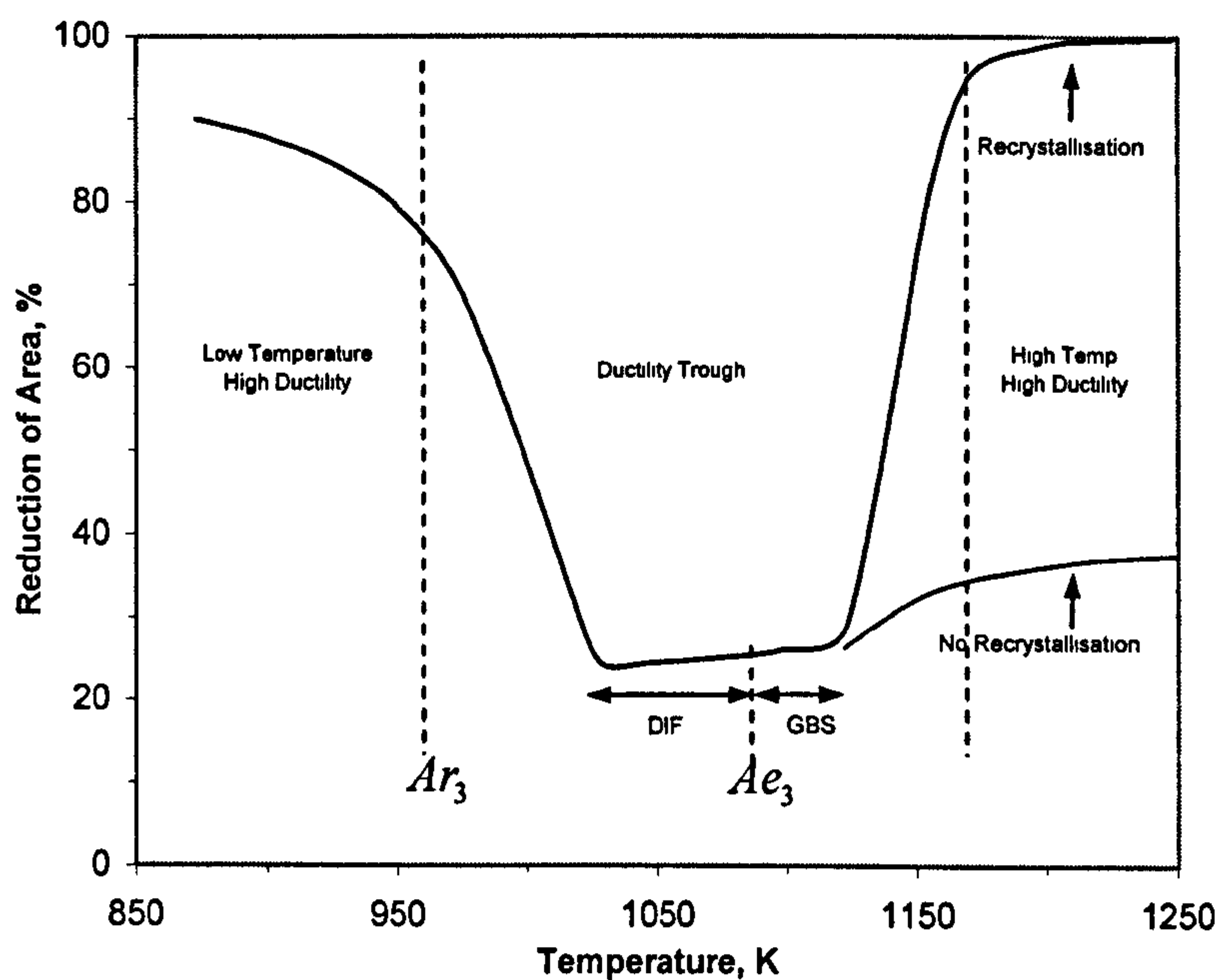


Figure 2.6: A schematic diagram of a typical hot ductility curve.

Although these three regions are of the most interest in this study due to the temperature at the straightener, another region of reduced ductility of concern in continuous casting exists at temperatures approaching the melting point and found within the mould. Low ductility observed within about 50K of the solidus is related to the solidification process of the steel, see Figure 2.7. This region of reduced ductility is known as hot tearing.

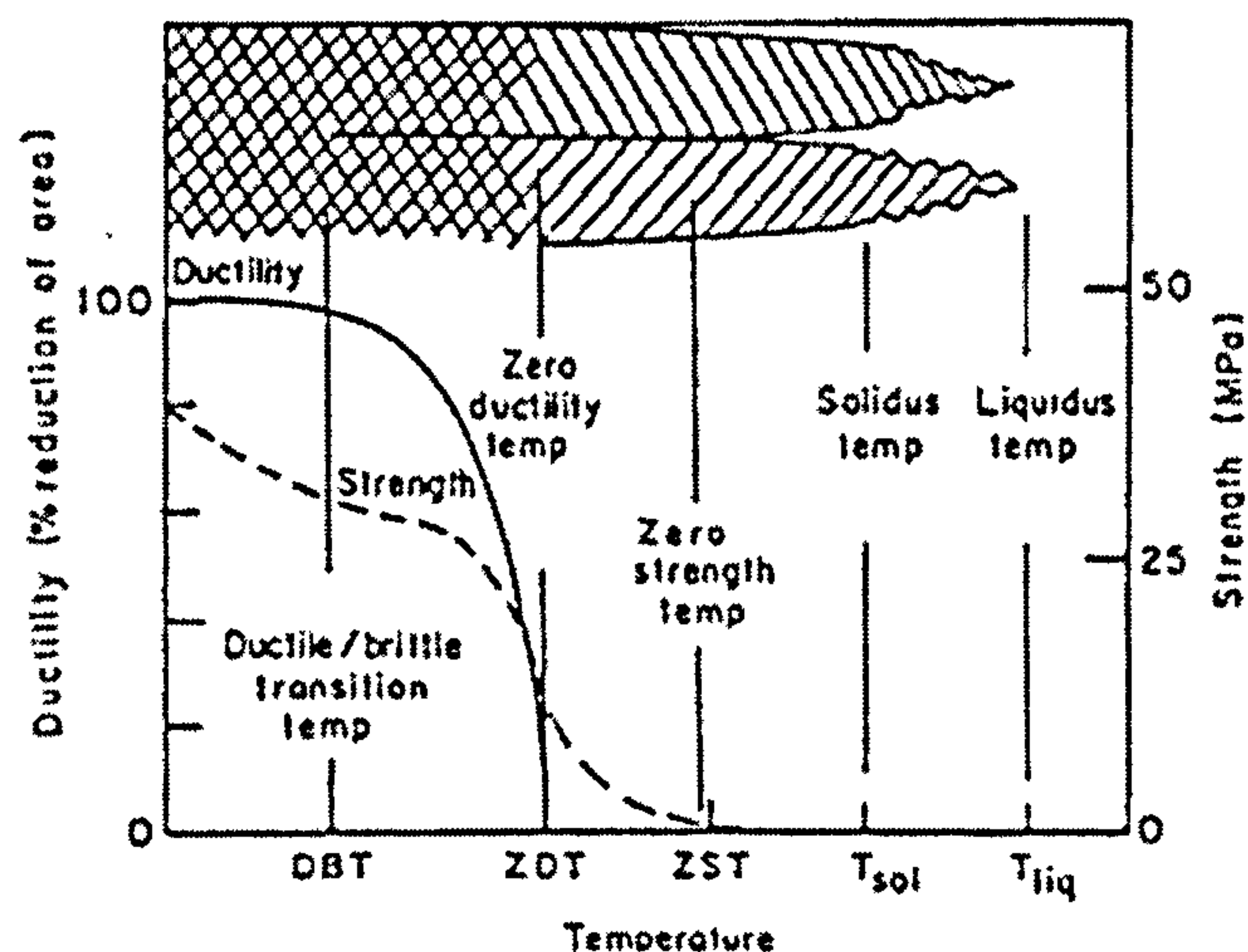


Figure 2.7: Schematic diagram of reduced ductility in the high temperature, low ductility region.²⁵

It is easiest to explain why the change in hot ductility occurs in Figure 2.6 by taking each of the three regions in turn, these being:

- The trough or region of embrittlement.
- A high ductility, high temperature region (HDHT).
- A high ductility, low temperature region (HDLT).

2.2.1 The Ductility Trough

The poor ductility that is encountered in this region is always related to intergranular failure at the γ grain boundaries, the fracture facets are either smooth or covered in fine dimples,² see Figure 2.8. This indicates that there are two distinct failure mechanisms acting in the ductility trough observed at test temperatures from as low as 973K to as high as 1473K. As mentioned earlier, the temperature at which the strand is straightened in commercial practice falls within this range, with transverse cracks often being observed at strain rates between 10^{-4} and 10^{-3}s^{-1} . Understanding what influences the hot ductility in this region is vital if solutions are to be found to reduce the occurrence of this cracking.

²⁵ H.G. Suzuki et al: In "100th ISIJ Meeting", October 1980.

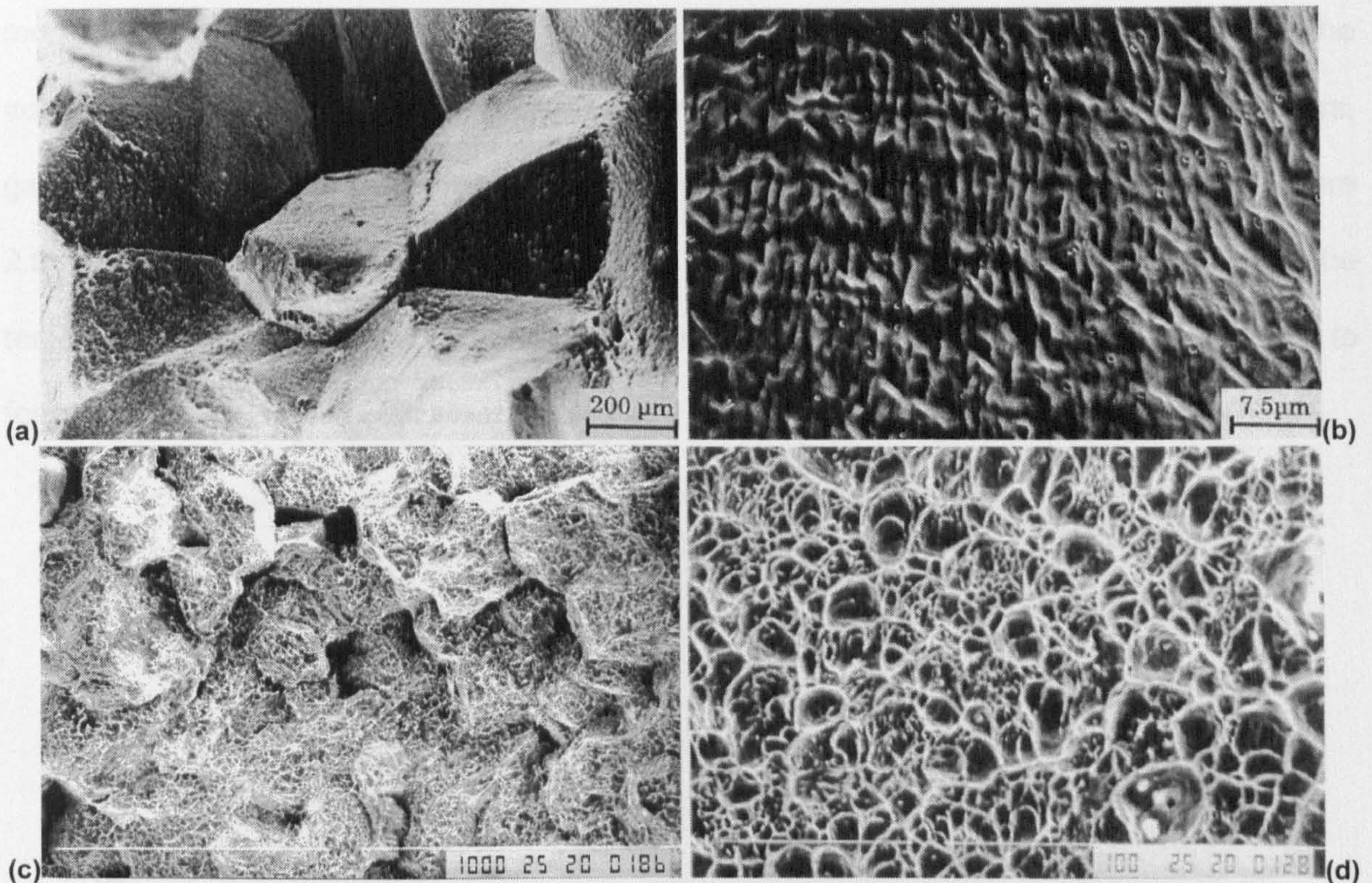


Figure 2.8: (a) C-Mn-Al steel showing flat facets on fracture surface; (b) enlarged view of a showing lack of voiding around MnS inclusions;² (c) intergranular microvoid coalescence type fracture in C-Mn-Al steel²⁶ and (d) ductile dimples showing voiding around inclusions within the thin film of ferrite.²⁷

The intergranular failures with dimpled fracture facets can be due to one of two microstructural features being present at the austenite grain boundaries and leading to excessive strain concentrations; these are thin ferrite films and precipitate free zones.

2.2.2 Thin Ferrite Films

Thin ferrite films form around the austenite grain during the austenite to ferrite transformation and intergranular failure can occur when the thin films are around 5 to 20 μm in thickness.² The α phase in iron-based alloys is softer than the γ at a given temperature.²⁸ This is due to ferrite having a higher stacking fault energy than austenite, and therefore

²⁶ A. Cowley, R. Abushosha and B. Mintz: Mat. Sci. and Technol., 1998, 14, pp. 1145-1153.

²⁷ R. Abushosha, S. Ayyad and B. Mintz: Mat. Sci. and Technol., 1998, 14, pp. 346-351.

²⁸ P.J. Wray: Met. Technol., 1981, 12, p. 466.

more rapid recovery.²⁹ As the ferrite film is generally much softer and more ductile than the austenite grains, the strain will tend to concentrate within the ferrite; ductile voiding occurs, generally around MnS inclusions formed at the austenite grain boundaries^{2,30,31}, see Figure 2.9. In an unstrained sample, the thin films of ferrite would only start to form when the temperature had dropped to the A_{r3} ; this being the temperature at which ferrite begins to form in unstrained austenitic steel, cooled at a given rate.

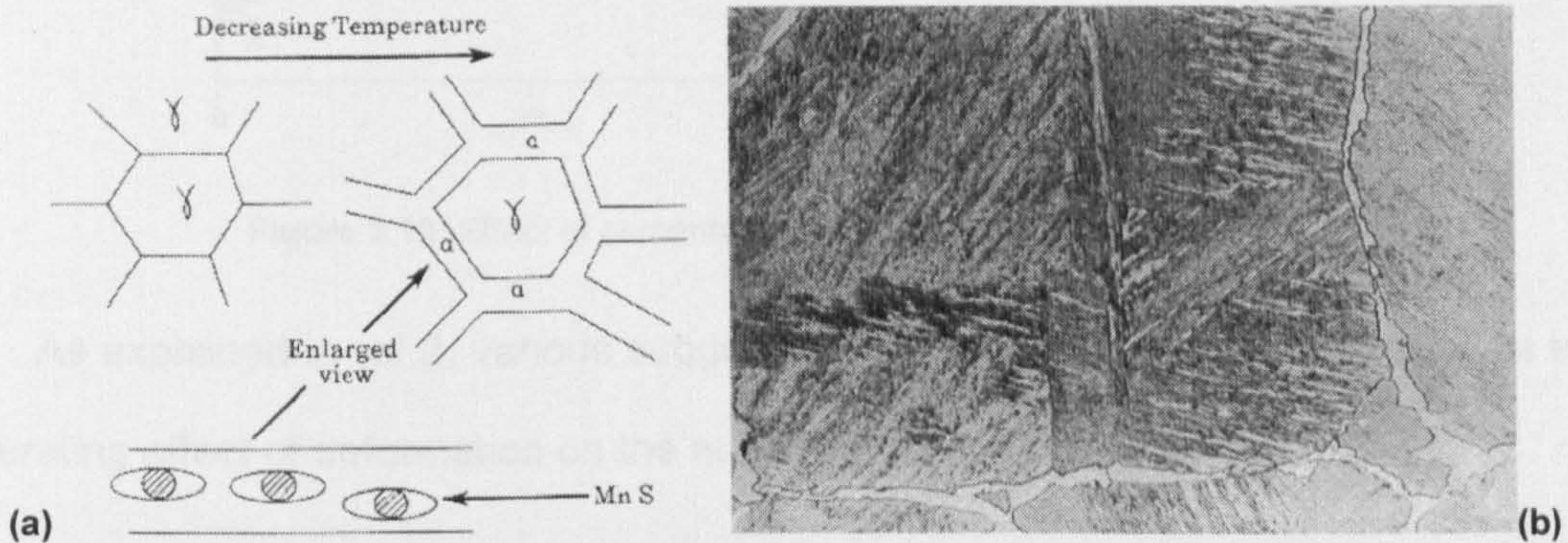


Figure 2.9: (a) schematic diagram showing mechanism for transformation induced intergranular failure;² (b) ferrite films at the boundaries of γ grains in a C-Mn-Al steel tested at 1023K with $A_{e3}=1085\text{K}$ and $A_{r3}=973\text{K}$ and cooling rate of 60Kmin^{-1} .²⁶

Previous work^{32,33,34} has shown that the rate of the γ to α transformation significantly increases if strain is applied at temperatures between the A_{e3} and A_{r3} ; the presence of this deformation causing ferrite to form at times and temperatures that would not otherwise be the case. Often the thickness of the strain induced ferrite films do not increase substantially until the A_{r3} is reached. Lowering the test temperature further, before the tensile test, results in ferrite forming normally and in large amounts. The ductility can be seen to recover fully when there is around 50 percent ferrite present; this can be seen in Figure 2.10.

²⁹ J. Lewis, J.J. Jonas and B. Mintz: ISIJ Int. 1998, 38, 3, pp. 300-309.

³⁰ B. Mintz, R. Abushosha and M. Shaker: Mat. Sci. Technol., 1993, 9, p. 907.

³¹ G.I.S.L. Cardoso and S. Yue: 31st Mechanical Working and Steel Processing Conf., ISS of AIME, Chicago, 1989, p. 585.

³² A. Sandberg and W. Roberts: Thermomechanical Processing of Microalloyed Austenite, ed. By A.J. DeArdo, G.A. Ratz and P.J. Wray, TMS-AIME, Warrendale, PA, USA, 1982, p. 405.

³³ R.K. Amin and F.B. Pickering: Thermomechanical Processing of Microalloyed Austenite, ed. By A.J. DeArdo, G.A. Ratz and P.J. Wray, TMS-AIME, Warrendale, PA, USA, 1982, p. 377.

³⁴ M. Umemoto, H. Ohtsuka, H. Kato and I. Tamura: Proc. Int. Conf. On Structure and Properties of HSLA Steels, Wollongong, Australia, 1984.

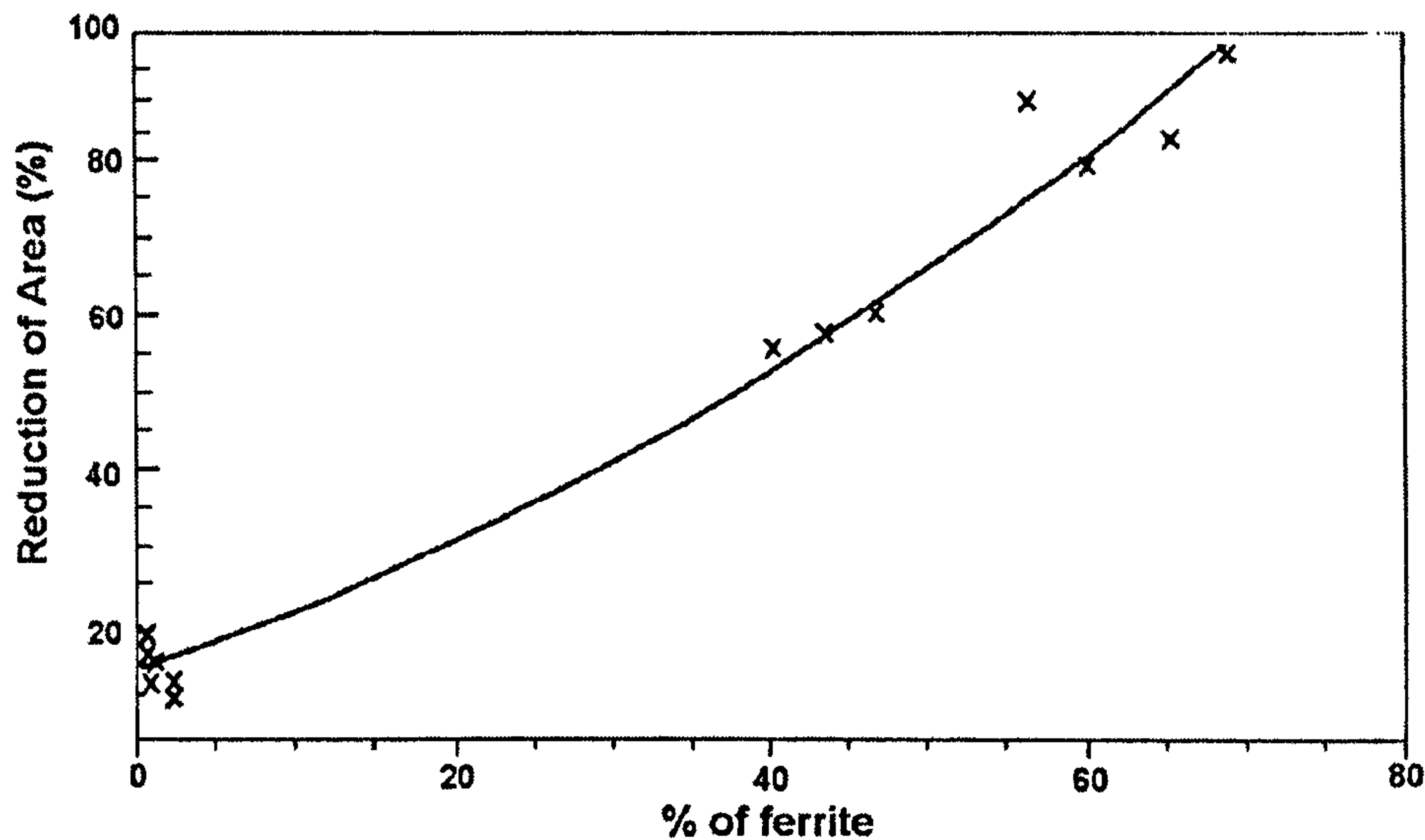


Figure 2.10: Effect of percentage ferrite phase present on hot ductility.⁸

As explained in ref 2, various suggestions have been put forward to account for the accelerating effect of deformation on the nucleation of ferrite:

1. The deformation results in local grain boundary migration which form bulges at the austenite grain boundaries, which then act as nuclei.³²
2. Sub-grains are formed near the boundaries, raising the locally stored energy.³³
3. The increased dislocation density in deformed austenite increases the strain energy, thus favouring ferrite nucleation.³⁵

Many investigations^{31,36,37,38} have shown that the thin films of ferrite observed are deformation induced; although much of the work that has been done shows deformation induced ferrite (DIF) to form readily in fine grained material, there is limited positive confirmation of its formation in coarse grained material at low strains (~2%) such as

³⁵ M. Umemoto and I. Tamura: in ref 28, personal communication, Kyoto University, Japan, 1985.

³⁶ T. Maki, T. Nagamichi, N. Be and I. Tamura: Tetsu To Hagane, 1985, 71, p. 1367.

³⁷ D.N. Crowther and B. Mintz: Mat. Sci. and Technol., 1986, 2, p. 671-676.

³⁸ D.P. Rizio, R.B. Oldland and B.W. Borland: in 'Physical Metallurgy of Thermomechanical Processing and other Metals, Thermec 88', p. 178; 1988, Tokyo, ISIJ.

experienced in the straightening operation. Essadiqi and Jonas ³⁹ have shown that deformation induced ferrite can be produced in fine grained ($\sim 25\mu\text{m}$) low C, Mo steel under strain and strain rate conditions similar to those in the straightening operation. Similarly, Mintz *et al* ⁴⁰ have shown that DIF can be produced in large quantities, close to equilibrium volume fractions, in a C-Mn-Al steel after strains as little as 0.15 at low strain rates (3×10^{-3} to 3×10^{-4}).

Wedge shaped cracks are often present at the interface between the prior austenite grain boundaries and the thin films of ferrite, ³⁷ see Figure 2.11. These are assumed to form by displacement of the austenite grains along the softer ferrite films rather than by conventional grain boundary sliding.²

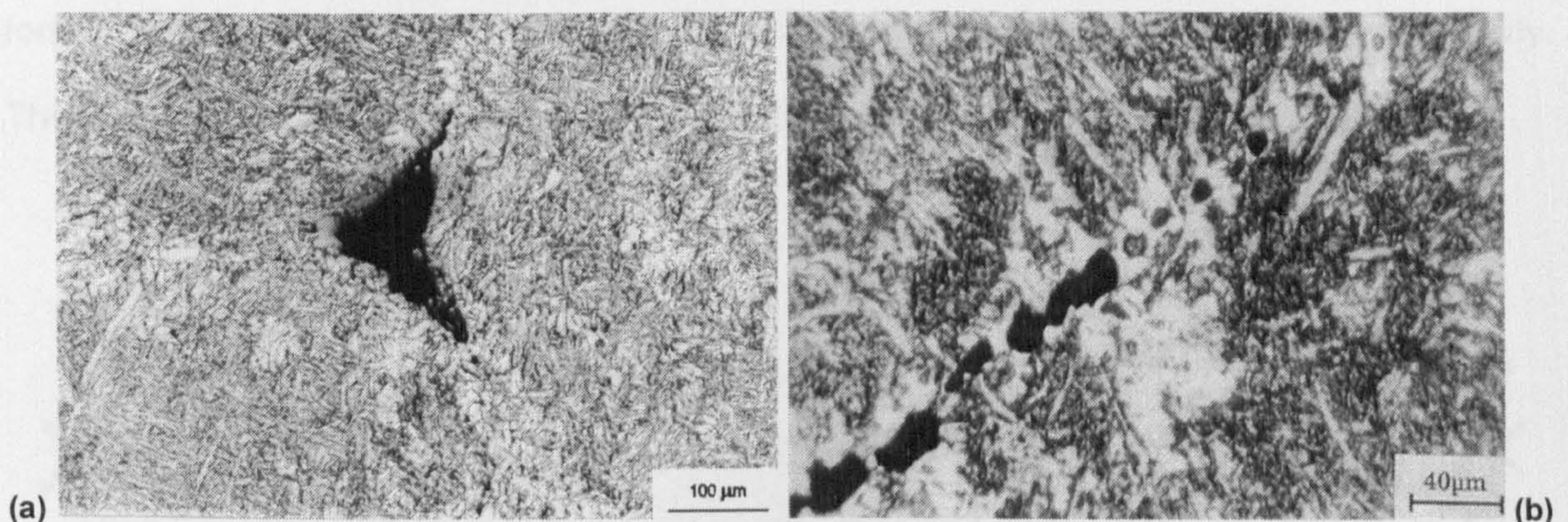


Figure 2.11: (a) A typical wedge type crack formed in a Nb containing steel ⁴¹ and (b) enlarged view showing microvoid nucleation at inclusions.²

2.2.3 Precipitate Free Zones

In Niobium containing steels that have been solution treated before cooling, precipitation takes place during deformation in the austenite. The formation of weaker precipitate free zones can occur on the edges of the grain boundaries, see Figure 2.12.

³⁹ E. Essadiqi and J.J. Jonas: Metall. Trans., 1988, 19A, p. 417.

⁴⁰ B. Mintz, J. Lewis and J.J. Jonas: Mat. Sci. and Technol., 1997, 13, pp. 379-388.

⁴¹ Z. Mohammed: Hot Ductility of Steels, PhD Thesis, 1988, City University London, UK.

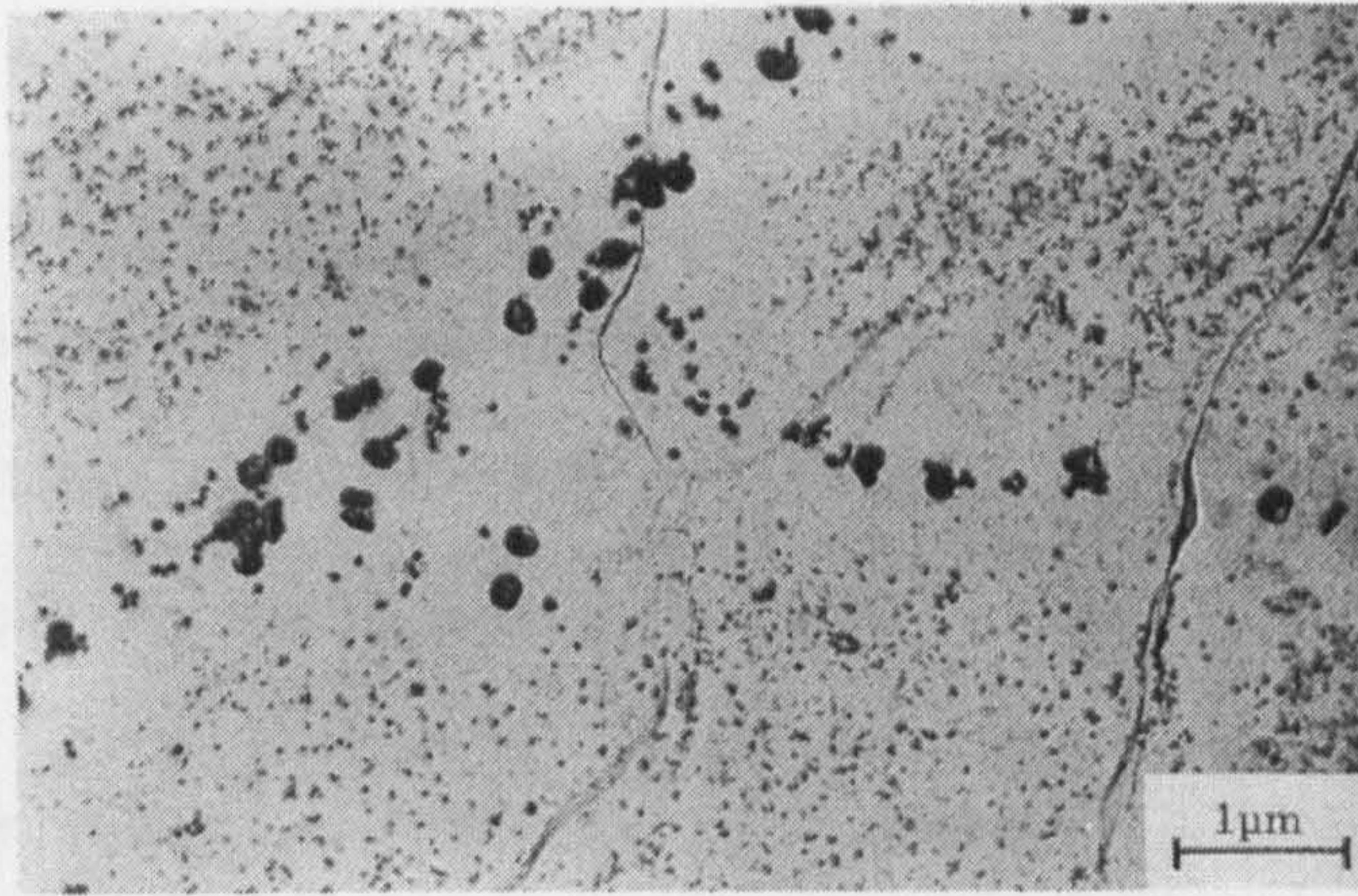


Figure 2.12: Precipitate free zone around the grain boundary in a Nb-containing steel, fractured at 950K. The grain boundary contains fine precipitates of Nb(CN) and coarse MnS inclusions.⁴²

These precipitate free zones are formed by diffusion and can be 500nm wide.⁴² Fine precipitation can be seen to take place within the matrix, causing strengthening, and microvoid coalescence can then take place around in the relatively weak PFZs. This void formation occurs at the Nb(C,N) or AlN precipitates again contributing to the lack of ductility. This fracture process is illustrated schematically in Figure 2.13.⁴³

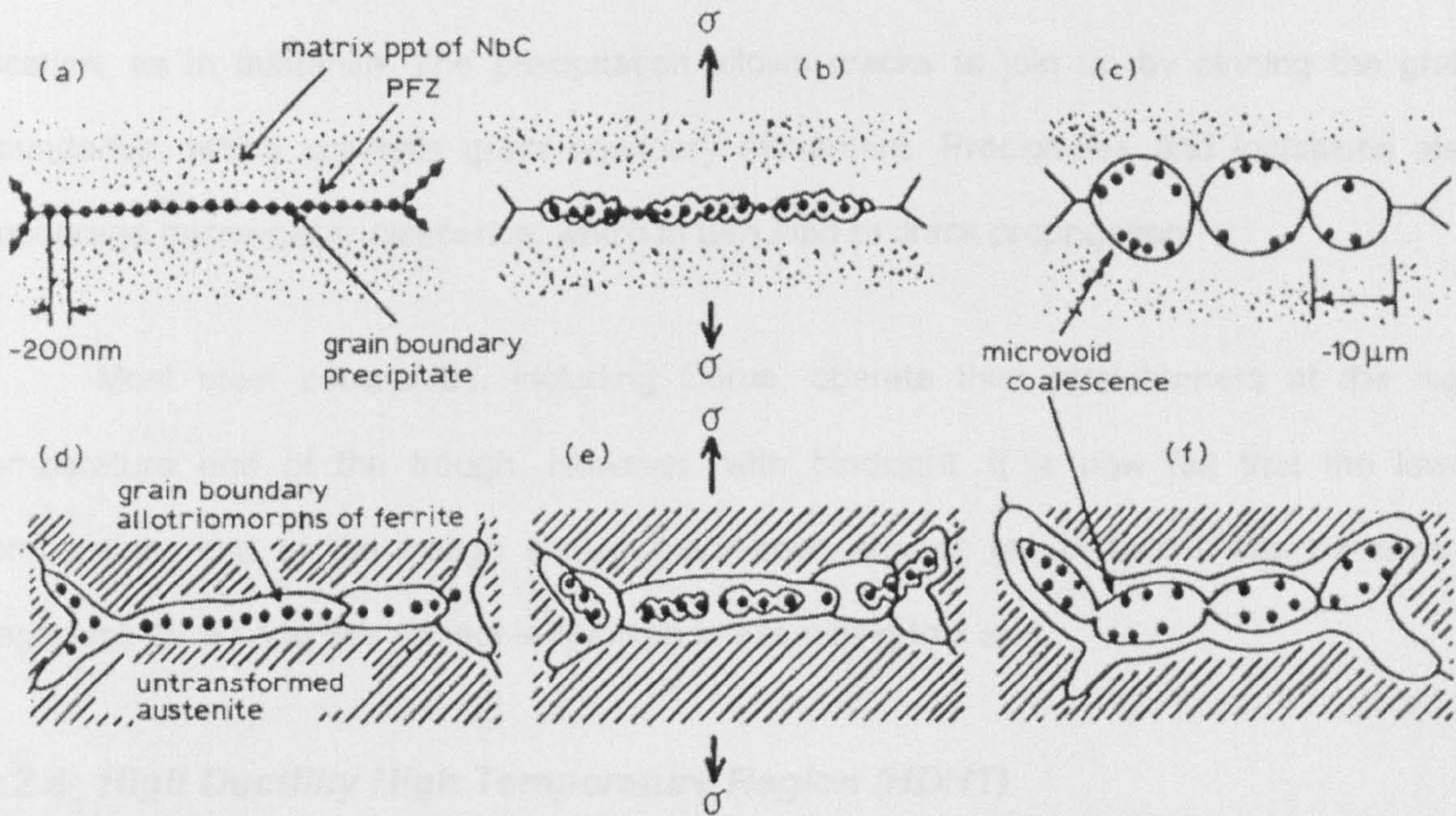


Figure 2.13: Schematic illustrations showing intergranular microvoid coalescence of Nb-bearing steels by deformation in (a)-(c) the low temperature region and (d)-(f) the duplex phase region.⁴³

⁴² B. Mintz, J.R. Wilcox and D.N. Crowther: Mat. Sci. and Technol., 1986, 2, p. 589.

⁴³ Y. Maehara and Y. Ohmori: Mat. Sci. Eng., 1984, 62, p. 109.

The size and shape of the ductility trough can be influenced by the composition and the microstructure of the steels. The two most important microstructural elements that effect ductility are the grain size and the occurrence of precipitates. Extensive creep studies have shown that the high temperature ductility increases as the grain size decreases. This increase in ductility is due to the following factors:

4. The increase in specific grain boundary area (for a given volume fraction of precipitate) reduces the precipitate density along the grain boundaries.
5. The increased occurrence of grain boundary migration due to the increased number of grain boundary nucleation sites.
6. The discouragement of crack propagation by the decrease in the crack aspect ratio (this controls the stress concentrations at the crack tip).

The refined grain size leads to reductions in both the depth and width of the trough. The effect that precipitates have on the hot ductility depends on their size, distribution and location; as in austenite, fine precipitation allows cracks to join up by pinning the grain boundaries, which prevents grain boundary movement. Precipitates and inclusions also encourage microvoid coalescence, which in turn lead to crack propagation.

Most steel companies, including Corus, operate their straighteners at the high temperature end of the trough. However, with hindsight, it is now felt that the lower temperature end of the trough should have been chosen (as in fact it was by several Japanese firms) and this project is involved in examining this end.

2.2.4 High Ductility High Temperature Region (HDHT)

In the HDHT region, the higher temperatures mean that the thin ferrite film is now entirely absent and the structure is entirely austenitic. This drastically reduces the strain concentration at the grain boundaries, which occurs when the ferrite film is present. Higher

temperatures also mean that less precipitation will occur and will also lead to lower flow stresses via increased dynamic recovery.

The main increase in ductility that is observed in laboratory tests in this region is usually associated with dynamic recrystallisation (DRX) which leads to an increase in the driving force for grain boundary migration; this improvement in hot ductility is illustrated in Figure 2.14. DRX does not normally occur in commercial continuous casting due to the small strains ($\sim 2\%$) involved at the straightener. This is still the case even with thin slab casting when pre-deformation is used and the grain size will be slightly finer. Results obtained experimentally for this side of the trough should therefore be used with caution when trying to predict the likelihood of transverse cracking occurring during the straightening operation. The effect of DRX on hot ductility will be discussed more fully in section 2.3.2.

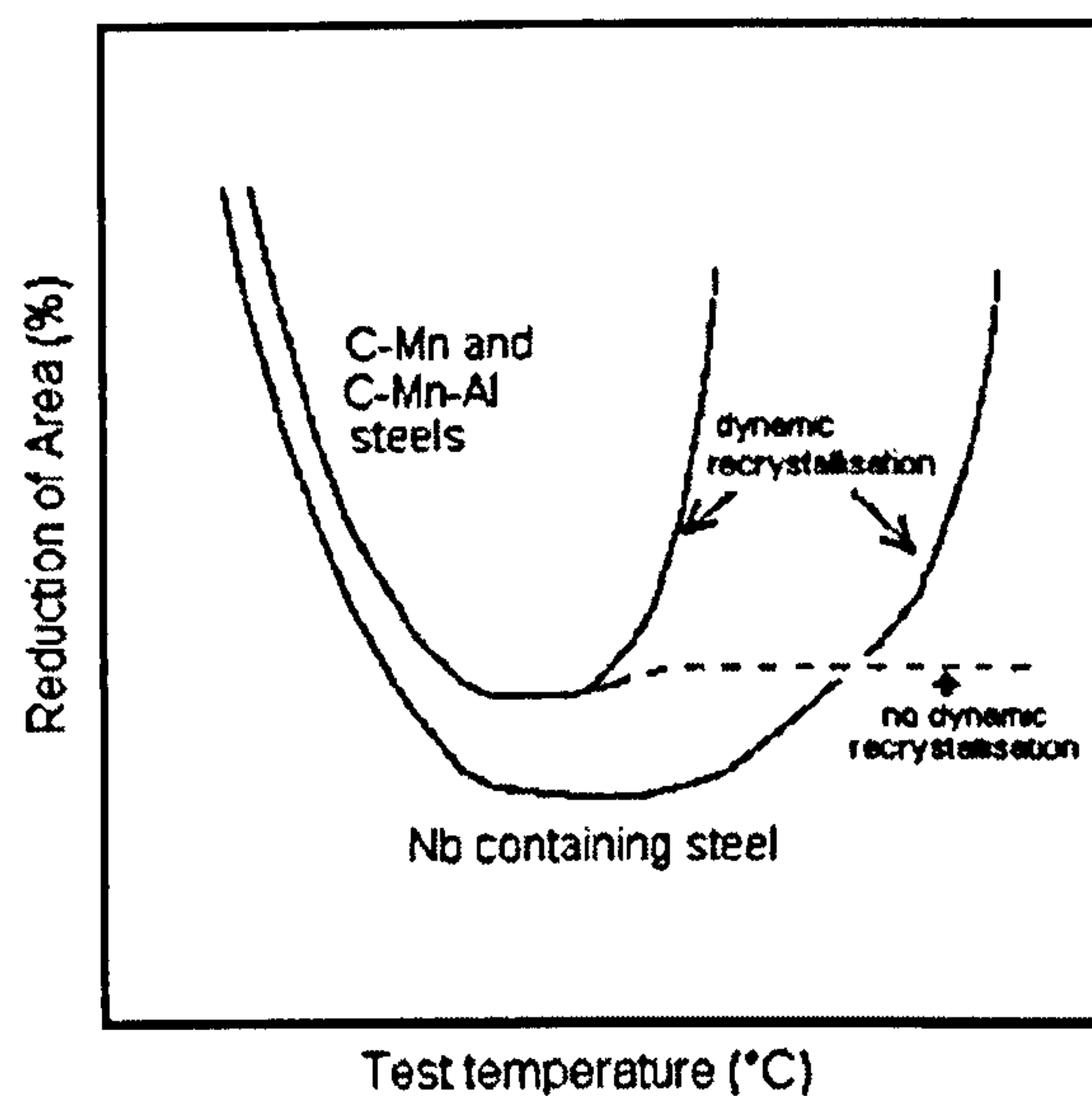


Figure 2.14: Schematic illustration showing the ductility levels that can be achieved with and without dynamic recrystallisation at the high temperature end of the trough.⁹

As a result of the grain boundary migration, cracks that have initiated are isolated from the prior γ grain boundaries and are not readily able to coalesce; crack growth is more difficult away from the grain boundaries. Generally the grain boundary migration is only possible when there is no film of ferrite present; this occurs at temperatures above the Ae_3 and thus good ductility often corresponds to the attainment of the Ae_3 temperature. This

high ductility is due to the cracks becoming isolated, and then growing into large elongated voids. The final failure occurs due to necking between these cavities and is a characteristic of the fracture surfaces obtained when testing in the HDHT region, see Figure 2.15. These massive cavities have been shown not to be due to second phase particles present within the matrix.^{44,45}

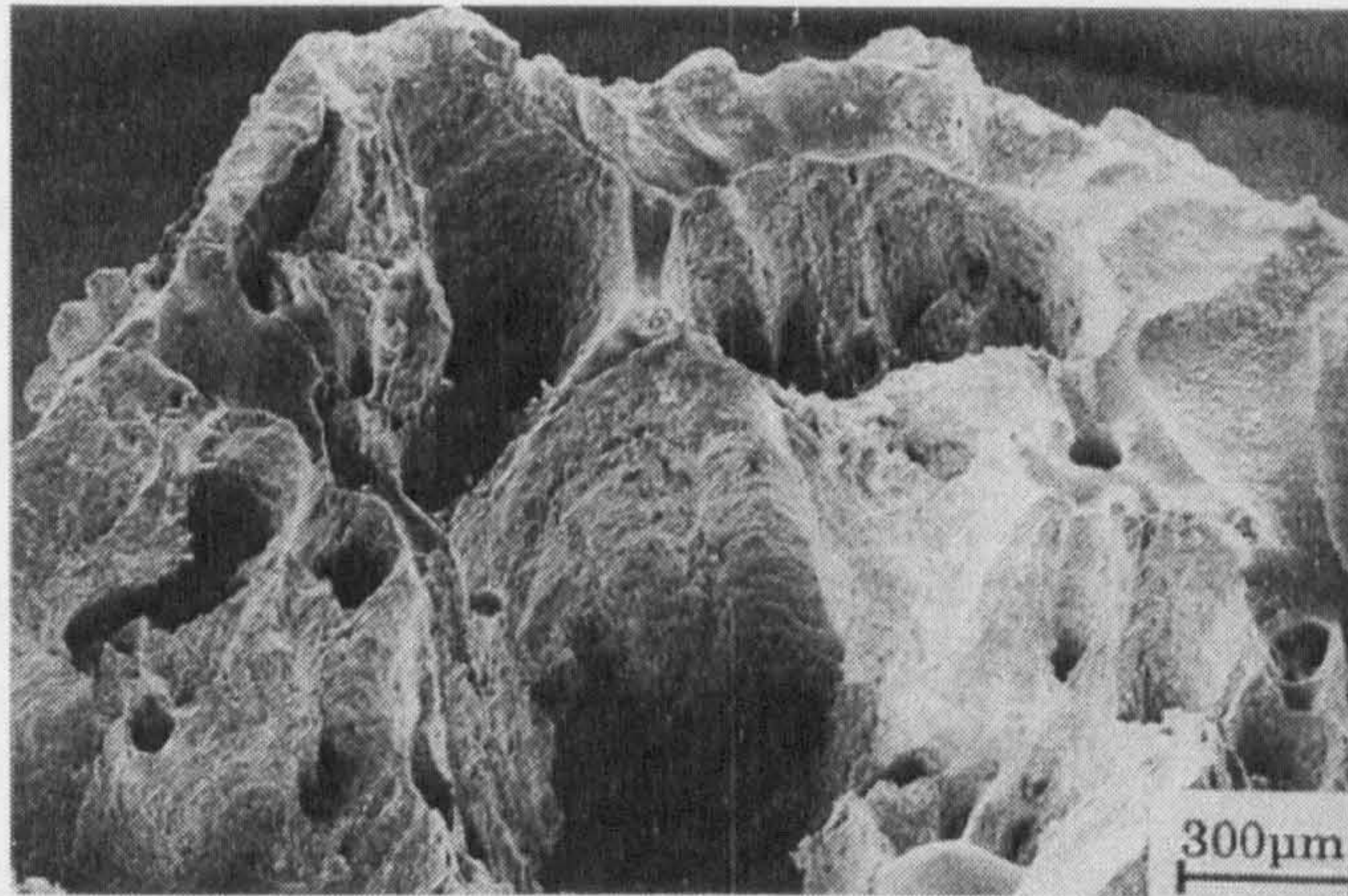


Figure 2.15: Typical high temperature ductile rupture failure observed in the HDHT region.⁴⁵

Many studies have shown that the HDHT region corresponds to the onset of DRX.^{24,46,47} However, in other studies^{44,47,48} DRX has been seen to occur throughout all or part of the ductility trough, suggesting that on occasions DRX needs to be more advanced than just the early stages in order to prevent intergranular failures. To fully understand the HDHT region, it is first necessary to understand what controls the A_{r3} temperature. If the A_{r3} temperature can be raised so that it approaches the A_{e3} temperature then, not only will the width of the trough be reduced, but large amounts of ferrite can form at the higher temperature thus improving ductility. The factors controlling the A_{e3} and A_{r3} temperatures, and hence production of DRX, form part of this current study.

⁴⁴ P.J. Wray: Metall. Trans., 1975, 6A, p. 1379.

⁴⁵ D.N. Crowther and B. Mintz: Mat. Sci. and Technol., 1986, 2, p. 1099.

⁴⁶ J.R. Wilcox and R.W.K. Honeycombe: Met. Technol., 1984, 11, p. 217.

⁴⁷ D.N. Crowther, Z. Mohamed and B. Mintz: Trans. ISIJ, 1987, 27, p. 366.

⁴⁸ B. Mintz, S. Yue and J. J. Jonas: in Proc. Int. Conf. on 'Recrystallisation in metallic materials', Wollongong, NSW, p. 553; 1990, Warrendale, PA, Met. Soc. of AIME.

2.2.5 High Ductility Low Temperature Region (HDLT)

The HDLT region starts when there is a relatively high volume fraction of ferrite surrounding the γ grains; these ferrite films are now thicker and more uniformly distributed. The strength differential between the austenite and ferrite phases diminishes with decreasing temperature; therefore, the strain no longer concentrates in the ferrite films.²⁸ In this region, low temperature ductile rupture occurs; voids that are nucleated at second phase particles within the grains grow and coalesce resulting in fracture.

A softening process known as dynamic recovery (discussed later in section 2.3.1) operates at all strains in the ferrite, due to α having a higher stacking fault energy;⁴⁹ this delays the onset of void nucleation and coalescence leading to good ductility.⁵⁰ Dynamic recovery occurs much more easily in ferrite which has 48 slip planes compared to austenite which only has 12. More deformation can thus be accommodated by the α phase such that grain boundary sliding is minimised resulting in high ductility.

2.2.6 Measurement of Hot Ductility

The closest simulation of the straightening operation in commercial continuous casting would be a hot bending test; due to complexity of the test apparatus required and difficulty in interpreting the results, it is not commonly used.^{23,51} Other methods such as a flange test⁵² and torsion testing⁵³ have been used, but the results are again difficult to interpret. The simple hot ductility test is by far the most commonly used laboratory test; this

⁴⁹ D.M. Keene, C.M. Sellars and W.J.McG. Tegart: in 'Deformation under hot working conditions', Iron and Steel Institute, London, 1968, 21.

⁵⁰ R.E. Smallman: Modern Physical Metallurgy, 1985, Butterworths and Co., ISBN 0750606290.

⁵¹ N.W. Blake: "Hot ductility of simulation castings", Rep. MRL/AMP/87/5, July 1987, BHP, Melbourne.

⁵² J.Y. Fu, C.I. Garcia, S. Pytel and A.J. DeArdo: in "Processing, Microstructure and Properties of HSLA Steels", 1988, 27, Warrendale, PA, Met. Soc. of AIME.

⁵³ L.E. Cepeda, J.M. Rodriguez-Ibabe, J.J. Urcola and M. Fuentes: Mater. Sci. and Technol., 1989, 5, p. 1191.

is mostly due to the ease by which it can be carried out, producing results that can be readily interpreted, and the fact that conventional tensile test machines (e.g. Zwick, Instron and Hounsfield) available in most research laboratories can be easily converted to accommodate this test. There are a number of types of hot tensile test, each with different degrees of complexity and varying suitability and success for predicting the likelihood of transverse cracking occurring at the straightener. Examples of the different types of hot tensile test are shown in Figure 2.16.

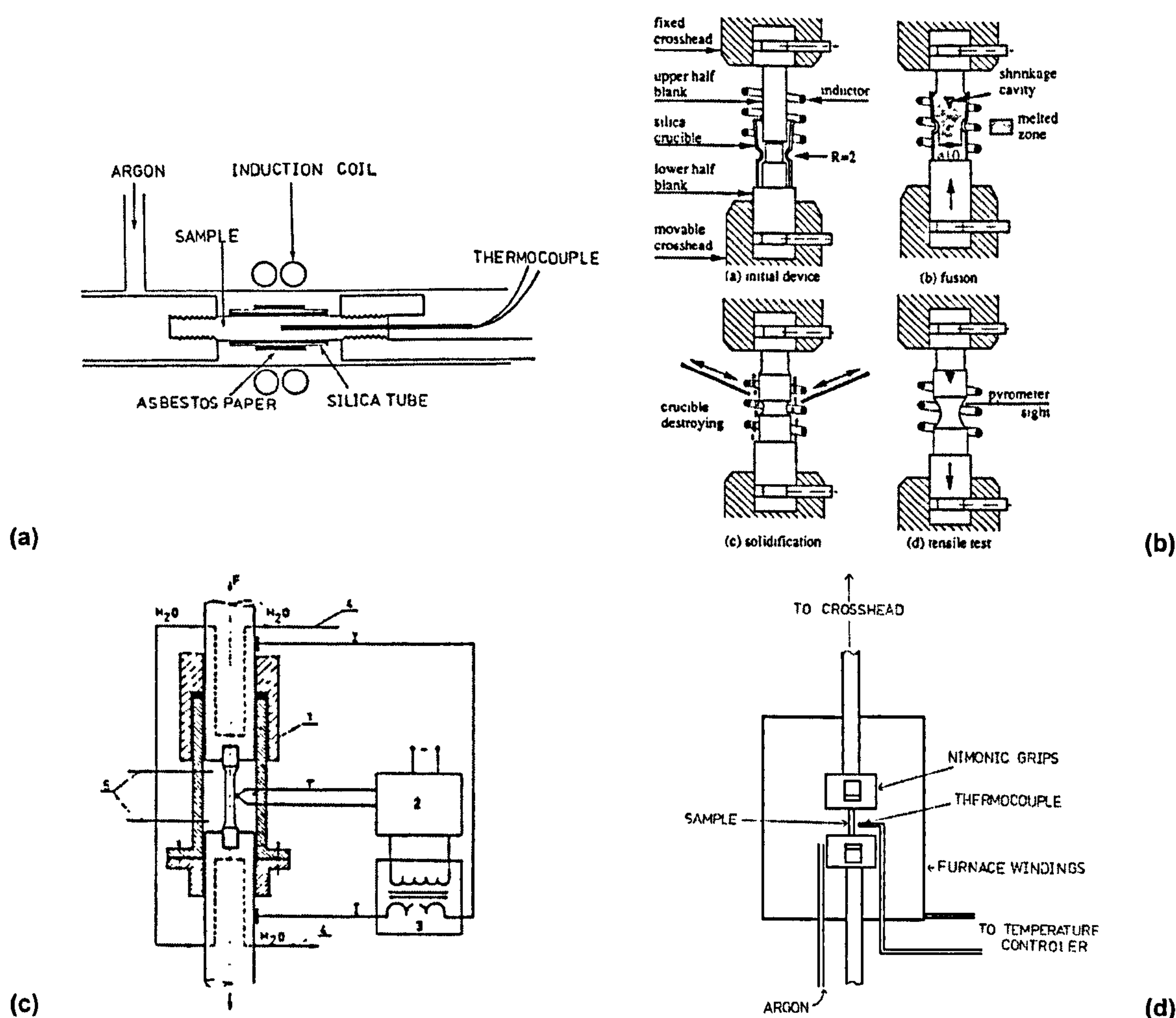


Figure 2.16: (a) Experimental arrangement for measuring hot ductility in the as-cast condition,⁵⁴ (b) Hot tensile test using as-cast notched specimen,⁵⁵ (c) hot tensile test employing resistance heating for solution treatment of specimen⁵⁶ and (d) using radiant heating for solution treatment.¹⁸

⁵⁴ B. Mintz and Z. Mohamed: "Hot Ductility of Directly Cast Microalloyed Steels", in Int. Symp. On Physical Simulation of Welding, Hot-Forming and Continuous Casting, CANMET, Canada, 1988.

⁵⁵ P. Deprez, J.P. Bricout and J. Oudin: Mat. Sci. and Eng., 1993, A168, pp. 17-32.

⁵⁶ S. Sladik and M. Longauerova: Metallic Materials, 1992, 30, No. 4, pp. 210-214.

In the apparatus shown in Figure 2.16 (a), a converted Hounsfield tensometer has been fitted with induction heating rig used to melt the sample; the molten steel is retained in the silica tube and then cast in situ and cooled to the test temperature. Some of the problems encountered using this method have been found to include temperature gradients along the specimen, and fractures occurring outside the melt zone at lower temperatures.

Figure 2.16 (b) shows a similar induction method, but this time using a notched specimen formed by fusing two blanks together. A calibrated conical shaped crucible ensures that the shrinkage cavity that can form is well away from the gauge length. This apparatus is therefore more involved and hence a more costly method than using that shown in Figure 2.16 (a). However, due to the notch failure always occurring in the melted zone and the gauge length in this case is definite; it has also been found to be of great interest as the test can produce the columnar grains present in commercially cast slabs, whereas without the notch, laboratory samples will only give equiaxed grains. Oudin *et al*⁵⁷ state that the notched test favours decohesion at the grain boundaries and related defects. Simple casting in-situ will simulate continuous casting more closely for segregation, grain size and dissolution of precipitates such as TiN and MnS, but not the grain morphology.

Figures 2.16 (c) and (d) show methods where samples are not cast in-situ, but are instead solution treated at temperatures high enough to allow the microalloying precipitates to dissolve. It has been shown⁵⁸ that solution treatment is the preferred route for hot tensile testing of microalloyed steels over casting in situ. Direct casting is only normally necessary when solution treatment is proved difficult, as is the case when studying steels with Ti precipitates, where a high temperature is required to take them into solution. The work that is undertaken in the Department of Mechanical Engineering at City University, and therefore that in the current study, uses apparatus similar to that shown in Figures 2.16 (a) and (d).

⁵⁷ J. Oudin, Y. Ravalard, J.C. Gelin, G. Lacombe and T. Labarthe-Vacquier: *Matér. Tech.*, 1988, 39, pp. 11-12.

⁵⁸ B. Mintz and R. Abushosha: *Mat. Sci. and Technol.*, 1992, 8, No. 2, pp. 171-177.

2.3 High Temperature Cracking and Softening Processes

Hot strength is strongly influenced by the temperature and strain rate; this is particularly the case when large strains (ϵ) are applied to materials at high strain rates at temperatures (T) in excess of $0.7 T_m$, where T_m is the melting point in Kelvin. During hot deformation, the strength and also the hot ductility of a steel will depend upon the balance between work hardening, dynamic softening (recovery and recrystallisation) processes, the composition and the test conditions (including temperature, ϵ and $\dot{\epsilon}$). Whether dynamic recovery or recrystallisation occurs is largely governed by the steel's composition and the deformation conditions, this is summarised in Table 2.1.

Group	Example	Dynamic	Static
A	Al, α -Fe, ferritic alloys	Recovery (all strains)	Recovery followed by recrystallisation
B	Cu, Ni, γ -Fe, austenitic alloys	Recovery (small strains) Recrystallisation (large strains)	Very limited recovery, followed by recrystallisation

Table 2.1: Possible softening processes occurring on hot deformation.⁵⁹

If work hardening predominates, the strength will be high but the ductility will be low. This situation is reversed if softening processes predominate, therefore resulting in high ductility. Various attempts have been made to discover a relationship between strength (σ), T and $\dot{\epsilon}$; the most successful of the early investigations would seem to be that of Sellers *et al.*⁶⁰ who proposed the following arrhenius type of rate equation:

$$\dot{\epsilon} = A(\sinh \alpha \sigma)^n e^{\left(\frac{-Q}{RT}\right)} \tag{2.3}$$

⁵⁹ C.M. Sellars and W.J.McG. Tegart: Int. Met. Rev., 1972, 17, 1

⁶⁰ C.M. Sellars and W.J.McG. Tegart: Mem. Sci. Rev. Met., 1966, 63, p. 731.

Where A , α and n are temperature independent constants, σ is the stress (either peak or applied), T is the absolute temperature, R is the Universal Gas Constant and Q is the activation energy.

The activation energy, Q , can remain unchanged over a wide range of strain rates, but different values may be obtained for creep and hot working conditions.⁶¹ For plain carbon steels deformed in the ferrite, Q can be taken as the activation energy for self diffusion (289kJ mol^{-1} in α -iron), indicating that the softening process is dynamic recovery; in this case, the value can remain constant over a wide range of strain rates. For austenitic steels, the value of Q is higher and is believed to be due to the operation of dynamic recrystallisation during hot working. For example, Perkins *et al.*⁶² estimated the value of Q for a 316L stainless steel, over a narrow range ($1273\text{-}1523\text{K}$ and $0.001\text{-}0.1\text{s}^{-1}$), to be about 600kJmol^{-1} ; this value is higher than the activation energy for self diffusion of 280kJ mol^{-1} .

Equation 2.3 may also be expressed in terms of the Zener-Holloman parameter, Z , where:

$$Z = \dot{\epsilon} e^{\left(\frac{Q}{RT}\right)} \quad (2.4)$$

Therefore, substituting for $\dot{\epsilon}$, equation 2.2 can be rewritten as:

$$Z = A(\sinh \alpha \sigma)^n \quad (2.5)$$

Previous studies have shown that this relationship can be successfully applied for a number of alloys, including plain carbon steels⁶³ and micro-alloyed steels in the austenitic state.⁶⁴ It is generally found that materials having a high stacking fault energy favour

⁶¹ J.J. Jonas, C.M. Sellars and W.J. McG. Tegart: In "Deformation under Hot Working Conditions", Special Report No. 108, London ISI, 1968, p.21.

⁶² R.A. Perkins, R.A. Padgett Jr. and N.K. Tunali: Metall. Trans., 1973, 4A, pp. 2535-2540.

⁶³ W.J. McG. Tegart: In "Ductility", Metals Park, Ohio, 1968, p. 133.

⁶⁴ J. Sanker, D.N. Hawkins and H.J. McQueen: Met. Technol., 1979, 6, p. 325.

recovery as thermally activated cross-slip is easy, these are Group A materials, see Table 2.1. Conversely, Group B materials have low stacking fault energy and allow dislocations to build up within the matrix and thus favour dynamic recrystallisation. These two processes will be discussed briefly in the following sections, but it should be noted that ferrite favours recovery, whereas austenite favours dynamic recrystallisation.

2.3.1 Dynamic Recovery

The microstructural evidence for dynamic recovery has been reviewed by Jonas *et al.*⁶², in which it is noted that the original grain structure becomes elongated in the direction of the applied strain and the boundaries appear fibrous. This boundary distortion is accompanied by sub-grain formation which results in the final structure containing narrow and well defined sub-grains. During straining, the dislocation density between the sub-boundaries remain constant and a situation is reached where dislocation generation and annihilation reaches an equilibrium; the strain hardening rate is reduced to zero and a steady flow is established.

In general, solid solution alloying additions make dynamic recovery more difficult as they increase the stacking fault energy and as a result increase the flow stress. Metals that contain stable second phase particle develop substructure more readily than equivalent particle free alloys. These particles stabilise the substructure and the sub-grain diameter is reduced to the order of the interparticle spacing. Particle coarsening is able to occur if the second phase particles are less stable; and is accelerated by hot deformation as the sub-boundaries allow diffusion to occur at a higher rate than within the lattice. This results in a decrease in the flow stress during hot deformation. Generally, ductility recovers when around 50% ferrite is present in the microstructure on the low temperature side of the ductility trough, see Figure 2.10.

2.3.2 Dynamic Recrystallisation (DRX)

At the high temperature end of the trough, ductility dramatically improves with the onset of DRX. Cracks that have formed at the original grain boundaries become isolated as the grain boundary moves away from the crack and new grains are formed; crack growth is then halted. It should be noted that DRX is not possible during conventional continuous casting since the strain involved in straightening (2%) is too small and the grain size is too coarse. Prasad *et al.*⁶⁵ consider DRX to be the single most important mechanism for bulk metal working and Jonas⁶⁶ emphasises its importance in the hot rolling of steel. However, it should be noted that the occurrence of DRX very much depends on processing conditions, e.g. strain rate and total strain. Although strain rates used in the hot ductility test are chosen to simulate the straightening operation, samples are strained to failure, whereas the total strains during straightening are much smaller (2%). DRX is not commonplace during slow rolling in plate, but is of vital importance during the rapid rolling of rods.

DRX is a very beneficial process during hot working, apart from improving workability by simultaneous softening, it 'breaks down' as-cast columnar grains to produce a wrought microstructure of acicular grains. DRX is traditionally associated with the hot working of low SFE metals like Cu and Ni, which exhibit flow softening after reaching a critical strain;⁶⁵ and normally occurs in the temperature range $0.7 - 0.8 T_m$ with intermediate strain rates of $0.1 - 1.0 s^{-1}$ for materials with low SFE; whereas it occurs at much lower strain rates, $0.001 s^{-1}$, for high SFE materials (e.g. f.c.c. metals typified by steel, Al and some of its alloys).⁶⁵

Stacking faults are planar imperfections in the normal stacking of planes within the lattice structure of a material; they increase the rate of work hardening by impeding the flow

⁶⁵ Y.V. Prasad, S. Sasidhara, R. Ravi and S. Yellapregada: Indian Institute of Science, 2003, <http://www.processingmaps.com/Graphics/content/Theory/Programs.htm>.

⁶⁶ J.J. Jonas: Mater. Sci and Eng., 1994, A184, pp. 155-165.

of dislocations.⁶⁷ Stacking faults have an energy associated with them as atoms either side of the fault are not in the positions they would be in a perfect lattice; this energy is generally small, but quantifiable, when compared with that of a normal grain boundary. Work by Prasad *et al.*⁶⁵ indicates that SFE is a very important parameter that can influence DRX characteristics. The higher the SFE, the closer are the partial dislocations to each other and the easier it becomes for cross slip to occur. This makes recovery more likely at higher temperatures than dynamic recrystallisation which requires a marked build up in dislocation density to set the process off.

Since DRX is not often possible during conventional continuous casting, the use of the high temperature end of the trough in predicting the likelihood of cracking has therefore to be treated with caution. Increasing the temperature at the straightener can nevertheless improve ductility as the particles will coarsen or the amount of precipitates formed in the boundary regions will decrease. Due to the difficulty in studying what is actually happening commercially during the straightening operation, it is assumed that this improvement is small as shown by the dashed curve in Figure 2.14.

However, in the present work the main focus has been on interpreting the hot ductility curve and hence the role of dynamic recrystallisation is important. The temperature at which DRX first occurs, T_D , can be found from when the curve of critical strain for DRX, ϵ_c , intersects the approximate horizontal line representing the ductility when no DRX is possible, ϵ_f , see Figure 2.17 (a). ϵ_c can be taken as the strain to the peak stress in the stress/strain curve, ϵ_p , which can be calculated. This model can be used to show how the curves are influenced by the increase in strain rate and refinement in grain size, Figures 2.17 (b) and (c) respectively.

⁶⁷ D.T. Llewellyn: Steels: Metallurgy and Applications, 2nd ed., 1994, Butterworth-Heinemann Ltd, ISBN 0-7506-2086-2.

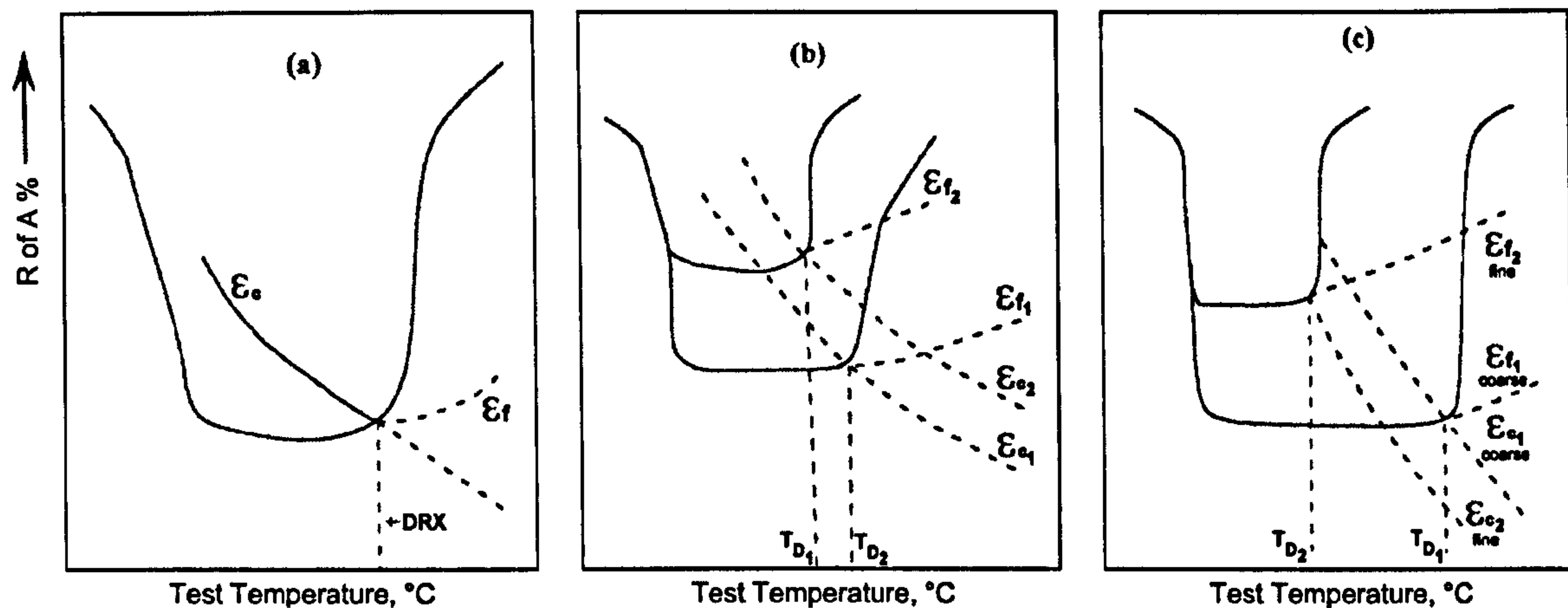


Figure 2.17: Schematic diagram showing (a) how the width of the ductility trough could be controlled by the dynamic recrystallisation (DRX); (b) how increasing the strain rate reduces the depth and width of the trough, ϵ_{c1} , ϵ_{f1} and T_{D1} refer to the lower strain rate and ϵ_{c2} , ϵ_{f2} and T_{D2} refer to the higher strain rate and (c) how refining the grain size reduces the depth and width of the trough, ϵ_{c1} , ϵ_{f1} and T_{D1} refer to the coarser grain size and ϵ_{c2} , ϵ_{f2} and T_{D2} refer to the finer grain size.⁶⁸

The nucleation of DRX takes place at existing boundaries at low strain rates. Poorly developed sub-boundaries pin sections of the original boundaries which bulge out and migrate relatively rapidly, this is because of the strain energy difference across the boundary. Refining the grain size increases the number of grain boundary nucleation sites thus making it easier for DRX and reducing the critical strain for DRX, ϵ_c . However, it should be noted that increasing $\dot{\epsilon}$, by increasing the strain energy of the unrecrystallised grains, results in more strain energy having to be pumped into the bulged region of the grain boundary to cause DRX. Hence the critical strain for DRX is increased.

Using this model, it can be explained how increasing the strain rate both increases the critical strain for DRX and also improves the hot ductility, see Figure 2.17 (b). Whereas increasing the strain rate improves the hot ductility, ϵ_{f1} to ϵ_{f2} , due to a reduction in the grain boundary sliding, the critical strain for DRX, ϵ_c , is also increased, ϵ_{c1} to ϵ_{c2} ; hence T_D occurs at a lower temperature as shown in Figure 2.17 (b). The change in T_D is dependant on the relative movements of ϵ_f and ϵ_c , and their sensitivity to $\dot{\epsilon}$ and grain size.

⁶⁸ B. Mintz, R. Abushosha and J. J. Jonas: ISIJ Int., 1992, 32, p.241.

The temperature for the onset of DRX can often be determined from the load-elongation curves and is characterised either by a sudden drop or oscillations in the flow stress. This effect of DRX on the load-elongation curve can be seen in Figure 2.18, below.

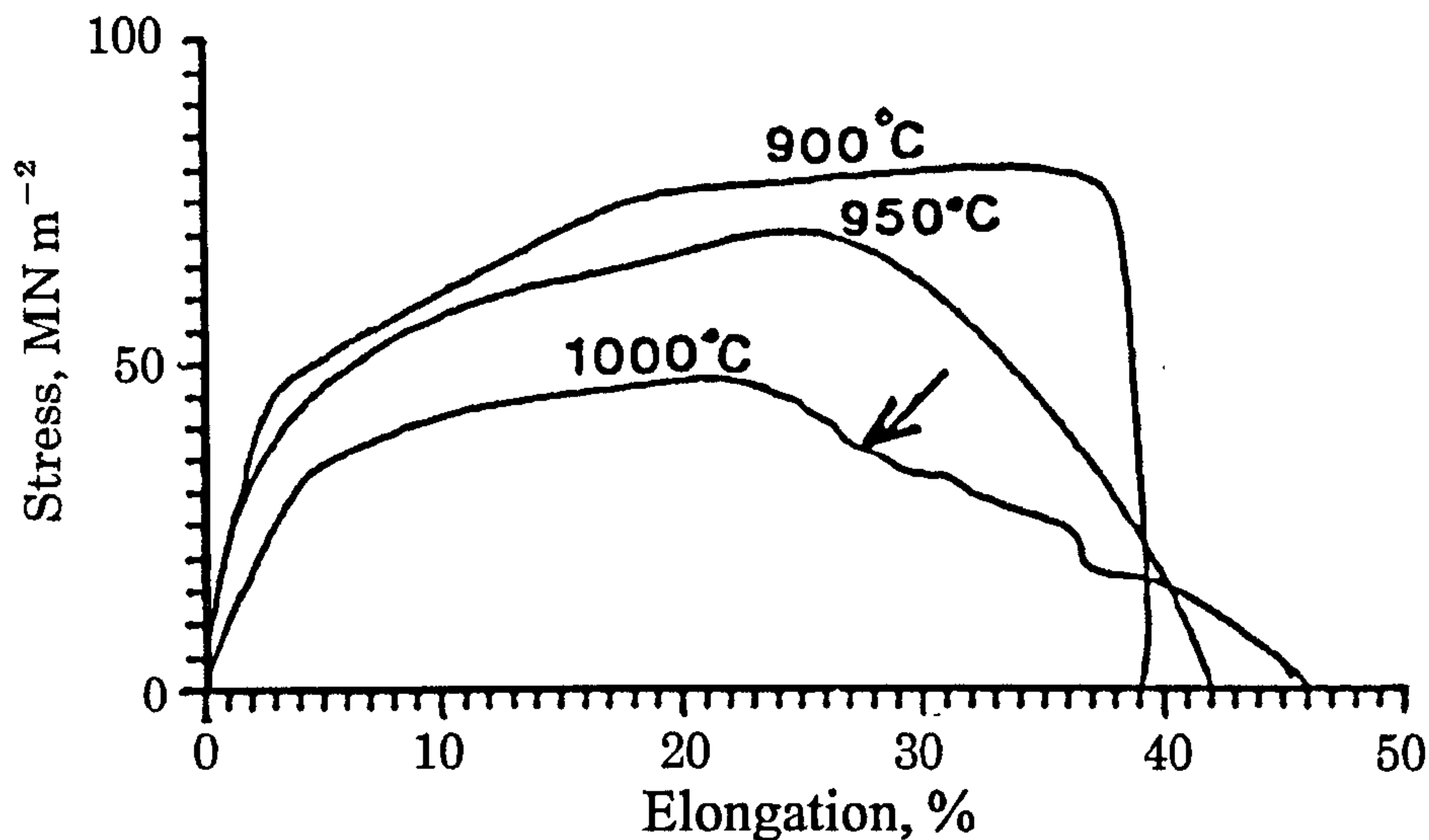


Figure 2.18: Stress-elongation curves for a C-Mn-Al-Nb steel, solution treated and tested in air, the arrow indicates that dynamic recrystallisation is occurring.⁶⁹

2.4 Influence of Processing Conditions and Composition

Processing conditions at the continuous caster and the composition of the steel being produced can be used to control the likelihood that transverse cracking will occur. Although production parameters and composition can be varied dramatically when studying hot ductility in the laboratory, it should be noted that these can not always be altered so greatly in commercial practice.

2.4.1 Influence of Process Variables on Hot Ductility

There are four test variables which can affect the hot ductility of steels; strain rate, thermal treatment, cooling rate and holding time. Since the effect of these variables have been discussed at length elsewhere,^{2,23} they will only be discussed briefly in the following sections.

⁶⁹ B. Mintz, R. Abushosha and D.N. Crowther: Mat. Sci. and Technol., 1995, 11, pp. 474-481.

Strain rate

The strain rate normally associated with the continuous casting straightening operation for 220mm thick strand is believed to be between 10^{-3} and 10^{-4}s^{-1} ; for thin slabs, ~50mm thick, this strain rate increases to 10^{-2}s^{-1} . These values can be calculated using Equation 2.2 given in section 2.1.2. The general effect of increasing the strain rate is to improve hot ductility. Increasing strain rate by an order of magnitude often increases R of A values by ~20%. Thus, in this respect thin slab casting should lead to better ductility. However, as will be seen from the section on cooling rate, the higher cooling rate associated with the cooling of thin slabs counteracts any benefit.²⁶ Higher strain rates improve hot ductility for a number of reasons; a) there can be insufficient time for strain induced precipitation, b) the amount of grain boundary sliding is reduced, c) the amount of time for diffusion controlled growth of voids at the boundaries is reduced, d) recent work³⁹ suggests that increasing the strain rate may favour the growth of deformation induced ferrite and so increase the volume fraction of ferrite to that required to give good ductility.

Thermal treatment

Thermal treatment has a major influence on the hot ductility and hence it is very important to make the experimental conditions as close to commercial practice as possible. A typical cooling cycle during continuous casting is shown in Figure 2.19. It can be seen that initially the cooling rate is very rapid as the water sprays hit the strand surface. The surface then heats up and a series of small temperature oscillations occur by the alternate impingement of water sprays and guide rolls on the slab surface.

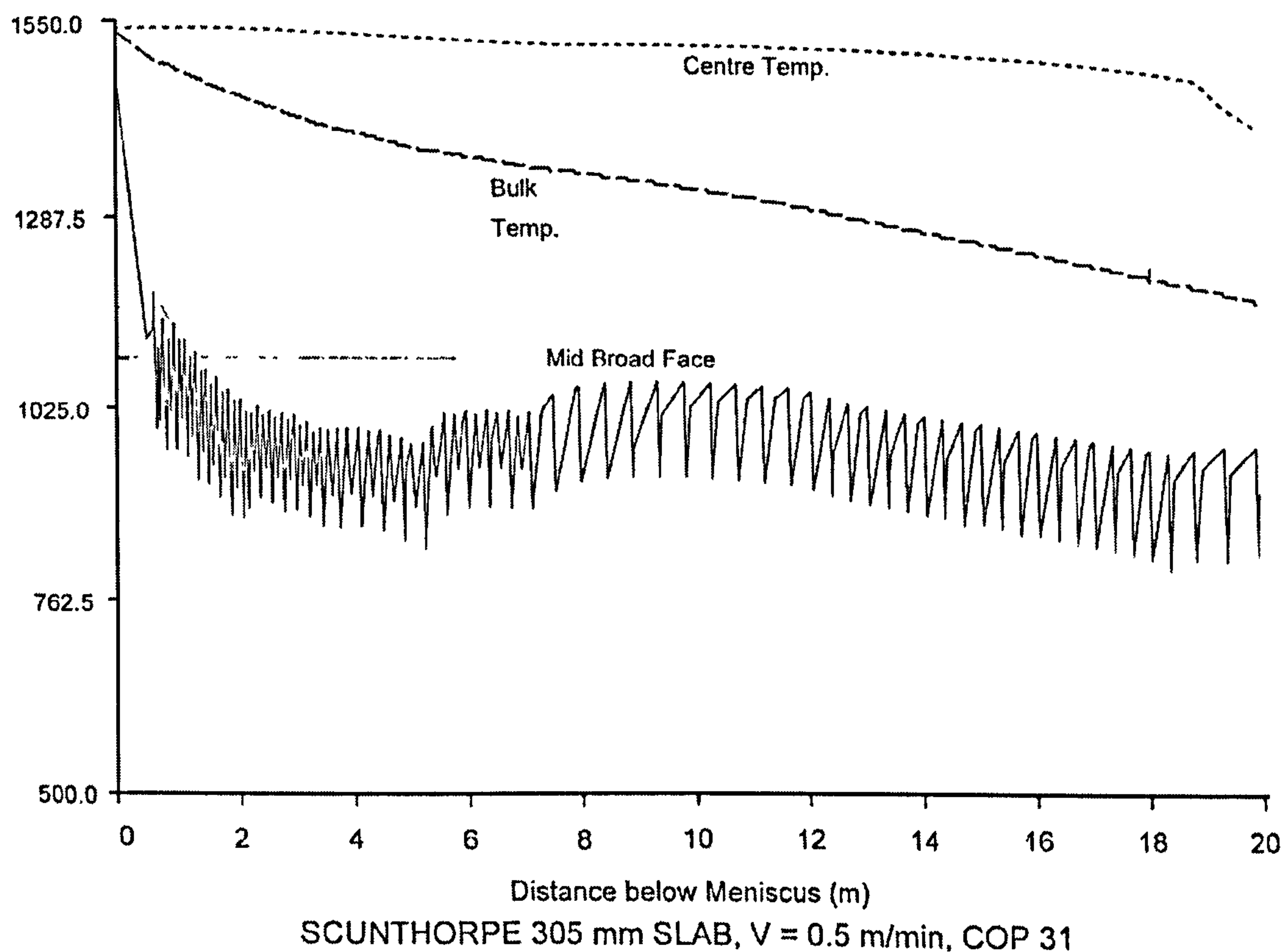


Figure 2.19: A typical temperature profile observed at a Scunthorpe continuous caster.

This undercooling has been found to deteriorate ductility due to enhanced precipitation and this occurs both for C-Mn-Nb and C-Mn-Al steels.^{34,70} Generally, there is limited scope for altering the cooling conditions during continuous casting. Ideally, coarse precipitation is favoured and this can be achieved by slow cooling rates, holding at high temperatures and possibly pre-deformation whilst the core is still liquid.

Influence of cooling rate

Previous work^{27,71} on C-Mn-Al and C-Mn-Nb-Al steels has shown that increasing the cooling rate always results in decreased ductility, although sometimes the differences were very small. Generally, increasing the cooling rate results in a finer precipitate and inclusion size and dispersion (and also worse ductility) as shown in Figure 2.20 (a) and (b). The effect

⁷⁰ B. Mintz, J.M. Stewart and D.N. Crowther: Trans. ISIJ, 1987, 27, p. 959.

of an increased cooling rate is very important in thin slab casting, Figure 2.20 (c) illustrates the deterioration in hot ductility observed in a Ti containing steel on increasing the cooling rate. The higher cooling rate produces finer precipitates and inclusion distributions, both of which encourage crack propagation along the austenite grain boundaries.

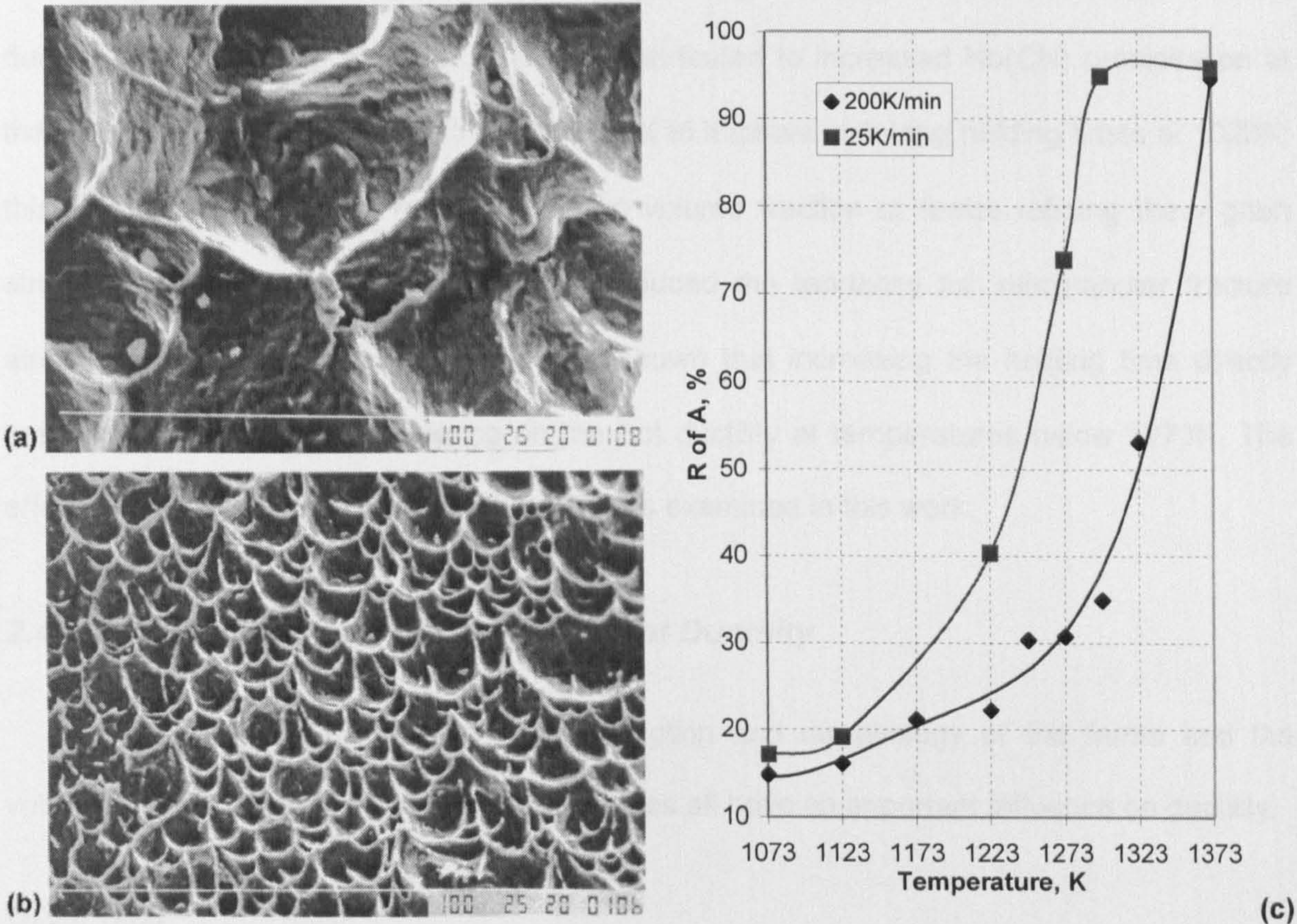


Figure 2.20: Fracture surfaces of a low Al steel tested at 1073K showing refinement of dimples and particles as cooling rate increases from (a) 25 Kmin⁻¹ to (b), 100 Kmin⁻¹. With the increase in cooling rate there is a corresponding drop in R of A from 52% to 24%.⁷² The influence of cooling rate on hot ductility for a C-Mn-Al steel with Ti addition and Ti:N ratio of 3.4:1 is shown in (c), data taken from ref. 72.

⁷¹ R. Abushosha, S. Ayyad and B. Mintz: Mat. Sci. and Technol., 1998, 14, pp. 227-235.

⁷² R. Abushosha, O. Cominelli and B. Mintz: Mat. Sci. and Technol., 1999, 15, pp. 278-286.

Holding Time

The hot ductility of a 0.054% Nb steel has been studied by Ouchi et al.,⁷³ where it was found that holding time can have a varied effect depending on the test temperature. Increasing the holding time in the temperature range 1073 to 1173K resulted in reduced ductility after reheating to 1273K. This was attributed to increased Nb(CN) precipitation at the γ grain boundaries. The ductility was found to improve with long holding times at 1023K; this was found to be due to the increased volume fraction of ferrite refining the γ grain structure after reheating to 1273K. This reduced the tendency for intergranular fracture along the γ grain boundaries. It was also shown that increasing the holding time directly before straining had little influence on the hot ductility at temperatures below 1273K. The effect of holding time on hot ductility will not be examined in this work.

2.4.2 Influence of Microstructure on Hot Ductility

The austenite grain size, volume fraction and morphology of the ferrite and the volume fraction, size and distribution of particles all have an important influence on ductility.

Grain Size

Finer γ grain size always leads to better ductility; the main reason for this being the decrease in the crack aspect ratio, which controls stress concentration at the crack tip. The effect of increasing grain size on hot ductility is illustrated in Figure 2.21. The benefit to ductility from refining the grain size is similar to case where the structure is either fully austenitic or contains the thin bands of ferrite surrounding the austenite grains.⁷⁴

⁷³ C. Ouchi and K. Matsumoto: Trans ISIJ, 1982, 22, p. 181.

⁷⁴ D.N. Crowther and B. Mintz: Mat. Sci. and Technol., 1986, 2, p. 951-955.

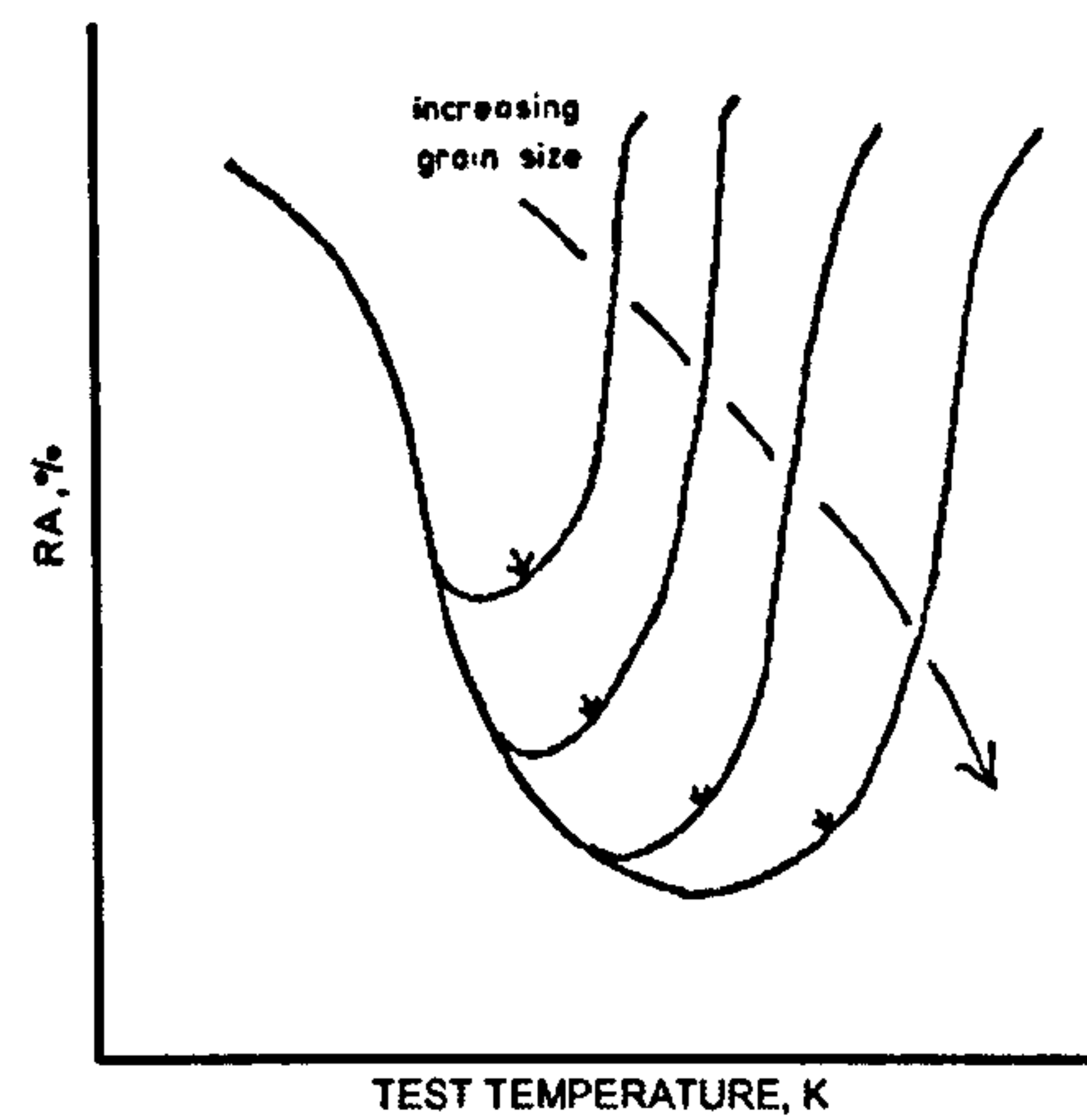


Figure 2.21: Effect of grain size on % R of A.⁷⁵

Form of Ferrite

The distribution of ferrite giving the worst ductility is when it forms thin bands surrounding the austenite grains which seems to be favoured by a coarse austenite grain size. Generally, since ferrite is softer than austenite, most of the strain concentrates there and, even though the local ductility is good, the overall ductility is low. Most importantly, this thin band of ferrite is encouraged to form on deformation and can form well above the A_{r3} , often to temperatures as high as the A_{e3} ; hence troughs can be very wide, $>100K$.

Below the A_{r3} , the amount of ferrite present increases rapidly and the band widens and the strain is then taken by a larger volume fraction of the material. There will always be a trough in steels, but the width of the trough will depend on how easy it is to thicken the ferrite film. Nevertheless in some steels, notably low C and Mn, the deformation induced ferrite has been found to form in large quantities just below the A_{e3} ; there is an indication that because deformation induced ferrite is diffusion controlled, higher A_{e3} temperatures will favour its production.¹¹

⁷⁵ B. Mintz and Z. Mohamed: Mat. Sci. and Technol., 1989, 5, pp. 1212-1219.

Precipitation

Unless the volume fraction of precipitates is very low and/or the size is sufficiently coarse, ductility is impaired. In the case of grain boundary sliding in the γ , fine precipitation pins the boundaries and it becomes much easier for cracks to join up; fine precipitation at the boundaries has the most detrimental effect on hot ductility. Nevertheless, fine precipitation in the matrix, as in Nb containing steels, by strengthening the matrix, increases the shear stress on the grain boundaries and also encourages sliding and crack propagation. Again precipitation is encouraged by deformation, the dislocation sites producing favourable nucleation sites for precipitation; both Nb(CN) and VN precipitate rapidly during the hot ductility test. The temperatures giving maximum rates of precipitation for Nb(CN), VN and AlN precipitation are 1223,^{76,77} 1158⁷⁸ and 1088K,⁷⁹ respectively.

Nb(CN) is particularly detrimental, precipitating within the matrix and at the γ grain boundaries in a fine form, and the boundaries are often associated with precipitate free zones. VN is less deleterious, as precipitation is coarser, in the V containing steels as a result of the higher solubility of V in the γ compared to Nb.

AlN precipitates very sluggishly and in normal solution treated hot tensile tests only precipitates out in high Mn steels (1.4% Mn) when the product of $[\text{sol.Al}]x[\text{N}]$ approaches 2×10^{-4} (e.g. 0.04% Al and 0.005 %N).⁸⁰ However, when temperature oscillations are introduced, AlN precipitates out at as low a product as 1×10^{-4} . Similar behaviour is noted for as-cast C-Mn-Al steels given a conventional cooling programme with no temperature cycling

⁷⁶ A. leBon, J. Rofes-Vernis and C. Rossard: Met. Sci. J., 1975, 9, p. 36.

⁷⁷ I. Weiss and J.J. Jonas: Metall. Trans., 1979, 10A, p. 831.

⁷⁸ M.G. Abken, I. Weiss and J.J Jonas: Acta Metall., 1981, 29, p. 111.

⁷⁹ W.C. Leslie, R.L. Rickett, C.L. Dotson and C.S. Walton: Trans. ASM, 1954, 46, p. 1470.

⁸⁰ D.N. Crowther, Z. Mohamed and B. Mintz: Metall. Trans., 1987, 18A, p. 1929.

due to the marked segregation of Al to the boundaries when solidification occurs (The concentration of Al at the boundaries can be increased by a factor of 6). Al additions have also been found to have a detrimental influence on the ductility of Nb containing steels by producing a finer precipitation of Nb(CN) rather than through AlN precipitation.¹²

The influence of TiN is complex; commercially Ti has been found to be a good element to add to reduce transverse cracking and improve surface quality. In the laboratory work, Ti additions have always been found to be detrimental to ductility due to the formation of very fine Ti rich particles. However commercially, coarse TiN precipitates are normally observed indicating possibly that the segregation to the grain boundaries is much more intense in commercial casts than in the as-cast small tensile samples.

2.4.3 Influence of Chemical Composition on Hot Ductility

The properties of steel can be massively altered by the addition of one or more different alloying elements. The first alloy steel was a high-manganese produced by Hadfield in 1882, the first high-speed steel by Taylor and White (USA) in 1900 and the first stainless steel by Brearley in 1913.⁸¹ Although many steels have large additions of the alloying element i.e. stainless steel, some elements only need to be present in tiny amounts to have a profound effect on the final properties of the steel and these steels are known as micro-alloyed. The following sections will discuss the effect on hot ductility of the elements which are importance in the present study.

Effect of Aluminium (Al)

Aluminium and, to a lesser extent, vanadium, niobium and titanium are used to control the austenitic grain size. Aluminium can also be added to remove dissolved oxygen from the melt. In the case of hot ductility, as already noted, AlN is detrimental to ductility.

⁸¹ R.A. Higgins: Properties of Engineering Materials, 2nd Rev. Ed, 1994, Publ. Edward Arnold, ISBN 0-340-60033-0.

Generally it is found commercially, that provided the soluble Al level does not exceed 0.04% in a steel with 0.005% N, there are no transverse cracking problems.

Effect of Boron (B)

Boron is a very powerful hardenability agent, and is 250 to 750 times as effective as nickel, 75 to 125 times as effective as molybdenum, and around 100 times as powerful as chromium. In order to obtain the desired effect in low-carbon steels, additions of only a few thousandths of a percent is required; however, the benefits are rapidly diminished with increasing carbon content. As no carbide formation or ferrite strengthening is produced, improved machinability and cold-forming capability often result from the use of boron in place of other hardenability additions.⁸² The influence of B on hot ductility is not clear.

Effect of Carbon (C)

For simple C-Mn-Al steels, the trough spans the temperature range from the A_{e3} to the A_{r3} . Thus in raising the C level, the trough is moved to the left in accord with the lower γ - α transformation. It should be noted that for very low C levels (0.04% C) the trough may be virtually eliminated as the high A_{e3} temperature ensures production of a large volume fraction of deformation induced ferrite just below the A_{e3} .⁸³ Steels with C levels above 0.25% give rise to very wide troughs due possibly to the prevention of DRX and increased grain boundary sliding. In Nb containing steels, C has little influence on the position of the trough due to the overriding influence of Nb(CN) precipitation in the austenite.

Steels with carbon in the peritectic range (0.1 - 0.15%) are particularly susceptible to transverse cracking. This is because coarse columnar grains are produced. The growth of such γ grains are impeded by having second phase particles, either to the left (the delta

⁸² E.P. DeGarmo, J. Temple Black and R.A. Kohser: Materials and Processes in Manufacturing, 7th ed, 1990, Macmillan Publ. Co., ISBN 0-02-946140-5.

⁸³ Private communication, B. Mintz, 2003.

phase, δ) or right (liquid phase) of the peritectic. A further reason for poor ductility is that during the peritectic transformation, from δ -ferrite to austenite, there is an accompanying contraction. This produces a gap between the shell and the mould wall resulting in a reduction of heat extraction by the mould. The thinner parts of the unevenly solidified shell are then more susceptible to breakage.²

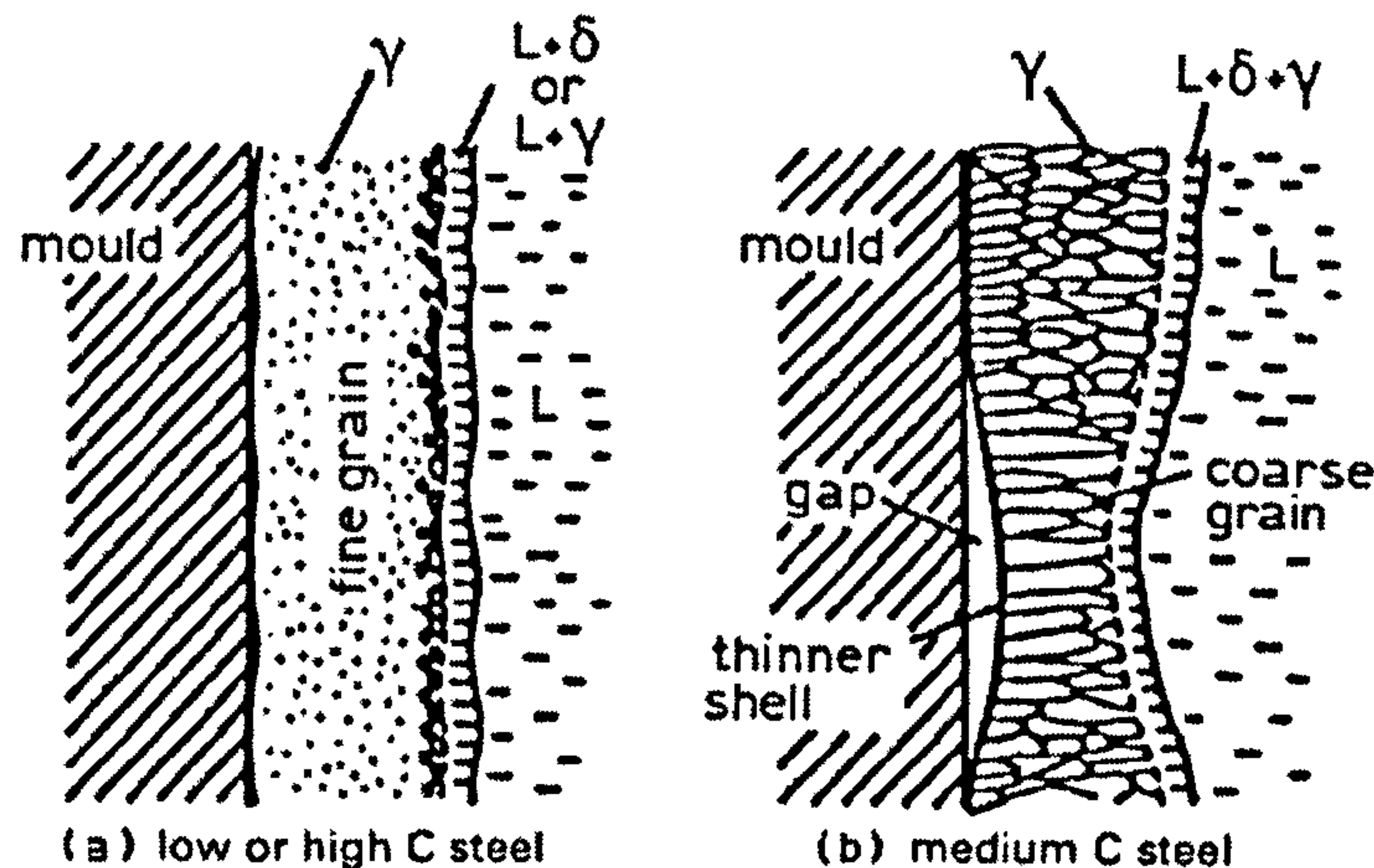


Figure 2.22: Schematic illustration showing austenite structure in the solidified shell.⁸⁴

Effect of Calcium (Ca)

Zirconium, caesium, and calcium control the shape of inclusions and thus promote toughness. By adding Ca, the S level is reduced so that the volume fraction of sulphide inclusions is decreased thus improving ductility.⁵

Effect of Copper (Cu)

Copper has been known to resist atmospheric corrosion for centuries, but has only recently been used as an addition to steel (in amounts from 0.10% to 0.50%) to provide this property. Low-carbon sheet steel and structural steels often contain a copper addition to enhance corrosion resistance, but this can result in deterioration in surface quality and hot-working behaviour.⁸²

⁸⁴ Y. Maehara, K. Yasumoto, Y. Sugitani and K. Gunji: Trans. ISIJ, 1985, 25, p. 1045.

As a residual, Cu has been shown to be detrimental to ductility,⁶⁹ due to fine copper sulphide (or oxysulphide) particles at the boundaries, which had formed on cooling as a result of oxidation and the presence of Cu according to the reaction:



Nickel in contrast, in combination with Cu improves ductility. By increasing the solubility of Cu in iron, Ni additions might be responsible for a reduced driving force for Cu precipitation; a Ni:Cu ratio of 2:1 is recommended. Sulphur levels are also advised to be kept low.

Effect of Chromium (Cr)

Although large percentages of chromium can impart corrosion resistance and heat resistance, in the amounts used in low-alloy steels these effects are minor. In these alloys, chromium serves primarily to increase hardenability and to increase strength, and an addition of less than 2% is generally employed. In many alloys, chromium and nickel are used together in a ratio of about one part chromium to two parts nickel. Combined with carbon, chromium carbides provide superior wear resistance.

There is again little information on the influence of small additions of Cr on the hot ductility of steel. Russian analysis⁸⁵ of works data suggests that a Cr level of 0.3% gives good ductility, but no explanation is given for this behaviour. High additions of Cr ($\geq 11\%$) result in the formation of ferritic or austenitic stainless steels, and information on these steels forms one of the chapters in this present thesis.

⁸⁵ S.D. Razumov, V.V. Zabitski, V.I. Umanets, V.I. Lebedev and V.A. Oburhov: Steel in the USSR, 1986, 16, pp. 225-228.

Effect of Molybdenum (Mo)

Molybdenum is used in alloy steels in amounts less than 0.3% to improve hardenability and increase strength properties, particularly at dynamic and high temperature conditions. Resistance to temper embrittlement is also attributed to the presence of molybdenum. Molybdenum carbides are extremely stable at elevated temperatures and are used in alloys to retain fine grain size and to provide strength and creep resistance at elevated temperature. Molybdenum carbides are also used in hot-work tool steels, such as those used in forging dies, to impart hardness that will persist at red heat.

There is little information as to the effect of Mo on the hot ductility of steels, but a normal Mo addition (0.2%)⁸⁶ has been found to result in improved ductility in an Nb containing steel. This may again be related, as with P, to segregation taking up vacant sites which Nb(CN) might otherwise have occupied.

Effect of Nitrogen (N)

Nitrogen is very detrimental to hot ductility as it forms fine nitrides with Al and many of the micro-alloying additions, although in itself it has little influence on hot ductility of high Mn steels (1.4% Mn).⁸⁷ It should therefore always be kept as low as possible. V containing steels generally give better hot ductility than Nb based steels; the product of [V][N] had to be as high as 1.2×10^{-3} (corresponding to 0.1% V and 0.012% N) to approach the low values of R of A exhibited by a 0.03% Nb, 0.005% N steel. Although V containing steels may show reduced tendency to exhibit transverse cracks compared, where ~0.005% N is present, the effect of N per se may be more serious in these steels as the detrimental precipitate is entirely N₂ based, i.e. VN, whereas for Nb it is generally a mixed carbonitride, Nb(CN), with carbon being the major constituent.

⁸⁶ R.E. Mercer and N.A. McPherson: AIME Steelmaking Conf. Proc., 1979, 62, p. 215.

⁸⁷ N.E. Hannerz: Trans. ISIJ, 1985, 25, p. 149.

However, the role of N in Nb steels may be more important than indicated from the foregoing paragraph. It should be noted that at constant Nb level (0.015%), it has been found that an increase in the N concentration from 0.002 to 0.006% markedly reduces the plasticity.⁷³ Low N levels promote the formation of $\text{NbC}_{0.85}$ particles, whereas high N concentration lead to the precipitation of $\text{NbC}_{0.6}\text{N}_{0.25}$. The higher ductility associated with NbC has been ascribed to its lower rate of precipitation in the austenite.

Effect of Niobium (Nb)

Niobium can be used for ferrite grain-size control as well as precipitation strengthening; its deleterious effect on hot ductility has been discussed previously in section 2.4.2 in relation to precipitation.

Effect of Nickel (Ni)

Nickel is commonly added to increase toughness and impact resistance primarily at low temperature. It is generally used in amounts from 2% to 5%, often in combination with other alloying elements. Alloys with 12% to 20% nickel and low amounts of carbon possess outstanding corrosion resistance. An iron and 36% nickel alloy, commonly known as Invar has a near-zero thermal expansion coefficient and is used for sensitive measuring devices.

As previously mentioned, nickel in combination with copper can improve ductility in solution treated and as-cast C-Mn-Al-Nb and C-Mn-Al specimens when an oxidising atmosphere is present. Burden *et al.*⁸⁸ have shown that very severe residual enrichment and grain boundary embrittlement can occur rapidly during commercial continuous casting due to the enhanced oxidation that is experienced. This can be caused by the water cooling sprays and reheating that occurs when the strand passes through the rolls. Therefore, laboratory testing may underestimate the influence of copper on hot ductility.

⁸⁸ M.H. Burden, G.D. Funnell, A.G. Whitaker and J.M. Young: in 'Solidification and casting of metals', pp. 229-236; 1979, London, The Metals Society.

The beneficial effect of a Ni addition can be used to exactly balance the detrimental effect of Cu. Mintz *et al.*⁶⁹ found that Ni additions sufficient to maintain a Cu/Ni ratio of 1:1 were effective in improving ductility; this work recommended that when Cu is added to continuously cast steel, Ni should be added in at least an equal quantity.

Effect of Phosphorus (P)

Phosphorus has been found to be detrimental to the hot ductility of steel if marked segregation occurs.⁸⁹ This leads to the formation of the low melting point Fe(Mn) phosphide phase which produces liquid films at the boundaries giving very low ductility. However, for P to cause problems the strain rate has to be higher than used in conventional continuous casting to prevent back diffusion of P from the grain boundaries to the matrix; the carbon level also needs to be greater than 0.25% to have sufficient segregation. Previous work by Mintz *et al.*¹² has found levels of up to 0.02% P to be beneficial for C-Mn-Nb-Al steels, and although P is normally considered to be detrimental, it is suggested that P takes up vacant sites at the boundaries where the more detrimental fine Nb(CN) precipitation would otherwise occur. Work by a number of other authors have also found P to be similarly beneficial to hot ductility.^{87,90,91,92}

At normal levels of P ($\leq 0.025\%$) and C levels $< 0.25\%$, the greater the P level up to 0.025%, the better the ductility and provided segregation is not too marked, the less susceptible the continuously cast slabs are to transverse cracking during straightening.¹¹

⁸⁹ S. Harada, S. Tanaka, H. Misumi, S. Mizoguchi and H. Horiguchi: ISIJ Int., 1990, 30, p. 310.

⁹⁰ H.G. Suzuki, S. Nishimura, J. Imanura and Y. Nakamura: Trans. ISIJ, 1984, 24, pp. 169-177.

⁹¹ E.P. George, R.L. Kennedy and D.P. Pope: Phys. Status Solids (a), 1998, 167, pp. 313-333.

⁹² K. Abiko: Phys. Status Solids (a), 1997, 160, pp. 285-296.

Effect of Sulphur (S), Manganese (Mn) and the Mn:S Ratio

Analysis of works data by Hannerz⁸⁷ showed that raising the S level invariably leads to reduced ductility and therefore an increase in transverse cracking. Reducing the S level in as-cast steel improves ductility and as previously mentioned the addition of Ca has also been found to be particularly beneficial.^{5,35,93,94} These findings are as expected, as intergranular failure is favoured by sulphides present at the boundaries and, when there are microalloying precipitates present, wide and deep hot ductility troughs are common.¹¹

Although reducing the S level will generally improve ductility, there is evidence to indicate that with Nb containing steels too low a S level (0.001%) may also cause cracking.⁹⁵ Thus, a Calcium addition may not always reduce the incidence of cracking. This may be because particles are required for nucleation of Nb(CN) at high temperatures so that there is less Nb available for precipitation in a fine form, which is detrimental to hot ductility, during straightening. The hot ductility of as-cast Nb containing steels is often much better than after solution treatment as a large percentage of Nb has been removed as the coarse eutectic. Whereas, after solution treating all the Nb is in solution and available for precipitating out in a fine detrimental form during deformation.¹¹

Manganese is added to most plain-carbon steels to combine with sulphur and produce soft manganese sulphides. This addition prevents formation of the low melting point iron sulphide, which coats grain boundaries and imparts brittleness to the metal. In alloy steels, manganese increases hardenability, slightly strengthens ferrite and lowers the martensite transformation temperatures; it is often added in amounts greater than 1.0%. In HSLA steels, 1.4% Mn results in the optimum strength and toughness. More than 1.4% Mn causes martensite to form and consequently the toughness deteriorates. When manganese

⁹³ T. Revaux, J.P. Bricout and J. Oudin: J. Mat. Eng. And Performance, 1996, 5, pp. 260-268.

⁹⁴ L.P. Karjalainen, H. Kinnunen and D. Porter: Microalloying in Steels. Ed. By J.M. Rodriguez-Ibabe, I. Gutierrez and B. Lopez, Trans. Tech. Publ., Switzerland, 1998, pp. 477-483.

⁹⁵ Private communication to B. Mintz, V. Ludlow, Corus, Teeside Technology Centre, 1998.

is added in large percentages (11% to 14%), an austenitic alloy is produced; high hardness, good ductility, high strain-hardening capacity, and excellent wear resistance make it ideal for impact-resisting tools and similar applications.⁸²

As previously mentioned, sulphur is usually not desired in steel because of the embrittling effect of the low melting point iron sulphide. In the form of manganese sulphide, however, sulphur is not harmful, provided that the sulphides are not large in quantity and are well dispersed. If manganese sulphide is present in large quantities and in the proper form, it can impart desirable machining properties. If there is a sufficiently high volume fraction of MnS present in an elongated form, a return to good ductility at the low temperature end of the trough has been observed in laboratory tests;⁷¹ although this is not an answer to the commercial problem of transverse cracking during the straightening operation. Studies of the effect of S and Mn:S ratio have been carried out by Wilber *et. al.*⁹⁶ Some free-machining steels have 0.08% to 0.1507 sulphur in combination with an increased manganese content. There is some doubt as to whether S reduces ductility by segregation to the boundaries on solidification or by the formation of small sulphides. Certainly fine sulphides are associated with poor ductility and these are produced on faster cooling.⁷¹

Effect of Silicon (Si)

In small percentages, silicon has an effect similar to that of nickel, increasing the strength properties with little companion loss of ductility. It is an important alloying element in certain high-yield-strength structural steels. It is also used in spring steels (in amounts of about 2%) and promotes the desirable large grain size in steels used for magnetic applications. Recent work⁹⁷ has shown that increasing the Si level by 1% moves the hot ductility curve by ~50K to higher temperatures in accordance with the increase in the A_{e3} temperature. However, for normal Si levels (0.2 - 3.0% Si) the effect is likely to be small.

⁹⁶ G.A.Wilber, R.Batra, W.F.Savage and W.J.Childs:Metall. Trans., 1975, 6A, p.1727.

⁹⁷ Private communication, B. Mintz, 2003.

3. Experimental Method

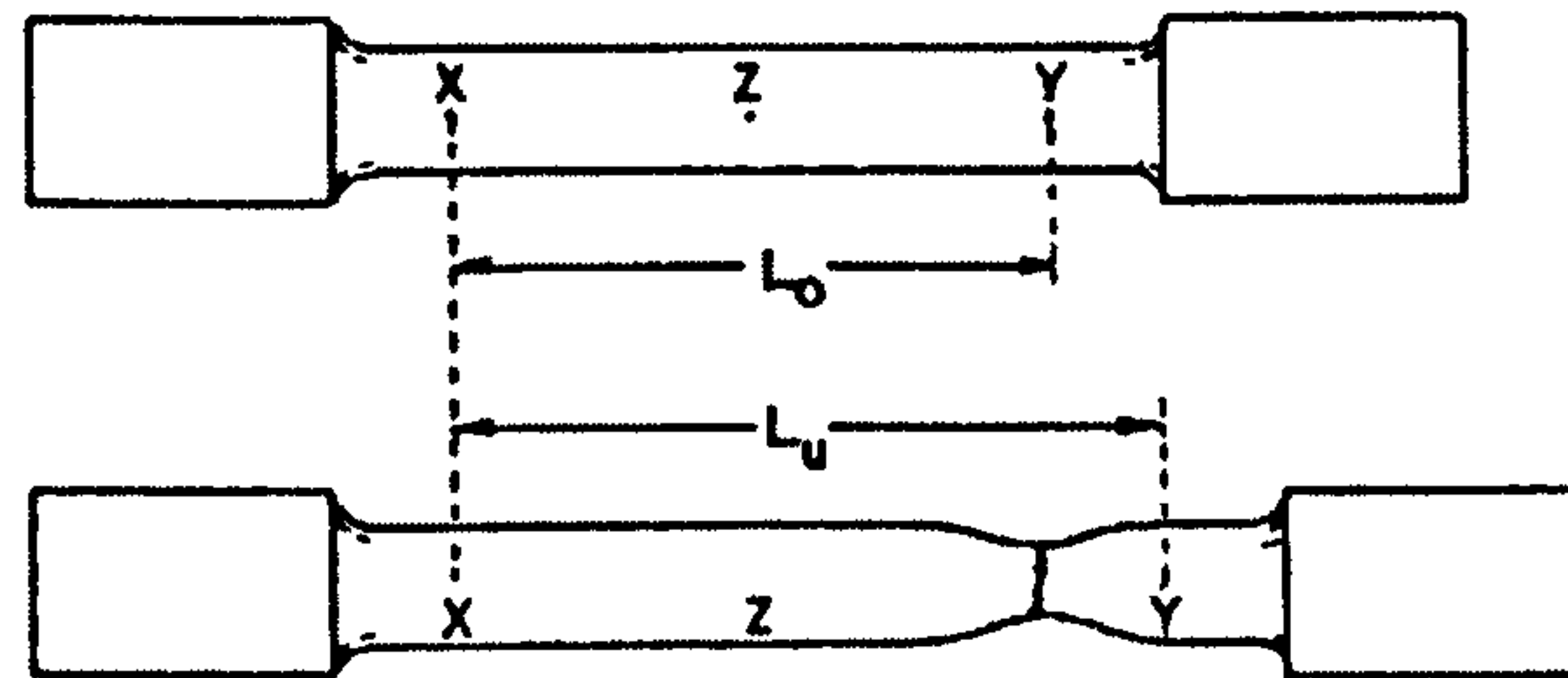
Many different methods have been used to determine the ductility of steels under hot working conditions, particularly the susceptibility to transverse cracking during the straightening operation. The only tests capable of providing quantitative data on the fracture behaviour are the tensile, torsion, and impact tests. The latter two testing methods have larger strains and strain rates than are experienced during the straightening operation and are therefore more suited to simulating the hot rolling processing.

The results obtained from the hot tensile test, using reduction of area values as a measure of ductility, have been found to correlate remarkably well with production experience at the straightener, where strain rates are in the range 10^{-3} to 10^{-4}s^{-1} . In the present study, only the hot tensile test using constant crosshead speeds are used. Two different methods of measuring the hot ductility were employed, and are described in sections 3.1.2 and 3.1.3.

3.1 Measurement of Hot Ductility

The ductility of samples tested using the hot tensile test can be measured from a) the amount of uniform elongation, b) the total elongation at fracture or c) the reduction of area at the point of fracture. In case a), this measurement is only useful if little or no necking has occurred, as sometimes happens with brittle intergranular fractures. This parameter is not suitable for use in the present study, as the ductility is known to vary widely over the test temperatures chosen. In case b), the total elongation is a measure of both the uniform elongation and the elongation due to necking at the point of fracture. The values of these two components are a complex function of test temperature, strain rate, composition and microstructure.¹⁸ Therefore, it is possible to obtain identical total elongation measurements from samples that have been tested at different temperatures and having very different

fracture geometries. Since a significant proportion of the plastic deformation will be concentrated in the necked region around the fracture, the percentage elongation between Z and Y will be greater than that between X and Y, as shown in Figure 3.1.



$$Elongation\% = \frac{(L_u - L_0)}{L_0} \times 100$$

Figure 3.1: Illustration of difficulty measuring total uniform elongation when necking occurs.⁸¹

Consequently, a quantitative measurement of the fracture strain at the point of failure is required; the Reduction of Area (R of A) measurement does not suffer from this difficulty and is unaffected by the actual fracture geometries. It has proven to be a very useful measure of the hot ductility, and has been used extensively. The reduction of area measurement is suitable for comparing the hot-ductility over a wide range of temperatures and is the parameter and that will be used in this study. The relationship between the fracture strain and the reduction in area at the fracture tip can be written as:

$$\varepsilon_f = \ln\left(\frac{A_0}{A_1}\right) \quad (3.1)$$

Where, ε_f is the fracture strain, A_0 the initial cross-sectional area, and A_1 the final cross-sectional area.

3.1.1 Measurement of Reduction of Area (R of A)

The R of A values were obtained from the fractured samples using a Vickers shadowgraph machine at a magnification of 12.5. The R of A was calculated for each fractured sample using measurements of the initial (D_i) and final diameters (D_f). The initial diameter, D_i , was measured using an accurate micrometer, as the machined sample is cylindrical. As the fracture surface was irregular, D_f was measured using the shadowgraph machine, and taking the average measurement of four diameters at 45° intervals of rotation for each half of the broken tensile. The final diameter, D_f , was therefore the average of eight measurements. The reduction of area (R of A) can then be calculated by using the following formula:

$$R\ of\ A = \frac{D_i^2 - D_f^2}{D_i^2 - D_i^2} \quad (3.2)$$

Where, D_t is the diameter of the hole drilled along the central axis to the midpoint of the induction samples for inserting a thermocouple; in this study, this diameter is 2mm and D_t^2 therefore equals 4mm². As the Instron samples have an external thermocouple attached to them, D_t^2 in this case is equal to zero.

After the R of A had been measured, one half of each sample was mounted in hot cured polymer resin, polished to one micron and then etched using 2% Nital for optical analysis. Carbon extraction replicas were made by deposition of C in a vacuum chamber. The fracture surface of the other half of the sample was studied using the scanning electron microscope (SEM). In order to assess the consistency of this method, repeated tests and sample measurements were carried out; the R of A results obtained were found to vary by no more than ±3% for the solution treated samples and ±5% for the as-cast samples.

3.1.2 The Induction test

In this study, two sets of test apparatus were used to measure hot ductility; the first of these is the induction set-up. The samples were tested in a converted Hounsfield tensometer, to which an induction coil had been fitted to melt the samples. The melting zone was approximately 22mm in length, situated at the mid-length position of the sample. The tensile samples were machined parallel to the rolling or forging direction and a 2mm diameter hole was drilled up to the middle of the sample so that the thermocouple could be inserted. The sample was fitted between the two grips with a silica tube having an initial 0.2mm clearance surrounding the mid-section to retain the steel when molten; it was protected from oxidation by surrounding it and the grips with 'T'-shaped silica tube through which argon was passed. The sample specifications are shown in Figure 3.2.

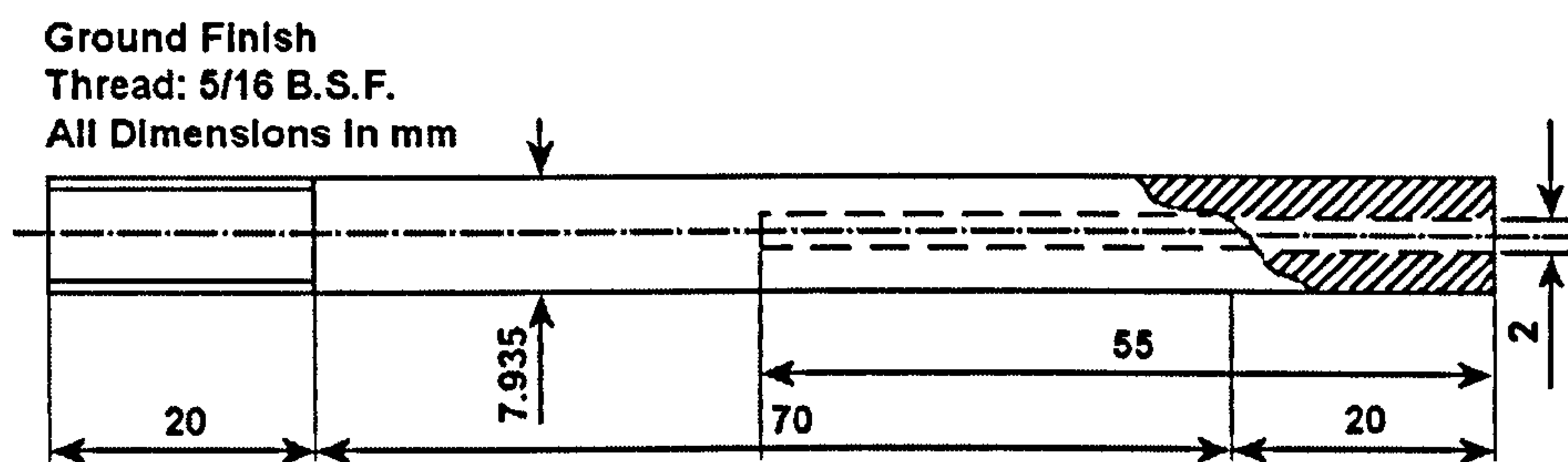


Figure 3.2: Schematic drawing of induction test specimen.

Prior to this study, the configuration of the Induction setup was of a more simple nature; the induction controller only allowed manual control of the temperature, which was measured using a platinum/platinum-13% rhodium thermocouple connected to a digital multimeter. The voltage measured with this multimeter then needed converting into temperature using a conversion chart and adjusting the values for the room temperature (generally taken as 293K). Work was undertaken by the author to upgrade this system to the current configuration as shown in Figure 3.3.

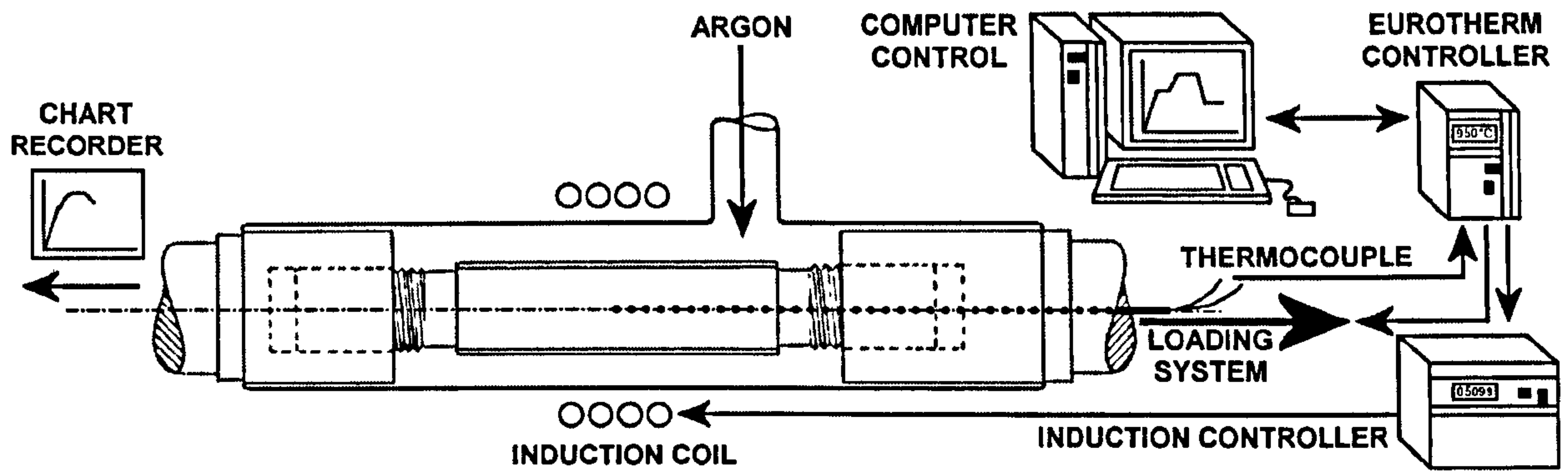


Figure 3.3: Schematic drawing of the induction hot-tensile apparatus.

A Eurotherm 2408 programmable controller was purchased to control a new induction unit, which allowed a remote device to control its output. The thermocouple was connected to the Eurotherm controller to provide the necessary feedback on temperature. The loading system was also upgraded to a 0.55kW A/C motor with digital controller linked to the Eurotherm controller for accurate control of its operation and therefore crosshead speed. The crosshead speed (mm s^{-1}) was calibrated against motor supply frequency (Hz), so that a specified strain rate could be applied to the sample, see Figure 3.4; i.e. a strain rate of $3 \times 10^{-3} \text{ s}^{-1}$ is obtained at 5.3Hz, using the gear ratio of 4:1 with a 22mm gauge length.

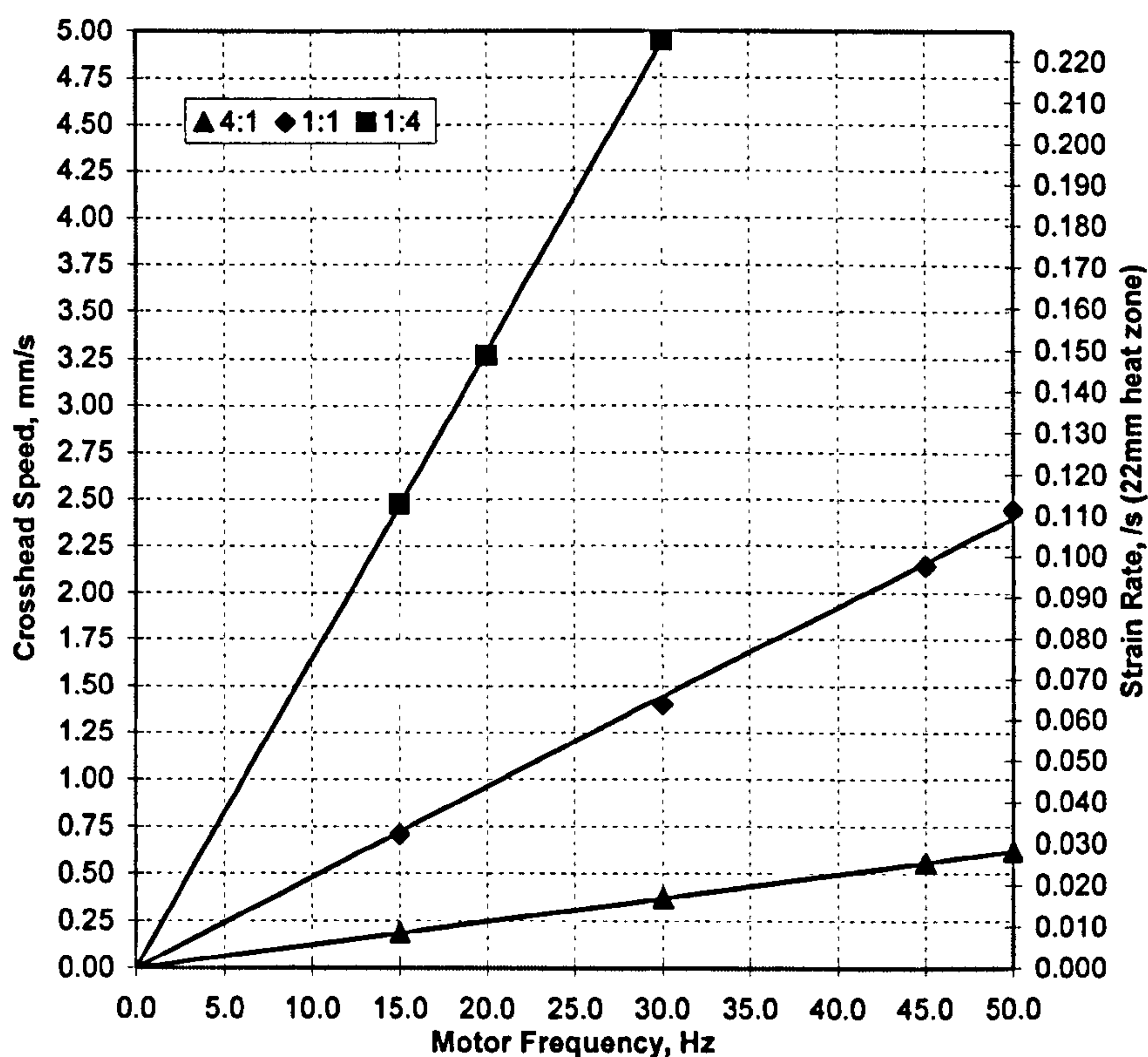


Figure 3.4: Calibration chart developed to select motor frequency required to give specified strain rate.

A software package supplied by Eurotherm was installed on a computer connected to the controller; this could control both the induction unit and the motor, download and upload heating/cooling cycles and also log the temperature measured during each test. Using these pre-recorded heating/cooling schedules, the control computer could melt, cool to test temperature and strain the samples to failure.

The temperature gradient along the central axis of the test specimen was examined by withdrawing the thermocouple from the centre in steps of 5mm and allowing the temperature to settle; a chart showing these results at different temperatures is shown in Figure 3.5. It can be seen that the temperature is relatively constant up to 5mm from the centre point and then starts to fall away more rapidly. On the basis of these tests, although the melted region of the sample is 22mm, the gauge length could be considered to be half this value. Therefore, only samples which failed within 5 to 6mm from the centre of the melt region were taken as being acceptable.

Due to the difficulty in knowing exactly where the strain is taken up in relation to the melt-zone, 22mm was taken as an arbitrary choice for use in strain rate calculations as R of A is not overly susceptible to this change; furthermore, consistency was maintained with previous work undertaken by the research group. Some tests, particularly those at the lower temperatures, needed repeating as fracture occurred outside this region. A solution to this problem would be to widen the induction coil, increasing the distance from the centre that the temperature remains near to the required test temperature.

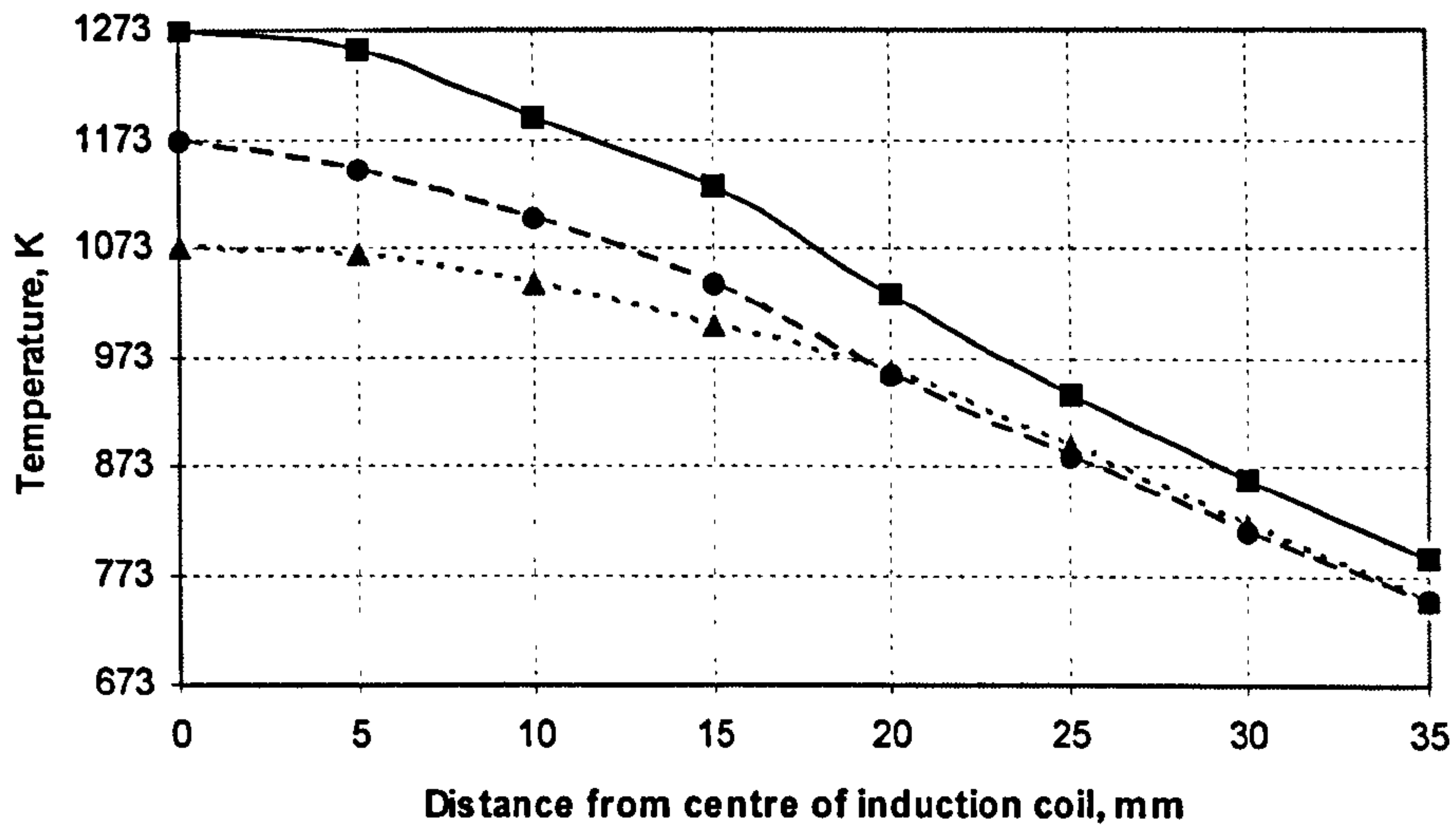


Figure 3.5: Temperature gradient along the central axis of sample heated to a constant temperature within the induction coil.

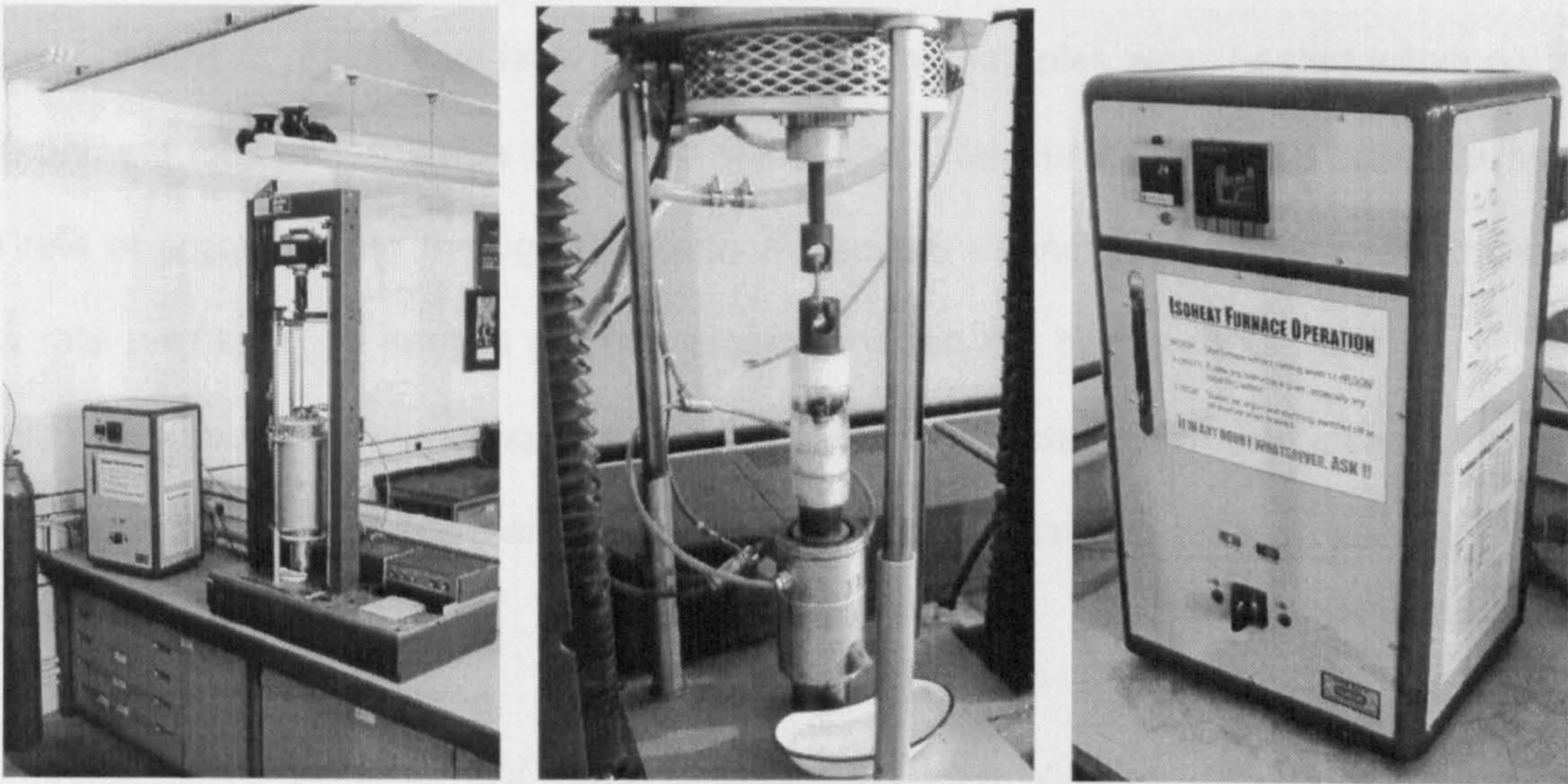
The samples were melted and held at 1815K for five minutes, cooled at either 200, 60 or 25Kmin⁻¹ to the required test temperature in the range 1273 - 973K, where they were held for a further five minutes before straining to failure. A nominal strain rate of 3x10⁻³s⁻¹ was used, which was calculated by dividing the crosshead speed by the gauge length of 22mm. During tensile testing, the chart recorder was used to produce a load versus elongation graph, which could also be used to identify whether dynamic recrystallisation had occurred. After failure, the microstructure of the fractured samples was "frozen in" by rapidly cooling by increasing the flow rate of Argon.

3.1.3 The Instron Test

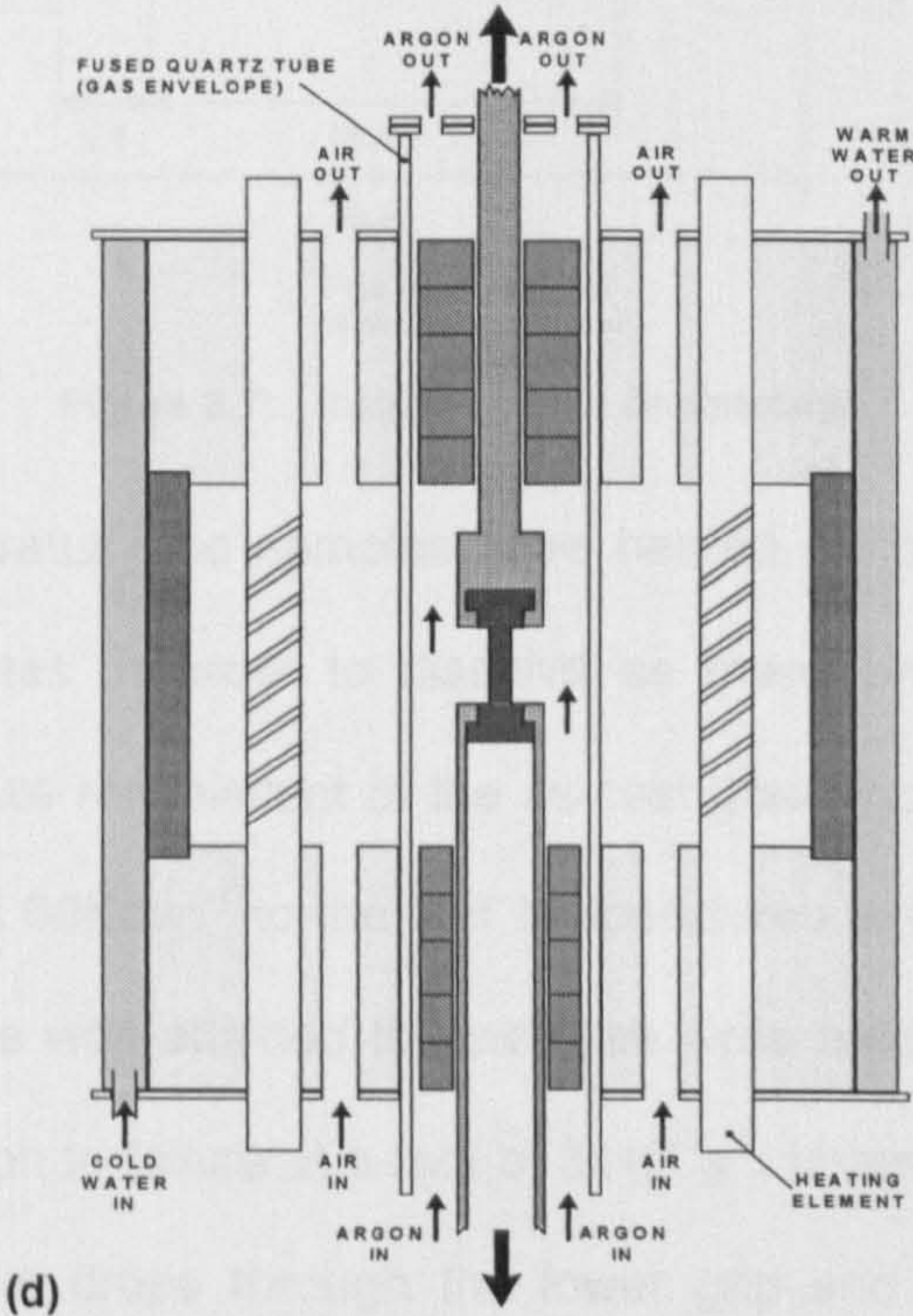
This apparatus consisted of a Model 1026 Instron machine to which a purpose built furnace, designed and manufactured by Isotherm Ltd, was fitted as shown in Figure 3.6 (a)-(c). The furnace was designed having the ability to cool at rates of up to 200 Kmin⁻¹ so that cooling conditions in both thin slab and conventional continuous casting could be simulated.

In order to achieve this cooling rate, heat must be removed rapidly from the heating elements and surfaces inside the furnace chamber. This is achieved by the use of a thin layer of very lightweight insulation; a water cooling jacket around the furnace shell; and the

facility of rapidly blowing compressed air through the furnace chamber and increasing the argon flow through the quartz tube containing the sample. A schematic diagram of the furnace chamber can be seen in Figure 3.6 (d).



(a) (b) (c)



(d)

Figure 3.6: Photographs of the Instron test apparatus, with (a) the furnace chamber closed and (b) open, (c) the furnace control unit and (d) a schematic diagram showing the construction of the Isoheat 'Rapid Cool' furnace attached to the Instron machine.

The samples used in the Instron test were electroplated with a 0.1mm thickness of nickel, using a Nickel Chloride and Boric Acid solution. Before inserting the samples into the grips of the Instron machine, they were also coated with aluminium oxide power mixed with ethanol to ensure they would be free to drop into the water for quenching immediately after failure. To further prevent oxidation during testing, the samples were heated within an inert environment maintained inside the fused silica tube. The Eurotherm 912S controller varies the rate of argon flowing through the furnace chamber during the test cycle. The minimum flow rate necessary to keep a positive pressure within the tube and to meet the required cooling was used during testing, but was increased to the maximum rate immediately after the sample had failed. The samples used in this test were prepared to the specification shown in Figure 3.7 by Corus:

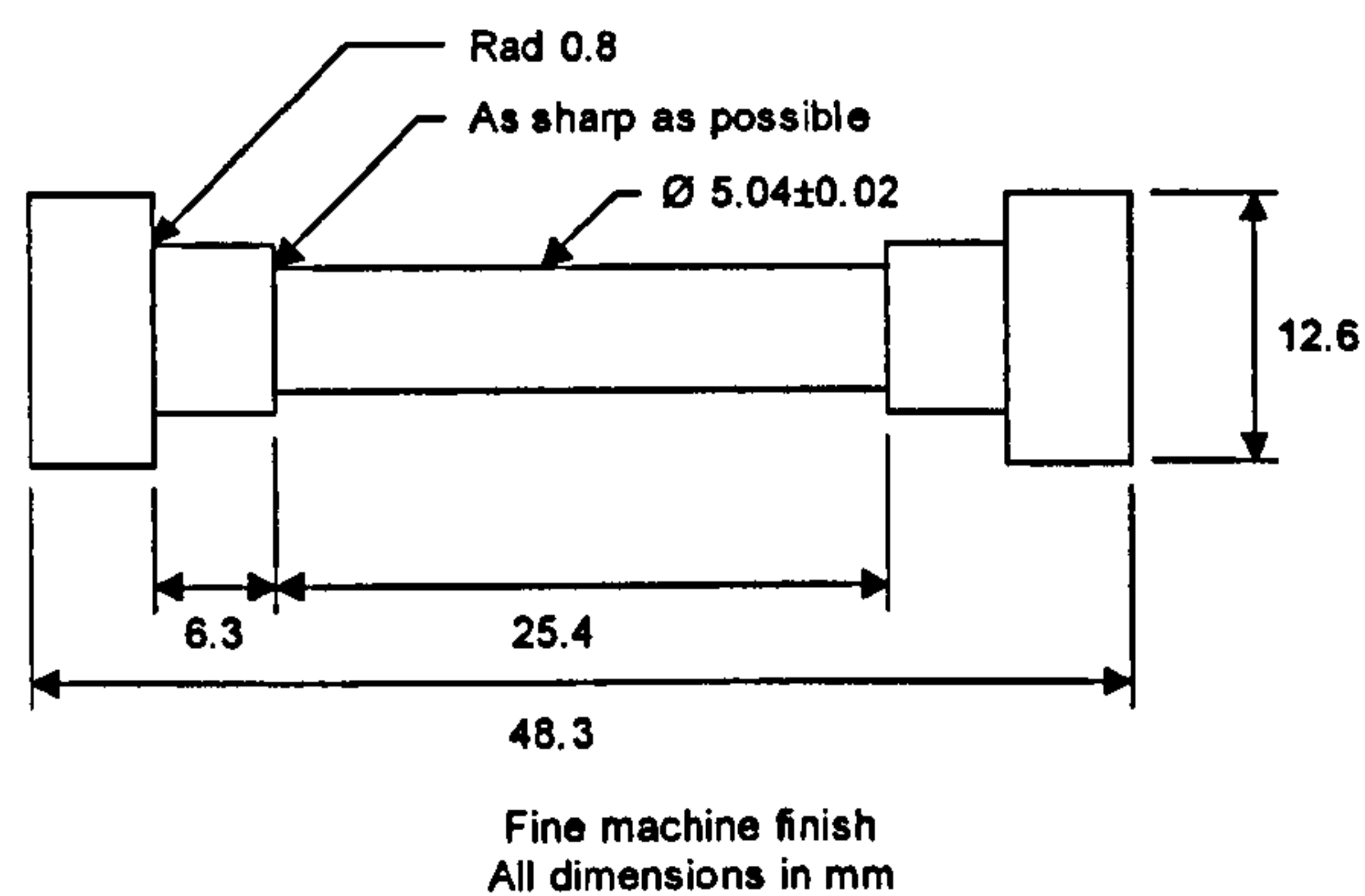


Figure 3.7: Instron Sample Dimensions.

Once in the apparatus, the samples were heated uniformly to 1603K where they were held for 12.5 minutes in order to dissolve as many precipitates as possible and produce a coarse grain size reminiscent of the as-cast grain size in continuously cast slab. They were then cooled at 60Kmin^{-1} to the test temperatures in the range of 873 to 1273K. Once the test temperature was attained the samples were held at this point for 5 minutes and then strained in tension to failure at a rate of $3 \times 10^{-3}\text{s}^{-1}$. Immediately following failure, the bottom half of the sample drops through the lower grip and is quenched to retain the structure present at failure. An example of a heating programme used in this study is shown in Table 3.1, below:

Segment Number	Type	Segment Details
1	Ramp	40 Kmin ⁻¹ → 1373 K
2	Dwell	5 minutes
3	Ramp	20 Kmin ⁻¹ → 1603 K
4	Dwell	2.5 minutes
5	Dwell	10 minutes
6	Ramp	60 Kmin ⁻¹ → 1293 K
7	Ramp	30 Kmin ⁻¹ → 1273 K
8	Dwell	5 minutes
9	Indefinite Dwell	Start Tensile Test

Table 3.1: An example Isoheat Furnace heating programme.

The quartz tube is highly efficient in allowing heat to transfer from the heating elements to the sample and is able to withstand the high cooling rates required. The temperature within the furnace is accurately controlled using the Eurotherm programme controller. This controller has the ability to select either of two thermocouples, work through complex heating/cooling programs, control both heating and cooling simultaneously, and to switch on auxiliary cooling if required during rapid cooling segments of the program.

As the fused silica tube is not entirely efficient in the transfer of heat to the sample, the control unit switches between two thermocouples during the heating cycle; one is positioned as close to the sample as possible, the other is outside of the fused silica tube. While the furnace is being heated to the solution temperature, 1603 K, the control unit relies on input from thermocouple outside the tube so as not to overheat itself causing damage. The thermocouple situated next to the sample is used, from segment 5 onwards, for the soaking and cooling sections of the heating program. This enables close control of the heat input and avoids overheating once the solid solution temperature is reached and avoids under cooling when the tensile temperature is reached.

The reliability of the temperature within the furnace was tested by placing two additional thermocouples in close proximity at the top and bottom of the gauge length of the sample. These not only allowed independent verification of the temperatures inside the silica tube, but also the temperature gradients from the top to bottom of the sample. The results of

this investigation are as shown in Figure 3.8. It can be seen that during the first heating segment, that the temperature lags behind that of the programme running on the temperature controller. This is due to the outer thermocouple being used by the furnace during heating, the heat transfer of the silica tube not being totally efficient and the relative difficulty in accurately controlling the heating of the furnace at lower temperatures. During the dwell cycles, e.g. sample straining, the temperature gradient settled to less than 5K.

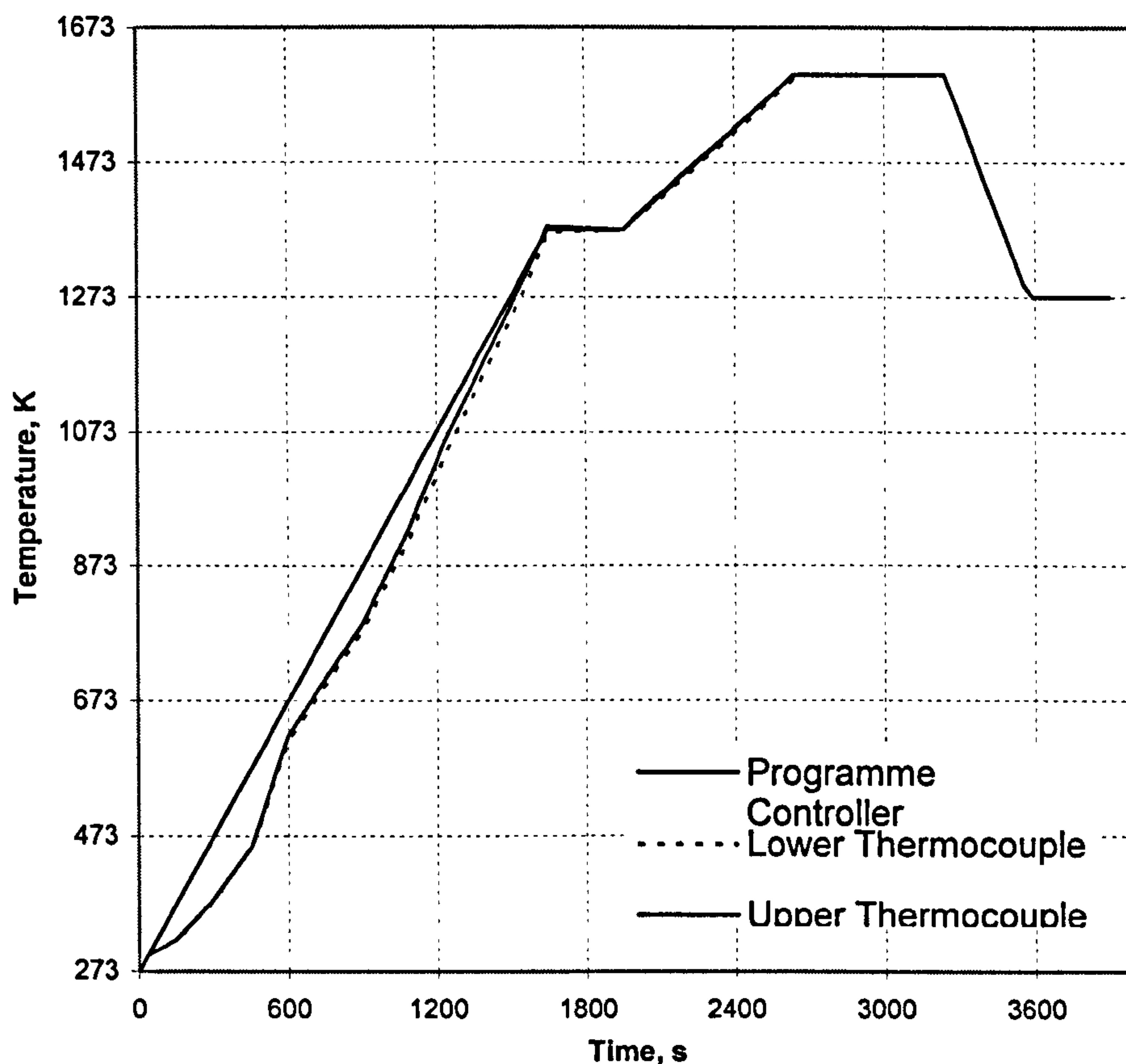


Figure 3.8: A chart showing how temperatures recorded at the top and bottom of the sample compared to the programme running on the Eurotherm measured using the inner and outer thermocouples.

3.2 Microscope Examination

Following the hot ductility testing, the Instron and Induction samples were examined using TEM, SEM and optical microscopy. A_{r3} temperatures were measured using dilatometry carried out by Corus; A_{e3} temperatures were calculated using the Thermocalc program. The methods of microscope examination used were as follows:

i. Optical Microscopy

The microscope used was a Nikon Optiphot connected to either a 35 mm black and white film camera or JVC TK-1280E Colour CCD video camera. The video camera was in turn connected to a film printer and also computer with a Picport colour video capture card installed. The quenched section of the Instron test specimens were used for optical and TEM measurements, the other portion being used for SEM examination. Specimens were taken near to the fracture surface in the longitudinal direction and mounted in a clear polymer resin using a Metaserv automatic mounting press. The clear polymer resin allowed an identification tag to be permanently fixed to the mounted samples.

ii. Scanning Electron Microscopy

The fracture mechanisms involved in the failure of the sample were studied using a Jeol T-200 SEM, operating at 25 kV. The fracture surface not used in optical microscopy was removed from the remainder of the test specimen and mounted in a holder using grub screws.

iii. Transmission Electron Microscopy

Some samples were prepared for TEM study from approximately 1 mm behind the fracture surface. The techniques used for the preparation and examination of these samples were similar to those used by Crowther.¹⁸

3.3 Grain Size and Type Measurements

The average grain sizes of the failed specimens were measured using the mean linear intercept method. Five sets of measurements were taken close the point of fracture which each included 100 point measurements. The prior austenite grain size was measured by counting the number of thin films of ferrite traversed in a test-line length. The percentage ferrite in these samples was measured in a similar manner, using a point counter to measure whether a grain under the cross hair at each position was ferrite or austenite.

4. Low Temperature Straightening

Most steel companies, including Corus, operate their straightener at the high temperature end of the trough, but it is thought that the lower temperature end probably should have been chosen. Since dynamic recrystallisation, which does not occur during straightening, dominates the high temperature end, recovery at the low temperature end is due to formation of around 40% ferrite. There is currently therefore much interest in examining this lower temperature end of the trough and this requires an understanding of what controls both the A_{r3} temperature and the production of deformation induced ferrite. If the A_{r3} temperature can be raised so that it approaches the A_{e3} , the width of the trough will be reduced allowing large amounts of ferrite to form at higher temperatures and this forms the basis of the following chapter. The work on this part of the programme has already been published ²⁶ and was awarded the Williams prize by the Institute of Materials, Metals and Minerals in 1998.

4.1 Introduction

Recent work ^{7,8,9,30} has gone far into interpreting the hot ductility curve and it has been possible to separate the contributions of deformation induced ferrite, grain boundary sliding and dynamic recrystallisation to hot ductility. In C-Mn and C-Mn-Al steels with low Al and N levels, the trough extends from the A_{e3} to the A_{r3} and is due to thin films of the softer deformation induced ferrite phase forming around the γ grains. Strain concentration occurs in these films causing ductile voiding to occur at the MnS inclusions at the boundaries and these cavities link up to give low ductility intergranular failure. As noted, the thin films of ferrite have been identified as being strain induced.

It has been shown ^{7,30} at the high temperature end of the trough in C-Mn-Al steels, in which no AlN precipitation has occurred, that full recovery in ductility corresponds to the onset of dynamic recrystallisation, this being able to isolate cracks formed at boundaries

and prevent them from growing. Without dynamic recrystallisation, removal of the thin films of ferrite above the A_{e3} does not lead to any marked improvement in ductility as grain boundary sliding in the γ occurs and this is just as detrimental. However, dynamic recrystallisation does not occur in the straightening operation during continuous casting as the grains are too coarse ($> 500 \mu\text{m}$) and the strain is too low (2%). Under these conditions improvements in ductility at high temperatures are small even when precipitation is present, as in Nb containing steels or C-Mn-Al steels having high Al and N levels. In contrast at the low temperature side of the trough, ductility improves dramatically when 30-40% ferrite is present in the structure. This involves working at temperatures 20 to 30K below the A_{r3} undeformed.

If the A_{r3} temperature can be raised so that it approaches the A_{e3} , large amounts of ferrite can then form at higher temperatures thus improving ductility as well as reducing the width of the trough. This requires an understanding of what controls the A_{r3} temperature and what controls the production of deformation induced ferrite. The A_{r3} can be raised by achieving slower cooling rates, refinement of grain size and raising the A_{e3} (i.e. lower C and Mn levels and higher Si and P levels). Recent work ⁸ has shown that refining the grain size has a remarkable affect in raising the A_{r3} under deformation conditions and this also needs to be explained.

Deformation has also been shown to be effective in raising the A_{r3} and for good ductility; and it is immaterial as to whether the ferrite is present prior to deformation or forms during deformation. A strain of ~5% has been shown to be adequate to form DIF.⁸ When ferrite first forms in coarse grained steel, it forms at the austenite grain boundaries, and it is likely at this early stage that there will be little difference in structure between pro-eutectoid ferrite and DIF. The major difference as far as ductility is concerned is that whereas a thin film of DIF can be present over a wide range of temperature resulting in poor ductility; the film rapidly thickens up as the temperature is decreased for pro-eutectoid ferrite.

4.2 Experimental Details

In this first part of the programme, four steels were chosen to give a wide range of A_{e3} and A_{r3} temperatures. The compositions of these four steels examined are shown in Table 4.1 and the A_{e3} , A_{r3} and A_{r1} temperatures are shown in Table 4.2. The A_{e3} temperatures were calculated using the 'Thermocalc' program⁹⁸ and the A_{r3} and A_{r1} temperatures measured using dilatometry. The steels were either 0.08% C, 0.6% Mn or 0.15% C, 1.4% Mn. Two of the steels were Nb free and the other two had an addition of 0.03% Nb. As well as these variations, Si was varied between 0.1 and 0.5% and P from 0.007 to 0.027%. Both of these two elements are known to have a powerful influence in increasing the A_{e3} and hence the A_{r3} temperature.

Steel	C	Mn	S	P	Si	Nb	Al	N
1	0.082	0.61	0.005	0.025	0.50	-	0.030	0.005
2	0.150	1.41	0.007	0.007	0.09	-	0.021	0.005
3	0.089	0.60	0.005	0.023	0.49	0.031	0.029	0.005
4	0.140	1.40	0.006	0.026	0.10	0.031	0.022	0.005

Table 4.1: Analysis of steels studied in this section, wt. %.

Steel	Transformation Temperature, K		
	A_{e3}	A_{r3}	A_{r1}
1	1154	1073	903
2	1085	973	775
3	1156	1010	823
4	1090	943	743

Table 4.2: Transformation temperatures of steels examined, K (at 60Kmin⁻¹).

The steels were heated to 1603K using the equipment shown in Figure 3.6 to produce the same coarse grain size held for 5 minutes, cooled at 60Kmin⁻¹ to test temperatures in the range 1273 to 873K, held for a further 5 minutes at the test temperature and strained in tension to failure at 3x10⁻³s⁻¹. Samples were quenched immediately after failure. A_{r3} temperatures were determined by dilatometry, following the above heating programme as closely as possible but without a hold at the test temperature; optical, TEM and SEM examinations were also carried out on the samples.

⁹⁸ B. Sundman, B. Jansson and J.-O. Anderson: Calphad, 1985, 9, p.153-190.

4.3 Results and Discussion

As would be expected, the higher C and Mn steels had the lowest A_{e3} temperatures, see Table 4.2. It is also interesting to note from Table 4.2 that although Nb has little influence on the A_{e3} it has a powerful effect in reducing the A_{r3} temperature.

The curves for the four steels are shown in Figure 4.1 and can be seen to be enormously different. Although the depth of the troughs are very similar, with minimum ductilities in the range 35 to 45% R of A, their width and position changes greatly.

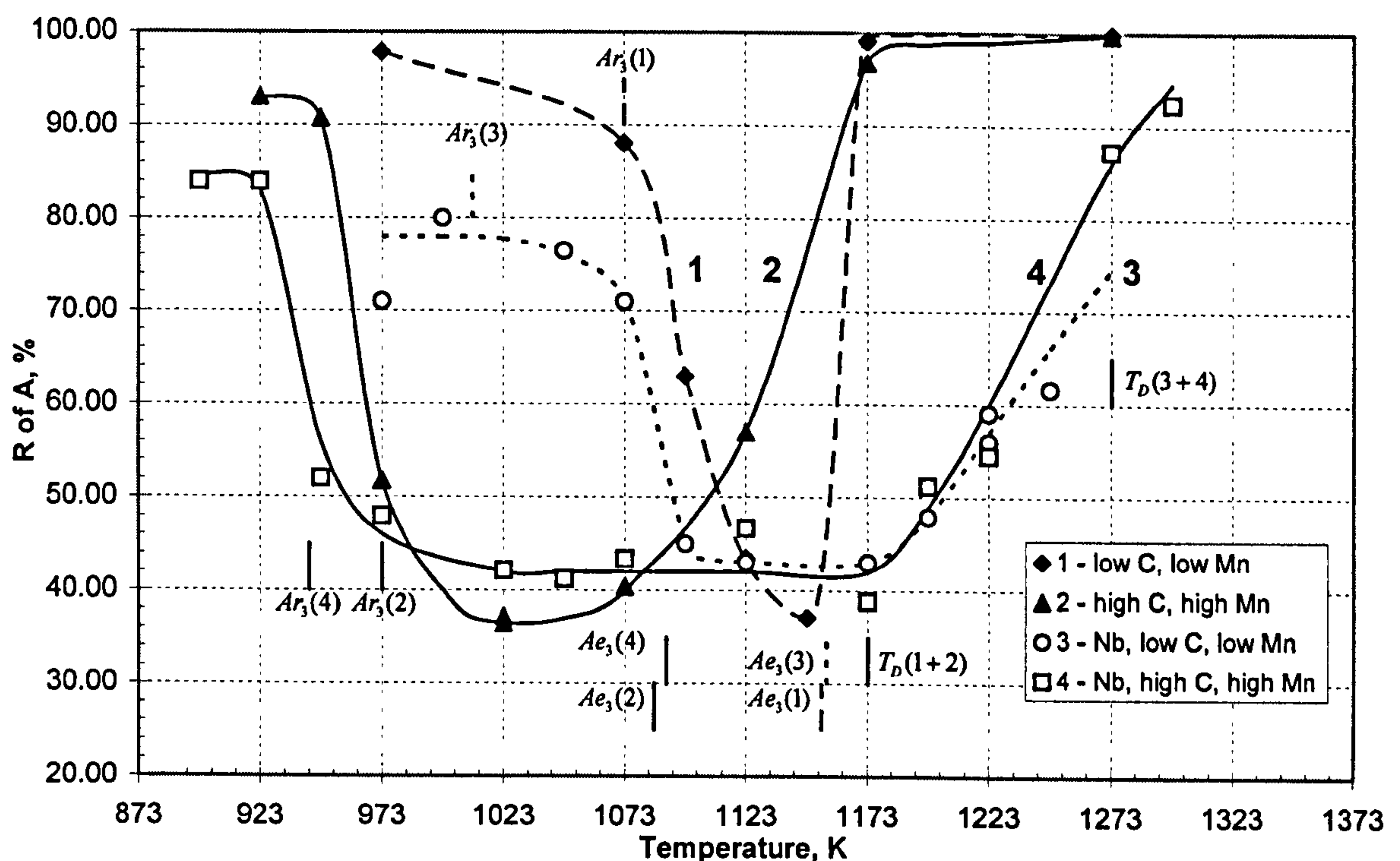


Figure 4.1: Hot ductility curves for steels 1 to 4, showing A_{e3} , A_{r3} and T_D temperatures.

Steel 1 (low C, low Mn) can be seen from Figure 4.1 to have the narrowest trough of approximately 30K; ductility starts to fall below the A_{e3} (1154K) and by the time the temperature has fallen to the A_{r3} (1073K), ductility has fully recovered. This indicates that the ferrite is deformation induced and, as will be seen from the discussion, can form in large quantities.

Steel 2 (high C, high Mn), which has a lower A_{e3} temperature (1085K) than steel 1, has a wider trough. Again ductility starts to fall at the A_{e3} , but this time only fully recovers below the A_{r3} (the A_{r3} is 973K and full recovery occurs at ~940K) suggesting that a thin band of ferrite forms and is not able to progress into the matrix until the normal transformation ferrite forms.

Adding Nb to steels 1 and 2 (giving steels 3 and 4) results in a widening of the trough on the high temperature side and ductility starts to fall well above the A_{e3} (1156K and 1090K respectively). In the case of steel 3 (low C, low Mn), ductility again fully recovers at the low temperature side only when the A_{r3} temperature (1010K) is reached. The widest trough, ~250K, is given by steel 4 (Nb + high C, high Mn); here the trough extends both at the high and low temperature ends.

Examination by TEM

Only steel 4, having high C, high Mn and containing Nb, was examined using TEM. A sparse matrix precipitation of Nb(CN) was found at test temperatures in the range 1073K to 1298K, as can be seen in Figure 4.2 (a), compared with what is normally found in Nb containing steels, Figure 4.2 (b).

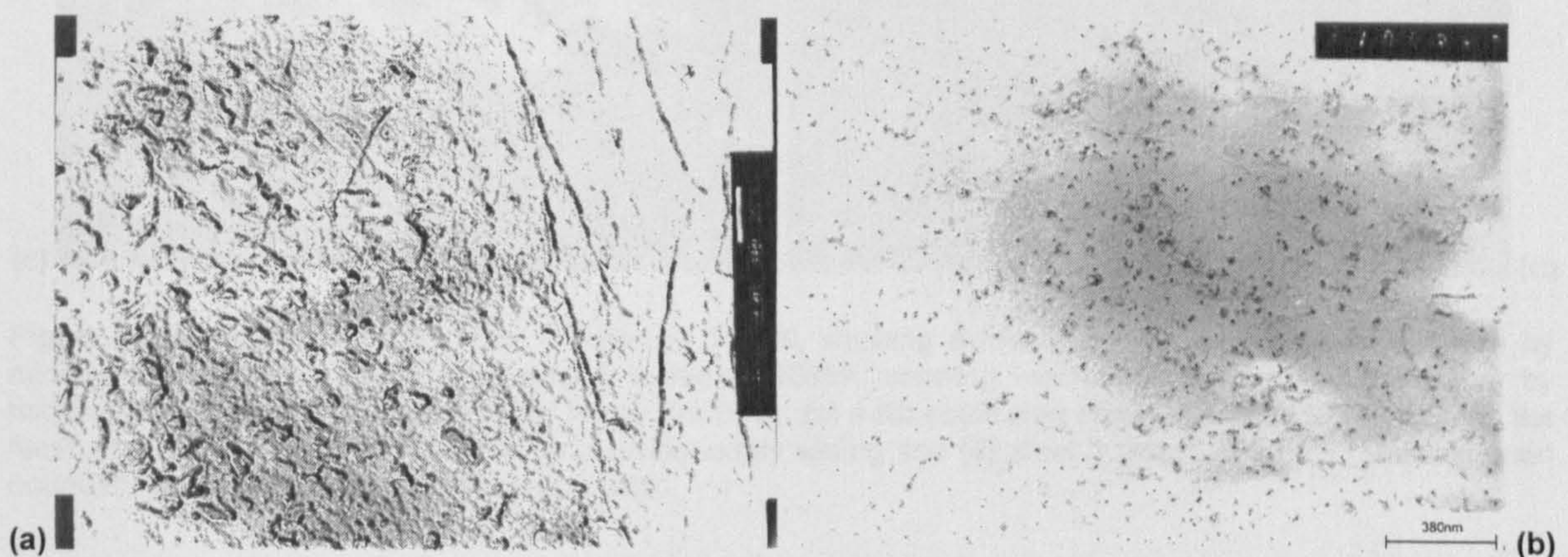


Figure 4.2: TEM Micrographs of (a) high Mn high C steel tested at 1173K, showing sparse precipitation of Nb(CN) and (b) typical Nb(CN) precipitation in a steel similar to (a) but containing 0.011% P, this steel has been cast and cooled to the test temperature of 1173K at 100Kmin^{-1} .⁹⁹

⁹⁹ R. Abushosha: Unpublished work, 1997.

Examination by SEM

Studying the four steels using the scanning electron microscope (SEM), it was seen that failures occurring in the trough and just below the A_{e3} temperature were of the microvoid coalescence type, see Figure 4.3 (a). Whereas, above the A_{e3} , low ductility intergranular failure characterised by fractures having smooth flat facets occurs; this is typical of when grain boundary sliding in the austenite is responsible for the intergranular failure,² Figure 4.3 (c). Figures 4.3 (b) and (d) show optical micrographs of these two failure modes of microvoid coalescence and grain boundary sliding, respectively.

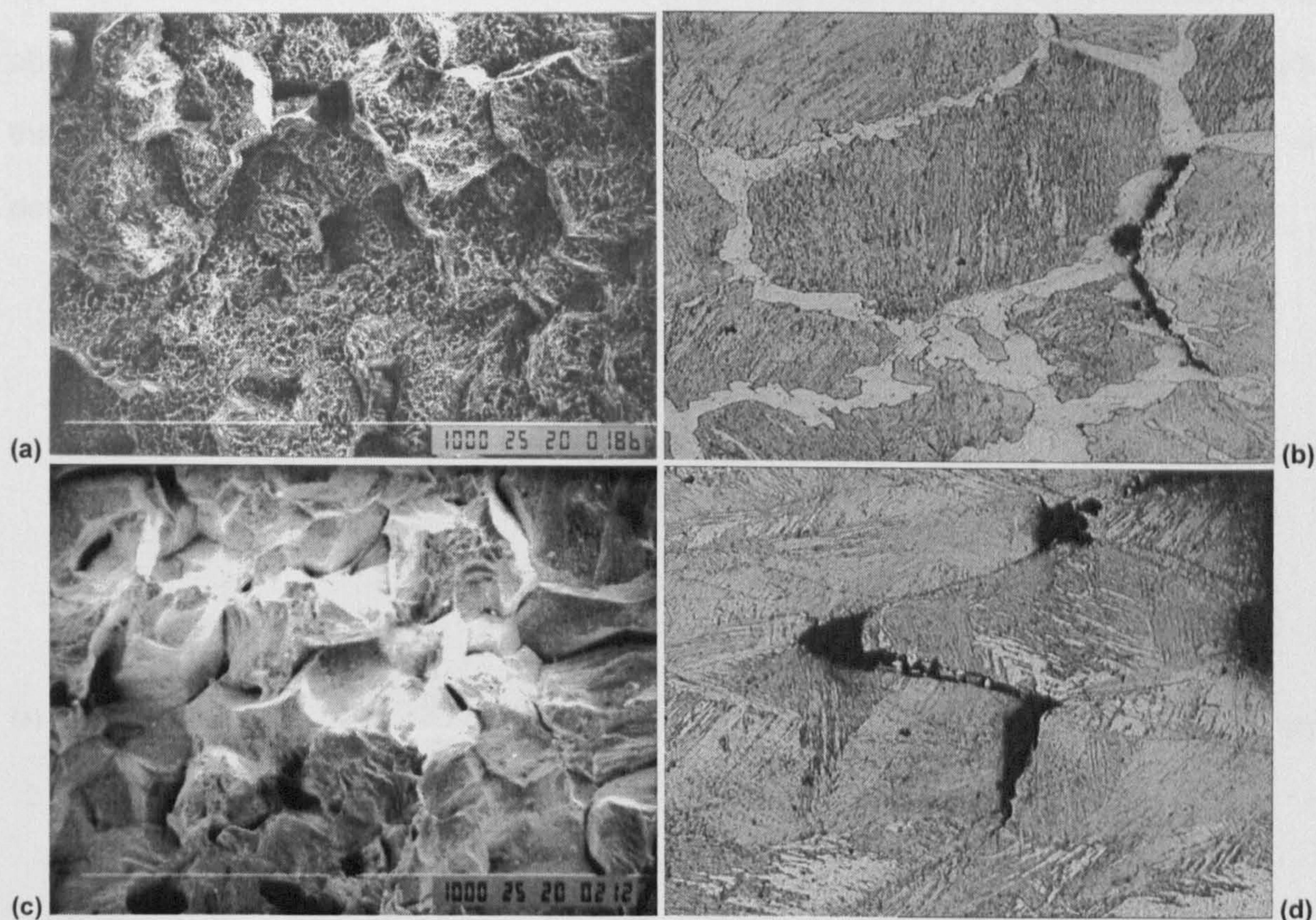


Figure 4.3: Micrographs of (a) steel 1 tested at 1148K, showing evidence of intergranular ductile failure by microvoid coalescence (SEM), (b) steel 3 tested at 1098K, showing mechanism of intergranular failure by microvoid coalescence within the softer ferrite film (x60), (c) a Nb containing steel tested at 1198K, showing flat facets indicating intergranular failure by grain boundary sliding and (d) steel 3 tested at 1198K, showing grain boundary sliding as the failure mechanism (x60).

4.3.1 Low Temperature End of the Trough

To investigate this part of the trough, samples which had been quenched after fracture were examined metallographically. It can be seen from Figure 4.4 (a), that at the minimum ductility temperature (1148K) for steel 1, the steel giving the narrowest trough, a thin band of ferrite surrounds the austenite grains; there is approximately 10% ferrite present and the R of A is 36%.

Decreasing the temperature to 1123K and then further to 1098K, Figures 4.4 (b) and (c) respectively, results in the formation of more and more ferrite; as these temperatures are above the A_{r3} , of 1073K, the ferrite must be deformation induced. The heavy substructure that can be seen in the ferrite, Figures 4.4 (c) and (d) also confirms that this ferrite is deformation induced.

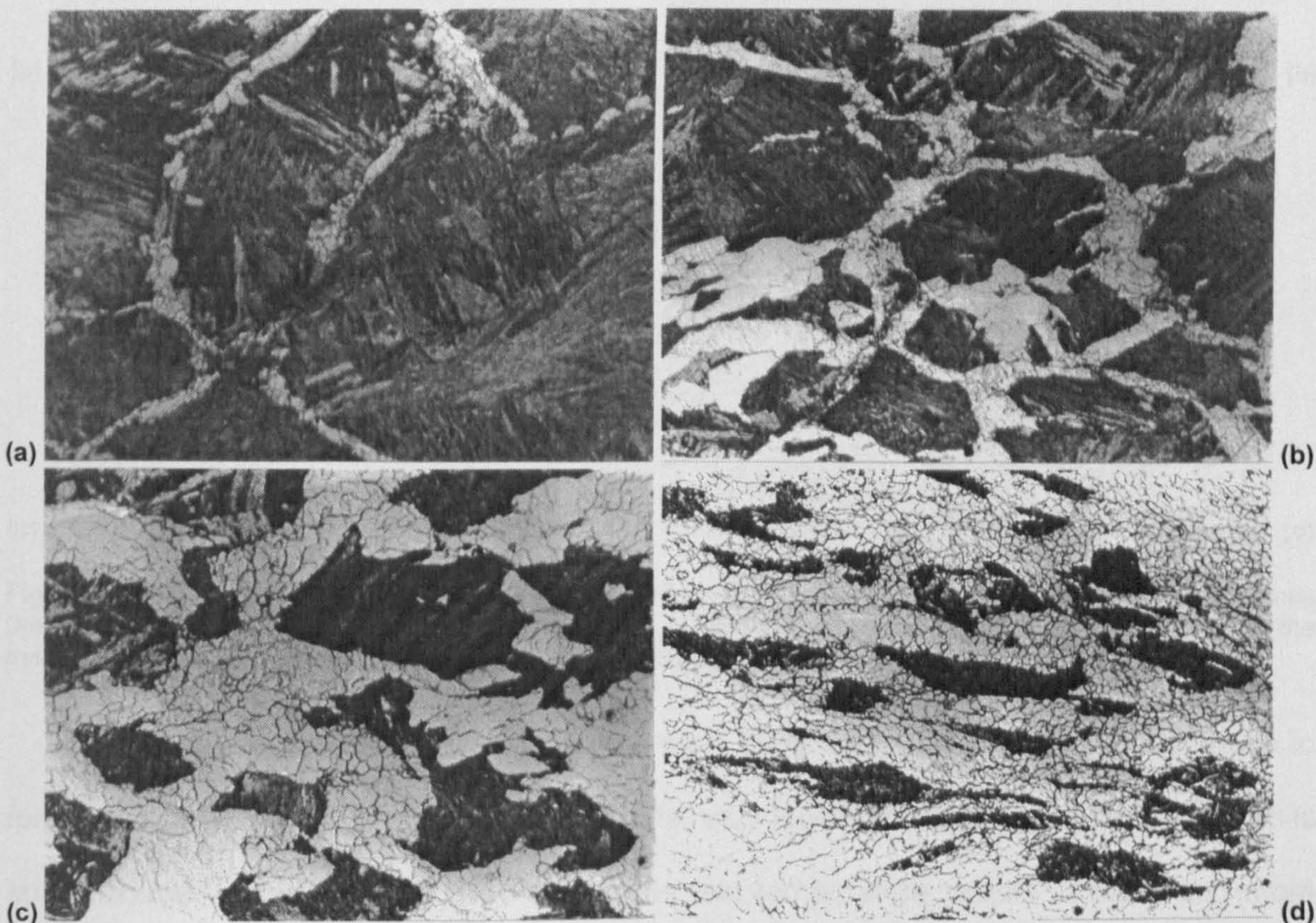


Figure 4.4: Micrographs of steel 1 (mag. x60) tested at (a) 1148K, thin films of ferrite surround austenite grain boundaries, 10% ferrite, 36% R of A, (b) 1123K, films have now developed, 27% ferrite, 48% R of A, (c) 1098K, marked substructure is apparent in ferrite, ~50% ferrite, 63% R of A and (d) 1073K, mostly ferrite with heavy substructure, 74% ferrite, 88% R of A.

In contrast in steel 2, a very thin band of ferrite is present as shown in Figures 4.5 (a) and (b). This gradually thickens as the temperature is decreased from 1073K to the A_{r3} temperature of 973K, Figures 4.5 (a), (b) and (c). However, the volume fraction of ferrite remains low so that strain concentration occurs and ductility is poor. Only when the temperature is reduced below the A_{r3} , 923K, are large amounts of ferrite produced, and now it is nucleated within the matrix, probably at inclusions and sub-grain boundaries as well as at the boundaries, see Figures 4.5 (c) and (d).

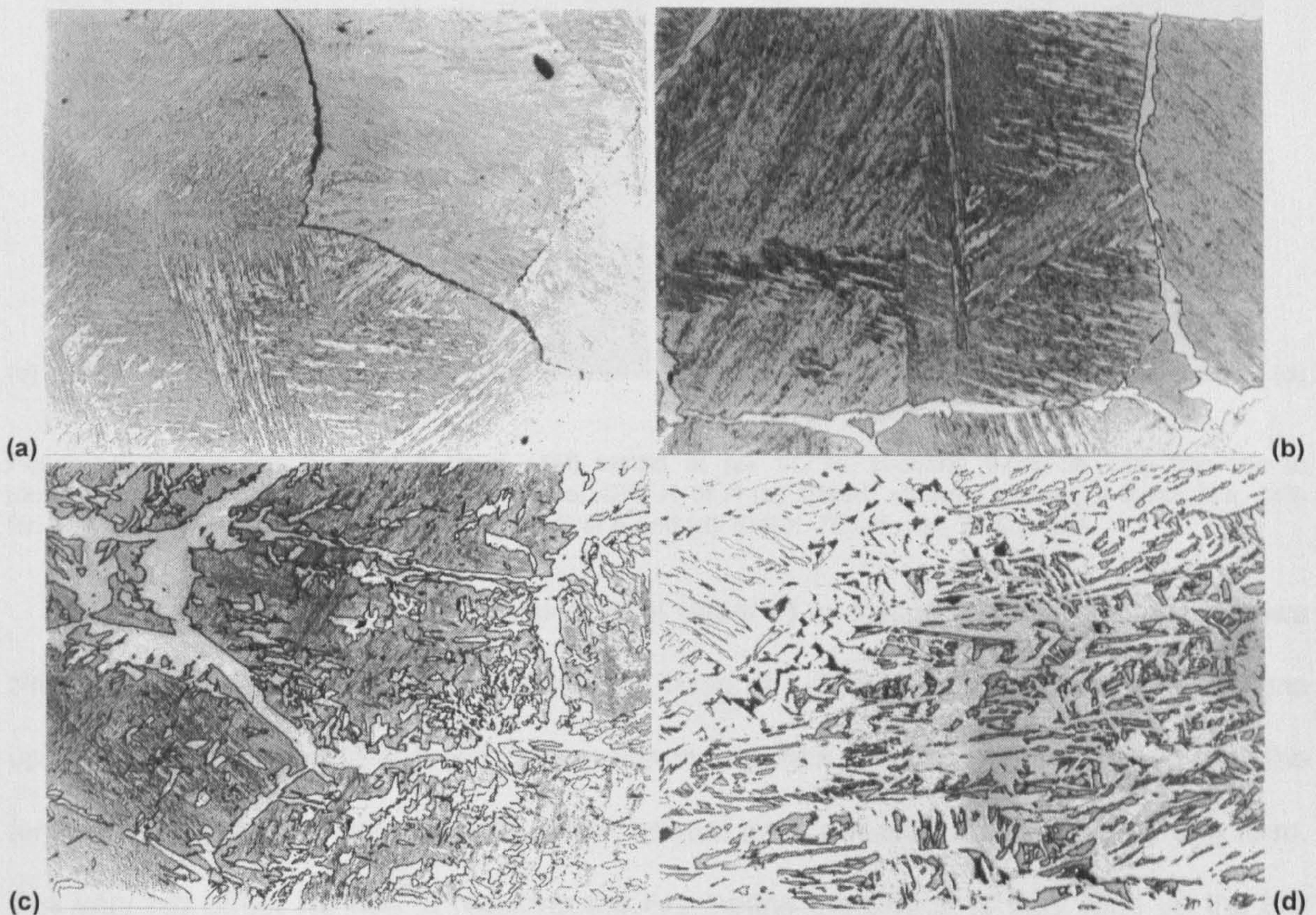


Figure 4.5: Micrographs of steel 2 (mag. x60) tested at (a) 1073K, showing very thin ferrite films at boundaries ($A_{e3} = 1085K$), (b) 1023K, showing growth of ferrite film, (c) 973K, the A_{r3} temperature, showing ferrite within the matrix and (d) 923K, showing much ferrite within the matrix.

For the low C, Low Mn, Nb containing steel (steel 3), like steel 1, ferrite first starts to form at 1123K in a very thin layer, <0.5% ferrite, very much above its A_{r3} of 1010K and so is strain induced, Figure 4.6 (a). Decreasing the test temperature results in more and more deformation induced ferrite being produced, see Figures 4.6 (a), (b) and (c), and at 1048K 75% ferrite has been formed, see Figure 4.6 (d).

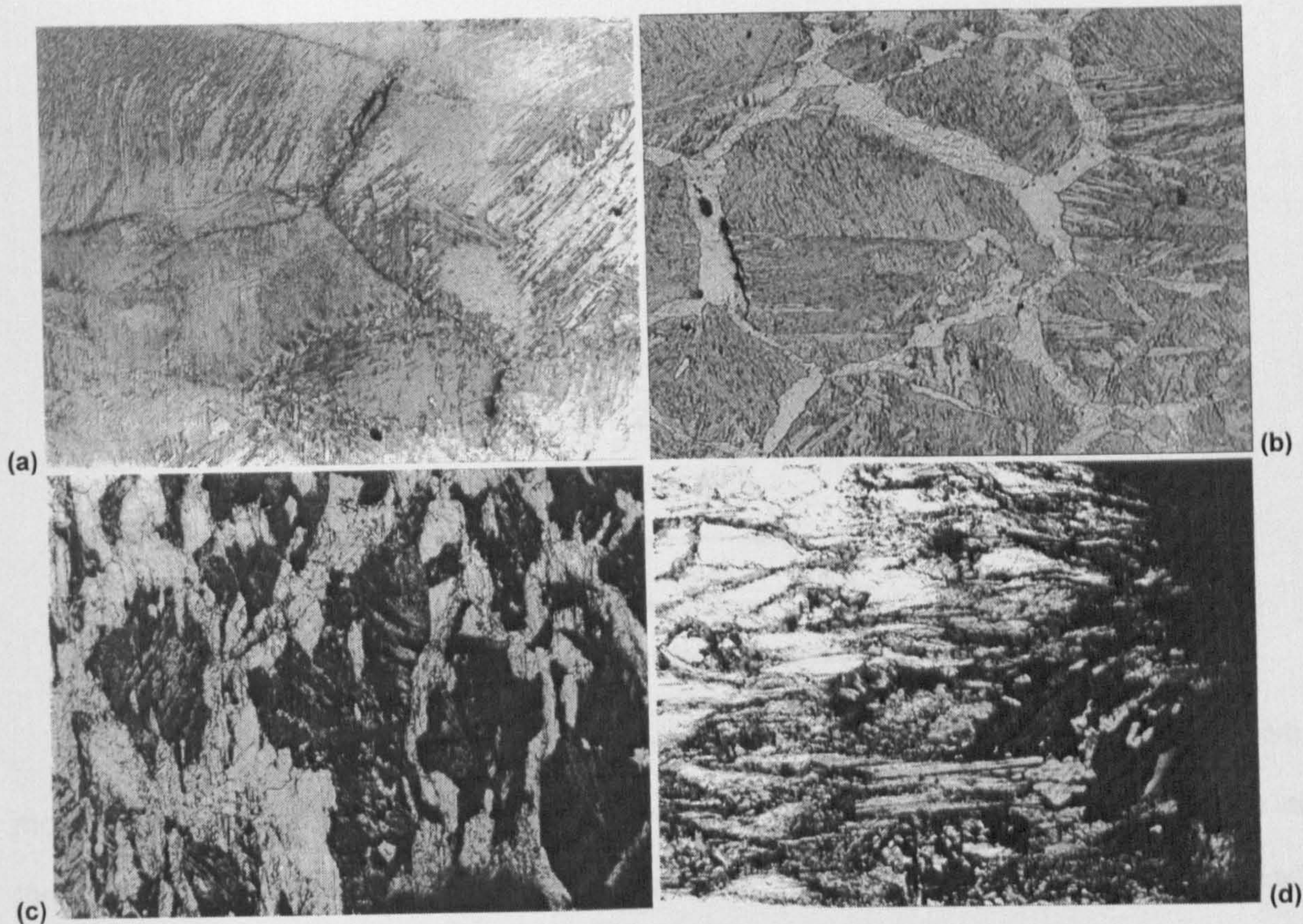


Figure 4.6: Micrographs of steel 3 (mag. x60) tested at (a) 1123K, showing ferrite in very thin film at temperatures of minimum ductility, <0.5% ferrite, 43% R of A (b) 1098K, showing growth of ferrite film, 24% ferrite, 47% R of A (c) 1073K, 45% ferrite, 72% R of A and (d) 1048K, 75% ferrite, 77% R of A.

The higher C, Mn, Nb containing steel (steel 4) in contrast to steel 3, again shows similar behaviour to steel 2 in that only a thin band of ferrite forms, but although it thickens up as the temperature is reduced, a high volume fraction of ferrite is not attained until the temperature has gone below the A_{r3} when normal transformation induced ferrite can form. The very big effect Nb has in reducing the A_{r3} means the trough is very wide on the low temperature side; this may be a major reason for Nb being such a deleterious element to have as it encourages crack formation over a very wide temperature range.

The curves of calculated percentage ferrite against test temperature for the four steels are given below in Figure 4.7.

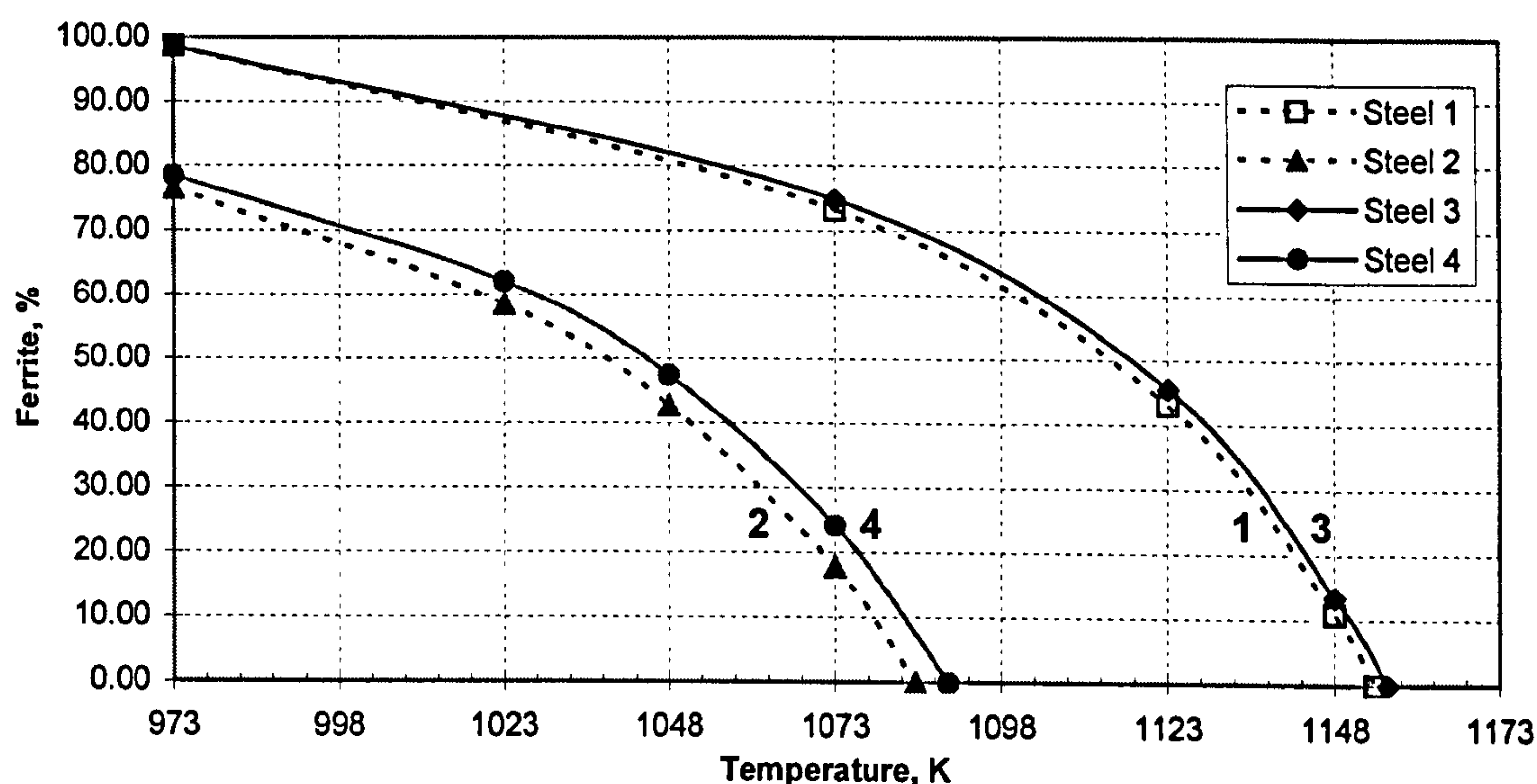


Figure 4.7: Calculated percentage ferrite present in the four steels.

It can be seen from Figure 4.7 that the low Mn steels (steels 1 and 3) always give more ferrite for a given temperature than the higher Mn steels. There is little difference in the percentage ferrite present with or without Nb. Figure 4.8 compares the calculated equilibrium ferrite values (solid line curves) to the observed (dashed line curves) and also gives the R of A hot ductility curves. It can be seen that although deformation induced ferrite at almost equilibrium values are achieved with steels 1 and 3 (lower Mn, lower C), Figure 4.8 (a), large amounts of ferrite are not formed in steels 2 and 4, the higher Mn and C containing steels, Figure 4.8(b) until the temperature is decreased below the Ar_3 .

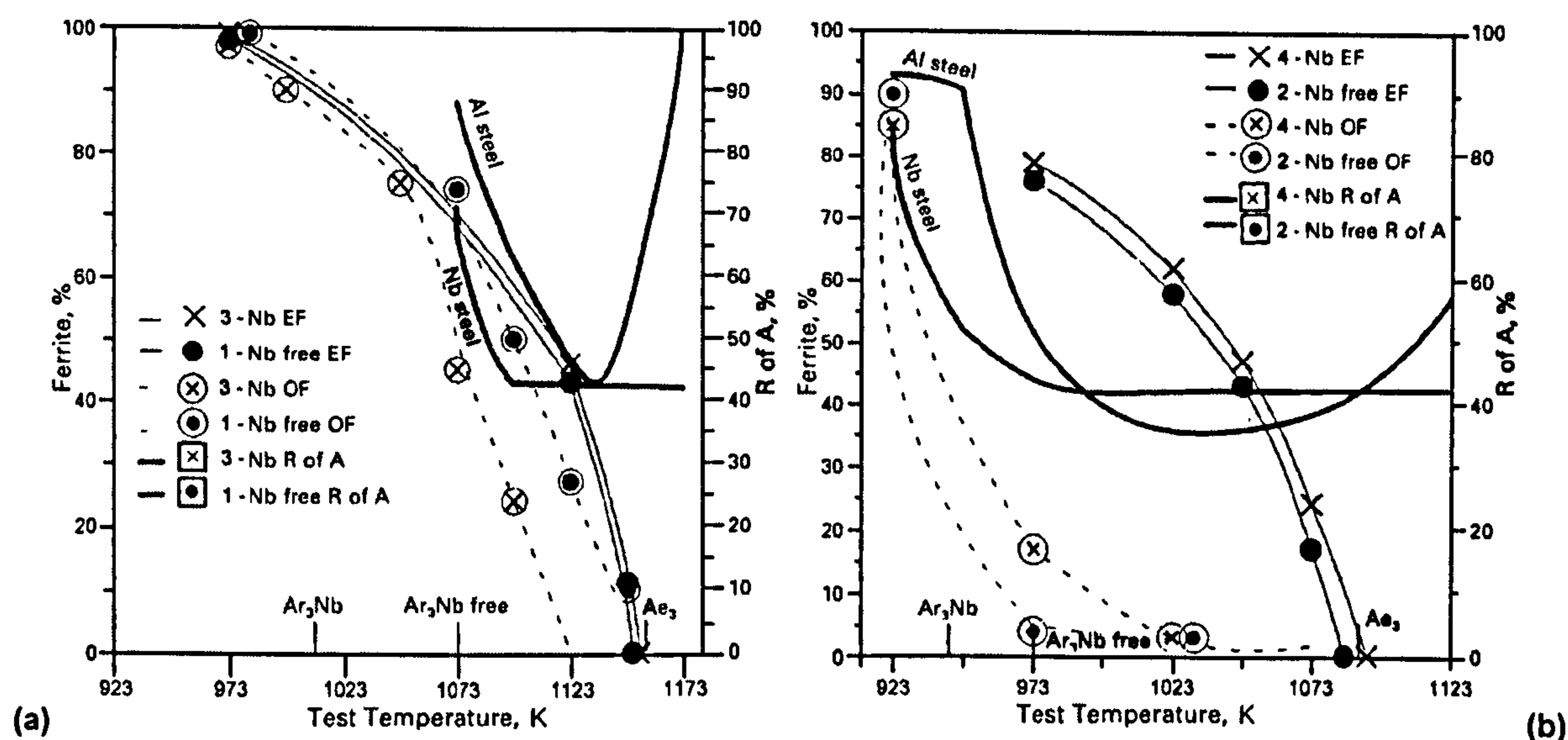


Figure 4.8: Influence of test temperature on observed and calculated % ferrite for (a) low Mn, low C steels 1 and 3 and (b) high Mn, high C steels 2 and 4. The relevant sections of the hot ductility curves are also included: EF – equilibrium ferrite, OF – observed ferrite.

4.3.2 High Temperature End of the Trough

Recovery at the high temperature end of the trough in these steels is always related to when dynamic recrystallisation is possible. In the case of plain C-Mn steels, it has been shown that dynamic recrystallisation only takes place when the thin film of deformation induced ferrite is no longer present, i.e. just above the Ae_3 .

In the case of Nb containing steels, the presence of Nb(CN) precipitation prevents dynamic recrystallisation until the temperature is sufficiently high to prevent pinning of the grain boundaries. In all cases, the temperature at which DRX occurs, T_D , can be obtained from the flow stress curves, when the stress reaches a peak and then dips and continues. The stress strain curves for the four steels studied can be found at the end of this section, Figures 4.10 – 4.13; the values of T_D for each of the steels can be found using these curves and are given in Table 4.3. A method of analysing these flow curves to more easily identify the temperature of the onset of DRX is presented in Chapter 5, Section 5.3.1.

Steel	T_D from load-elongation curve, K	T_D from metallography, K
1	1173	1173
2	1173	1173
3	1273	1223
4	1273	1273

Table 4.3: Temperatures for onset of dynamic recrystallisation, T_D .

T_D can also be obtained from metallographic examination of samples quenched after fracture, as illustrated in Figure 4.9. For these coarse grained steels, DRX always produces a fine grain structure in steels, Figure 4.9 (a). Generally, metallographic examinations are more accurate and give T_D temperatures either the same or 50K lower than from the flow stress curves. This is because the flow stress curves are measuring the overall sample and metallography looks at the localised region near to the fracture tip.

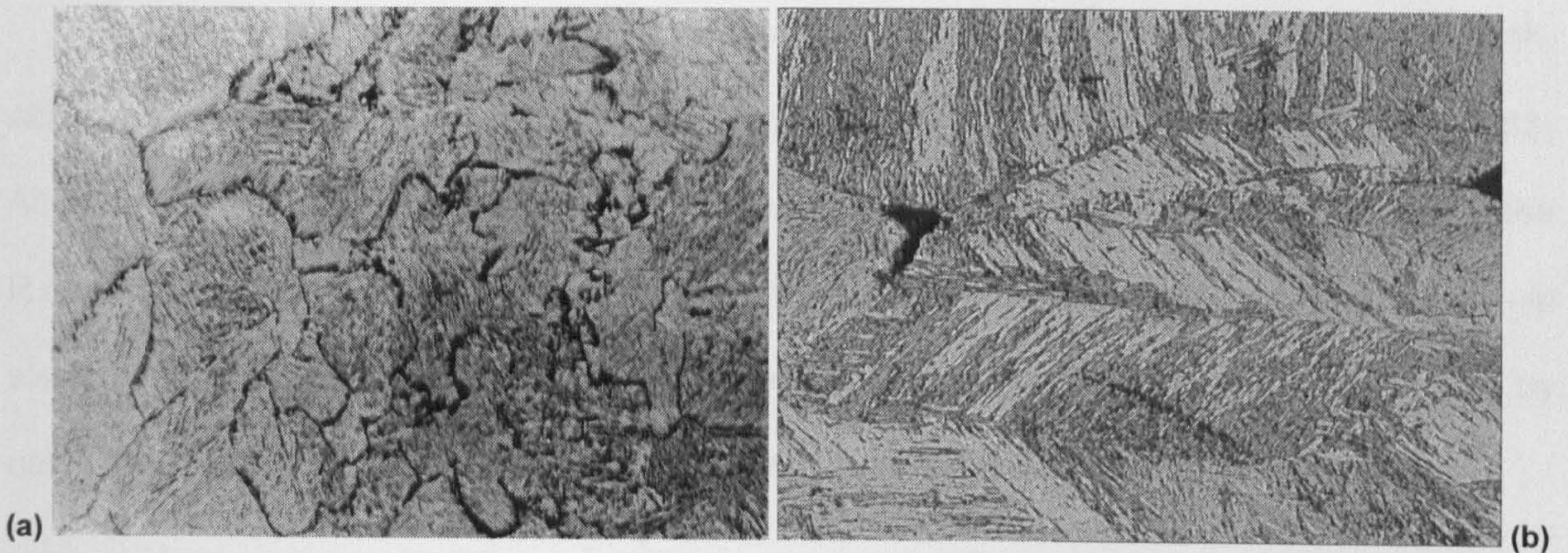


Figure 4.9: Austenitic grain structures (mag. x60) seen in (a) steel 2 (high Mn, high C, Al), showing dynamically recrystallised grains, tested at 1173K and (b) steel 3 (low Mn, low C, Nb), showing the original un-recrystallised austenitic structure and evidence of wedge cracking, also tested at 1173K.

4.3.3 Depth of the Trough

The depth of the trough is probably the most difficult part of the hot ductility curve to estimate. For simple C-Mn-Al steels, some attempt has been made to calculate the R of A values knowing the thickness or volume fraction of the ferrite band at the minimum ductility temperature. The minimum ductility can then be calculated using a model by Yamanaka *et al.*¹⁰⁰ assuming all the deformation takes place in the ferrite film. The equation for fracture is then given by Equation 4.1 below:

$$\varepsilon_f = V_\alpha \left(\frac{k(1-f)}{f} \right) \quad (4.1)$$

Where ε_f = fracture strain, V_α = volume fraction of ferrite and f is the inclusion volume fraction in the film and k is a constant taken as 0.000099. The value of f is believed to be related to the amount of sulphur in solution, at the solution temperature, which is available for precipitating out at the austenite grain boundaries on cooling to the test temperature. However, there are other factors that influence the depth of the trough such as grain size, strain rate and coarse precipitation. The size of the inclusions is also important as fast cooling produces finer inclusions and worse ductility.⁷¹

¹⁰⁰ K. Yamanaka, F. Terasaki, H. Ohtani, M. Oda and M. Yoshihara: Trans. ISIJ, 1980, 20, p. 810.

Refining the grain size and/or increasing the strain rate will both reduce the depth, whereas, increasing the precipitate volume fraction, or refinement, will increase the depth. All of these terms would need to be incorporated in Equation 4.1 to fully account for the R of A value. However as a first approximation, this equation can be used for C-Mn-Al steels. The influence of MnS precipitation and sulphur in solution can be accounted for by using the solubility product, given by Turkdogan ¹⁰¹ for Mn and S, as follows:

$$\log K_s = 2.929 - \frac{9020}{T} \quad (4.2)$$

where T is temperature in Kelvin and K_s is:

$$K_s = [S_{total} - S_{combined}] \left[Mn_{total} - \frac{\text{atomic wt. Mn}}{\text{atomic wt. S}} \times S_{combined} \right] \quad (4.3)$$

Using equations 4.1 and 4.2 for a temperature of 1603K, the amount of S in solution for steels 1 and 2 would be calculated to be 0.0035 and 0.0016 %, respectively. Thus on the basis solely of sulphide inclusions in the ferrite band, one would expect steel 1 to have the lower R of A. However, as can be seen on comparison of Figures 4.4 (a) and 4.5 (a), the band of ferrite is much thicker in steel 1 than in steel 2 at the minimum ductility temperatures and hence a greater strain can be accommodated in the ferrite band in steel 1; this counteracts the detrimental influence of more sulphides.

The percentage ferrite for steels 1 and 2 at the minimum ductility temperature is 10% and 3%, respectively. Using Equation 4.1, the R of A values for steel 1 and 2 are 38% and 29% respectively which compares favourably with the theoretical values of 37% and 36%. Table 4.4 lists the values of the percentage S in solution at 1603K, the grain size, minimum ductility temperature, percentage of ferrite and the R of A values both observed and calculated using equation 4.1.

¹⁰¹ E.T. Turkdogan, S. Ignatowicz and J. Pearson: J. Iron Steel Inst., 1955, 180, p. 349.

Steel	% Mn	% S in solution	% Ferrite	Min. Ductility Temp., K	Grain Size, μm	Observed R of A, %	Calculated R of A, %
1	0.61	0.0035	10	875	290	37	38
2	1.41	0.0016	3	750	620	36	29
3	0.60	0.0035	23	825	450	42	-
4	1.40	0.0016	2	800	530	42	-

Table 4.4: Calculated and observed R of A values for the four steels.

C-Mn-Al-Nb Steels

The addition of Nb to C-Mn-Al steels generally results in both wider and deeper troughs. Dynamic precipitation of Nb(CN) is very marked in Nb containing steels after solution treatment; and their poor ductility can be attributed to the combination of extensive matrix and γ grain boundary precipitation and the tendency to form precipitate free zones which lead to strain concentration at the boundaries.

Previous work ¹⁰² indicates that at 1223K, the temperature for the maximum rate of dynamic precipitation of Nb(CN), precipitation is very rapid and, with the strain rate in use, is often complete within the time of the test, so that equilibrium conditions for precipitation can be assumed. Thus, in addition to the sulphides and ferrite volume fraction, precipitation is important and one would expect deeper curves. However, as can be seen from Figure 4.1 and Table 4.4, the addition of Nb appears to have little influence on the depth of the trough. This is most likely due to the relative insensitivity of Nb additions to ductility at the high level of P used in these steels (0.025% P), see Table 4.1.

Previous work ^{12,103} has noted that a high P content improves the ductility of Nb containing steels. It has been suggested that P segregates to the boundaries and occupies deformation sites there in preference to Nb(CN) so that the P reduces the amount of

¹⁰² B. Mintz and Z. Mohamed: in Proc. 7th Int. Conf. on Fracture, Houston, TX, 'Advances in fracture research', ed. K. Salama et al., Oxford, Pergamon, 1989, 4, pp. 2545-2553.

¹⁰³ B. Mintz and J.M. Arrowsmith: Sheffield Int. Conf. on 'Hot working and forming processes', ed. C.M. Sellars and G.J. Davies, 1979, London, The Metals Society, pp. 99-103.

Nb(CN) precipitation. Certainly, the Nb(CN) precipitation found in steel 4 (Nb + high C, high Mn), the only steel to be examined with the TEM, was very much less than has been noted previously¹⁰⁰ in similar steels having P levels more in accord with modern steel making practice; compare Figures 4.2 (a) and (b). Analysis of commercial data,^{12,85} relating the composition to the incidence of transverse cracking, has also found that high P levels reduce the problem. No attempt has been made to modify Equation 4.1 to take account of the Nb(CN) precipitation and therefore, no calculations have been made for the Nb containing steels.

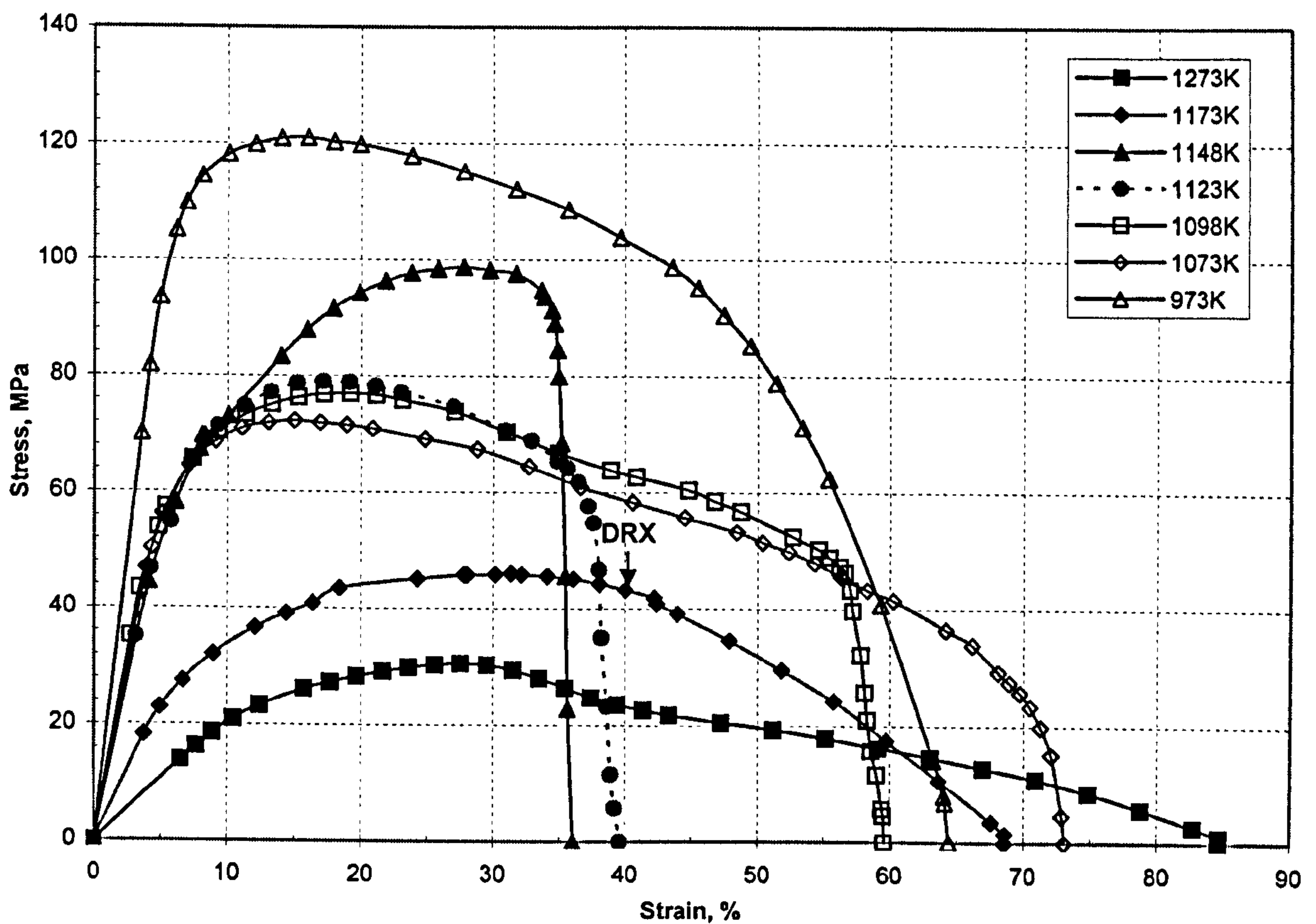


Figure 4.10: Stress strain curves for steel 1, showing onset of dynamic recrystallisation.

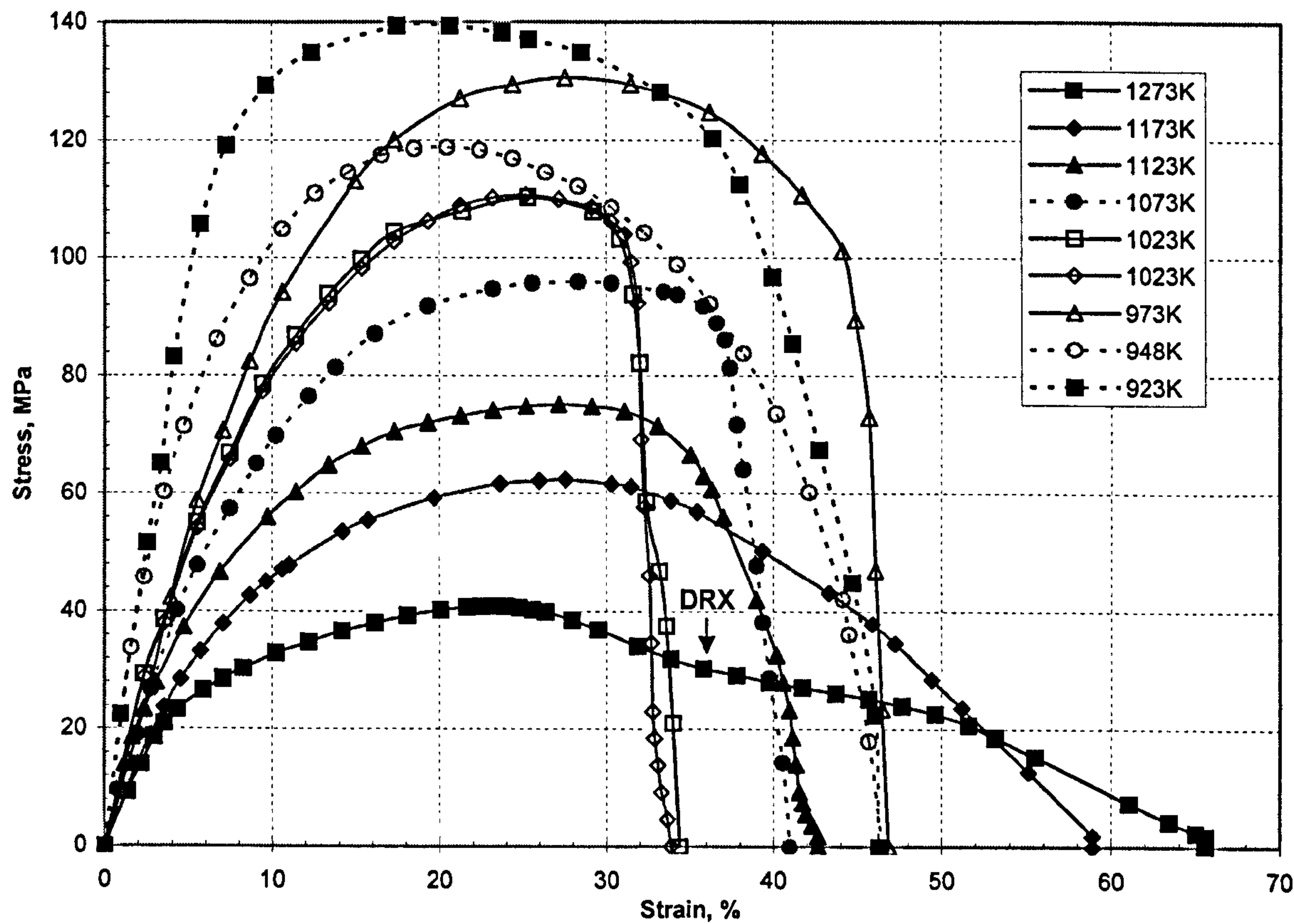


Figure 4.11: Stress strain curves for steel 2, showing onset of dynamic recrystallisation.

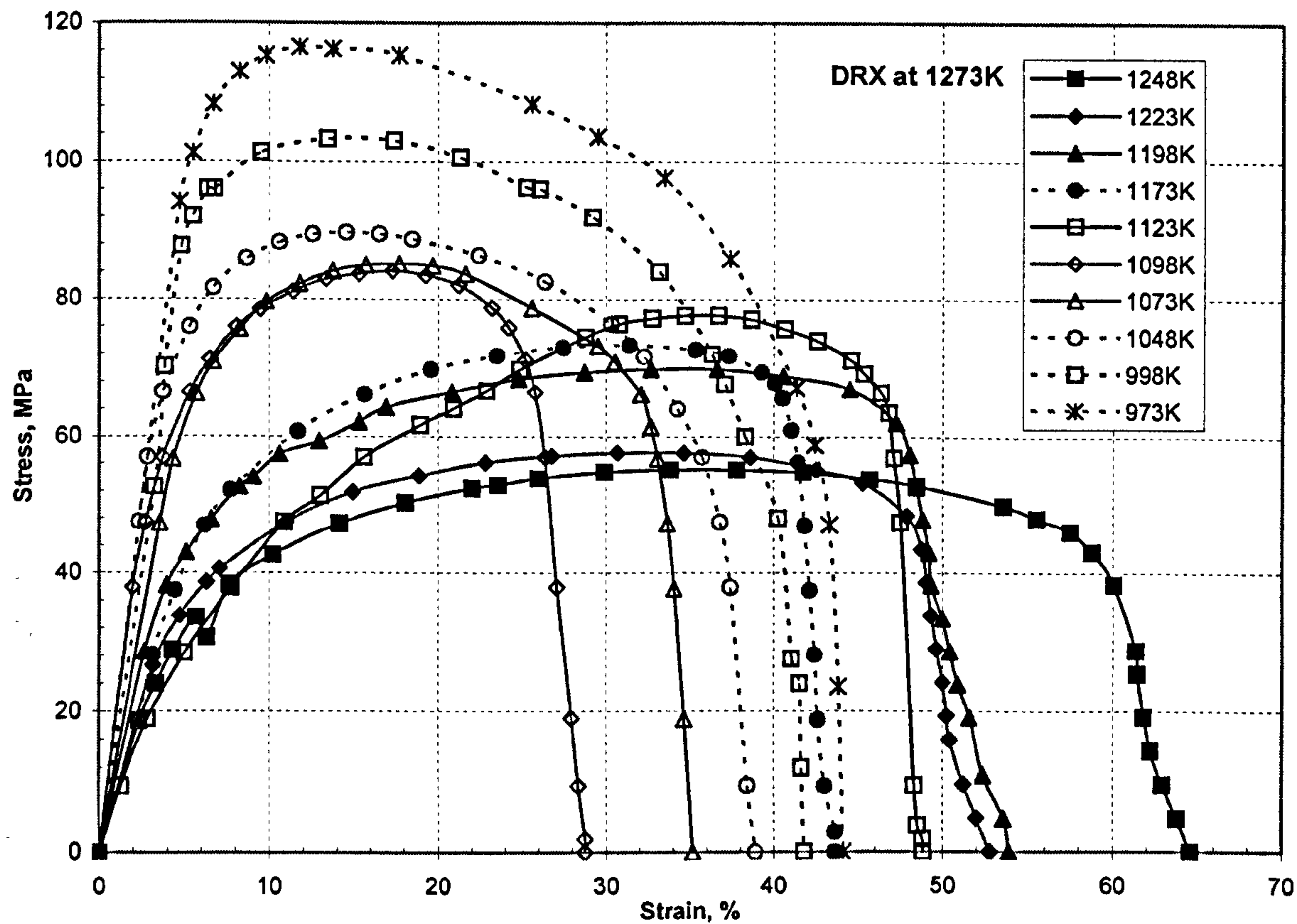


Figure 4.12: Stress strain curves for steel 3, showing no evidence of dynamic recrystallisation.

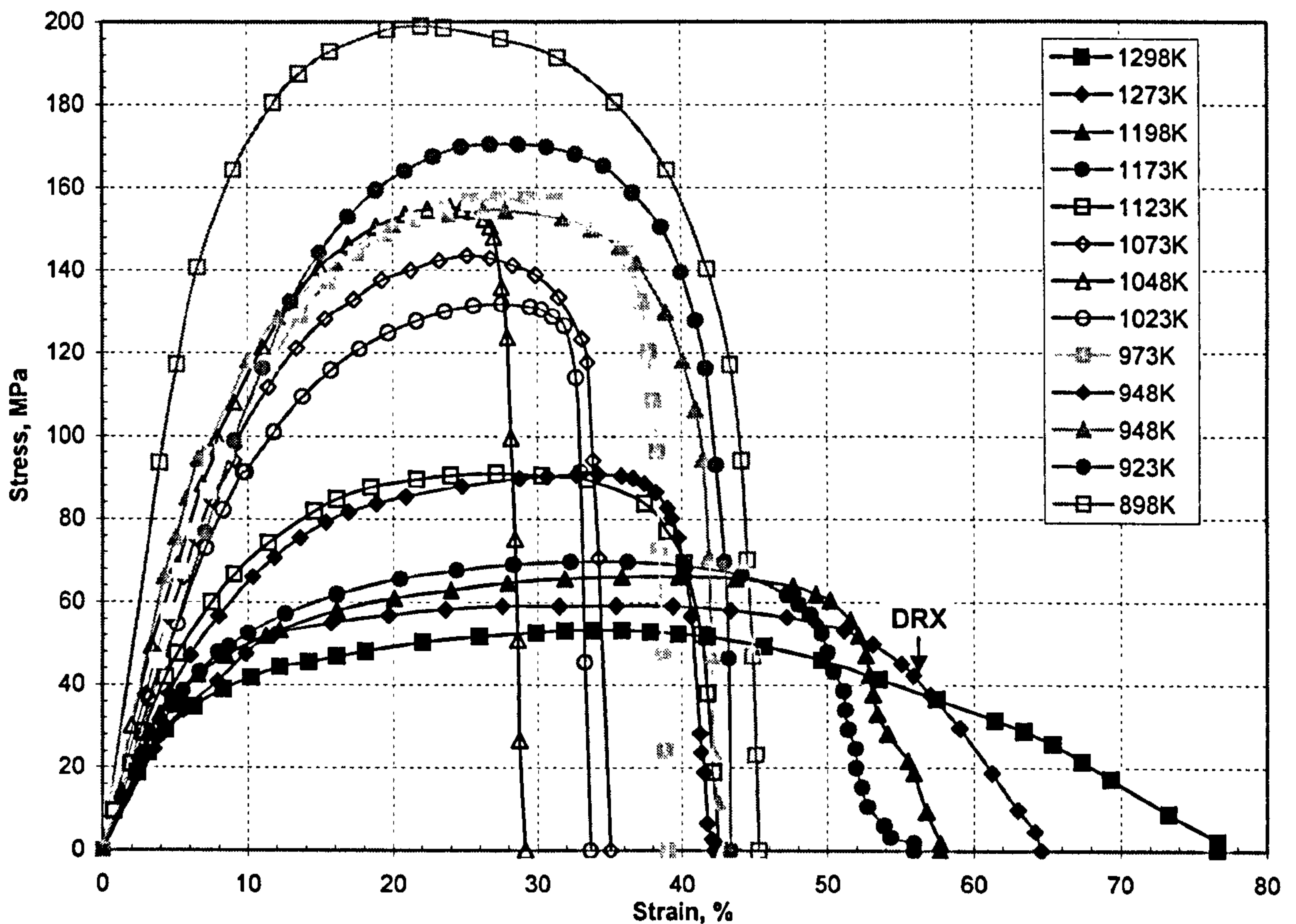


Figure 4.13: Stress strain curves for steel 4, showing evidence of dynamic recrystallisation.

4.4 Conclusions

In the four steels examined, the depth of the troughs were found to be similar, independent of the presence or absence of Nb. This insensitivity to the presence of Nb is believed to be due to the high P level in these steels reducing the amount of Nb(CN) precipitation in the grain boundary region.

Steel 4 (high C and Mn, C-Mn-Al-Nb) had the widest trough which extended for over 200K. In this steel, the trough below the A_{e3} temperature is due to the presence of a thin layer of DIF surrounding the γ grains. Since α is softer than γ , all the strain concentrates in these films; this causes voiding around the MnS inclusions resulting in low ductility intergranular ductile failures. The deformation induced ferrite at the γ boundaries is not able to develop into the matrix as the temperature is reduced and ductility only improves when the temperature has fallen below the A_{r3} (undeformed) and the normal transformation

induced ferrite forms in large quantities. Strain is then taken up more homogeneously in the structure and ductility therefore improves. Above the Ae_3 , the trough is extended to higher temperatures by grain boundary sliding in the γ and ductility improves gradually owing to coarsening of the Nb(CN) precipitates and the onset of DRX.

The narrowest trough was given by steel 1 (low C and Mn, C-Mn-Al); in this steel ductility recovered very rapidly on either side of the Ae_3 temperature. Above the Ae_3 , with the absence of Nb(CN) precipitation, DRX occurred easily. Below the Ae_3 , ductility improved rapidly owing to the formation of large amounts of DIF close to equilibrium volume fractions.

Steel 2 (high C and Mn, C-Mn-Al) had a trough which was extended at the low temperature end, below the Ae_3 in the same way as steel 4 (high C and Mn, C-Mn-Al-Nb). DIF only formed as thin films resulting in poor ductility. Above the Ae_3 , ductility again started to recover due to DRX, but this recovery was slower than for steel 1 (low C and Mn, C-Mn-Al), possibly because the Ae_3 temperature is lower reducing the driving force for DRX.

Steel 3 (low C and Mn, C-Mn-Al-Nb) gave a similar curve to steel 4 (high C and Mn, C-Mn-Al-Nb) at the high temperature end of the trough above the Ae_3 , owing to Nb(CN) delaying the onset of DRX. At the low temperature end, ductility still remained poor below the Ae_3 for about 30K, but further reduction in temperature caused ductility to improve and the curve then followed that for steel 1 (low C and Mn, C-Mn-Al) as large amounts of DIF were formed.

It is not entirely clear what is responsible for producing the large amounts of DIF in steels 1 and 3 (low C and Mn) which results in a narrowing of the trough. It is possible that a high transformation temperature may encourage the formation of DIF. This in itself may be enough and the presence of a high Si content in these steels will further raise the transformation temperature. However, another possible explanation is that the high Si

content could strengthen the ferrite sufficiently to encourage more of the γ to transform to α under deformation. However, further work is required to clarify these explanations.

When straightening at the low temperature side of the trough, compositional changes which raise the A_{r3} will always enable the straightening operation to be carried out at higher temperatures without risk of cracking. However, it is unclear at the present time whether the necessary requirement of having ~50% ferrite present can be achieved by very low deformation (2 - 4%) or whether much lower temperatures are needed to ensure that the ferrite is present before the straightening operation. Much lower temperatures would require either slower casting speeds, faster heat removal from the strand or a larger distance between the mould and the straightener. These process changes could result in productivity losses, higher thermal stresses on the solidifying strand or expensive machinery alterations.

5. Influence of Cooling Rate and Sulphides on Hot Ductility

5.1 Introduction

With the move to thin slab casters, it is important to assess the influence of faster cooling rates. In particular, faster cooling rates are likely to accentuate the fine strain induced precipitation of Nb(CN) making ductility worse and for plain C-Mn steels produce a finer distribution of sulphides which will also adversely affect the ductility. This section gave an opportunity to assess the importance of sulphides in influencing the hot ductility trough, as well as the influence of cooling rate on the A_{r3} .

Ductility troughs are commonly seen in steels tested in the temperature range 973K - 1273K with low strain rates of $\leq 10^{-3} \text{s}^{-1}$ and are accompanied by low ductility intergranular fractures.^{12,24,48,74,104} These intergranular fractures have been shown to occur normally either by strain concentration in the ferrite films forming around the γ grains,³⁸ or by precipitation at the γ grain boundaries; this precipitation prevents the movement of the boundaries and allows cracks formed by grain boundary sliding to link up.^{12,24,74,104,105} Nevertheless, hot ductility troughs have on occasions been observed in the γ phase, at low strain rates, without fine precipitates being present.⁷⁵ The failures that are observed have flat facets and show little evidence of voiding around the MnS inclusions, indicating that grain boundary sliding is the operative failure mechanism.³⁸

The trough in plain C-Mn steels is due to the formation of ferrite which occurs on transformation from the γ phase and is formed at the γ grain boundaries. In coarse grained material, the ferrite forms as a thin band around the γ grains and because it is generally softer than the γ , on deformation most of the strain concentrates within this film. On

¹⁰⁴ H.G. Suzuki, S. Nishimura, J. Imamura and Y. Nakumura: Trans. ISIJ, 1982, 22, p. 48.

¹⁰⁵ G.D. Funnell and R.J. Davies: Met. Technol., 1978, 5, p. 150.

deformation, voiding occurs around the MnS inclusions and the cavities produced gradually link up to give intergranular failure. Thus, as with ductile fracture, one would expect the volume fraction, size and shape of the inclusions to influence the R of A values.

As well as the depth of the trough being influenced by the MnS, the width has also been shown to be influenced by these Mn sulphides.⁷¹ At the low temperature end of the trough, elongated coarse MnS inclusions can encourage the formation of ferrite and hence cause ductility to improve more readily. At the high temperature side, the finer sulphides that can precipitate out at the γ boundaries on cooling to the test temperature can delay the onset of dynamic recrystallisation and hence widen the trough at this end.

This experiment was intended to obtain the relative importance of the form and distribution of sulphides at the boundaries, and to investigate the effect they have on the width and depth of the hot ductility curve or whether it is only micro-alloying additions that widen and deepen the trough. It was also hoped to gain useful information as to how the higher cooling rates, that thin slab casters are exposed to, influence cracking.

5.2 Experimental Details

C-Mn-Al steels were chosen for examination at two levels of Mn, 0.3 and 1.4% and two levels of S, 0.004 and 0.01 to 0.02% sulphur. The casts were supplied as 15mm hot rolled plate. Tensile samples (taken along the rolling direction) were solution treated at 1603K to allow varying amounts of sulphur to go back into solution, held for 5 minutes at this temperature and then cooled to test temperatures in the range 1273 – 973K. After holding for a further 5 minutes at the test temperature, the specimens were strained to failure at a strain rate of $3 \times 10^{-3} \text{ s}^{-1}$. Samples were quenched immediately after failure.

In addition, tensile samples from selected steels were cast at 1813K, held 5 minutes and cooled at 60 K min^{-1} to the same test temperature range. After holding these induction samples a further 5 minutes at test temperature, they were strained to failure at a strain rate of $3 \times 10^{-3} \text{ s}^{-1}$ based on an average gauge length of 22mm, i.e. length of molten sample within the induction coil. The compositions for these four steels are shown in Table 5.1.

Steel	Plate Code No.	C	Mn	Si	S	P	Al	N
5	P7H45	0.1	0.33	0.31	0.009	0.019	0.025	0.0049
6	P7H47	0.1	0.33	0.31	0.004	0.017	0.029	0.0046
7	P7H48	0.1	1.47	0.30	0.004	0.018	0.025	0.0041
8	P7H46	0.1	1.36	0.30	0.020	0.020	0.025	0.0047

Table 5.1: Analysis of steels studied in this section, wt. %.

These steels had Mn and S levels such that at 1603K either a) most of the S is in solution and available for precipitating out in the ferrite bands as spherical particles or b) the S will remain mainly as elongated MnS. It was expected that for the low Mn steels, all of the S will be in solution at 1603K for the lower S steel (0.004%) and most of the S, (0.006%) for the higher sulphur steel. For high Mn steels, little S will be in solution at 1603K, but will instead be mainly in the form of elongated MnS. The transformation temperatures of the four steels are shown in Table 5.2. Dilatometry followed the sample heating programme as closely as possible; however, the maximum temperature was limited to 1653K and the samples were not held for 5 minutes at the test temperature.

Steel	Transformation Temperatures, K		
	Ae3	Ae ₁	Ar ₃
5	1147	988	1071
6	1147	988	1083
7	1105	942	999
8	1109	946	999

Table 5.2: Transformation temperatures of steels examined, K (at 60Kmin⁻¹). The A_e temperatures were calculated using the Thermocalc program and the A_r temperatures by dilatometry.

5.3 Results and Discussion

Table 5.3 shows the amount of S in solution at 1603K and wt. percent of MnS that can be produced on cooling, assuming all S is re-precipitated out (relative atomic mass [Mn+S]/S multiplied by %S in solution = 2.714 x %S). It can be seen that most, or all, of the S is taken into solution for the low Mn steels 5 and 6, but only ~0.0016% for the high Mn steels - independent of whether the total S content is 0.004 or 0.020%. The calculated equilibrium curve of %S in solution against temperature is shown in Figure 5.1.

Steel	Wt. % Mn	Wt. % S	Wt. % S in Solution at 1603K	Wt. % MnS precipitation on cooling (spherical particles)
5	0.33	0.009	0.0062	0.017
6	0.33	0.004	0.0040	0.011
7	1.40	0.004	0.0015	0.004
8	1.36	0.020	0.0017	0.005

Table 5.3: Amount of S in solution at 1603K and the quantity of MnS able to precipitate out on cooling to the test temperature.

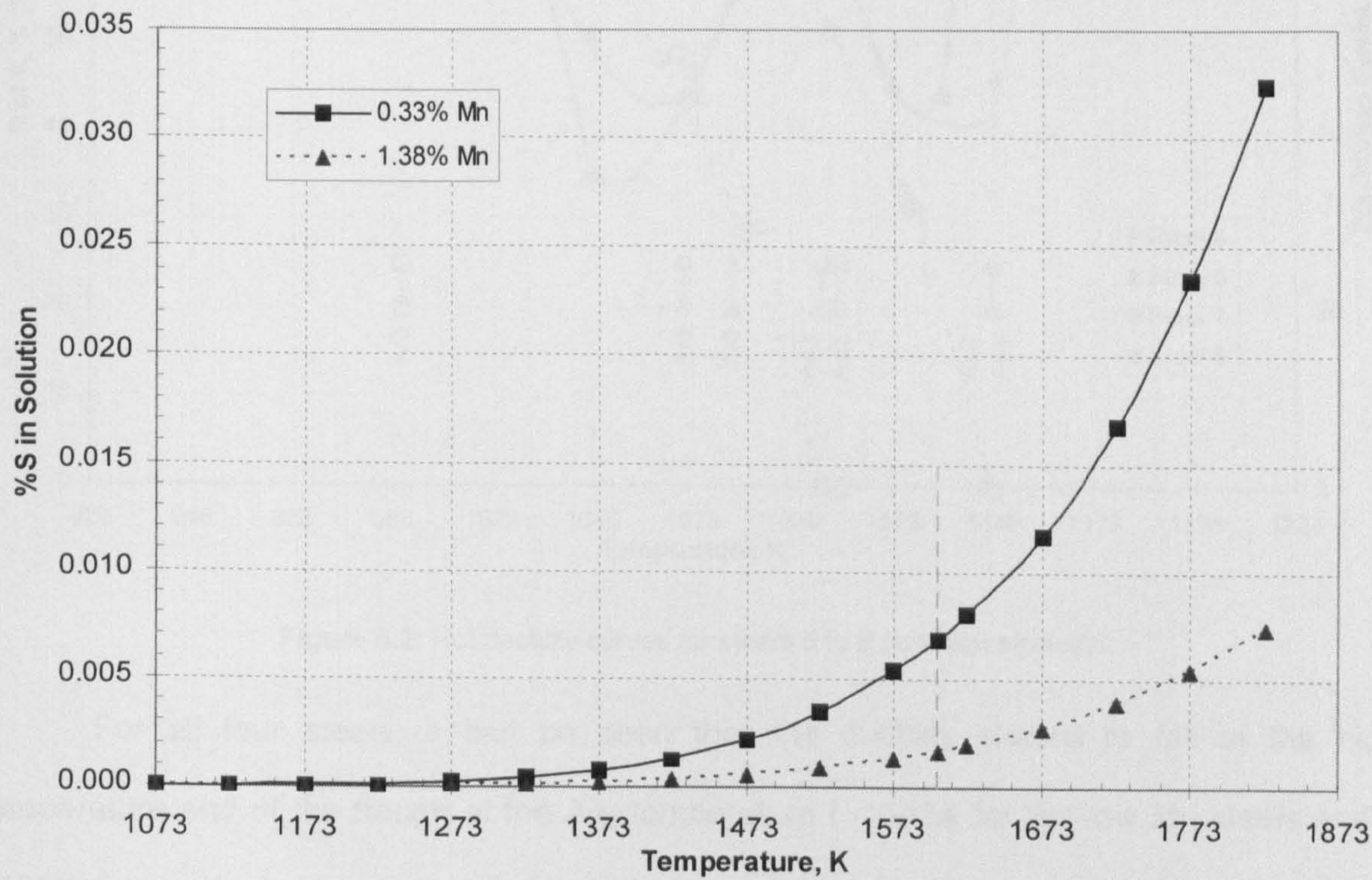


Figure 5.1: Calculated equilibrium %S in solution versus temperature for the two Mn levels.

The hot ductility curves for the four steels studied are shown in Figure 5.2, and can be seen to divide themselves into two groups, one for the low Mn steels, in which the trough occurs in the narrow temperature range ~ 1098K to 1148K, and the other for the high Mn steels in an equally narrow lower temperature range ~ 1033K to 1093K. The sulphur content can be seen to have only a small influence on the hot ductility behaviour. The equilibrium amounts of ferrite present (dashed curves) and the A_{e3} and A_{r3} temperatures, calculated using the Thermocalc program and measured from dilatometry respectively, are also shown on this figure.

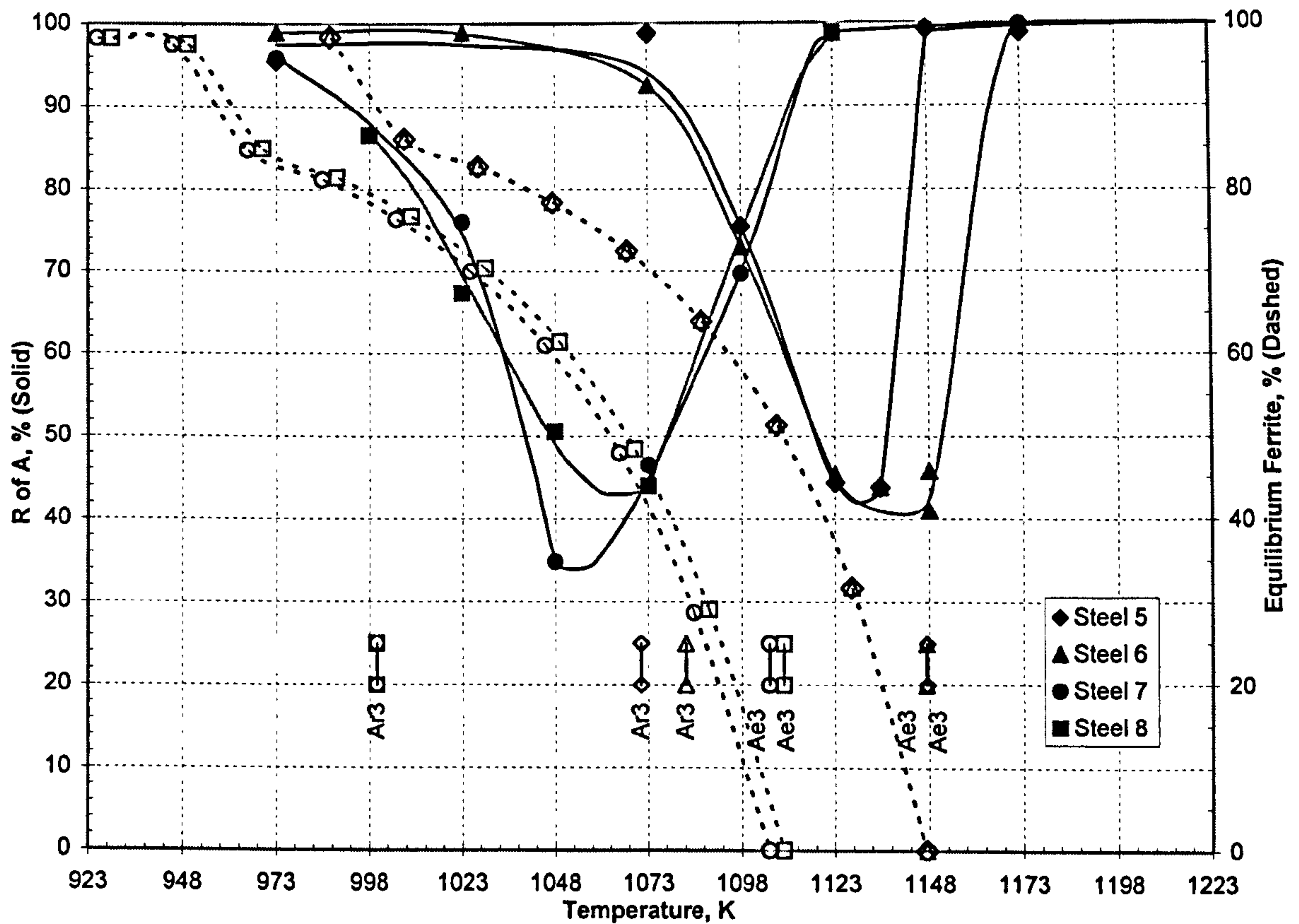


Figure 5.2: Hot ductility curves for steels 5 to 8 (solution treated).

For all four steels, it can be seen that the ductility started to fall at the high temperature end of the trough at the Ae_3 temperature ($\sim 1143K$ for the low Mn steels and $\sim 1103K$ for the high Mn steels). As seen in the previous chapter and previous work,⁷² the troughs were caused by a thin band of ferrite which rapidly increased in thickness as the temperature fell below the minimum ductility temperature, see Figures 5.3 – 5.6. For example for steel 5, Figure 5.3, the thin film of ferrite forms at 1123K, Figure 5.3(b), and this rapidly increases in thickness, (c) and (d), as the temperature decreases to 1073K when ductility fully recovers, Figure 5.2. Behaviour is similar for the other steels, Figures 5.4 – 5.6. The Ar_3 temperatures were always well below the Ae_3 temperatures, see Table 5.2, indicating that all the ferrite associated with the trough was deformation induced.

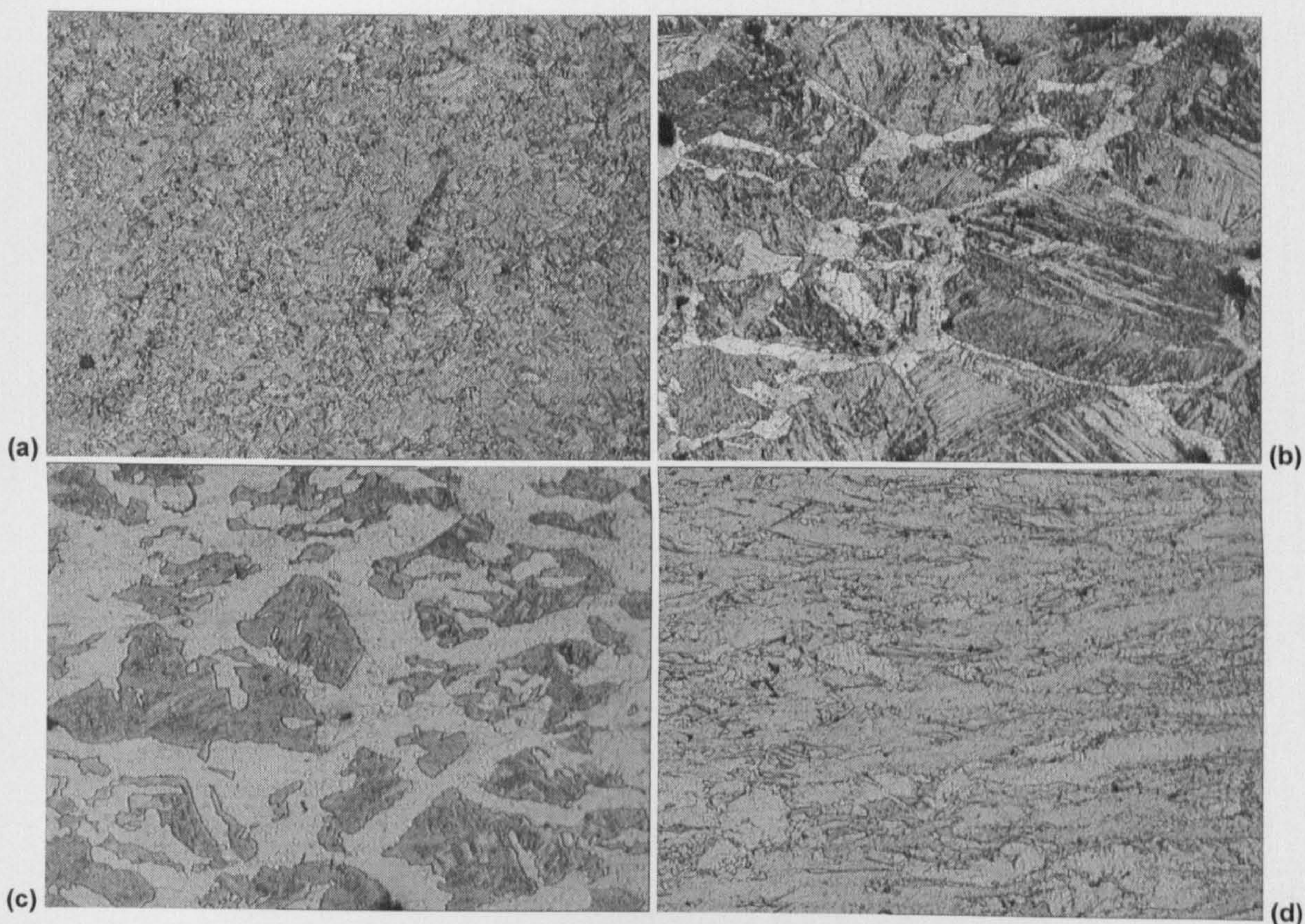


Figure 5.3: Digital micrographs (mag. x60) of steel 5 at (a) 1148K, fully austenitic (b) 1123K, thin ferrite film (c) 1098K, thickened films + ferrite in matrix, and (d) 1073K, structure nearly fully ferritic.

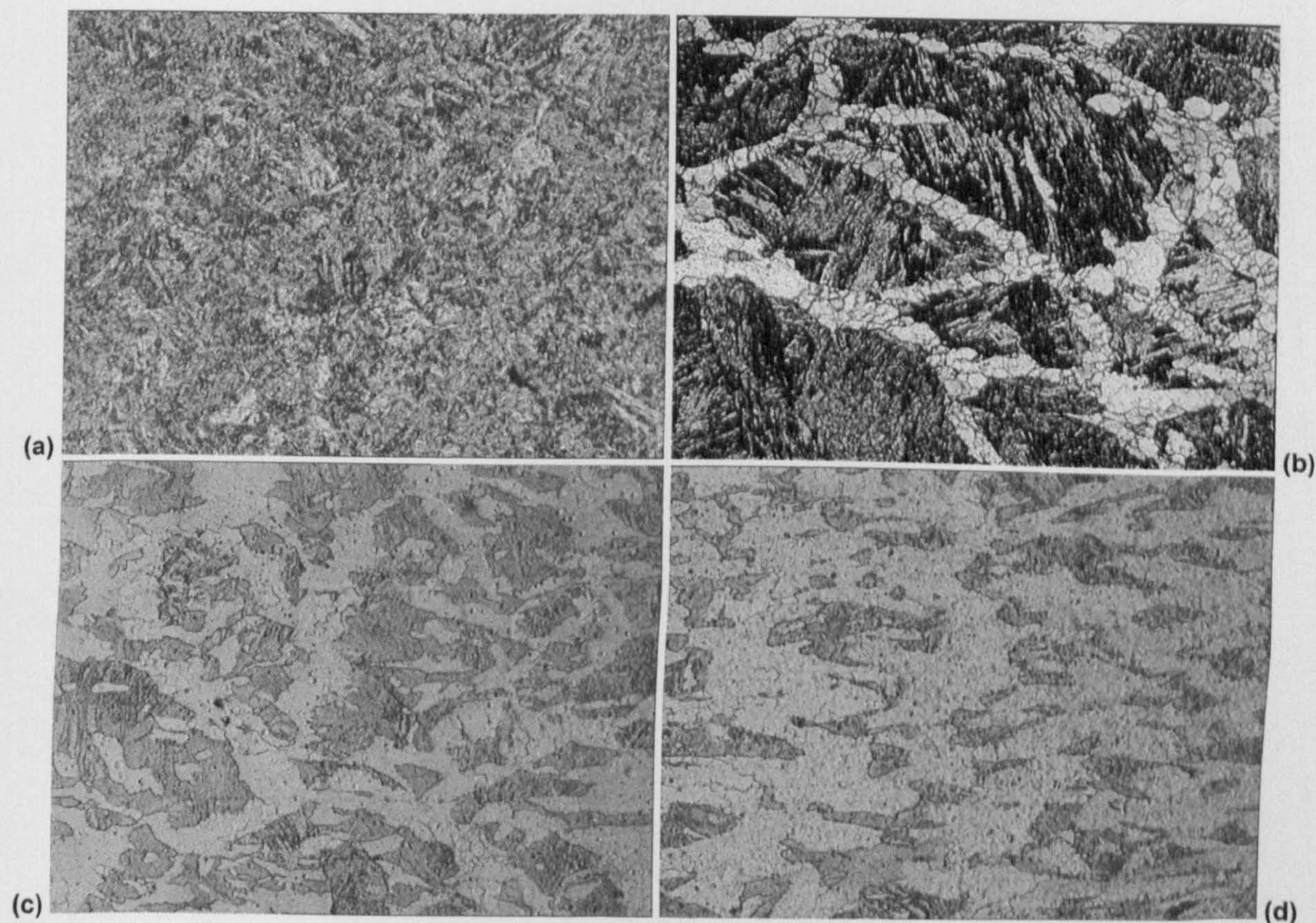


Figure 5.4: Digital micrographs (mag. x60) of steel 6 at a) 1173K, fully austenitic b) 1123K, thin ferrite film c) 1098K, thickened films + ferrite in matrix, and d) 1073K, structure nearly fully ferritic.

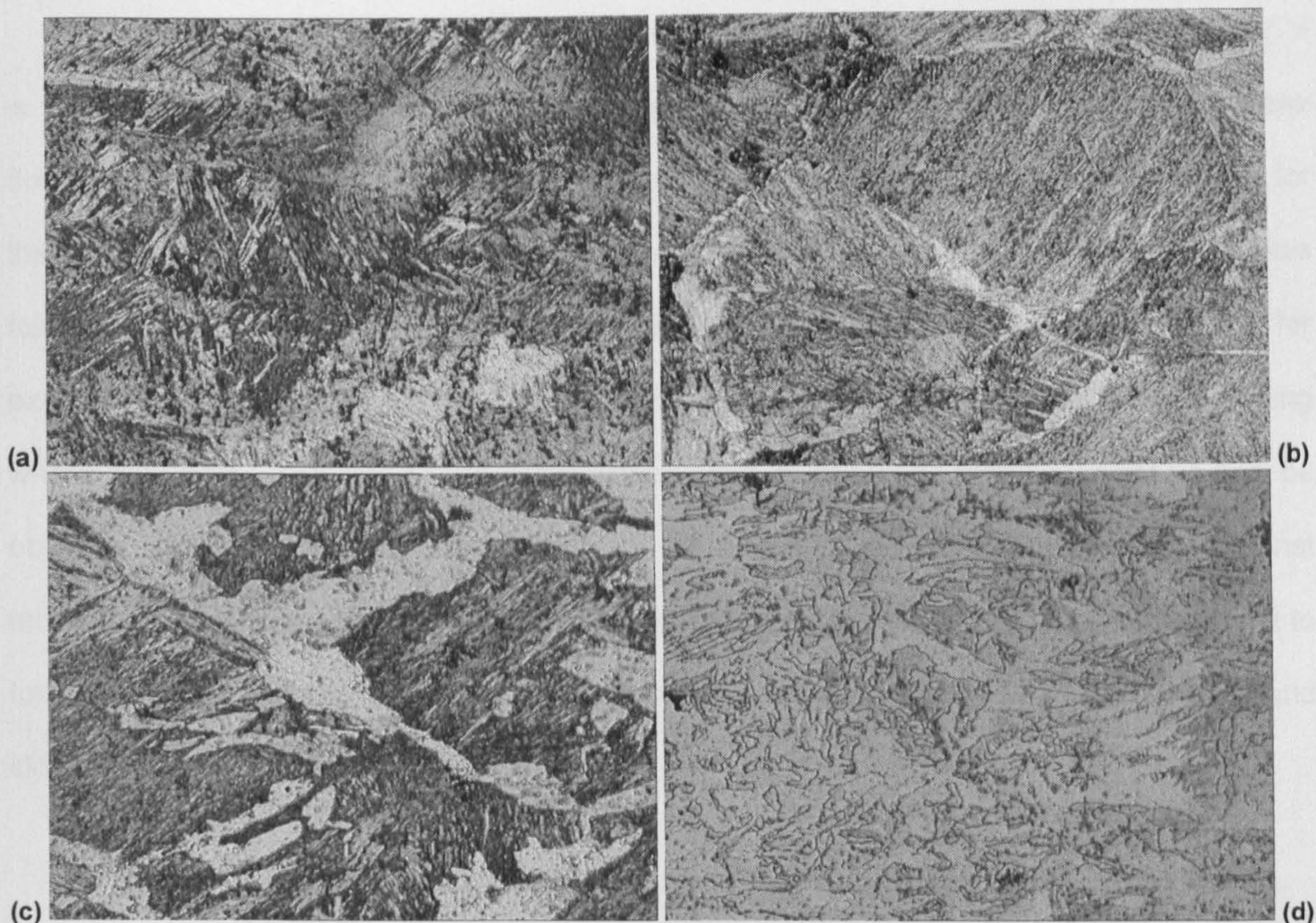


Figure 5.5: Digital micrographs of steel 7 (mag. x60) at (a) 1073K, fully austenitic (b) 1048K, thin ferrite films, (c) 1023K, thickened films + ferrite in matrix, and (d) 973K, nearly fully ferritic.

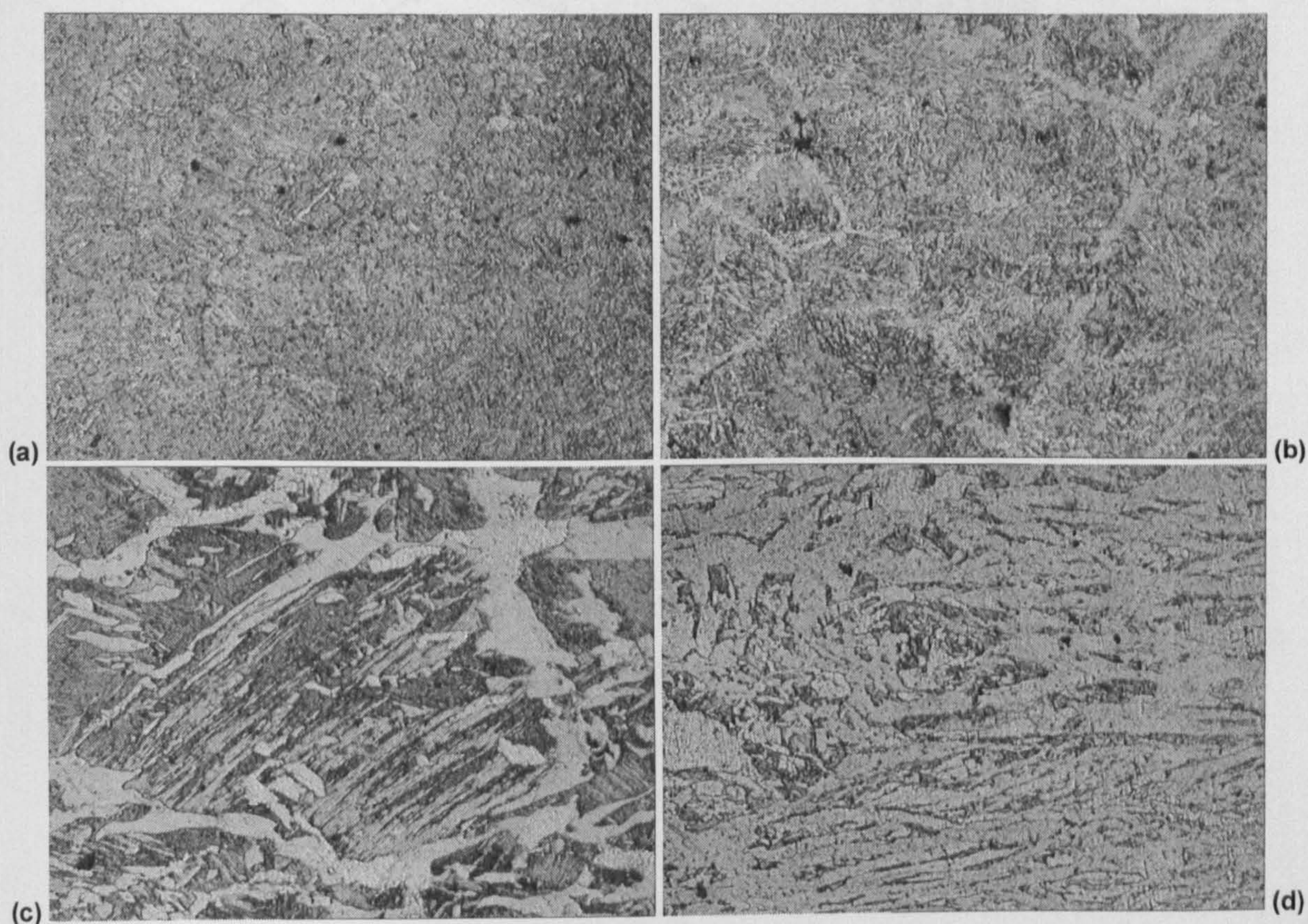


Figure 5.6: Digital micrographs (mag. x60) of steel 8 at (a) 1123K, fully austenitic (b) 1073K, thin ferrite film (c) 1023K, thickened films + ferrite in matrix, and (d) 998K, structure nearly fully ferritic.

The flow curves for the steels examined are given in Figures 5.7 – 5.10. However, it is not easy to identify the temperature for the start of dynamic recrystallisation from these flow curves by load fluctuations, this is because similarly shaped curves are produced for the onset of DRX and for when DIF first forms; in both cases, there is a drop in stress followed by an extensive elongation prior to fracture. This can be seen from Figure 5.7, for example, where the curves at 1073 and 1173K have similar shapes; the 1073K curve being where DIF forms and the 1173K curve when DRX is possible. More information can be obtained by drawing the curves of strain to the peak stress and the peak stress against temperature, Figures 5.11 and 5.12 respectively. Figure 5.12 shows that it is more difficult to form DIF in high Mn steels; this is because of the lower transformation temperature and slower diffusion rates.

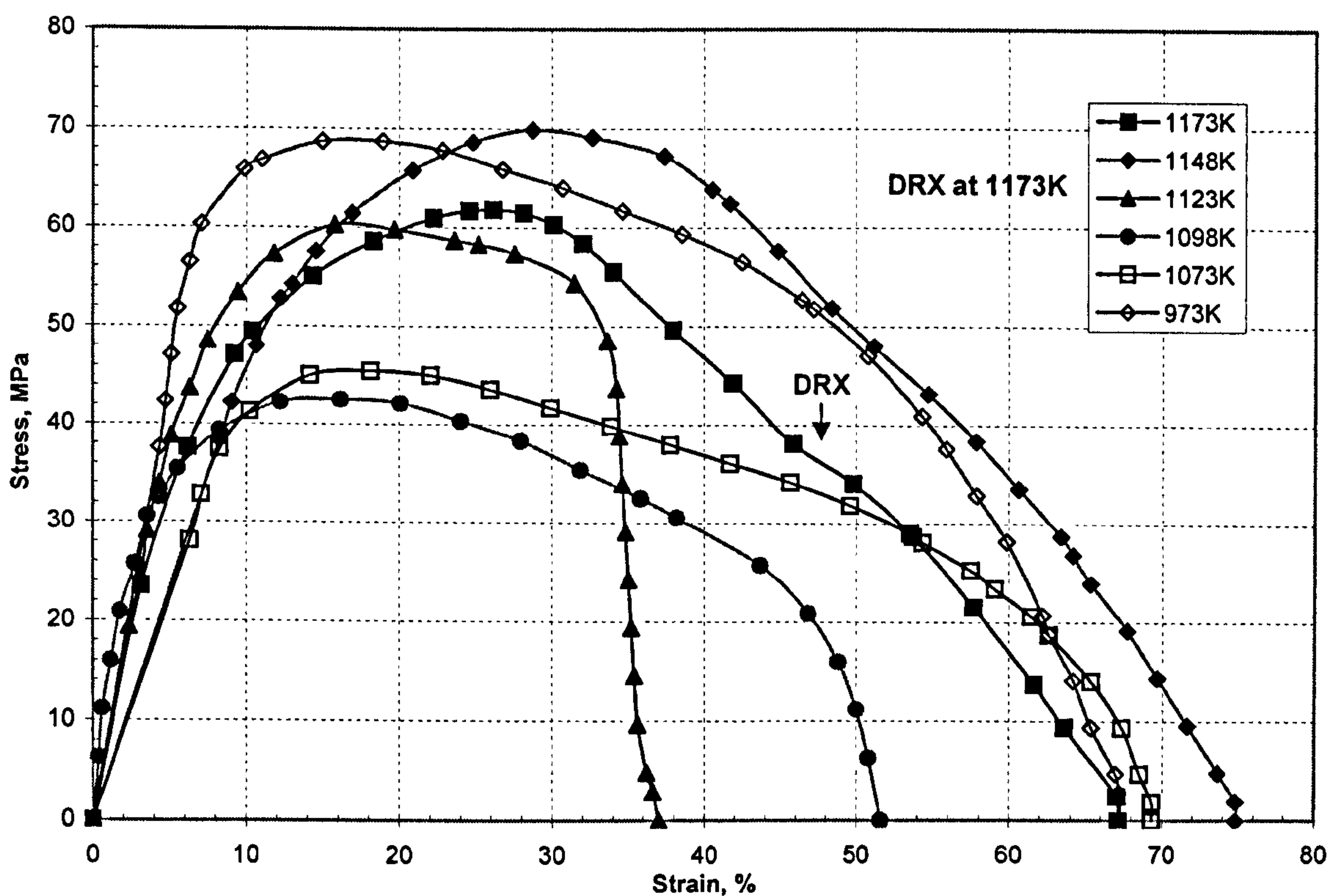


Figure 5.7: Stress strain curves for steel 5, showing onset of dynamic recrystallisation.

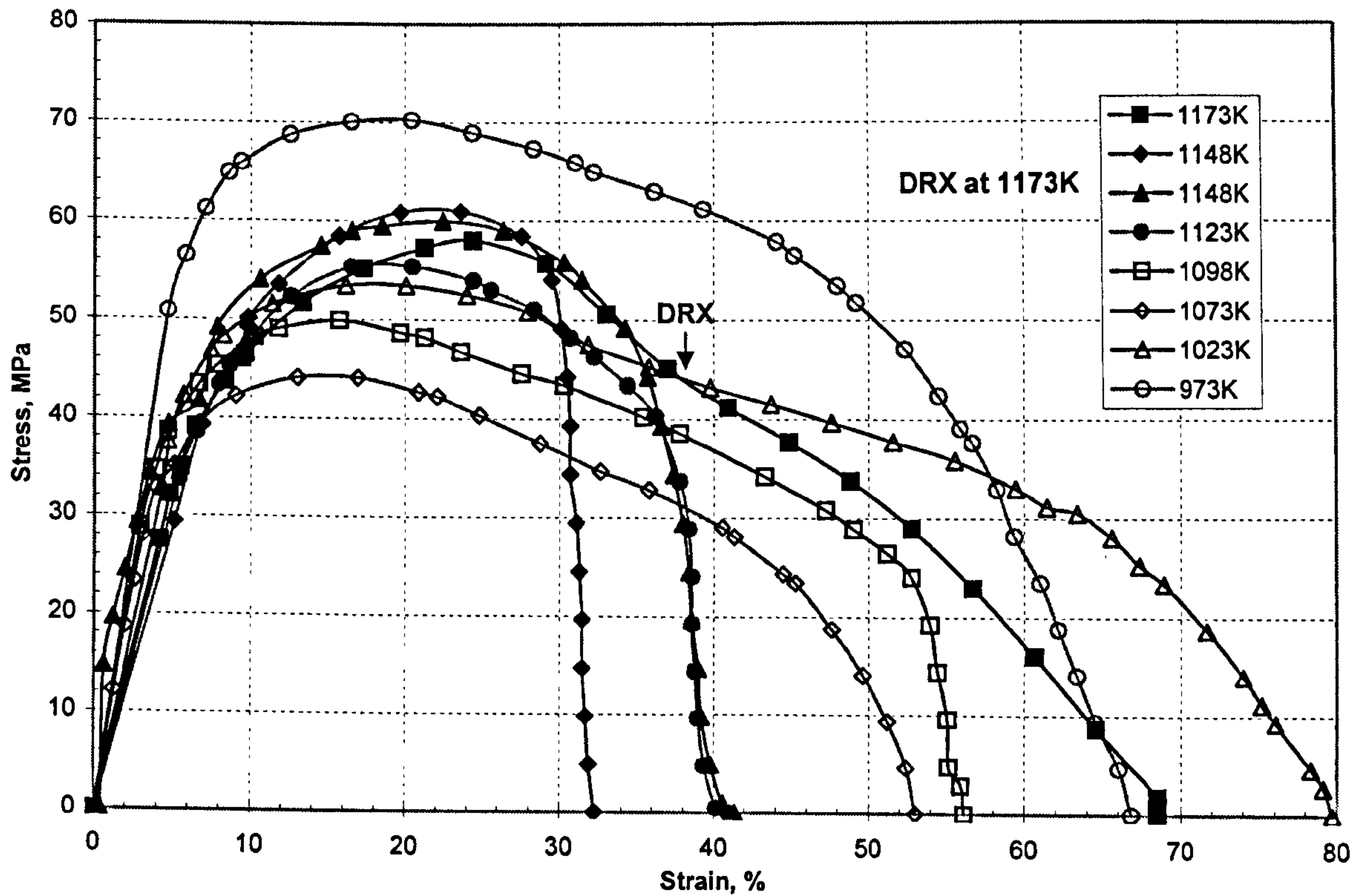


Figure 5.8: Stress strain curves for steel 6, showing onset of dynamic recrystallisation.

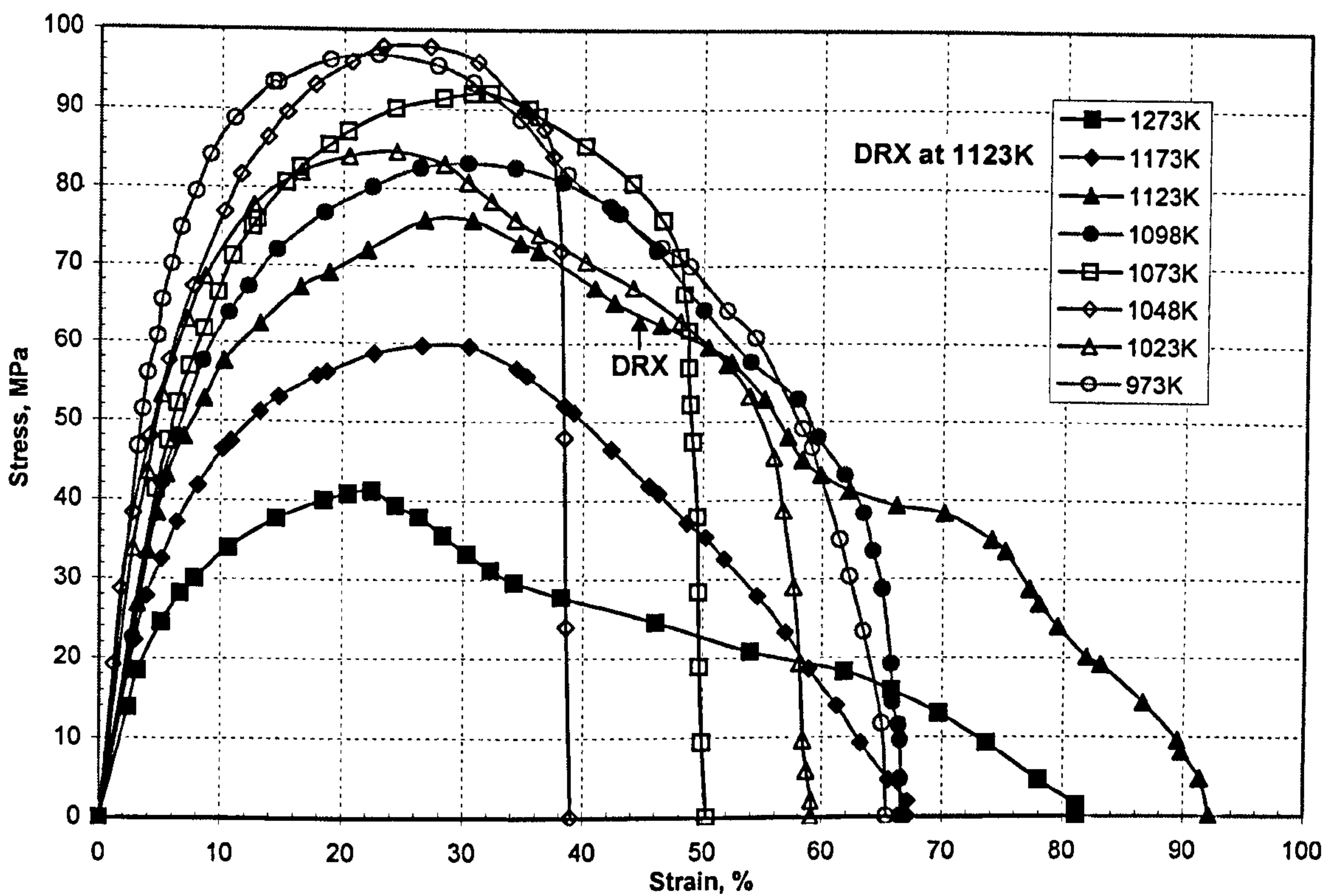


Figure 5.9: Stress strain curves for steel 7, showing no evidence of dynamic recrystallisation.

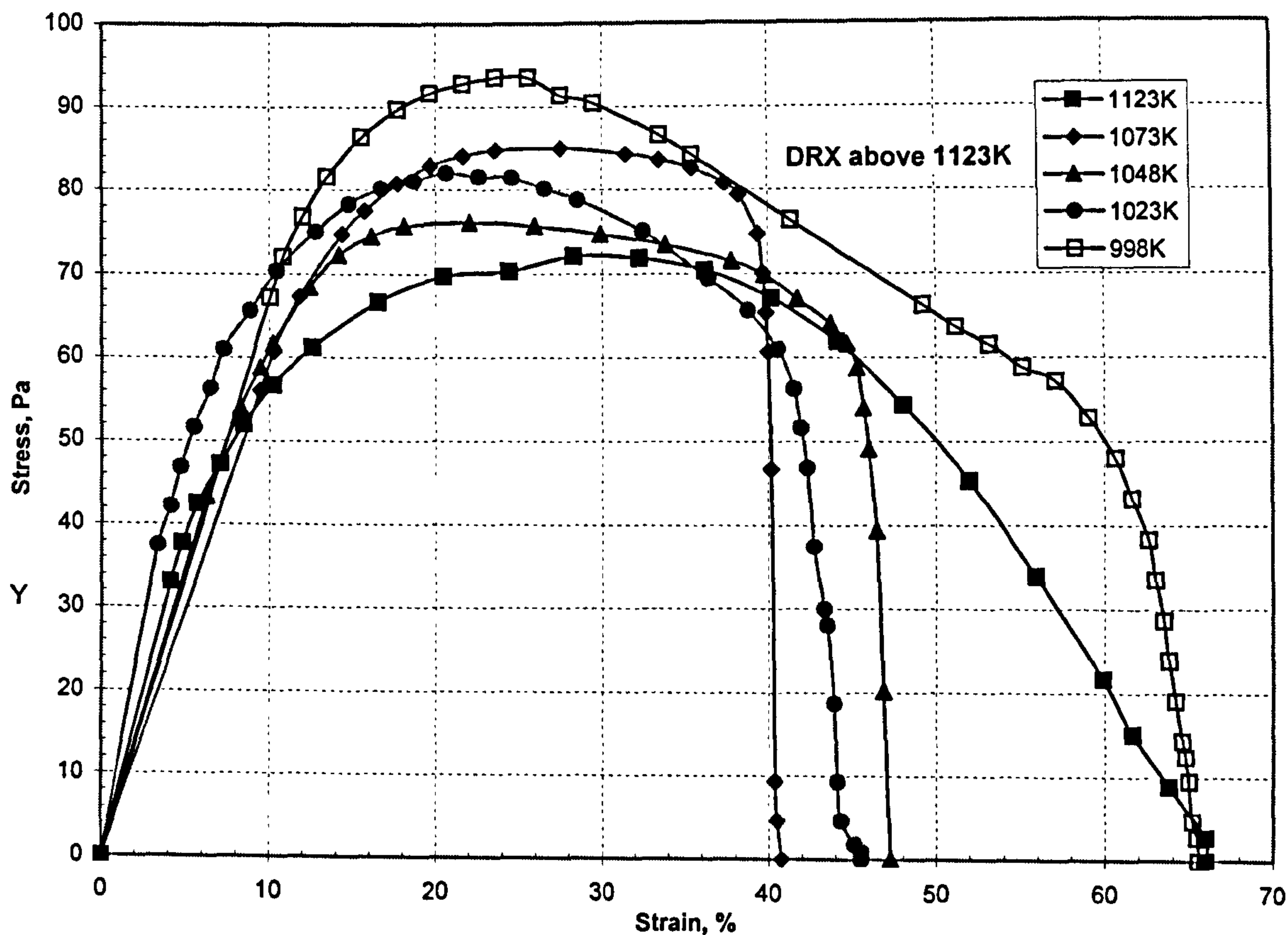


Figure 5.10: Stress strain curves for steel 8, showing evidence of dynamic recrystallisation.

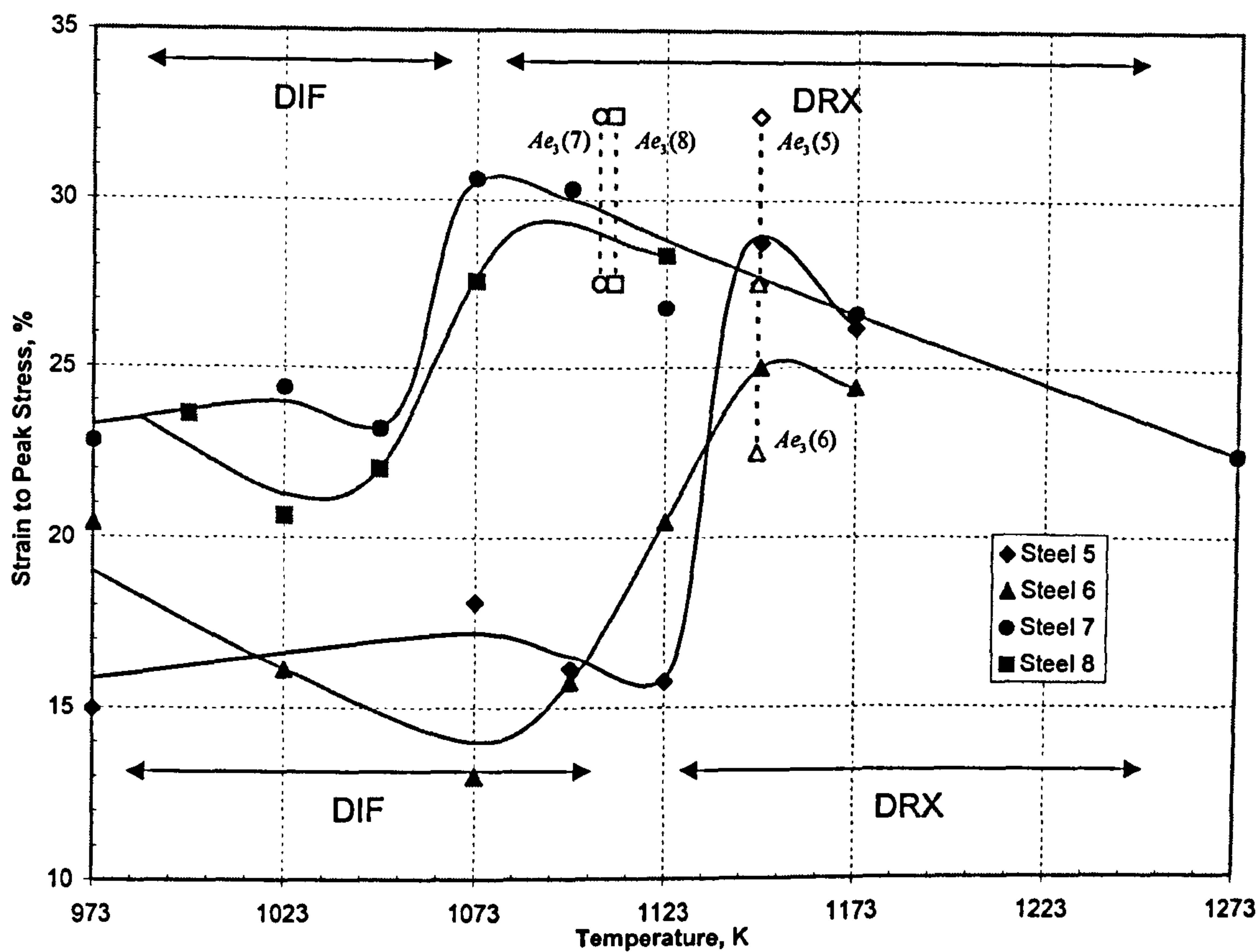


Figure 5.11: Curves of the strain to the peak stress against temperature for steels 5 to 8.

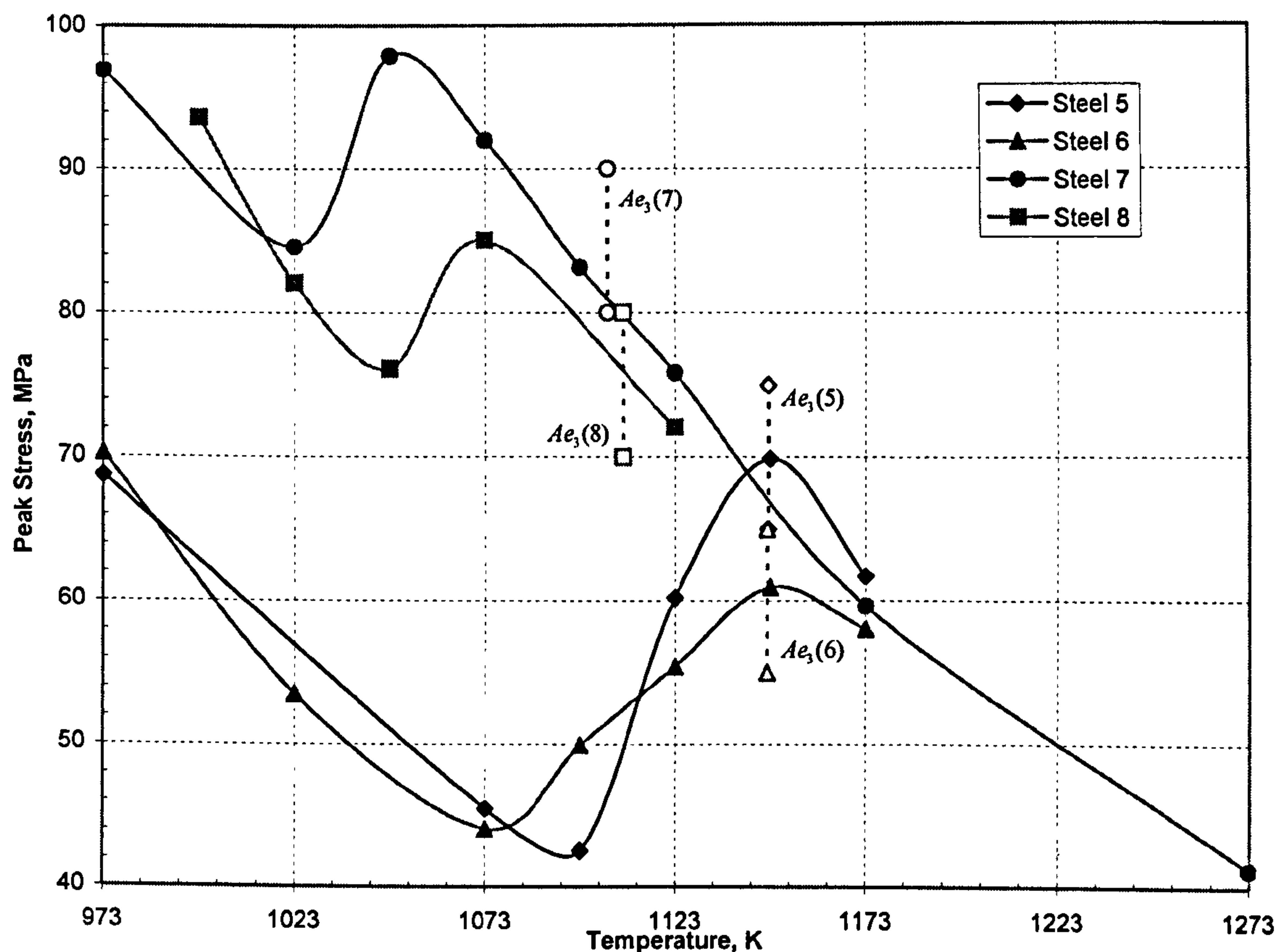


Figure 5.12: Curves of peak stress against temperature for steels 5 to 8.

5.3.1 Analysis of Flow Curves

a) Flow curves in present chapter 5

For the low Mn steels, steels 5 and 6, it can be seen from Figure 5.11 that there is a peak strain for the production of deformation induced ferrite of about 15% throughout the temperature range 973K to 1098K (It should be noted that as for dynamic recrystallisation, the critical strain for deformation induced ferrite is likely to be significantly less than the strain to the peak stress). The maximum stress throughout this temperature range decreases with increase in temperature, Figure 5.12.

On raising the temperature above ~1113K for the high S steel, steel 5, and 1143K for the low S steel, steel 6, both the peak strain and peak stress increase, Figures 5.11 and 5.12 respectively. This is a clear indication that the softening process has changed from the production of deformation induced ferrite to the onset of dynamic recrystallisation. Thus, at

the low Mn level, dynamic recrystallisation requires both higher strains and stresses. Increasing the temperature once dynamic recrystallisation can occur leads to the normal reduction in peak stresses and strains.

For the high Mn steels, steels 7 and 8, greater stress and strain is required for the formation of deformation induced ferrite than with the low Mn steels, Figures 5.11 and 5.12. It can be seen that it is far more difficult to produce deformation induced ferrite in the high Mn steels. The maximum stress progressively decreases with temperature, independent of whether deformation induced ferrite or dynamic recrystallisation is the operative mechanism.

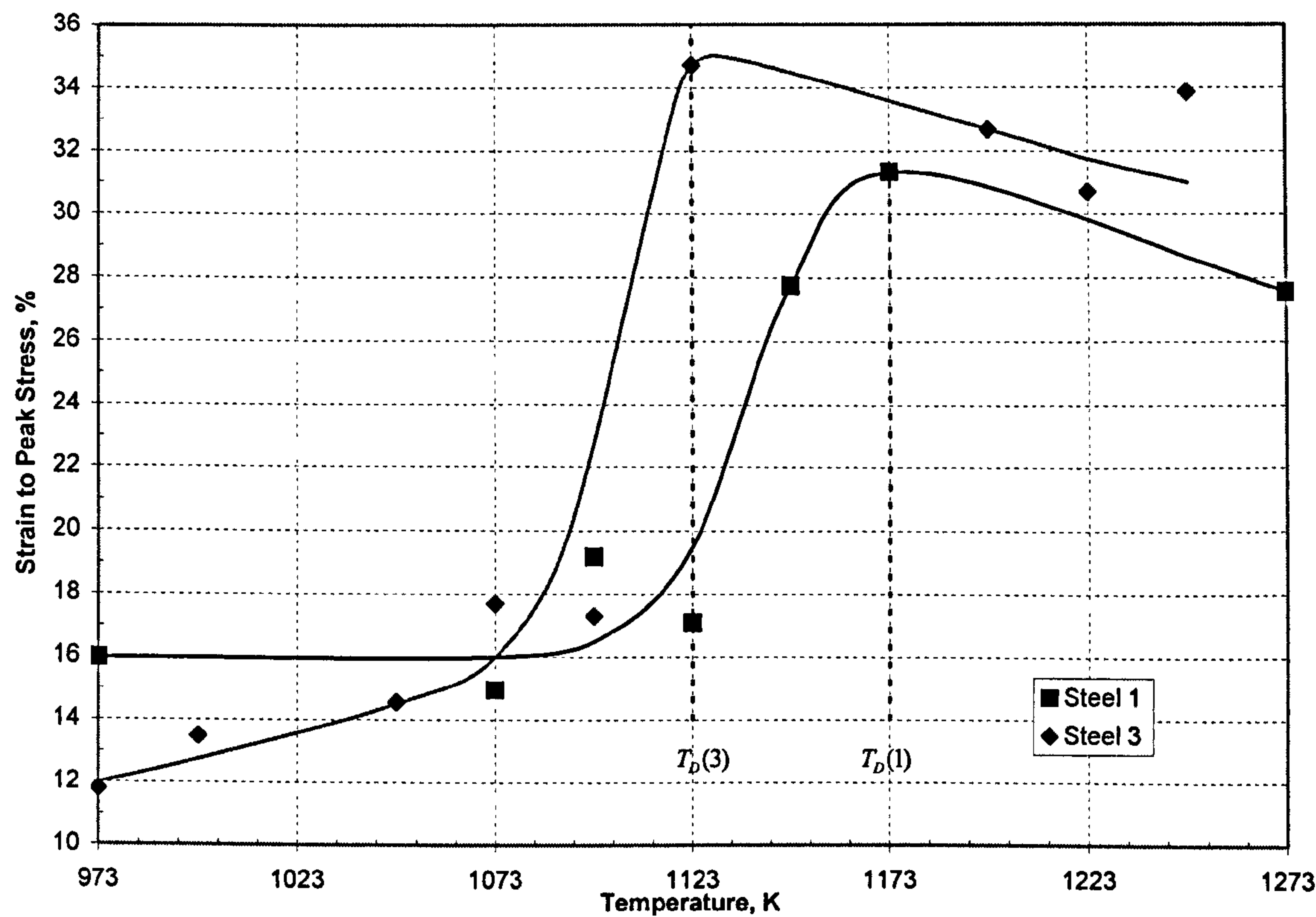
In the present work, it has been shown that sulphur/sulphides do not generally have a major influence on the hot ductility of solution treated C-Mn-Al steels, Figure 5.2. This is because, for the steels examined, the temperature range in which a thin band of ferrite surrounds the γ grain boundaries is very limited. As such, the trough is governed mainly by the A_{e3} and A_{r3} temperatures, which are little influenced by the sulphur levels.

b) Analysis of flow stress curves in previous chapter 4

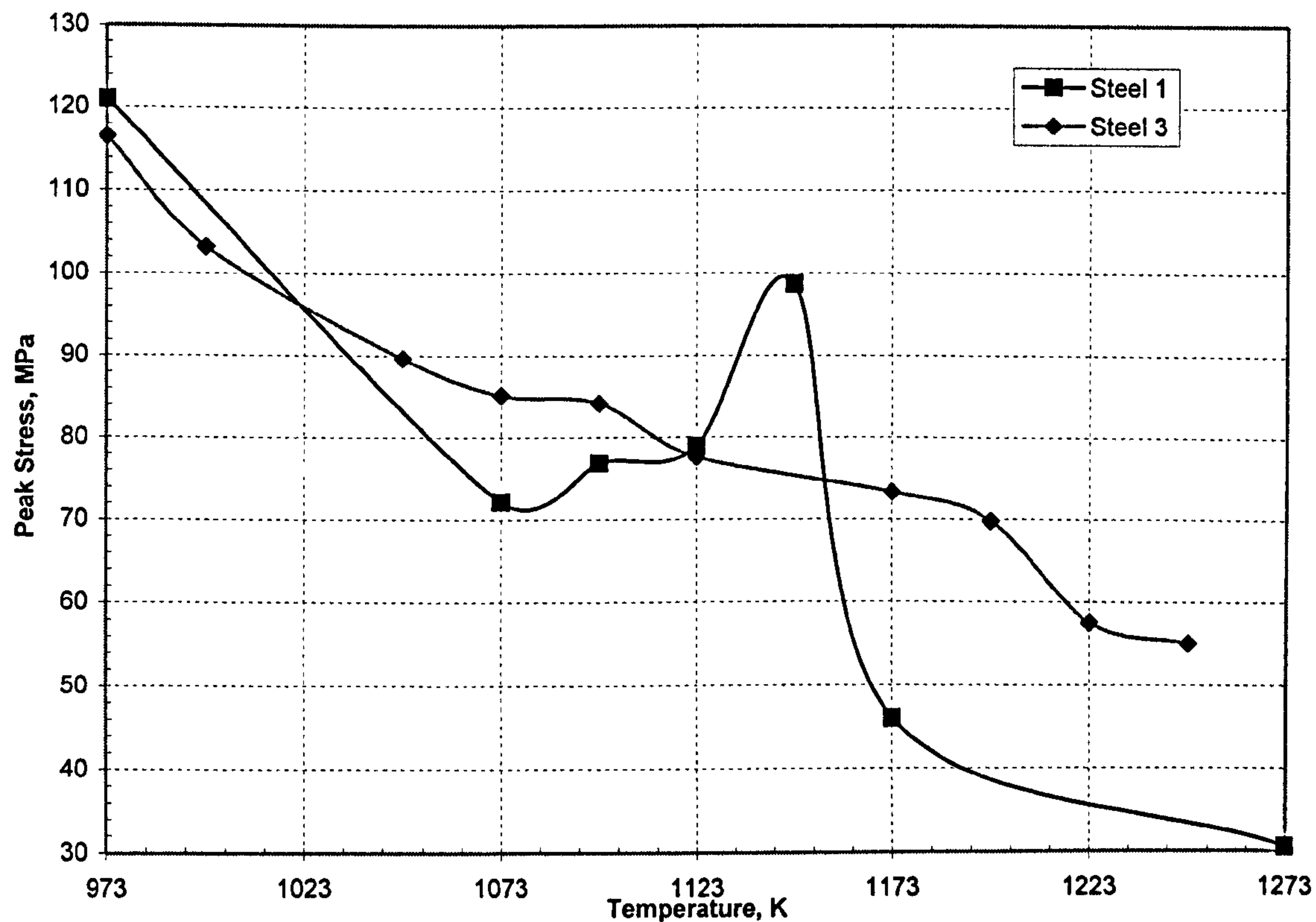
The same approach can also be used for the steels with narrow troughs that were examined in the previous chapter, chapter 4, steels 1 and 3. The curves of strain to the peak stress against temperature and peak stress against temperature are given in Figure 5.13a and 5.13(b) respectively. Again, the temperature for the onset of dynamic recrystallisation, T_D , can be readily determined from Figure 5.13(a). For the Nb containing steel, steel 3, the curve of peak stress v temperature does not show a peak at T_D , Figure 5.13(b), but this may be because insufficient testing was carried out to establish the peak. It can be seen that once dynamic recrystallisation is established, that both the strain to the peak stress and peak stress for a given temperature are higher for the Nb containing steel 3.

For the steels having the wide troughs, 2 and 4, the situation is more complex, see Figures 5.14(a) and 5.14(b). Two salient points can be noted in Figure 5.14(a), the first relates to the A_{r3} temperature, below which large amounts of ferrite are formed prior to deformation. This leads to a reduced strain to the peak stress as the temperature is reduced – this being normal work hardening behaviour for ferrite. Above the A_{r3} , only a very small amount of ferrite forms under deformation and for the plain C-Mn steel, the strain is approximately constant throughout this range from 973 to 1173K. The next salient point is when dynamic recrystallisation can take place, and the strain to peak stress gradually falls with temperature. One would estimate this for the plain C-Mn steel to be between 1173 and 1273K.

In the case of the Nb containing steel, steel 4, the A_{r3} temperature can be clearly identified in Figure 5.14(a) as 953K, but above this temperature, the strain first decreases and then increases again, through the temperature range 953 to 1193K. Again, only a small amount of ferrite forms between the A_{r3} and A_{e3} , 953 and 1090K and above this temperature it would appear that deformation is solely in the austenite without DRX occurring. Recrystallisation probably occurs at a temperature between 1193 and 1273K, when the strain starts to decrease with the increase in temperature.

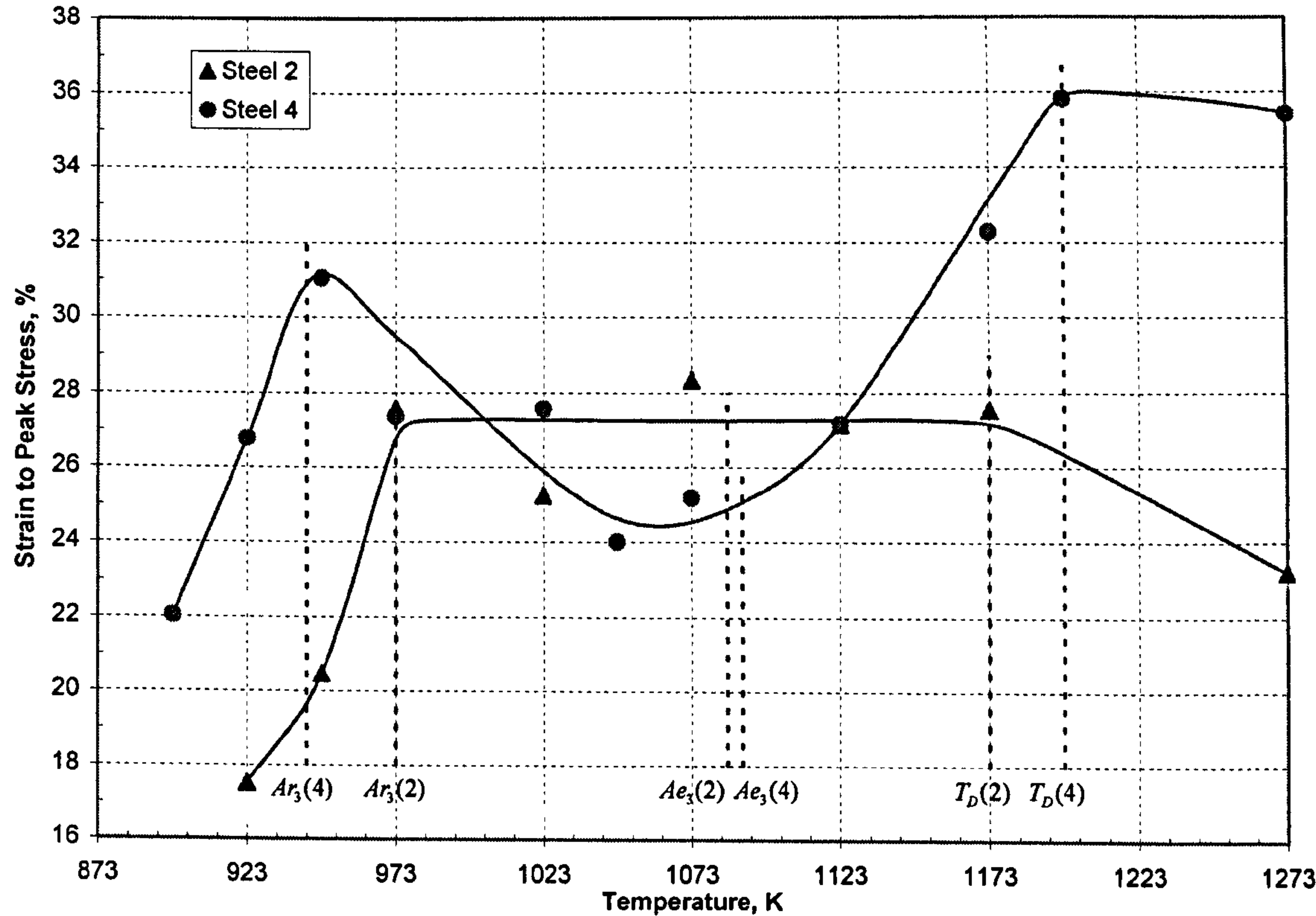


(a)

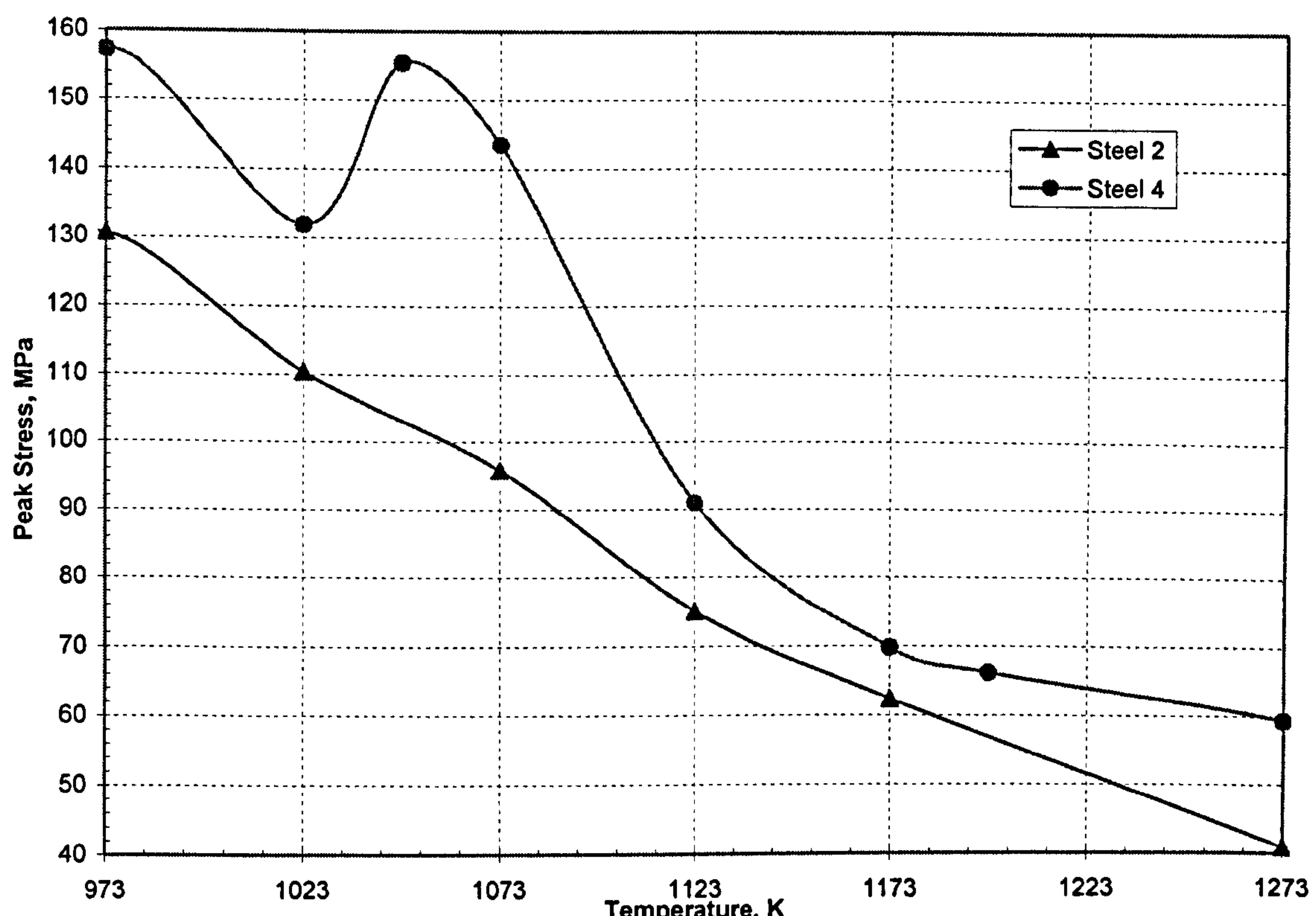


(b)

Figure 5.13: Curves of a) strain to the peak stress and b) peak stress against temperature for steels 1 and 3.



(a)



(b)

Figure 5.14: Curves of a) strain to the peak stress and b) peak stress against temperature for steels 2 and 4.

5.3.2 Conditions required for obtaining a narrow trough

For the steels examined in this chapter, steels 5 to 8, ductility recovery at the low temperature end of the trough is due to the formation of large amounts of deformation induced ferrite (DIF) just below the A_{e3} giving relatively narrow troughs. Deformation induced ferrite formed very readily in these steels in almost equilibrium amounts even in the high Mn steels, as can be seen from Figure 5.15 which plots the equilibrium and observed amounts of ferrite against temperature. When this happens there is no defined depth to the trough and it is not possible to accurately determine the depth. Thus, although the amount of S in solution varied considerably both in solution at 1603K and in the volume fraction of sulphides present, the actual "depth" of the trough changed little, see Table 5.4 and Figure 5.2.

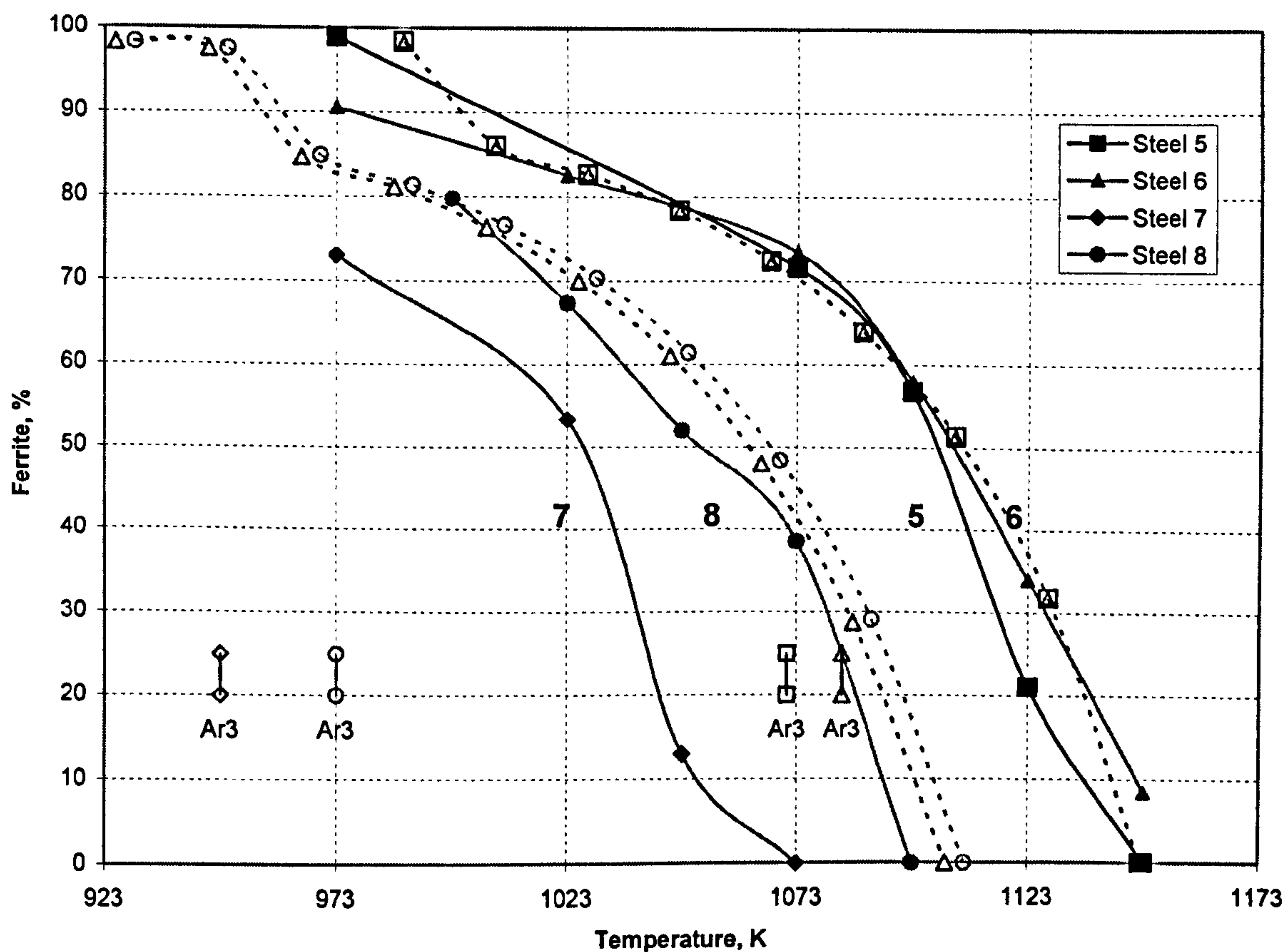


Figure 5.15: Curves of equilibrium (dashed) and observed (solid) percentage ferrite for steels 5 to 8.

Steel	Wt. %S	Wt. %Mn	Tot. Vol. fract. elongated MnS after hot rolling	S in solution at 1603K, wt. % x10 ⁻³	Volume fraction spherical MnS precipitating after solution treatment
5	0.009	0.330	0.048	6.249	0.033
6	0.004	0.330	0.021	4.000	0.033
7	0.004	1.470	0.021	1.546	0.008
8	0.020	1.360	0.107	1.678	0.009

Table 5.4: Percentage S in solution at 1603K and the volume fraction of MnS present in the steels after both hot rolling and solution treatment.

It can be seen from Figure 5.2, which plots equilibrium volume fraction of ferrite against temperature, that as in the previous chapter, there is a good relationship between this and the R of A values. The previous chapter had suggested that narrow troughs could only be formed at high A_{e3} temperatures of $\sim 1153\text{K}$, i.e. since DIF is diffusion controlled, the higher temperatures should encourage its formation.

However, in the present instance, the narrow troughs are being produced at much lower temperatures of $\sim 1103\text{K}$. It may be that the present work has just covered the A_{e3} temperature range in which the changeover from a wide to a narrow trough occurs. In the previous chapter, the A_{e3} temperatures for the wide troughs were 1085K to 1090K , whereas in this chapter the lowest A_{e3} temperature is 1105K and this gives a narrow trough. It may necessitate having a temperature greater than 1100K to obtain this narrow trough. Thus, one method of narrowing the trough is to have lower C levels. When the C level is 0.15-0.2% in a 1.4% Mn steel, a very wide trough occurs, since only a thin film of ferrite forms around the γ boundaries and the temperature has to go below the A_{r3} to produce large volume fractions of ferrite. Often this deep trough can exist over 150K from the A_{e3} to 30K below the A_{r3} . However, when the C level is reduced to $<0.1\%$, DIF forms very readily just below the A_{e3} leading to a narrow trough and improved ductility. Commercially, it has been found that reducing the C level in a 1.4% Mn, Nb containing steel from 0.12 to 0.08% can lead to much reduced cracking and this could possibly be the reason.¹⁰⁶

¹⁰⁶ B. Mintz: Private communication, 1998

5.3.3 Influence of S and Sulphides

Surprisingly, there is little obvious influence of the sulphur level in the hot ductility curves for these narrow troughed steels. For the low Mn steels, the curves were very similar even though there were big differences in the amount of dissolved sulphur at 1603K. Indeed the higher S containing steels gave slightly better ductility. For the high Mn steels, again the curves were very similar for the two sulphur levels, but the steel with the higher total S containing steel gave slightly better ductility.

For these steels, the formation of ferrite is the main factor controlling the trough and the higher S levels, by providing more MnS particles, will encourage ferrite formation and may give better ductility. This is confirmed for steel 8, the steel with the greatest volume fraction of elongated MnS inclusions, in which ductility at the low temperature side of the trough is observed to recover more quickly than for the lower sulphur containing steel 7, Figure 5.2. At 1098K, it can be seen that the elongated sulphides act as nucleation sites for ferrite formation so enhancing its production, Figure 5.16. Although the ferrite here is surrounding the MnS inclusions within the grains, recovery in ductility at the low temperature end of the trough is likely to be mainly dependant upon the volume fraction of ferrite independent of where it is situated.

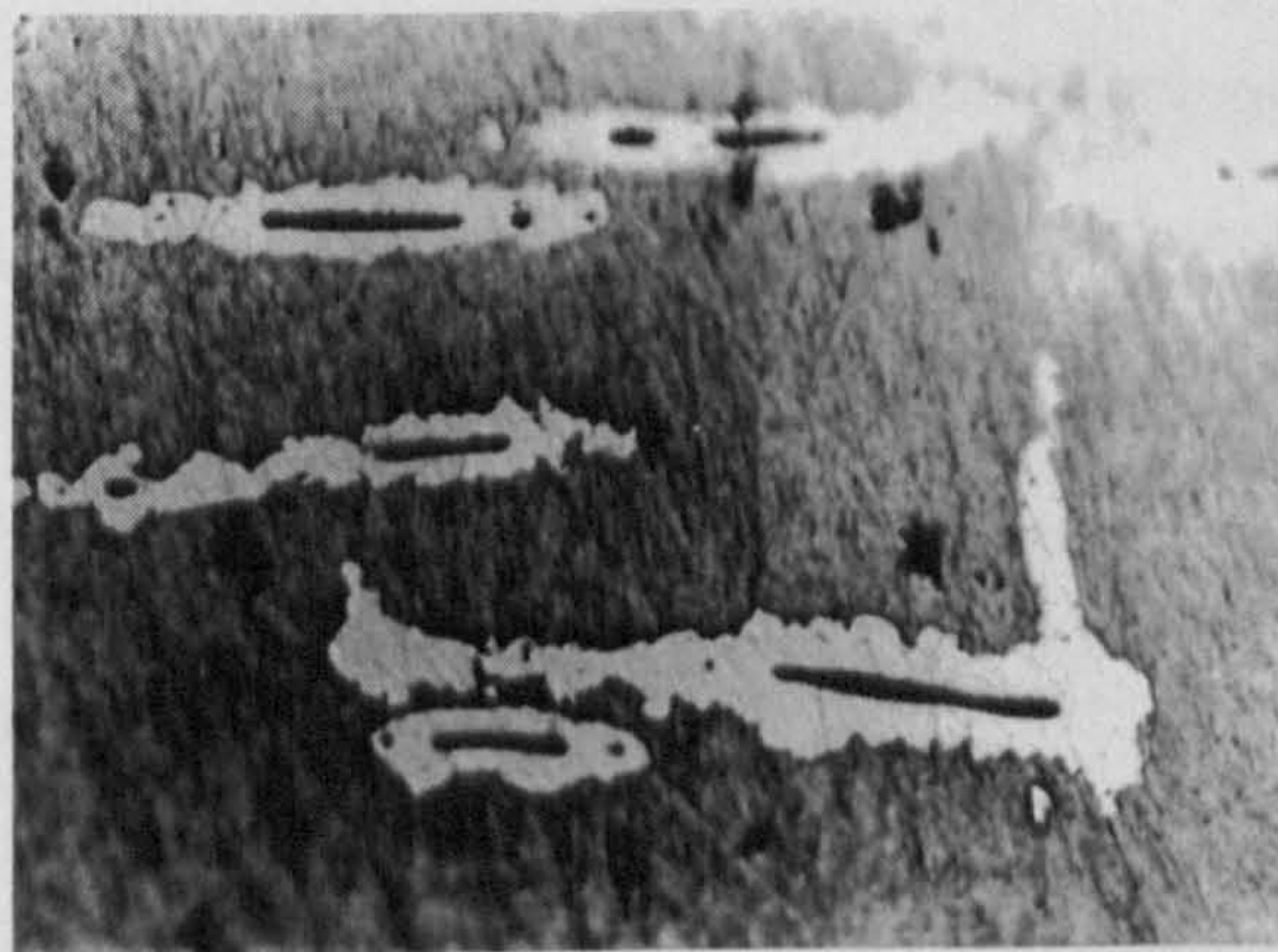


Figure 5.16: Elongated MnS inclusions encouraging the formation of DIF in steel 8. Steel tested at 1098K (mag x800).

This observation is in accord with previous work,⁴ which shows that increasing the volume fraction of elongated MnS inclusions encourages ferrite formation, but the present work indicates this is a relatively small effect compared with that of reducing the C content. Any influence of sulphur on hot ductility may only become important with wide troughs and the sulphides can then have an important influence on ductility as there is then only a thin band of ferrite at the austenite grain boundary. The exercise needs to be repeated on higher C (0.15%) and 1.4% Mn steels, which should result in a wide trough being observed.

5.3.4 Influence of Cooling Rate

The typical influence of cooling rate on hot ductility is shown in Figure 5.17 for a steel previously examined by the research group at City University and having a similar composition to that of steel 6. The work clearly shows that increasing the cooling rate from conventional rates ($25\text{-}60\text{Kmin}^{-1}$), to that appropriate for thin slab casting (200Kmin^{-1}), leads to worse ductility and, as has been noted in other recent work,⁴⁻⁷ is due to finer precipitation and finer inclusion distributions. Ductility as a result is worse, presumably because the finer the precipitation the more closely spaced are the particles along the boundary and the easier it is for cracks to interlink. Thus, transverse cracking might be expected to be more of a problem in thin slab casting particularly as there is no opportunity for surface inspection. Only limited testing at cooling rates other than 60Kmin^{-1} using the steels in the current programme was able to be carried out; however, the initial findings were in agreement with the results shown in Figure 5.17.

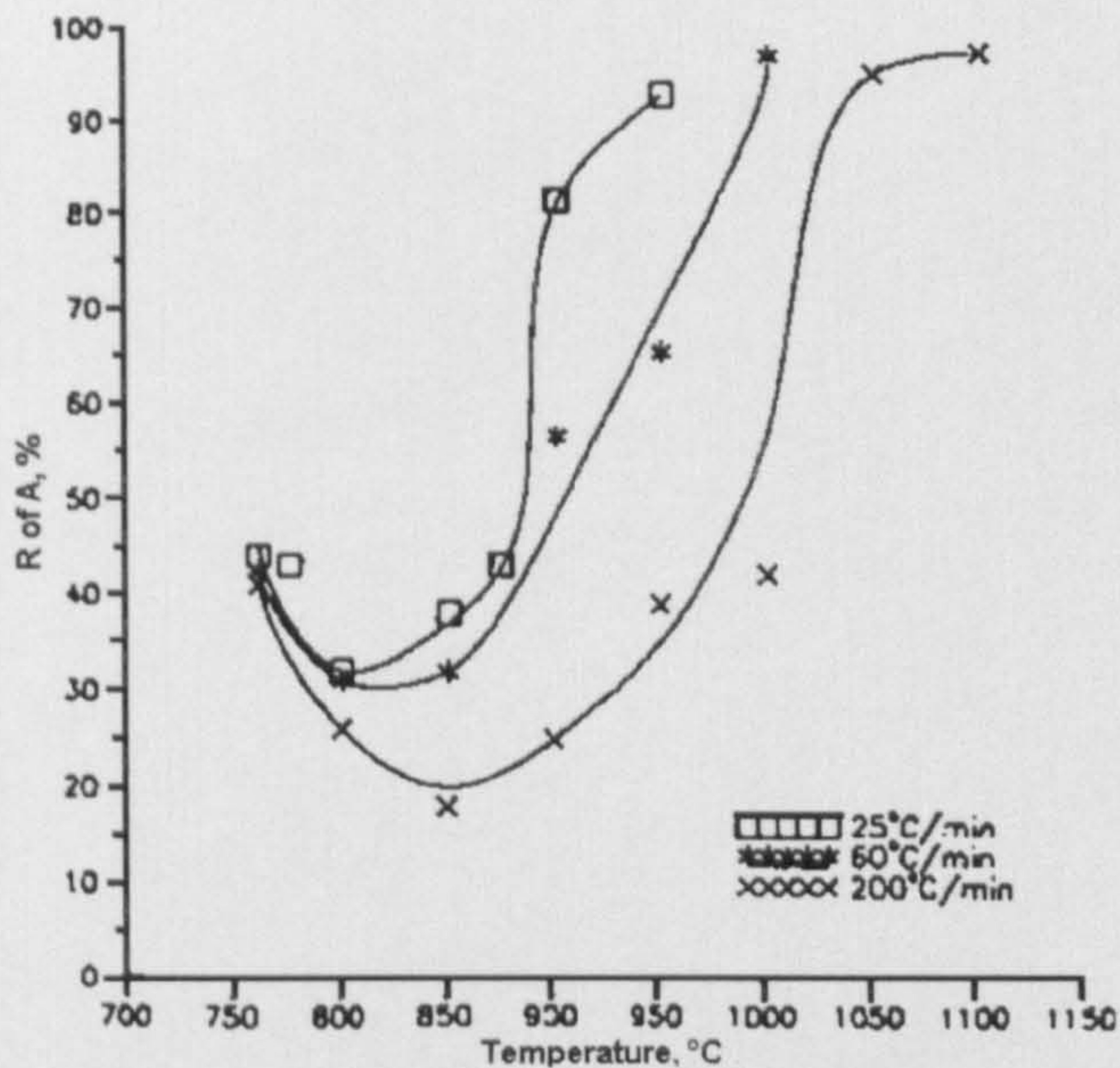


Figure 5.17: Hot ductility curves for a typical as-cast C-Mn-Nb-Al steel, given different cooling rates to the test temperature.¹⁰⁷

Increasing the cooling rate would be expected to lower the Ar_3 and for steels showing the wider troughs, extend the troughs even more. However, in the present case, increasing the cooling rate from 25 to 200 $Kmin^{-1}$ can be seen from Table 5.5 to give very variable results, from very little influence to a marked decrease in the Ar_3 and Ar_1 temperatures.

Steel	Plate Code No.	Ar3 Transformation Temperatures, K		
		25 K min ⁻¹	60 K min ⁻¹	200 K min ⁻¹
5	P7H45		1071	
6	P7H47		1083	
7	P7H48	-	999	999
8	P7H46	989	999	932

Table 5.5: Ar_3 transformation temperatures for steels 5 to 8 at cooling rates of 25, 60 and 200 $Kmin^{-1}$.

The average effect, as one would expect, was to decrease these temperatures. In this respect, increasing the cooling rate might be expected to move the hot ductility curves to lower temperatures. In fact, the ductility curves move to higher temperatures on increasing the cooling rate, i.e. worse ductility, indicating that the detrimental influence of precipitation is even worse than that given in Figure 5.18

¹⁰⁷ B.Mintz, R. Abushosha, S.Y. Ayyad and GISL Cardoso: HSLA '95, Proc. Of the Conf. on HSLA steels, China Science and Technology Press, China, (1995), pp. 342-345.

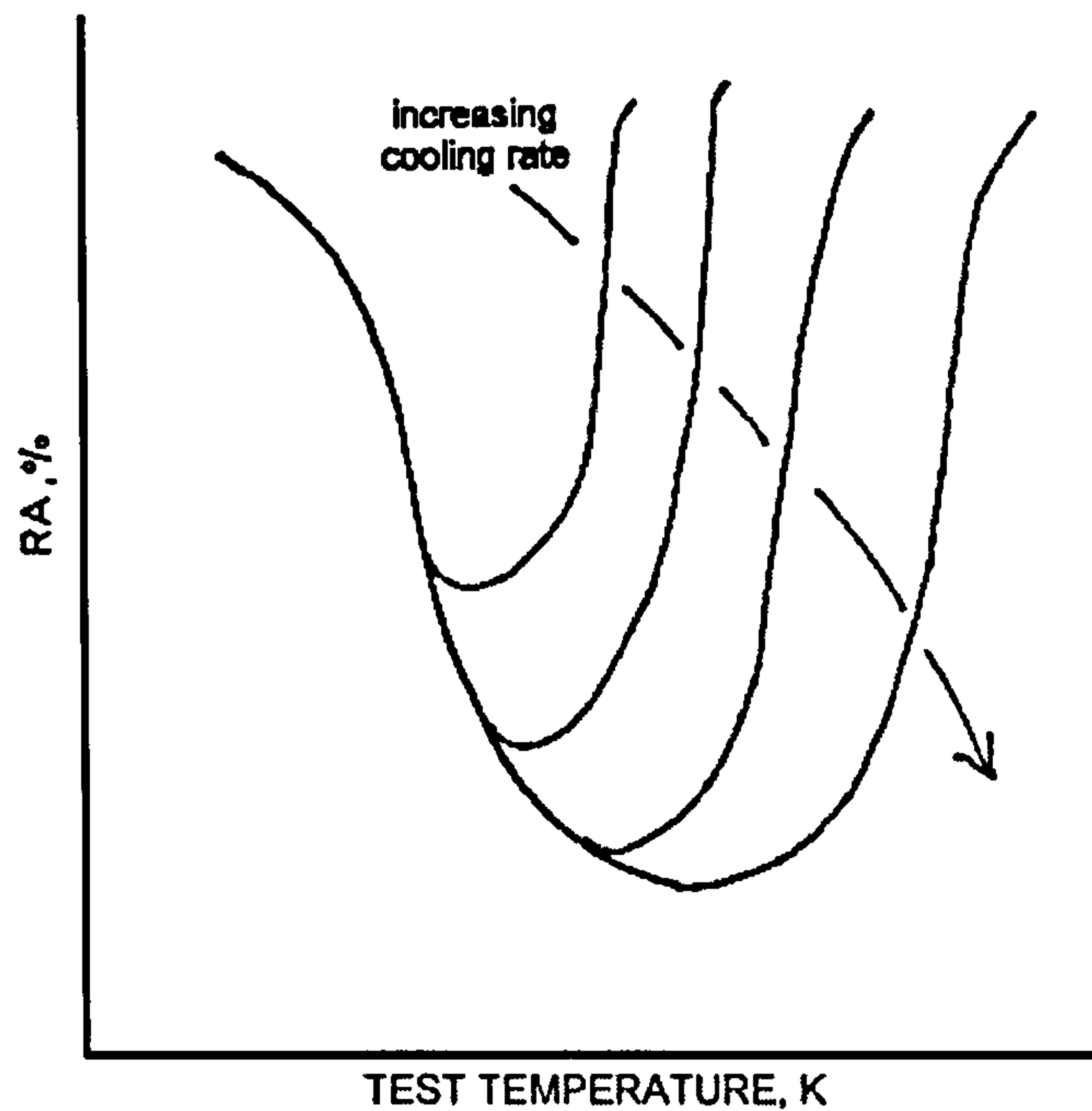


Figure 5.18: Schematic diagram showing the effect of cooling rate on hot ductility (based on Figure 2.21⁷⁵ showing grain size having a similar effect on the hot ductility curve).

5.3.5 As-Cast Samples

Again the influence of raising the S level from 0.004 to 0.019% only had a very small affect on the hot ductility, Figure 5.19. However, for as-cast steels, because all the sulphur is in solution on solidification, a large amount of sulphides are able to precipitate out at the austenite grain boundaries. The presence of a larger volume fraction of sulphides in the higher sulphur steel led to dynamic recrystallisation being delayed so that ductility at the high temperature end did not start to recover until slightly higher temperatures. Similar behaviour has been noted previously on similar steels.⁴ However, sulphur may have a more pronounced influence at higher C levels, when wide troughs are possible. It should be noted that the ductility trough is deeper for as-cast samples than for the solution treated samples; this is due to more sulphur being available for precipitating out at the interdendritic and austenite grain boundaries.

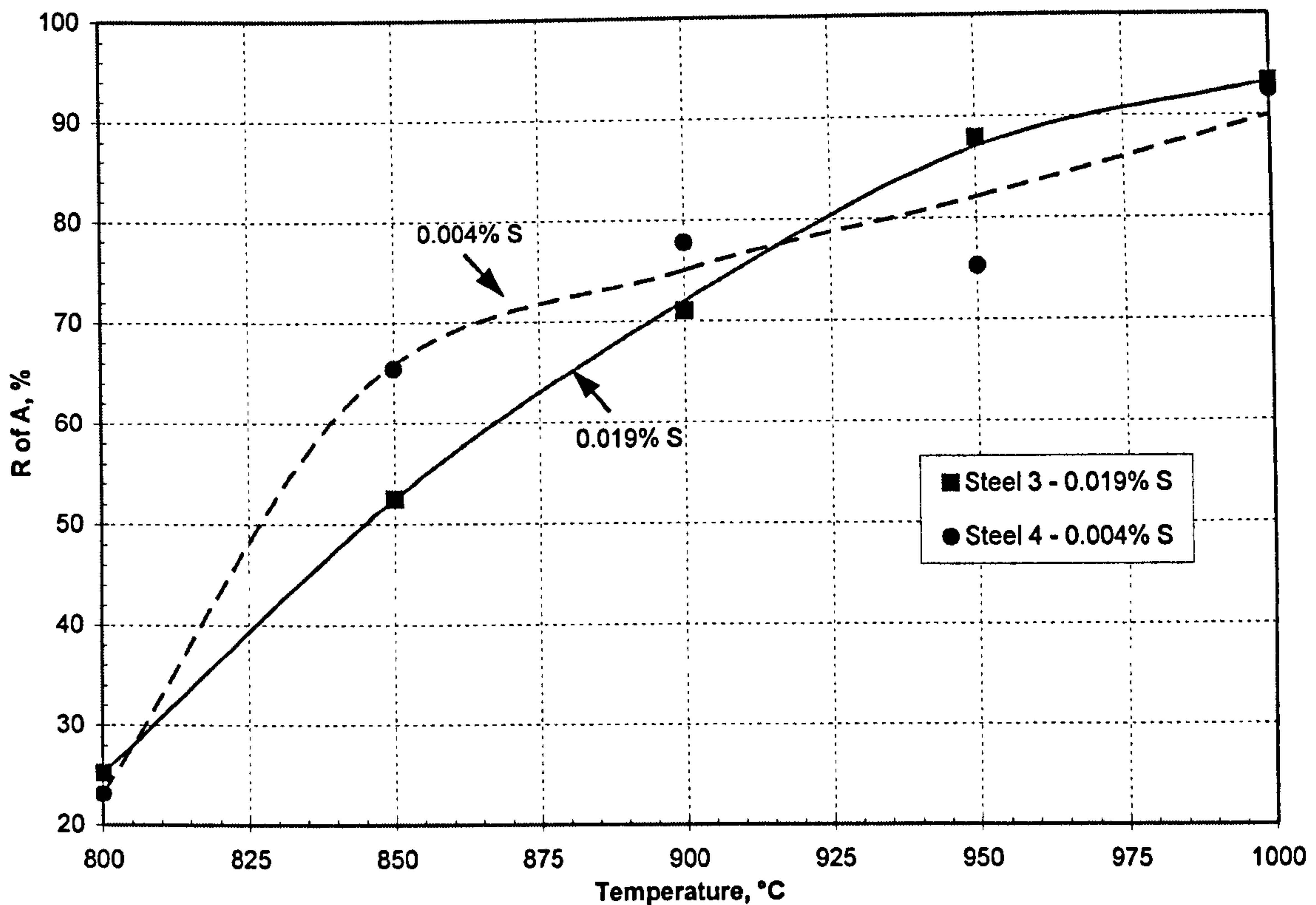


Figure 5.19: Hot ductility curves for as-cast steels, showing little change with percentage sulphur present.

5.4 Conclusions

1. The ductility troughs obtained for the four steels in this chapter can be seen to be grouped as the low Mn (steels 5 and 6) and high Mn (steels 7 and 8) containing steels; the low Mn and high Mn steels giving narrow ductility troughs of approximately 60K centred at ~1135K and ~1060K respectively. There is also a similar displacement in the positions of the observed and calculated curves of percentage ferrite against temperature. This is in agreement with the reduction of transformation temperatures as Mn levels increase; the higher Mn steels have A_e temperatures approximately 40K lower than the lower Mn steels, whereas the A_{r3} temperatures were much lower (~100K). Dilatometry and metallography show that the ductility troughs are caused by the presence of a thin film of deformation induced ferrite.

2. In the present work it has been shown that sulphur and sulphides do not generally have a major influence on the hot ductility of solution treated C-Mn-Al steels for the compositions examined. This is because for these steels, the temperature range in which a thin band of ferrite forms around the γ grains is very limited. Deformation induced ferrite readily forms in large amounts at temperatures close to the A_{e3} . As such, the trough is governed mainly by the A_{e3} and A_{r3} temperatures, which are little influenced by sulphur levels.

There is some indication that a high volume fraction of elongated MnS inclusions allow recovery in ductility to occur more rapidly on the low temperature side of the trough as has been noted in previous examinations. However, this again is only a small effect. Wider troughs, in which the presence of a thin band of ferrite occurs over a wide range of temperature, as with the Nb containing steels or higher C or Mn containing plain C-Mn steels might be expected to be more influenced by the level of sulphur, particularly with regards to the depth and this requires further investigation.

In the as-cast steels, large amounts of sulphides are able to precipitate out at the austenite grain boundaries because all the sulphur is in solution. This makes it more difficult for dynamic recrystallisation to occur, thus extending the trough to higher temperatures.

3. Increasing the cooling rate results in worse ductility, previous work showing this to be due to finer sulphides and precipitation. For the range of cooling rates investigated, 25 to 200 K min⁻¹, the decrease in A_{r3} temperatures as the cooling rate increases is relatively small.
4. This work has also clearly shown that the width of the trough can be narrowed by reducing the carbon and manganese levels, and to produce a trough <60K the A_{r3} temperature should be greater than 1103K. Recovery in the ductility at the high temperature end in these hot-rolled and solution treated steels generally corresponds to

the onset of dynamic recrystallisation. However, the strains that are required are much greater and the grain sizes too coarse to allow dynamic recrystallisation to occur in the commercial straightening operation during continuous casting.

At the low temperature side of the trough, recovery in ductility corresponds to the formation of a large amount of ferrite (~40%) and therefore any changes in composition that could raise the A_{r3} would be beneficial, e.g. lower C or Mn levels. These changes to the composition would be expected to reduce the width of the trough, thus reducing the risk of transverse cracking.

6. Mathematical Modelling

The work in this chapter followed on from previously published work by Mintz *et al.*^{9,30} and has been published in two papers.^{108,109} This exercise was intended to attain a better understanding of what controls the width of the trough and to develop a model which can be applied to a wide selection of steels. The role of strain rate, grain size and particles in controlling the width and depth of the trough were examined.

6.1 Introduction

Steels generally exhibit poor ductility when tested at a low strain rate in the temperature range 1273 to 973K. The poor ductility on the high temperature side of the trough can be due to either grain boundary sliding in the γ , which is exacerbated by the presence of particles at the boundaries, or to the phase transformation when a thin film of the softer ferrite forms around the γ grains allowing strain concentration to occur.² Recent work has shown that in coarse grained steel, the major improvement in hot ductility that occurs at the high temperature end of the trough is due to the onset of dynamic recrystallisation (DRX).^{2,30,48} Cracks that form prior to recrystallisation then become isolated and further development is prevented.²

Without DRX, intergranular failure occurs, which at lower temperatures is due to the presence of deformation induced ferrite, and at higher temperatures is due to boundary sliding. Both failure modes give rise to similar R of A values, so that the transition from one failure mode to the other as the temperature is raised is not always recognised when it occurs. Without DRX, the fracture strain remains fairly constant with increasing temperature, as although raising the temperature reduces the flow stress, the beneficial influence this has

¹⁰⁸ B. Mintz, R. Abushosha, A. Cowley: *Mat. Sci. and Technol.*, 1998, 14(3), pp. 222-226.

¹⁰⁹ B. Mintz, A. Cowley, R. Abushosha and D.N. Crowther: *Mat. Sci. and Technol.*, 1999, 15(10), pp. 1179-1185

on the hot ductility is balanced by an increase in the rate of grain boundary sliding. The strain to the peak stress, ε_p , can be calculated from the following equation.

$$\varepsilon_p = A d_0^{0.5} Z^{0.15} \quad (6.1)$$

where A is a constant, d_0 is the γ grain diameter in μm , and Z is the Zener-Holloman parameter ($Z = \dot{\varepsilon} \exp(Q/RT)$), where $\dot{\varepsilon}$ is strain rate, Q is activation energy, R is the gas constant and T is absolute temperature. The constant A has been shown for simple C-Mn and C-Mn-Al steels to be 6.3×10^{-4} for grain sizes in excess of $200 \mu\text{m}$ and Q has been taken as 290 kJ mol^{-1} .^{48,68}

The critical strain for dynamic recrystallisation, ε_c , is always less than ε_p , a typical value being $0.83\varepsilon_p$.¹¹⁰ A model has recently been proposed in which the temperature at which the onset of DRX occurs in a tensile test, T_d , can be obtained from where the curve of ε_c (critical strain for DRX) v temperature and ε_f v temperature "curve" intersect as shown in Figure 6.1. In this model, changes of ε_f with strain rate, grain size and precipitation are considered much more marked than that undergone by ε_c . Lowering the strain rate, coarsening the grain size and increasing precipitation all lower ε_f . The relative movement of the curves with changes in these variables has been shown in Figure 2.17, and illustrates that whereas grain coarsening and precipitation will lead to a rise in T_d (extends trough), increasing the strain rate lowers T_d (narrows trough).

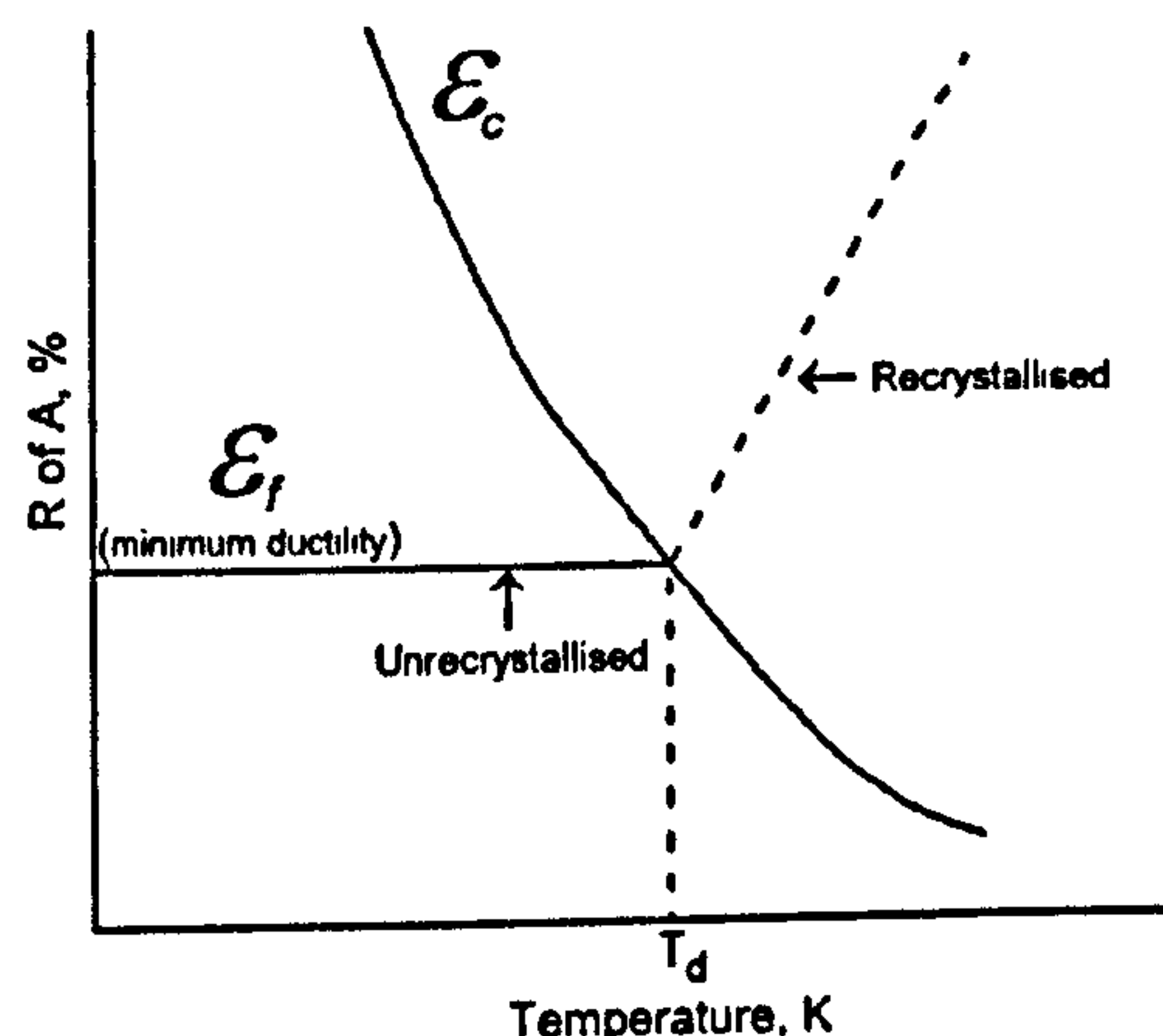


Figure 6.1: Schematic diagram showing how depth of the trough controls the temperature for onset of DRX, T_d .

¹¹⁰ C. Rossard: in 'Microstructure and Design of Alloys', 1973, London, The Institute of Metals, 2, p. 175.

The experimental work in this chapter was divided into two sections; one section was aimed at predicting the hot ductility curves in plain C-Mn steels and the other extended this work by looking more closely at the influence of the critical strain for DRX using an austenitic stainless steel in which no phase change could take place. The work on simple plain C-Mn steels was intended to show how the ductility curves can be predicted and how they could be used in relation to the problem of transverse cracking during continuous casting. The trough in these simple steels has been shown to be due to strain concentration causing voiding to occur around MnS inclusions in the softer ferrite films that form around the γ grains. In this case, DRX is often prevented by the presence of a film of strain induced ferrite at the boundaries and only when the temperature is above the Ae_3 can DRX occur, improving ductility. Because of the importance of the phase transformation in influencing the hot ductility behaviour, it is important to investigate whether the model investigated can be used equally successfully when grain boundary sliding alone is responsible for the intergranular failure. Therefore, an austenitic stainless steel was also examined in which no phase transformation was possible.

6.2 Experimental Details

As previously mentioned the work in this chapter was split into two sections, one using two simple plain C-Mn steels and the other an austenitic stainless steel; the compositions are given in Table 6.1. The plain C-Mn steels were provided by Corus, Swinden Technology Centre and the testing was carried out within the research group at City University. The stainless steel was provided by TWI and compression tests were carried out by Professor B. Mintz while on sabbatical at McGill University, Montreal using an MTS machine provided by Professor J.J. Jonas.

Steel	C	Mn	Si	S	P	Al sol.	N	Cr	Mo	Ni	V	O
9	0.095	0.31	0.28	0.032	0.010	0.032	0.004	-	-	-	-	-
10	0.110	0.32	0.32	0.003	0.010	0.037	0.003	-	-	-	-	-
11	0.014	1.70	0.40	0.006	0.013	-	0.130	25.5	2.16	22.4	0.11	0.002

Table 6.1: Analysis of steels studied in this section, wt. %.

As the focus of this chapter is on modelling of the ductility curve, the experimental results obtained from testing these steels formed the required input data. However, brief accounts of the experimental details are given below.

The plain C-Mn steels were 50 kg laboratory made vacuum melts which were rolled to 12 mm thick plate. Induction tensile specimens with dimensions as shown in Figure 3.2 were machined from these plates with their axes parallel to the rolling direction. These specimens were placed in the induction unit so that approximately 22 mm at the mid-length position could be heated to the desired temperature. The specimens were heated to 1703 K (in 15 min), held for 10 min and cooled at a rate of 100 Kmin^{-1} to test temperatures in the range 1073 – 1373 K. They were then held for 5 minutes at this temperature and strained to failure at a strain rate of $5 \times 10^{-4} \text{ s}^{-1}$. More information about the experimental details of this work can be found in reference 111, but is not regarded as being necessary for the purpose of this chapter which deals only with the modelling of the ductility curves.

The austenitic steel studied was supplied as 15mm thick hot rolled plate and compression samples 11.4 mm long and 7.6 mm in diameter were machined from the plate with their axis parallel to the rolling direction. The experimental details for the tensile¹¹² and compression¹⁰⁹ testing for this steel have been detailed elsewhere, so again will only be discussed briefly. For the tensile samples, grain sizes of 40 and 325 μm were examined and were obtained by heating the samples to 1273 and 1603 K respectively. After being held at these temperatures for 5 minutes, the samples were cooled at 60 Kmin^{-1} to test temperatures in the range 1273 to 973 K; they were then tested to failure at four different strain rates, 3×10^{-1} , 3×10^{-2} , 3×10^{-3} and $3 \times 10^{-4} \text{ s}^{-1}$, and quenched immediately after fracture.

¹¹¹ B. Mintz, R. Abushosha, O.G. Cominelli and M.A. Loyola de Oliveira: In Proc. Conf. 'Thermec 97' Wollongong, Australia, July 1997, Dept. Materials Engineering, University of Wollongong.

¹¹² B. Mintz, M. Shaker and D.N. Crowther: *Mat. Sci. and Technol.*, 1997, 13(3), pp. 243-249.

Due to the difficulty in identifying whether DRX had occurred from the tensile flow curves, as necking takes place, compression testing needed to be employed as well as the more conventional tensile test. As much of the information available on the values of the activation energy for DRX, Q , and the constant, A , used in equation 6.1, is only available for the commonly used stainless steels, not the complex austenitic stainless steel used in these experiments, these were therefore determined experimentally from the compression test results. The furnace attached to the MTS compression machine had a maximum temperature of 1448 K (i.e. a lower temperature than used for the tensile samples) and therefore the compression samples were held at this temperature for a longer time of 15 minutes to compensate. However the grain size for these samples was found to be 240 μm , which is finer than the 325 μm obtained in the tensile tests.

6.3 Results and Discussion

6.3.1 Simple C-Mn Steels

The hot ductility curves for steels 9 and 10, high and low sulphur respectively, are shown in Figure 6.2. The A_{r3} , A_{e3} and T_d temperatures for the two steels are also shown in order to aid discussion. The A_{e3} temperatures were calculated using Andrews formula¹¹³ and found to be equal for the two steels, the A_{r3} was established from dilatometry and T_d , the temperature for the onset of DRX, obtained from the load-elongation curves. The minimum ductilities of ~20 and ~38% R of A for steels 9 and 10 respectively have been projected across, and the point of intersection with the curves of ϵ_c against temperature indicates where ductility will improve due to DRX. The minimum ductilities can be converted to true strain using the following relationship, where ϵ_f is the strain to fracture.

$$\epsilon_f = \ln[100/(100 - R \text{ of } A)] \quad (6.2)$$

¹¹³ K.W. Andrews: J. Iron Steel Inst., 1965, 203, p. 721.

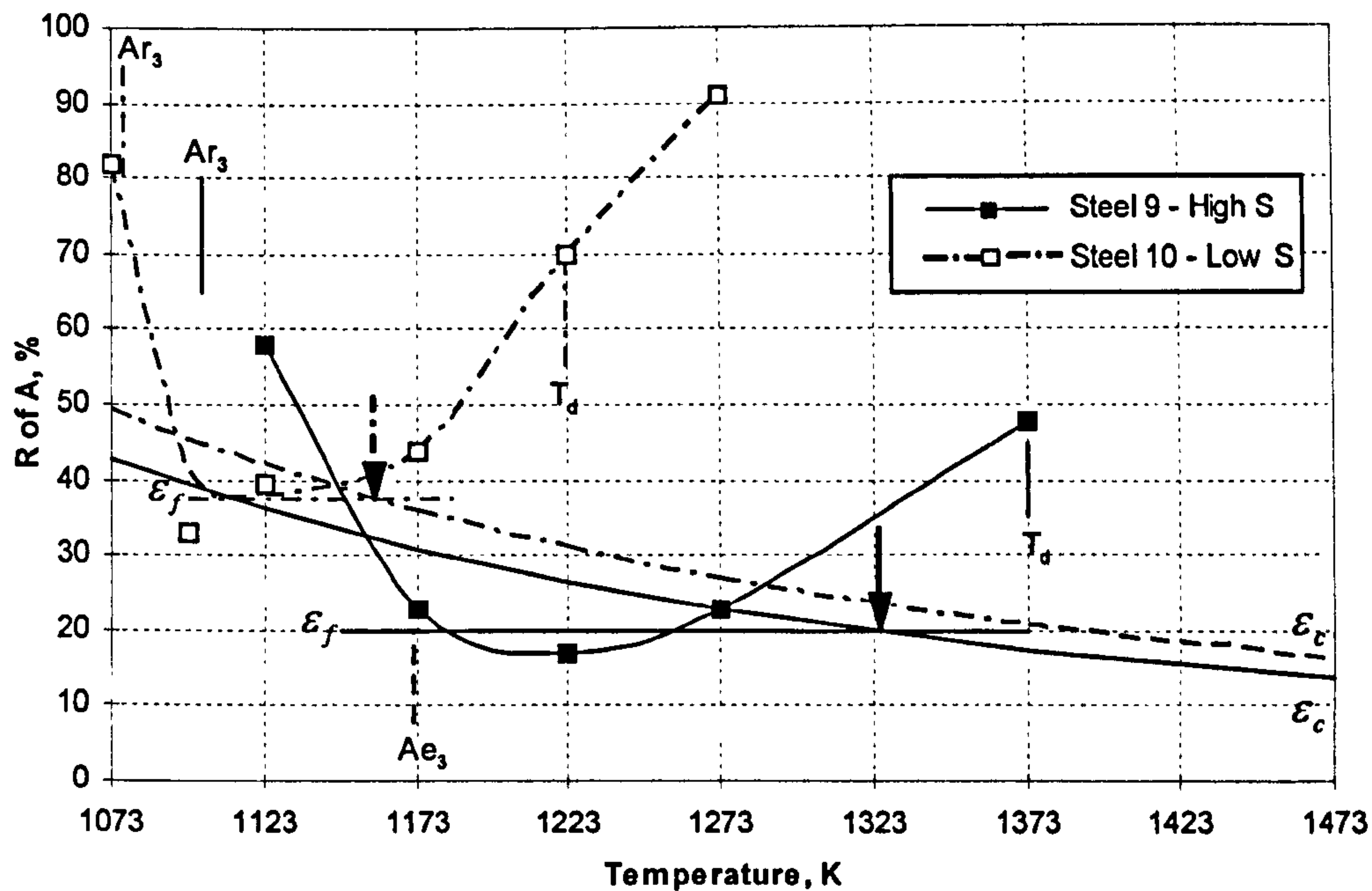


Figure 6.2: Hot ductility curves and ϵ_c against temperature for the C-Mn-Al steels 9 and 10, having high and low sulphur respectively. Arrows indicate the point at which the projected base of the trough intersects the curve of ϵ_c against temperature and therefore when ductility will start to improve.

Depth of the Ductility Trough

Intergranular failure within the ductility trough has been shown to occur by one of two mechanisms; microvoid coalescence taking place at inclusions below the A_{e3} and grain boundary sliding in the austenite at higher temperatures.² The depth of the ductility trough is similar for these two mechanisms and it is rare to see significant changes in R of A values either side of the A_{e3} temperature. In the absence of DRX, the ductility has been shown to remain essentially parallel to the temperature axis.^{2,30} The depth of the trough is known to depend on $\dot{\epsilon}$, grain size and the inclusion or precipitate distribution at the boundaries and within the matrix.²

The depth of the trough reduces with increasing strain rate as there is less time for voids to grow and join when failure is of the microvoid coalescence type and limits the amount of grain boundary sliding when failure is in the austenite.² Refining the grain size normally results in improved ductility as it becomes more difficult for cracks to propagate and the shorter crack length results in less stress concentration. The austenite grain sizes for the low and high S steels were 950 and 650 μm respectively, and this would have been expected to result in better ductility for the high S steel. However, when the grain size

exceeds 200-400 μm , the effect of grain size on ductility becomes very small,⁵⁸ and would explain the results seen in the present work.

The particle volume fraction and distribution also plays a significant part in controlling the ductility and when the failure in the trough is intergranular, it is these particles at the γ grain boundaries that control the ductility. Furthermore, if there are no microalloying additions and the soluble Al and N levels are too low to form AlN precipitates,² as in these two steels, then it is the inclusions that are responsible for the trough.

Recent work on C-Mn steels indicates that the ductility is controlled by sulphides at the boundaries⁷¹ and not grain boundary segregation of sulphur locally weakening the bonding.¹¹⁴ These sulphides form when the elongated MnS inclusions, as were shown in Figure 5.16, partially dissolve at 1703K and are re-precipitated in a fine spherical form in the boundary region on cooling to the test temperature.⁷¹ These sulphides can be readily identified in sections that are taken parallel to the rolling direction, Figure 6.3. Using the solubility data of Turkdogan et al.,¹⁰¹ 0.0137 and 0.003%S dissolves in the high and low sulphur steels respectively at a temperature of 1703K. When a larger volume fraction of MnS precipitation forms at the boundaries, the closer is the inter-particle spacing and the greater the ease for voids forming around the precipitates to link up resulting in failure. It is therefore to be expected that the high sulphur steel has the deeper ductility trough.

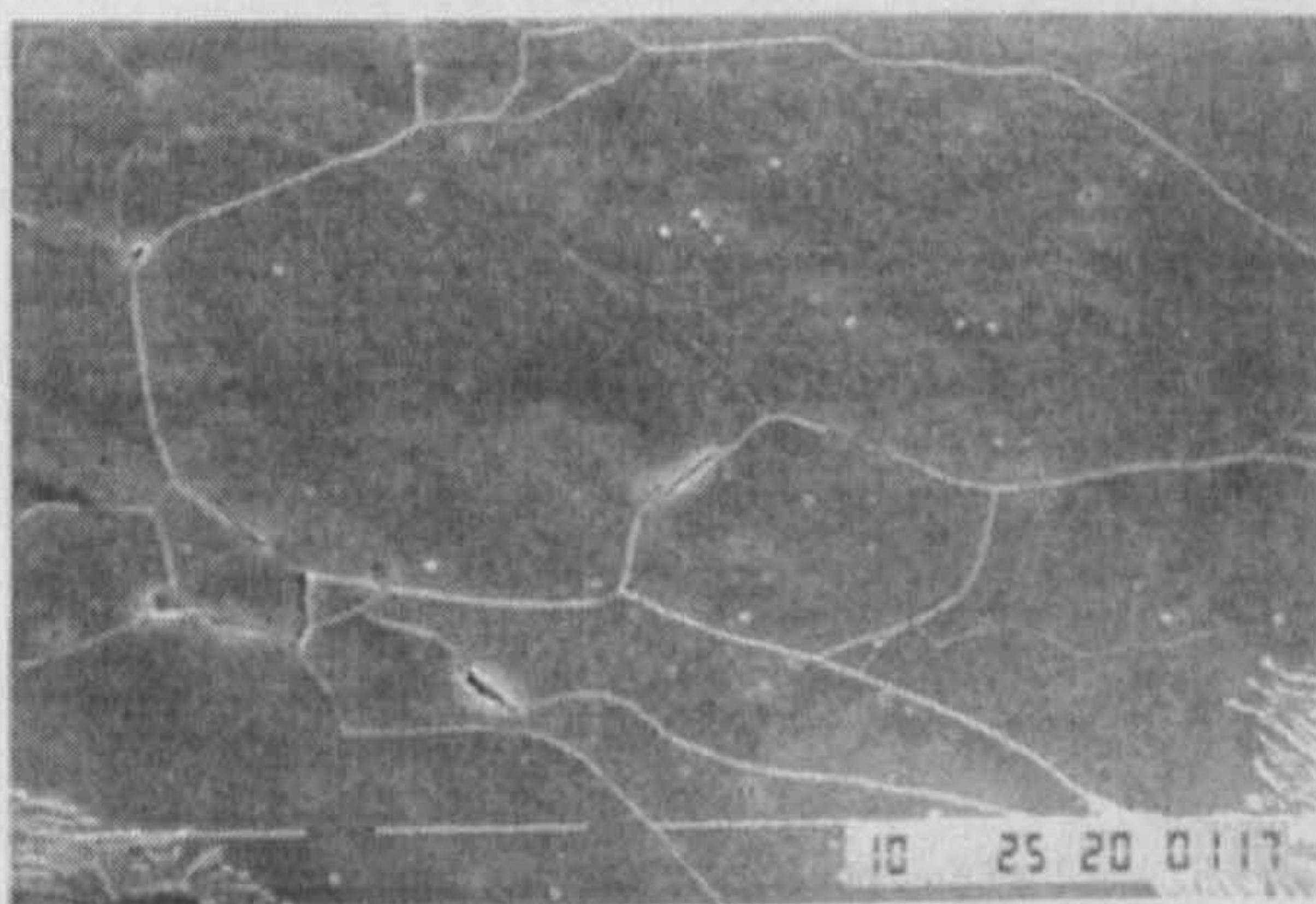


Figure 6.3: Spherical MnS precipitates found in C-Mn steel with a high S level. Tested at 1123K, $3 \times 10^{-4} \text{ s}^{-1}$ with a cooling rate of 10 Kmin^{-1} and giving R of A=55%. (mag x1150)

¹¹⁴ H. Kobashi: Trans. ISIJ, 1991, 31, p. 268.

The work on these two C-Mn steels has used the model of Yamanaka *et al*¹⁰⁰ to calculate the minimum ductility and assumes that all the deformation takes place in the ferrite film. Gurland and Plateau¹¹⁵ have derived the following relationship for the fracture strain, ε_{f_a} .

$$\varepsilon_{f_a} = k \left(\frac{1-f}{f} \right) \quad (6.3)$$

where k is a constant and f is the volume fraction of inclusions. Using the law of mixtures, Yamanaka *et al*.¹⁰⁰ have developed this equation further to account for the situation where both ferrite and austenite are present.

$$\varepsilon_f = (V_\alpha + R V_\gamma) k \left(\frac{1-f}{f} \right) \quad (6.4)$$

where V_α and V_γ are the volume fractions of α and γ respectively, $R = \varepsilon_\gamma / \varepsilon_\alpha$ where ε_α and ε_γ are the strains in the α and γ respectively. It is believed that when failure occurs in the trough, virtually all the strain is taken up in the softer ferrite films surrounding the austenite grains. Therefore, to a first approximation, the equation for fracture strain, ε_f , then simplifies to:

$$\varepsilon_f = V_\alpha k \left(\frac{1-f}{f} \right) \quad (6.5)$$

The calculated values of ε_f converted to R of A together with the experimentally observed R of A values for steels 9 and 10 are given in Table 6.2. Also shown in this table are recent values obtained experimentally and calculated from other low C (~0.1%) steels in which the volume fraction of sulphides can be calculated and the ferrite volume fractions have been estimated.^{71,116,117,118} The value of k has been taken as 0.0008 to give the best fit to the data and the calculated values are plotted against the observed values in Figure 6.4.

¹¹⁵ J. Gurland and J. Plateau: ASM Trans., 1963, 56, p. 442.

¹¹⁶ G.I.S.L. Cardoso: PhD Thesis, 1986, City University London, UK.

¹¹⁷ G. S. I. L. Cardoso, B. Mintz and S. Yue: Ironmaking and Steelmaking, 1995, 22, p. 365.

¹¹⁸ A. Cowley: Unpublished work, City University, London, UK, 1997.

Data Source	Mn, %	S in Sol., %	Cooling rate, K min ⁻¹	Ferrite, %	Test Temp., K	Strain Rate, s ⁻¹	R of A, %	
							Observed	Calculated
Ref. 18	1.40	0.0016	60	7	750	10 ⁻³	37	46
Ref. 16	1.39	0.0016	60	3	800	10 ⁻³	35	25
Ref. 18	0.61	0.0035	60	12	875	3x10 ⁻³	35	40
Ref. 11	0.58	0.0036	60	8	850	3x10 ⁻³	44	28
Ref. 16	0.39	0.0053	60	6.5	850	10 ⁻³	16	26
Steel 10	0.32	0.0137	100	14	900	5x10 ⁻⁴	22	14
Steel 9	0.31	0.003	100	14	850	5x10 ⁻⁴	40	50

Table 6.2: Calculated and observed R of A values for a selection of C-Mn-Al steels.

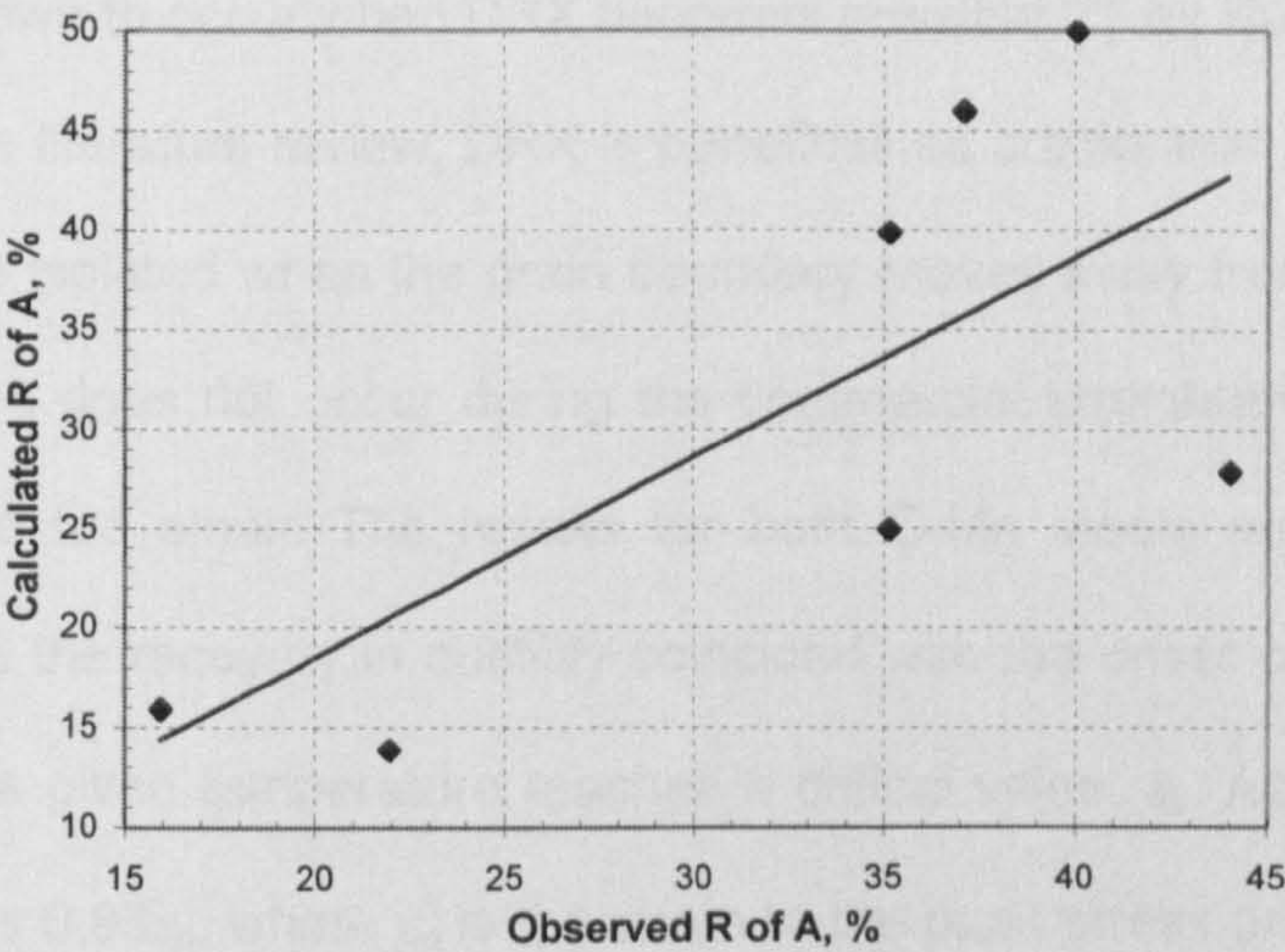


Figure 6.4: Calculated R of A values from Table 6.2 plotted against those observed experimentally.

The thickness of the ferrite films around the γ grains, i.e. the percentage ferrite present, cannot be calculated at present and has to be experimentally determined. There is a trend from Table 6.2 for the higher Mn steels to exhibit thinner ferrite films. The present work also does not make allowances for inclusion size which are dependant on the cooling rate; the faster the cooling rate, the finer the inclusions. Therefore, some re-adaptation may be required to account for the influence of inclusions and precipitation on the strain to fracture, ϵ_f . The effect of precipitation is generally taken account of by the higher Q values in the Zener-Holloman parameter, Z. Recent work⁷¹ has shown that, for a given volume fraction of inclusions, ductility decreases with decreasing inclusion size. This may be related to finer distributions of inclusions at the grain boundaries providing easier paths for cracks to join together. The effect of inclusion distribution is likely to be relatively small compared to that of the volume fraction of inclusions.

Increasing the strain rate should also improve ductility, but the current work has only studied a narrow range of strain rates. For a complete analysis of the ductility curve, it would require the incorporation of terms for both $\dot{\epsilon}$ and the cooling rate, which controls the size of the sulphides, into Equation 6.1.

High Temperature Ductility Recovery

The recovery in ductility on the high temperature side of the trough in coarse grained steels has been shown to occur when DRX becomes possible,^{2,30} as illustrated in Figure 6.1. As mentioned in the literature review, DRX is beneficial as cracks that have formed at grain boundaries become isolated when the grain boundary moves away from the crack and new grains are formed; it does not occur during the commercial straightening operation as the strains involved are too small. The results for both C-Mn steels are in agreement with previous work,² and the recovery in ductility coincided with the onset of DRX, which occurs when the strain at a given temperature reaches a critical value, ϵ_c . As discussed earlier, a typical value for ϵ_c is $0.83\epsilon_p$, where ϵ_p is the strain to the peak stress and is calculated using Equation 6.1. Previous work on C-Mn steels^{48,68} has shown that it is better to use ϵ_p in calculating the strain required for ductility improvement, this is due to recrystallisation in the boundary regions needing to be sufficiently advanced to prevent crack from joining together.

Assuming that there is very little change in ϵ_t up to the temperature when DRX is possible then the point at which the horizontal line, for the un-recrystallised state, intersects the curve of ϵ_p against temperature is when the ductility will recover, as shown in Figure 6.1. It can be seen from Figure 6.2 that this point of intersection is also the temperature where ductility measured experimentally can be seen to recover in both the high and low S steels. However, it should be noted that for the low S steel this point is very close to the Ae_3 temperature; and because this steel has a coarser grain size, the curve of ϵ_p against temperature is also higher in comparison to the high S steel.

The A_{e3} temperature is important in determining the onset of DRX as the thin films of ferrite that form around the γ grains make it difficult for DRX to occur.^{2,30} In steels having a 'finer' grain size ($d_0=200\text{ }\mu\text{m}$), this is particularly the case as ε_c is relatively small; the ductility does not recover at the point of intersection of the two curves, as would be expected, recovery is delayed until the A_{e3} temperature is exceeded and ferrite can no longer form.

Low Temperature Ductility Recovery

Ductility recovery at the low temperature side of the trough corresponds to a large volume fraction of ferrite being present ($\geq 45\%$), i.e. the amount of ferrite that can form before¹¹⁷ or during deformation at temperatures close to the A_{e3} .¹¹⁸ The equilibrium percentage ferrite present at temperatures below the A_{e3} for a typical 0.1C-0.6Mn steel is shown in Figure 6.5a, calculated using the 'Thermocalc' program.⁹⁸ Figure 6.5(b) shows the relationship between R of A values and the percentage ferrite present for similar steels studied in previous work.¹¹⁷ It can be seen from Figure 6.5(b) that 60% R of A can be obtained from a steel with 45% ferrite present and this proportion of ferrite would be present at 30-40 K below the A_{e3} temperature, Figure 6.5(a). In the case of the ductility trough, the ferrite controlling ductility is DIF and can form at temperatures as high as the A_{e3} .

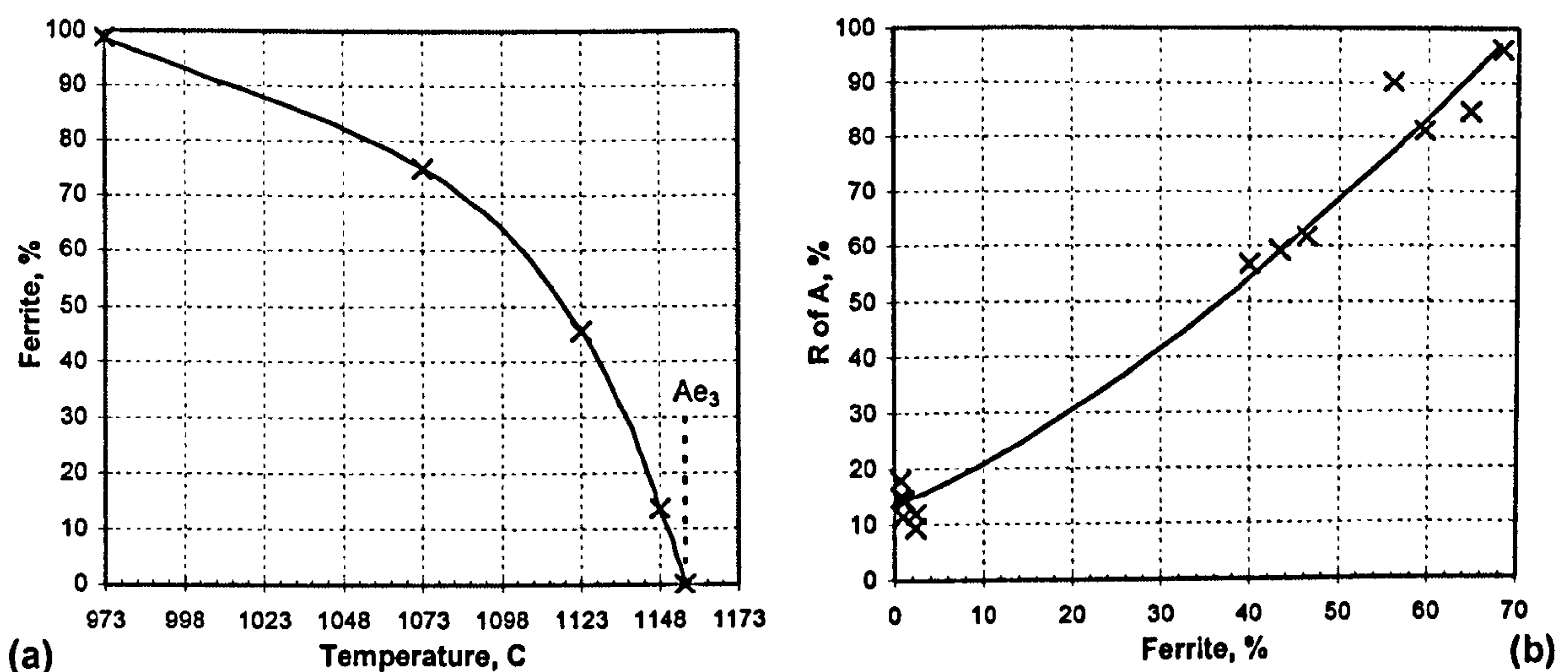


Figure 6.5: (a) Equilibrium percentage ferrite at temperatures below the A_{e3} for typical 0.1C-0.6Mn steel calculated using the 'Thermocalc' program⁹⁸ and (b) the influence of percentage ferrite on hot ductility.¹¹⁷

It is generally found that ductility will first start to recover at either 20-30 K below the A_{r3} (undeformed) temperature or at 20-30 K below the A_{e3} temperature; there is little evidence to suggest that ductility will start to recover at temperatures between these ranges. The poor ductility seen in the trough is due to thin films of DIF forming around the γ grains.² Virtually all the strain concentrates in these films as they are relatively soft compared to the γ grains, and as long as the films do not work harden, ductility remains poor.

The stress acting in the boundary region appears to dictate whether ductility starts to recover below the A_{e3} or below the A_{r3} ; at higher stresses DIF is more likely may spread into the γ grains and there may be a critical stress for this to happen. Therefore, at higher strain rates and finer grain sizes the A_{e3} temperature would be the controlling factor for ductility recovery.^{7,40} The spread of the ferrite into the γ is probably always due to the thin films of ferrite work hardening until its strength reaches that of the γ and therefore deformation becomes homogeneous. When DIF starts to spread, equilibrium amounts of ferrite quickly form.⁴⁰

MnS inclusions provide good nucleation sites for transformation ferrite and even more so for DIF,⁷¹ and when coarser elongated MnS inclusions are present, the stress concentration at their tips encourages the formation of ferrite even more, Figure 6.6. It is therefore interesting to note that ductility recovers just below the A_{e3} in the high S steels, which have high volume fractions of elongated MnS inclusions. However, the low S steel requires temperatures below 1098 K for ductility recovery. If the ferrite volume fraction can be increased, then ductility can be improved. In the present work the grain size is coarse and the strain rate very low; therefore, recovery readily occurs keeping the ferrite soft and resulting in strain concentration within the ferrite films and low ductility intergranular failure. For the low S steel, the width of the trough extends from the A_{r3} (undeformed) to the A_{e3} and for recovery to occur ferrite must be present before deformation. For the high S steel, the large amounts of DIF forms around, and also within, the γ grains encouraged by the high MnS volume fraction, and ductility recovers at the low temperature end close to the A_{e3} .

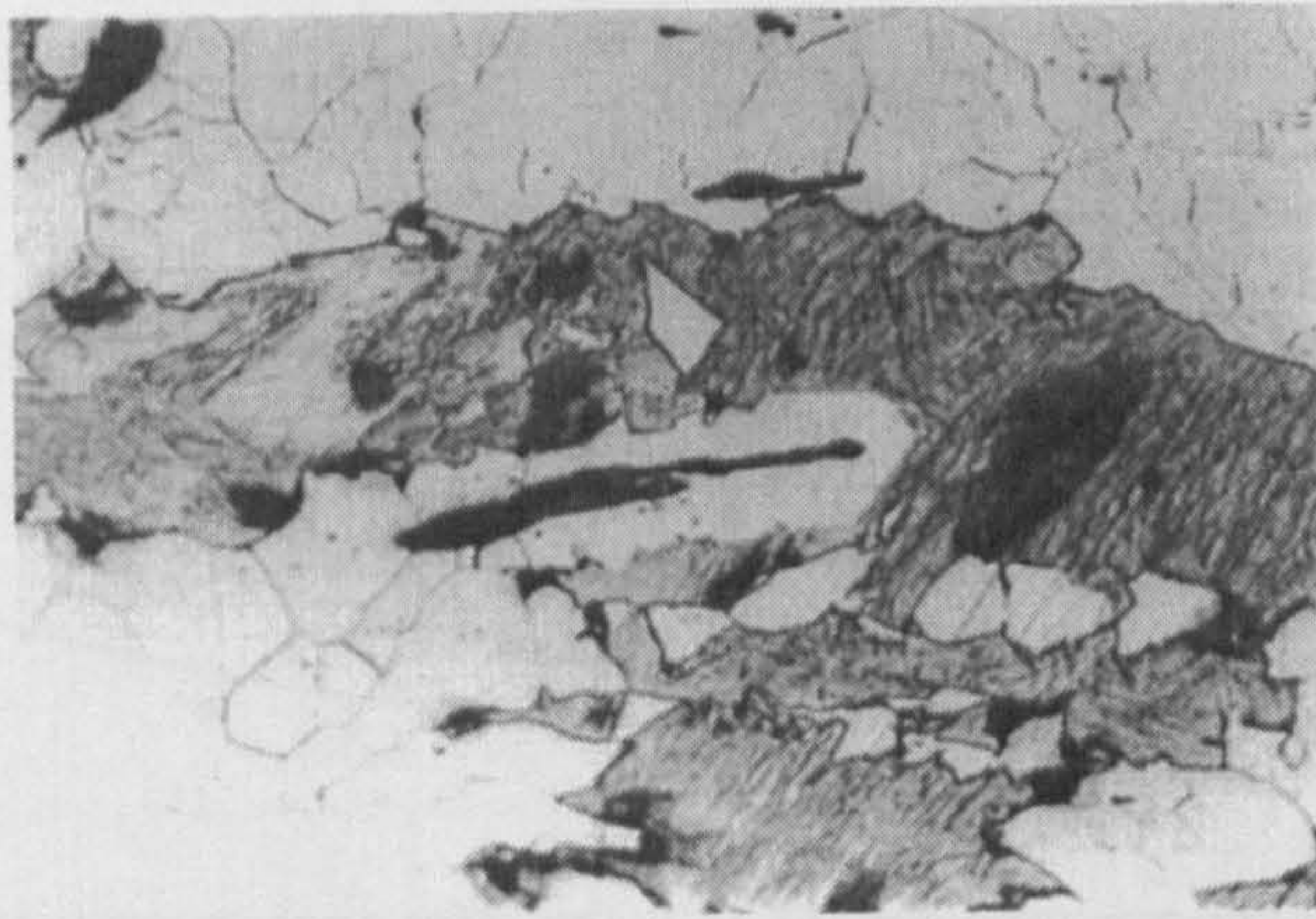


Figure 6.6: Elongated MnS inclusions favouring ferrite nucleation, high S steel tested at 1123 K. (mag x482)

6.3.2 Grain Boundary Sliding in Austenitic Stainless Steel

Coarse Grain Size

As mentioned earlier, an austenitic stainless steel where no phase transformation was possible was used to see if the model can be successfully applied when grain boundary sliding (GBS) alone is responsible for intergranular failure. The depth of the trough is similar, independent as to whether GBS or phase transformation is the operative mechanism for intergranular failure. In order to calculate the curves of ε_p against temperature, the grain size and the constants Q and A needed to be determined experimentally. The γ grain size, determined by the linear intercept method, was found to be 240 μm . The value of Q , 450 kJmol^{-1} , was determined from the curve of $\ln \varepsilon_p$ against $1/T$, and A , 1.45×10^{-4} , by fitting Equation 6.1 to give the best agreement with the experimental results. Using these values, the curve of ε_p against temperature can be calculated and the strain value converted to R of A values using Equation 6.2. The calculated curves and the experimentally determined values of ε_p against temperature are shown in Figure 6.7.

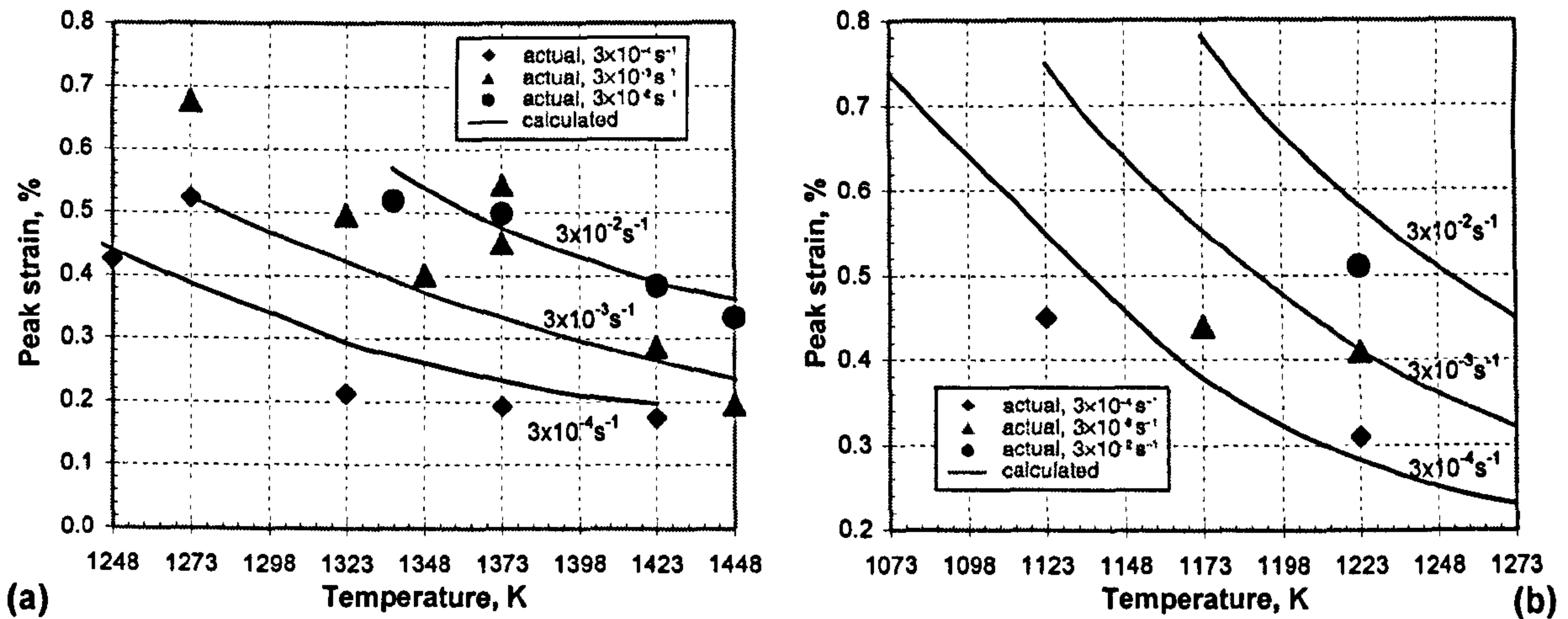


Figure 6.7: Calculated curves and experimentally determined values of ε_p against temperature for (a) coarse grain size, 240 μm (after Ref. 108) and (b) fine grain size, 40 μm .

To predict the T_d temperature from the curve ε_p against temperature the depth of the ductility trough must be known and there is no theoretical model to calculate this for grain boundary sliding. Figure 6.8 shows the hot ductility curves obtained previously¹¹² for these steels by tensile testing and the present calculated values for the curve of ε_p against temperature. The values of T_d are obtained by projecting the depth of the ductility trough across as shown. The hot ductility curves are those taken from the tensile samples having a grain size of 325 μm (coarser than the 240 μm compression samples) and strained to failure at four strain rates; 3×10^{-1} , 3×10^{-2} , 3×10^{-3} and $3 \times 10^{-4} \text{ s}^{-1}$.

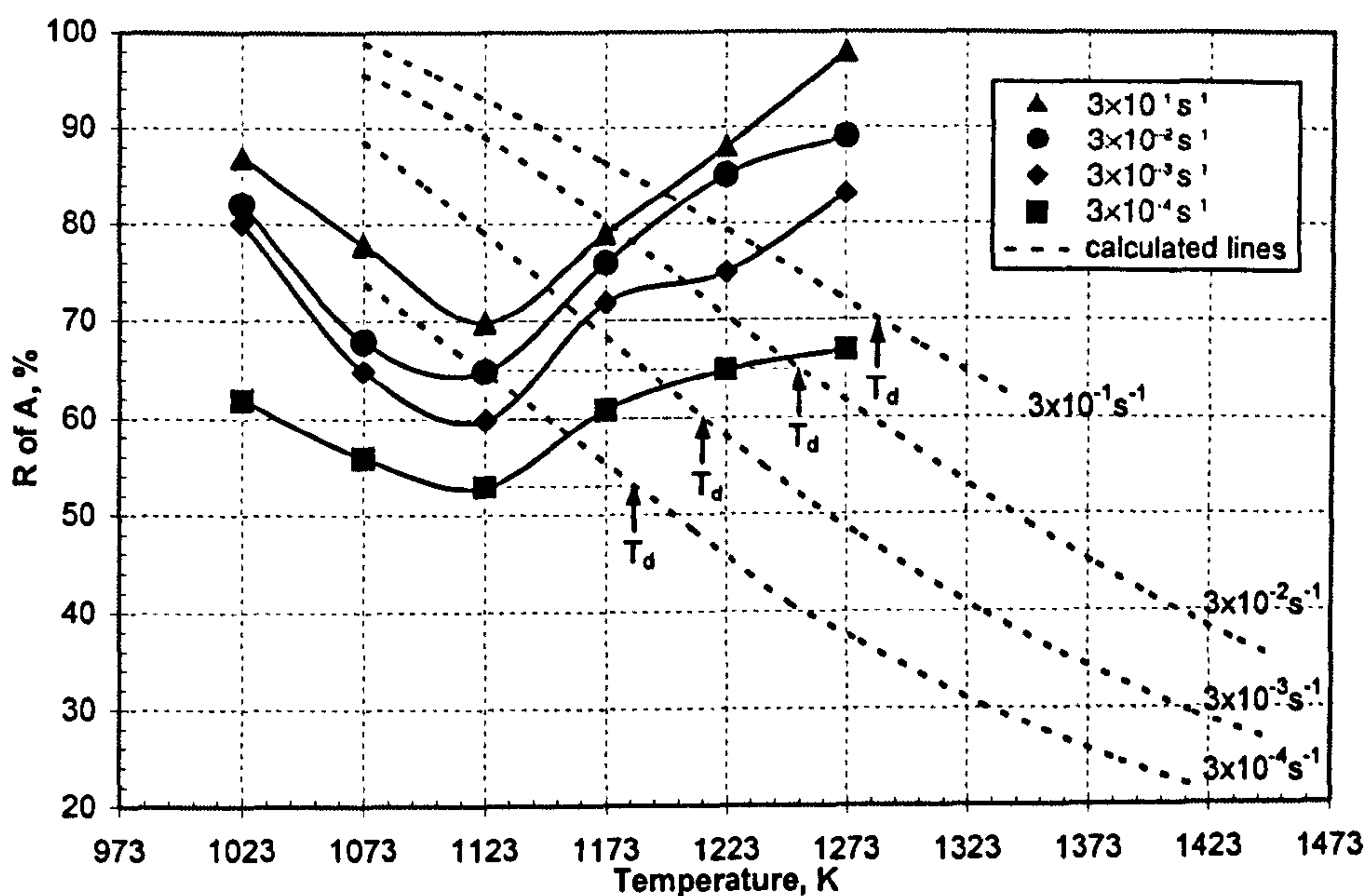


Figure 6.8: Hot ductility curves obtained from tensile tests and calculated ε_p converted to R of A values against temperature for the coarse grained samples, T_d for each strain rate is marked by an arrow (after Ref. 108).

The values of T_d for strain rates of 3×10^{-4} , 3×10^{-3} , 3×10^{-2} and $3 \times 10^{-1} \text{ s}^{-1}$, are 1188, 1213, 1248 and 1293 K, respectively. Experimentally, DRX was found to occur at lower temperatures than expected, e.g. for $3 \times 10^{-3} \text{ s}^{-1}$ recrystallisation was first observed at 1173 K, whereas the predicted temperature was 1213 K. Better agreement in this case between the experimental and calculated values were found using ϵ_c rather than ϵ_p . However, it was found that ductility could improve without DRX if the strain rate was high enough, $3 \times 10^{-1} \text{ s}^{-1}$, so that GBS was suppressed. Furthermore, at very low strain rates, cracks developed to such a degree by GBS that DRX was too late to prevent failure. In fact, only at a strain rate of $3 \times 10^{-3} \text{ s}^{-1}$, i.e. the strain rate pertinent to the straightening operation in continuous casting, was the model found to be satisfactory.

Fine Grain Size

Ductility troughs were not seen with the finer grain size and ductility was excellent (>90% R of A) for all temperatures examined, Figure 6.9. This indicates that in the fine grained condition, 40 μm , DRX would occur at temperatures >973 K. Metallographic examination confirmed that DRX did in fact occur throughout the whole temperature range examined. The ductility troughs for all strain rates have been completely removed by refining the grain size; this is shown in Figure 6.9 where the curves of ϵ_p against temperature would intersect the ductility curves (100% R of A) below the temperature range studied, i.e. less than 973 K. Even at the lower R of A values that were seen in the coarse grained condition, DRX would still have occurred before fracture when using the calculated curves of ϵ_p against temperature for the fine grained condition.

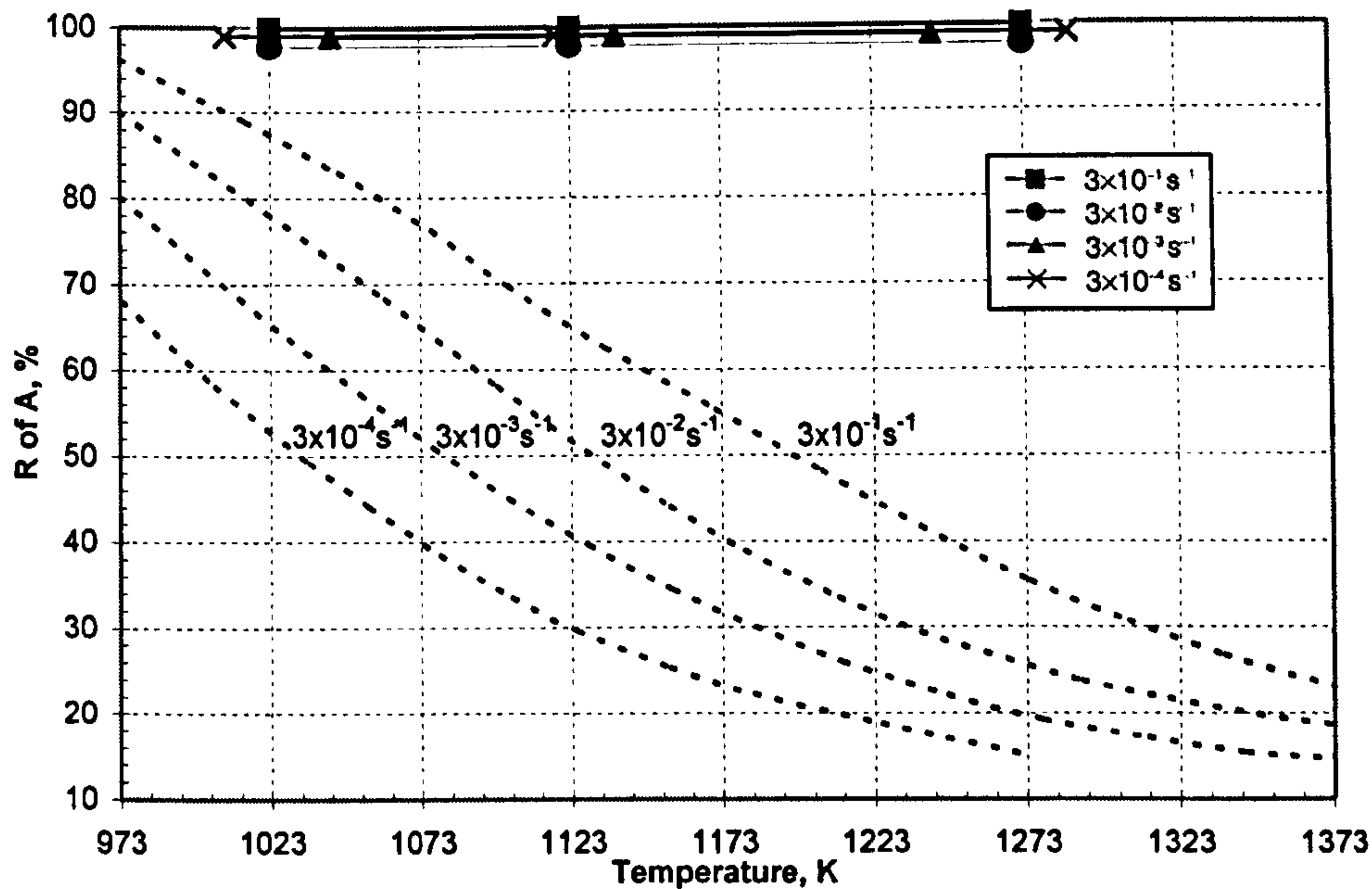


Figure 6.9: Hot ductility curves and calculated peak strain, ϵ_p , converted to R of A values against temperature.

The present work indicates that for coarse grained stainless steel this simple model can only be used to predict T_d for strain rates around 10^{-3} s^{-1} , i.e. the strain rate experienced at the straightener. However, DRX does not occur during the commercial straightening operation as the strain is too low and the grain size too large. Therefore, information derived from this model for the high temperature end of the curve must be used with caution when attempting to predict the likelihood of transverse cracking during continuous casting. At strain rates above and below 10^{-3} s^{-1} , GBS was dominant in controlling the recovery of ductility. Increasing the strain rate reduced both the width and depth and the trough. At higher strain rates, the time for cracks to grow is reduced and at lower rates, the cracks develop to such a degree that DRX is no longer able to restore ductility.

Metallographic Evidence for Coarse Grained Austenitic Steel

Low Temperature End of the Trough

Metallographic examination confirmed the effect of $\dot{\epsilon}$ on GBS since the length of cracks at the γ boundaries increased as the strain rate decreased, as shown in Figure 6.10. At the lowest strain rate of $3 \times 10^{-4} \text{ s}^{-1}$, the minimum ductility was only able to improve a small amount with increasing temperature, even at the highest temperature of testing, 1273 K.

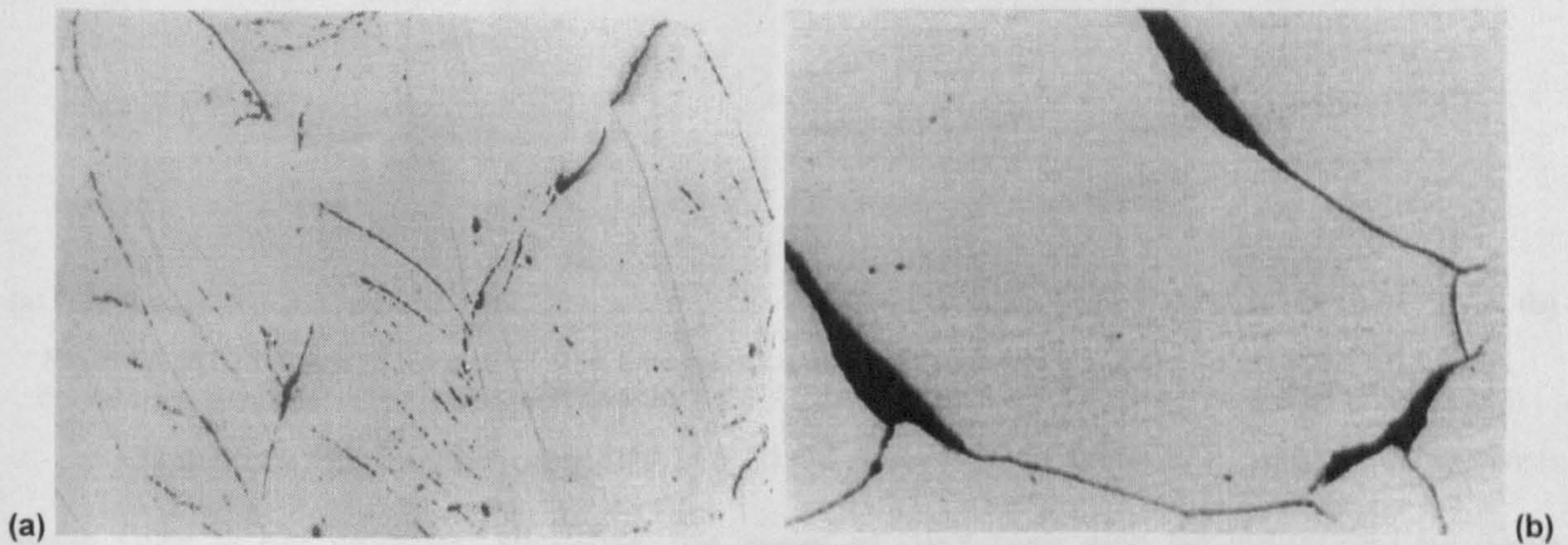


Figure 6.10: The influence of $\dot{\epsilon}$ on the length of cracks formed by grain boundary sliding, (a) $3 \times 10^{-1} \text{ s}^{-1}$ and (b) $3 \times 10^{-4} \text{ s}^{-1}$, both samples being tested at the minimum ductility temperature of 1123 K (mag x120).

Although GBS can occur in austenite without particles being present at the boundaries, it is generally accepted that there must be some particles present for a trough to form. Grant *et al.*^{119, 120} have shown that crack or cavity formation by GBS in creeping alloys occurs more easily in the presence of grain boundary particles. At the low temperature end of the trough in this steel, 1123 K, the boundaries become saturated with precipitation, Figure 6.11(a), but ductility is able to recover and give high R of A values as grain boundary sliding is reduced at lower temperatures.

¹¹⁹ N.J. Grant and A.W. Mullendore: 'Deformation and fracture at elevated temperatures', 1965, Cambridge, MA, MIT Press.

¹²⁰ I. Servi and N.J. Grant: Trans. AIME, 1951, 191, p. 917.

High Temperature End of the Trough

Fewer but coarser precipitates are formed at higher temperatures, 1273 K, as shown in Figure 6.11(b). The particles in this stainless steel were found to be chromium carbides¹¹², whereas in simple C-Mn and micro-alloyed steels these would be AlN, Nb(CN) or TiN etc.

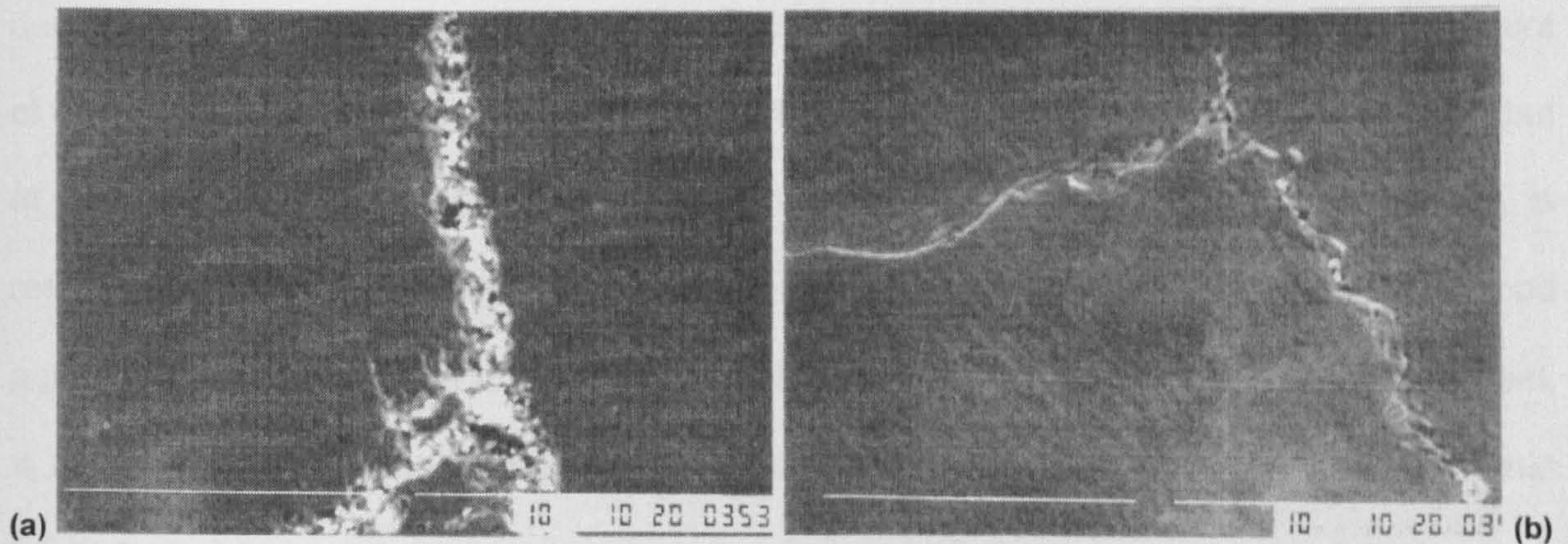


Figure 6.11: Influence of temperature on amount of carbides precipitated at γ grain boundaries, (a) 1123 K, boundaries saturated with precipitation and (b) 1273 K, considerable reduction in precipitation. (SEM x1200)

Therefore, higher temperatures would be expected to have improved ductility even when DRX is not possible. However, the onset of DRX may also be influenced by grain boundary particles and removal of these precipitates may promote recrystallisation. At the lowest strain rate, $3 \times 10^{-4} \text{ s}^{-1}$, GBS dominates the recovery of ductility, ductility only slightly recovering with the onset of DRX, from 53 to 67% R of A as shown in Figure 6.8. Metallographic examination of the coarse grained condition at 1123 K revealed serrated boundaries, Figure 6.12(a), marking the onset of DRX, but even at 1273 K, Figure 6.12(b), when DRX was well advanced there still was not a great improvement in the ductility.

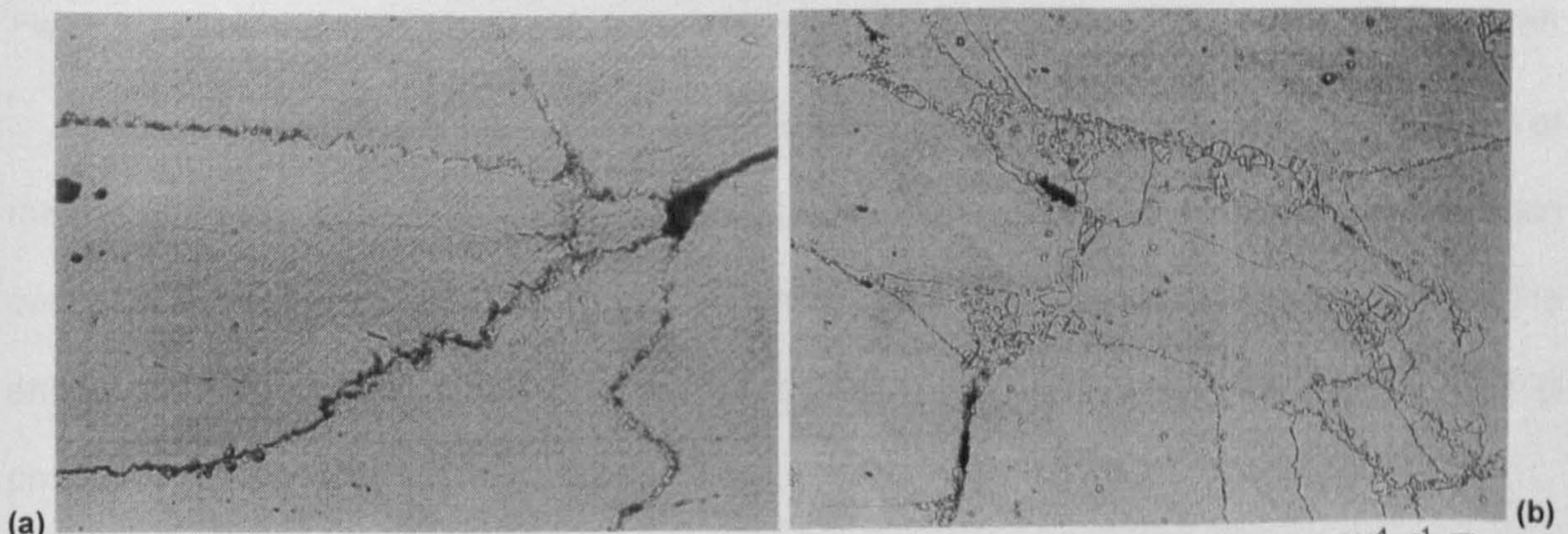


Figure 6.12: (a) Irregular serrated boundaries showing the early stages of DRX, 1123 K, $3 \times 10^{-4} \text{ s}^{-1}$. The cracks are sufficiently long enough to cause poor ductility even when DRX is well advanced at higher temperatures (b) Substantial DRX present at 1173 K, $3 \times 10^{-3} \text{ s}^{-1}$. (mag x120)

At the highest strain rate, $3 \times 10^{-1} \text{ s}^{-1}$, ductility recovers before DRX can occur and this was confirmed by metallographic examination where although ductility had almost fully recovered at 1223 K, there was no evidence that DRX had occurred, Figure 6.13. This is in accordance with T_d being calculated to be between 1248 and 1293 K. The improvement in ductility at the higher temperature can therefore arise either from a reduction in the amount of GBS or by DRX. DRX seems to be most effective at the lower strain rate of $3 \times 10^{-3} \text{ s}^{-1}$, but at $3 \times 10^{-4} \text{ s}^{-1}$ ductility does not fully recover following the onset of DRX. When DRX is responsible for recovery in ductility, the value used for ' ε_c ' is very important in obtaining good agreement with the temperature at which ductility recovers and for the coarse grained steel, ε_c more closely follows the experimental results than ε_p . However, it has been shown^{2,68} that DRX does not always result in ductility improving and often temperatures much higher than T_d , around 100 K in fine grained steels², are required before ductility recovers.

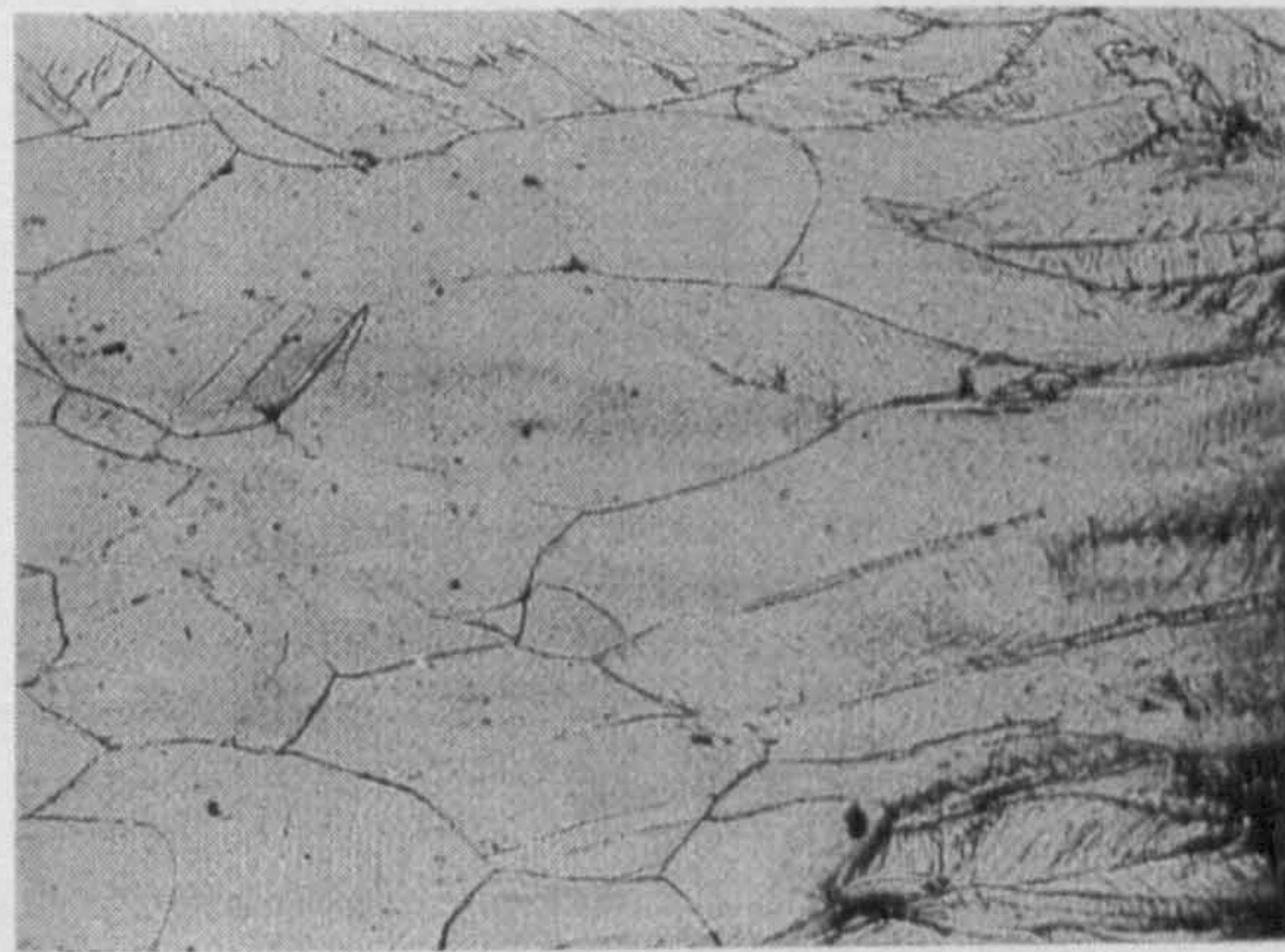


Figure 6.13: Coarse grained sample with good ductility and no evidence of DRX, 1223 K, $3 \times 10^{-1} \text{ s}^{-1}$. (mag x120)

It is clear from this work that in order to make the theory more universal, the depth of the trough needs to be theoretically determined for when grain boundary sliding is the main cause of intergranular failure. This will involve developing equations which include the effects of temperature, strain rate and precipitation size and distribution on the sliding process.

6.3.3 Relevance of the Hot Ductility Curve to Transverse Cracking

The two sections of the hot ductility curve that are relevant to the problem of transverse cracking at the straightener, during conventional continuous casting, form the curve ABC as shown in Figure 6.14. This is because DRX never occurs during the straightening operation, as the strains involved are too small ($\sim 2\%$) and the grain size is too coarse, sections CD and C'D' are not relevant. Although thin films of ferrite can form at very low strains, there is no evidence that the large amounts of DIF, which can be produced just below the A_{e3} in a tensile test, can also form at these low strains. Therefore, the depth of the trough is most important in predicting the likelihood of transverse cracking as it represents the ductility of the un-recrystallised grains.

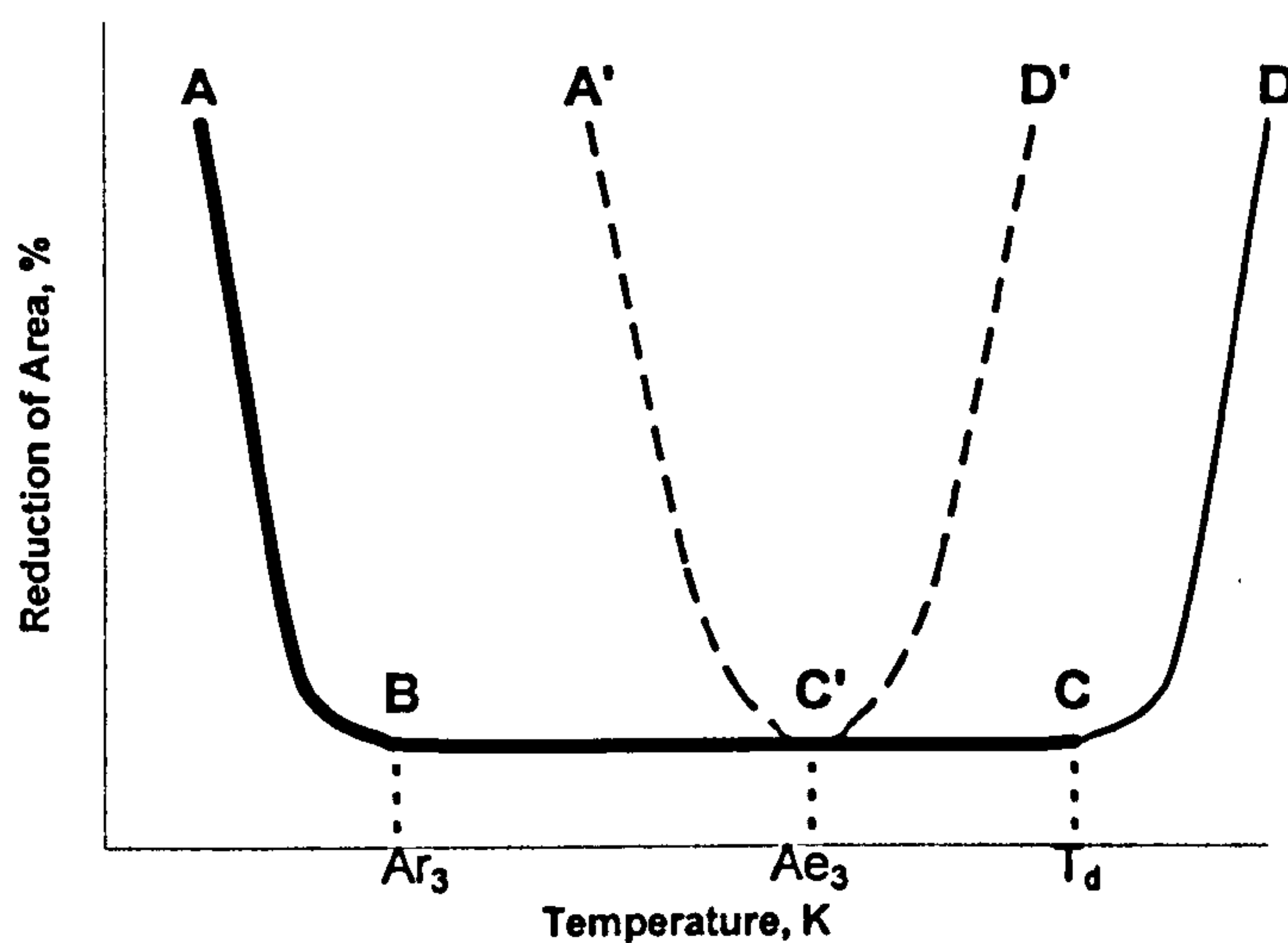


Figure 6.14: Schematic diagram highlighting the parts of the ductility curve that are relevant to the problem of transverse cracking.

6.4 Conclusions

1. This model was found to work reasonably well for very simple plain C-Mn steels, in which no microalloying precipitates were present, provided that the strain rate is about 10^{-3} to 10^{-4} s^{-1} and the cooling rate is in the range 60 to 100 Kmin^{-1} ; these are the conditions pertaining to conventional continuous casting. The model can be used to predict the ductility curve for a simple steel if the A_{e3} and A_{r3} (undeformed) temperatures are known along with the curves of ε_c and ε_f against temperature. The latter curve requires knowledge of the amount of S able to precipitate out at the γ boundaries and the ferrite volume fraction.
2. Recovery in ductility at the high temperature end of the trough for the C-Mn steels was found to take place at the point when DRX becomes possible. This occurs either when the curve of the strain to fracture, ε_f , either intersects the curve of critical strain for DRX, ε_c , or when the A_{e3} temperature is exceeded, whichever is the higher. Recovery at the low temperature end always occurs when substantial amounts of ferrite forms either before or during deformation.
3. For the austenitic stainless steel with the fine grain size of $40\mu\text{m}$, the model predicted that ductility would be excellent and DRX would occur throughout the entire temperature range; this is in accordance with the experimental and metallographic observations. DRX occurred at tensile strains lower than those causing failure in the coarser grained material throughout the temperatures range studied.
4. For the coarse grained austenitic stainless steel, ductility troughs were obtained with the minimum ductility values for all the strain rates studied occurring at 1123 K. Extensive networks of chromium carbides were found at the γ grain boundaries, which prevented DRX and instead encouraged cracks formed by grain boundary sliding to grow and

interlink. Recovery at the low temperature end was found to be due to a reduction in grain boundary sliding even though the carbides were still present. Whereas the recovery in ductility at the high temperature end was due to DRX occurring, but only at strain rates of $3 \times 10^{-3} \text{s}^{-1}$ as are found in the straightening operation during conventional continuous casting. Increasing the strain rate to $3 \times 10^{-2} \text{s}^{-1}$ resulted in less grain boundary sliding and ductility improved without DRX; whereas at very low strain rates of $3 \times 10^{-4} \text{s}^{-1}$, grain boundary was increased sufficiently such that DRX had little influence on the ductility.

5. The model used was found to work reasonably well for very simple plain C-Mn steels in which no microalloying precipitates were present. However, for the austenitic stainless steel clearly the model needs to take into account grain boundary sliding and a creep type model of the form given in reference 11 needs to be incorporated.

7. Influence of Columnar Grains

Transverse cracking during the straightening operation, as has already been mentioned, has been a subject much studied due to the cost and quality implications involved. Cracks form on the top surface and edges of the continuously cast strand during the straightening operation; these cracks can penetrate to a depth of up to 15mm, requiring scarfing for removal. An austenitic stainless steel slab having a coarse columnar structure emanating from the surface into the interior was chosen to study the effect of the columnar grains, as it would be expected to retain its grain structure down to room temperature. The work on this part of the programme has already been partly published.¹²¹

7.1 Introduction

The influence of grain size on hot ductility has been well established. As can be seen from Figure 7.1, R of A values increase as the grain size refines and shallower and narrower troughs are also observed. However, it can also be seen that above a grain size of 300 μ m, the change in R of A is relatively small. The curve in Figure 7.1 was established for essentially equiaxed grain structures, these being the shape that is invariably produced on solution treating. However, even when the small tensile samples have been melted in-situ and cooled to the test temperature, the grain size in the as-cast region is still equiaxed.

However, Mintz *et al.*² have noted from examination of transverse cracks on the surface of slabs, that cracks always propagate from the surface along the long boundary of the columnar grains. When columnar grains are not present, such severe cracking is not observed. Vodopivec *et al.*¹²² have also suggested that this cracking may be caused by the presence of a coarse dendritic structure which is favoured by Al in solution to at least 0.04%.

¹²¹ B. Mintz, A. Cowley and R. Abushosha: *Mat. Sci. and Technol.*, 2000, 16, pp. 1-5.

¹²² F. Vodopivec, M. Torkar, M. Debelak, M. Kmetec, F. Haller and F. Kaucic: *Mat. Sci. and Technol.*, 1988, 25, p. 917.

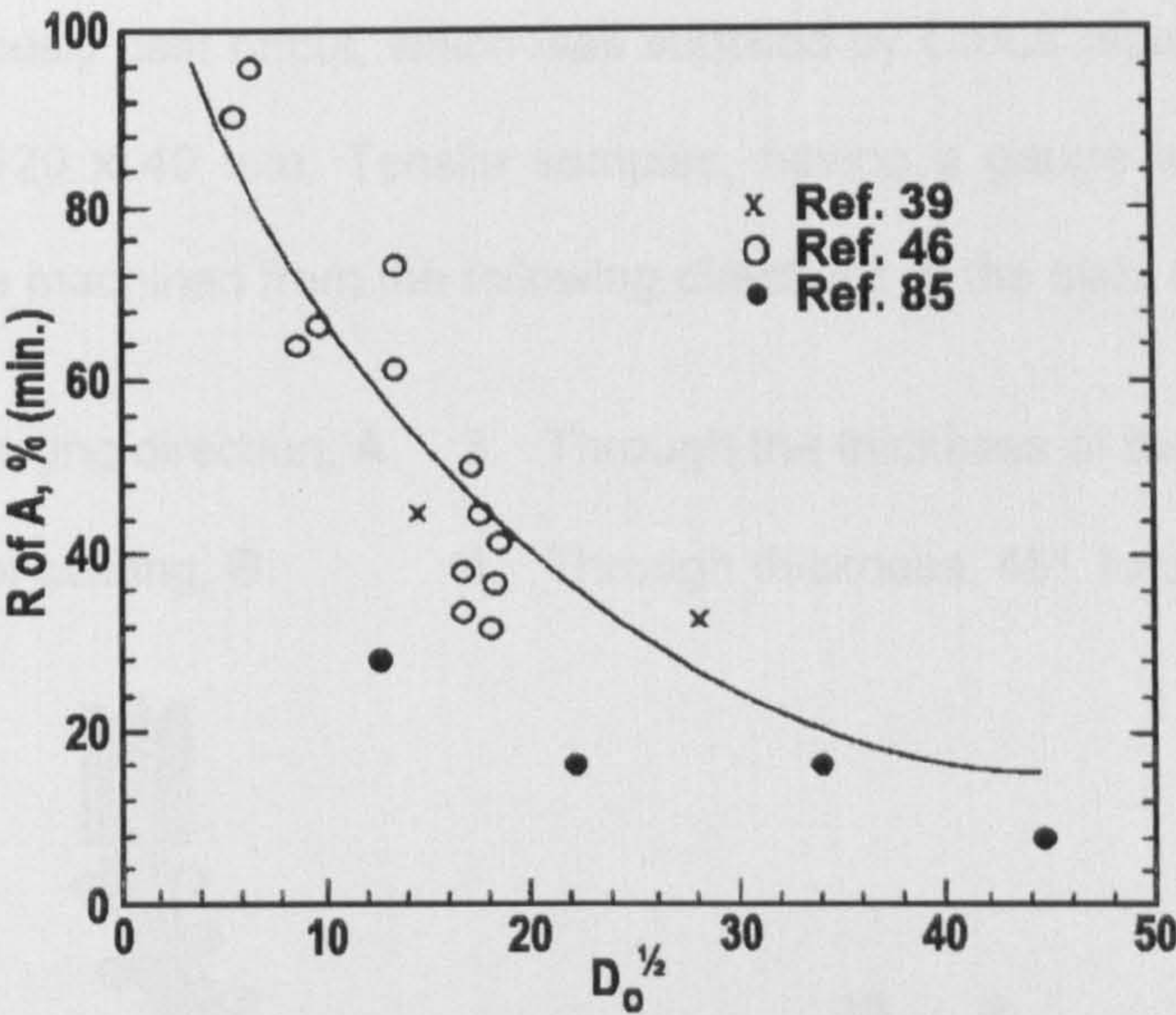


Figure 7.1: Influence of initial undeformed grain size after heat treatment, D_o , on minimum R of A value.²

The boundary length of the columnar grains can be up to 10mm compared to the ~1mm equiaxed grains that can be produced on casting. Such a length of boundary in the long direction of a columnar grain oriented normal to the tensile stress, that is produced during the straightening operation, might be expected to cause deterioration in ductility. There are of course difficulties in examining the influence of columnar grain orientation within the tensile specimen on ductility. Investigation was required to ascertain the importance of the presence of columnar shaped grains on ductility for HSLA steels. Even if columnar grains are present in the as-cast slab, reheating to a temperature of 1603K will cause them to recrystallise into equiaxed.

7.2 Experimental Details

In order to test these ideas, a continuously cast slab of austenitic stainless steel having columnar grains present at room temperature was chosen; the steel will maintain this columnar structure at 1603K and the composition is as shown in Table 7.1.

Steel	C	Mn	S	P	Si	N	Cr	Ni	Mo	V
12	0.14	1.63	0.003	0.012	0.27	0.054	25.1	20	0.054	0.05

Table 7.1: Compositions of the steel studied in this section, wt. %.

The continuously cast offcut, which was supplied by Corus' Scunthorpe Works, had dimensions 200 x 120 x 40 mm. Tensile samples, having a gauge length of 25mm and diameter 5mm, were machined from the following directions in the slab, see Figure 7.2.

1. Transverse to casting direction, **A**.
2. In the direction of casting, **B**.
3. Through the thickness of the slab, **C**.
4. Through thickness, 45° to casting direction, **D**.

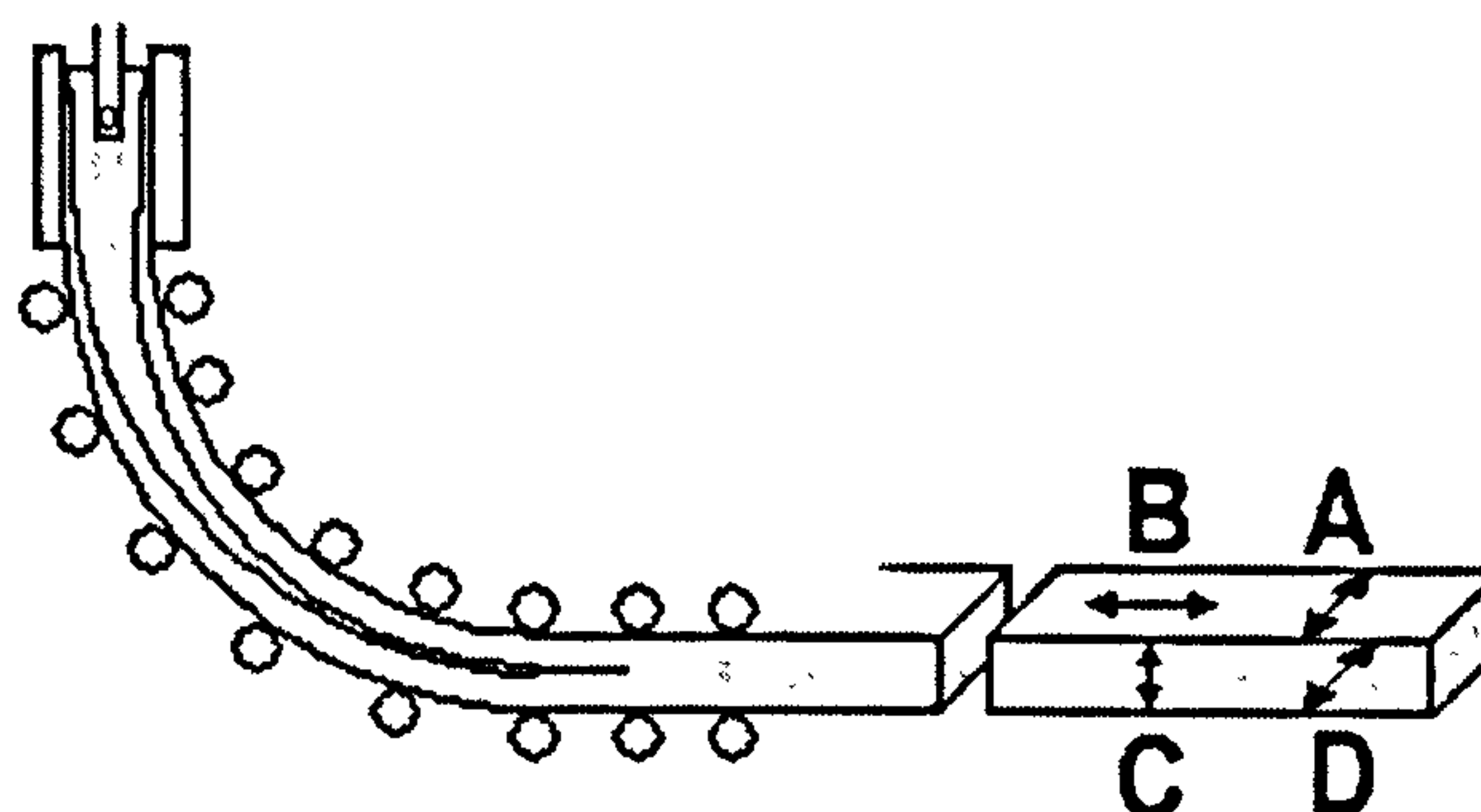


Figure 7.2: Sample directions.

The samples were heated to 1603K, held for 5 minutes and cooled at 60Kmin^{-1} to test temperatures in the range 1273K to 973K, held for 5 minutes at temperature and then strained to failure at $3 \times 10^{-3}\text{s}^{-1}$.

7.3 Results and Discussion

The hot ductility curves for the 4 directions A, B, C and D are given in Figure 7.3. Ductility in the through-thickness direction, C, is excellent having >85% R of A throughout the whole temperature range. However, it can be seen that ductility deteriorates as the test direction changes from C to D then A to B, ductility at test temperatures of 973K dropping to a minimum of 55% and at 1273K, a minimum of 35%. Thus, ductility is worse when the tensile direction is perpendicular to the long columnar boundary, as it is when the straightening operation takes place.

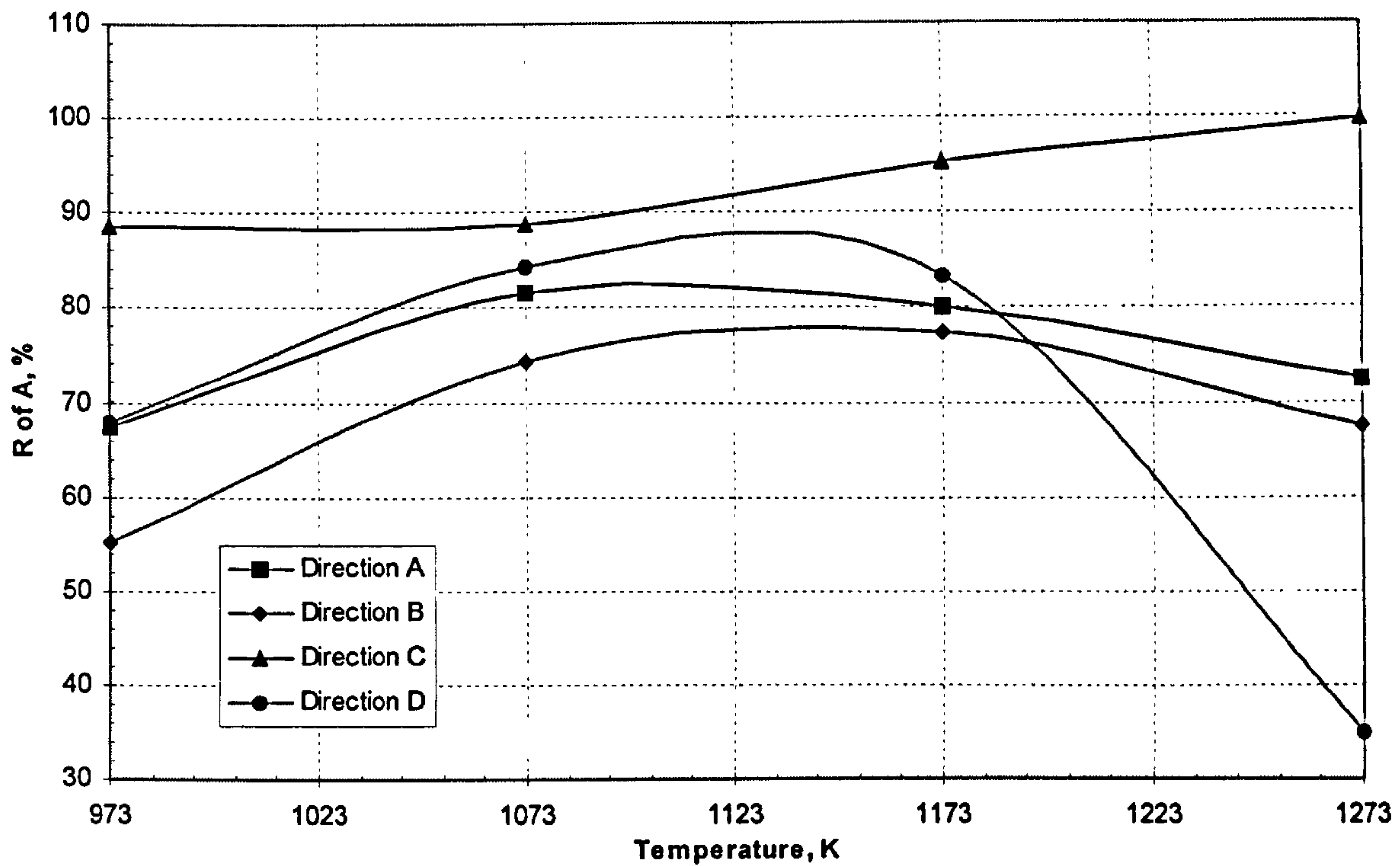


Figure 7.3: Hot ductility curves for the four sample directions studied; A - transverse direction, B - casting direction, C - through thickness direction and D - through thickness at 45° to casting direction.

The stress-strain curves for samples from the four directions tested in the temperature range of 973 to 1273K are given in Figures 7.4 to 7.7.

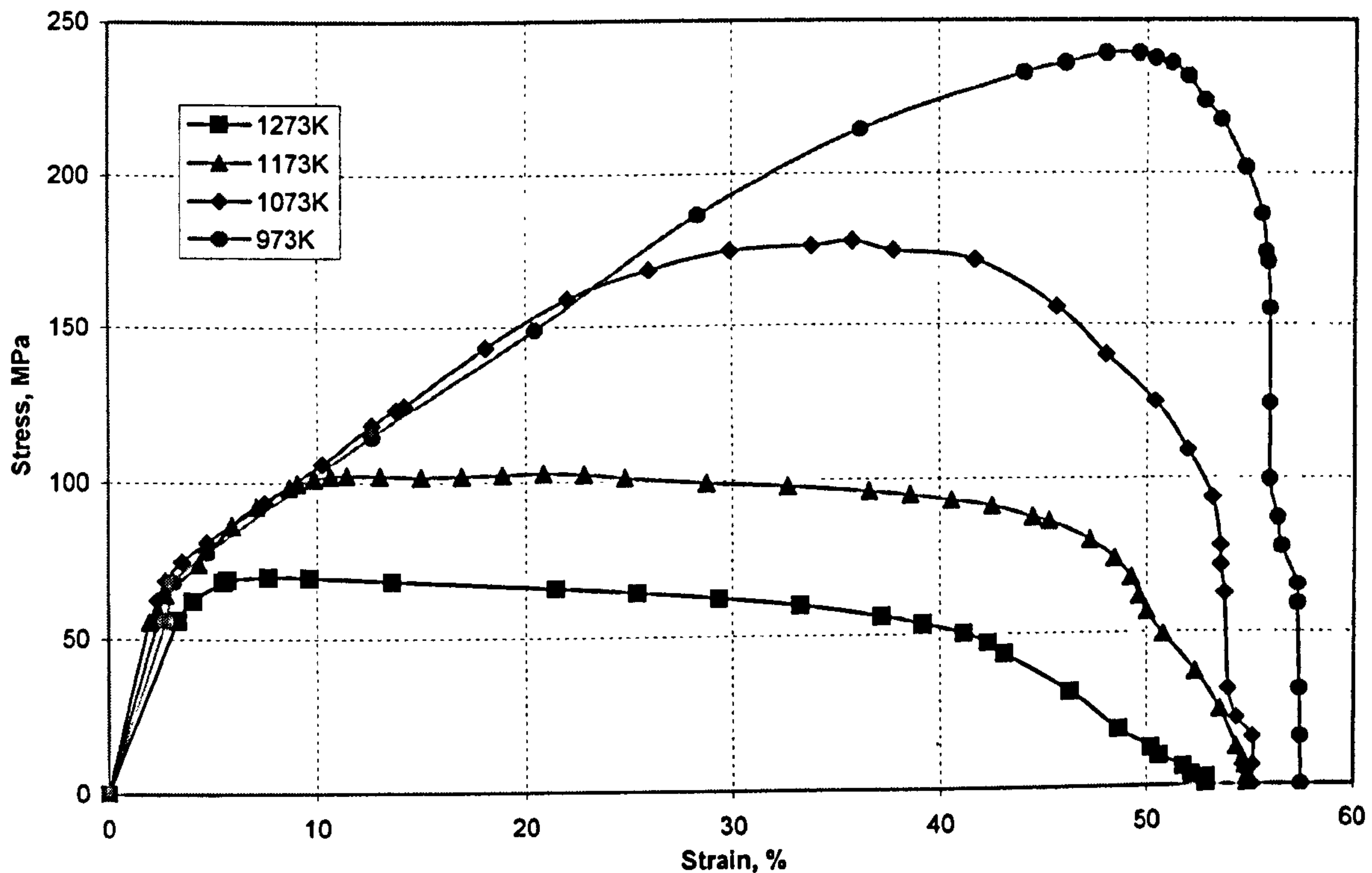


Figure 7.4: Stress - strain curves for samples taken transverse to the casting direction (A).

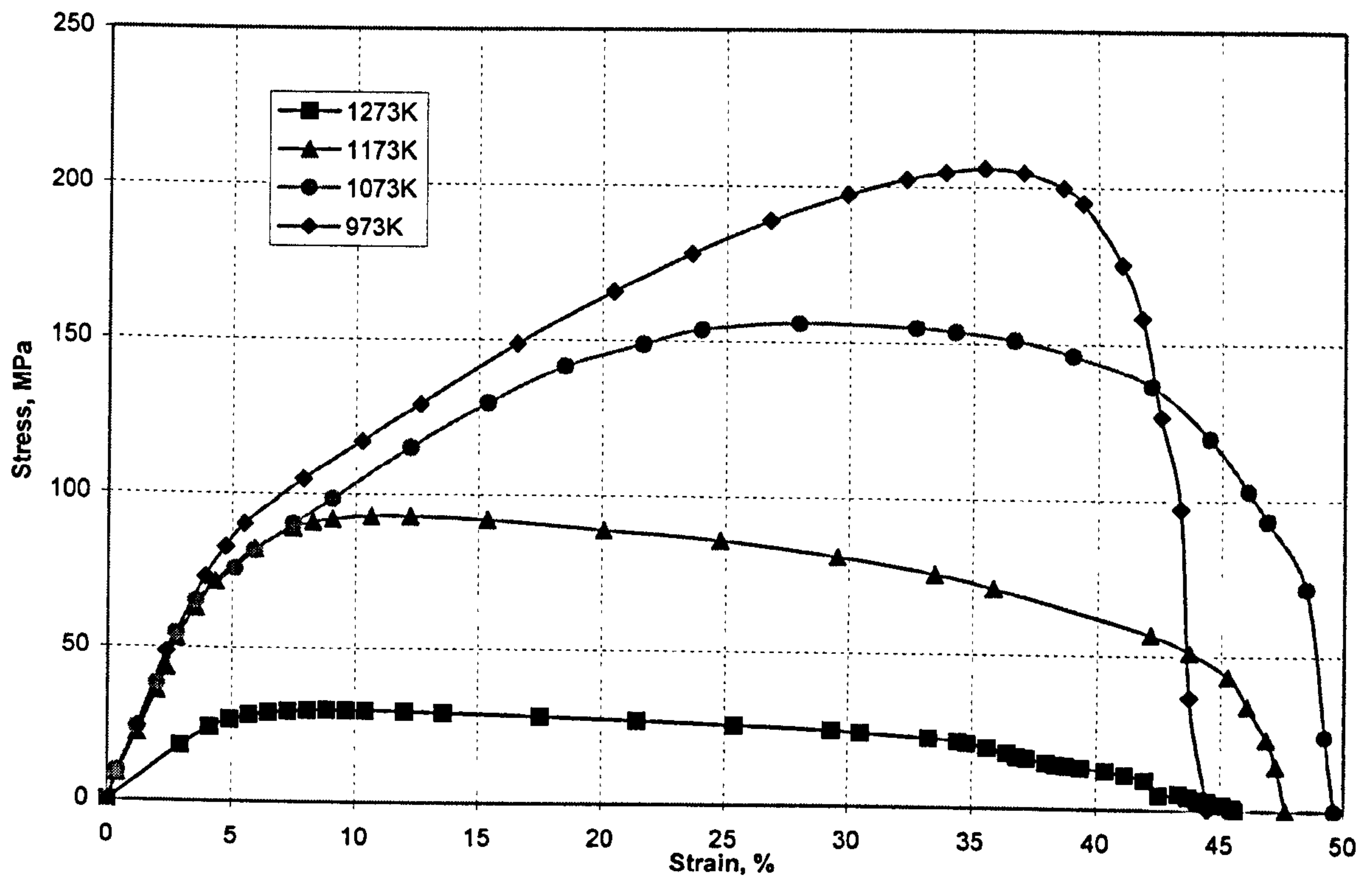


Figure 7.5: Stress – strain curves for samples taken parallel to the cast direction (B).

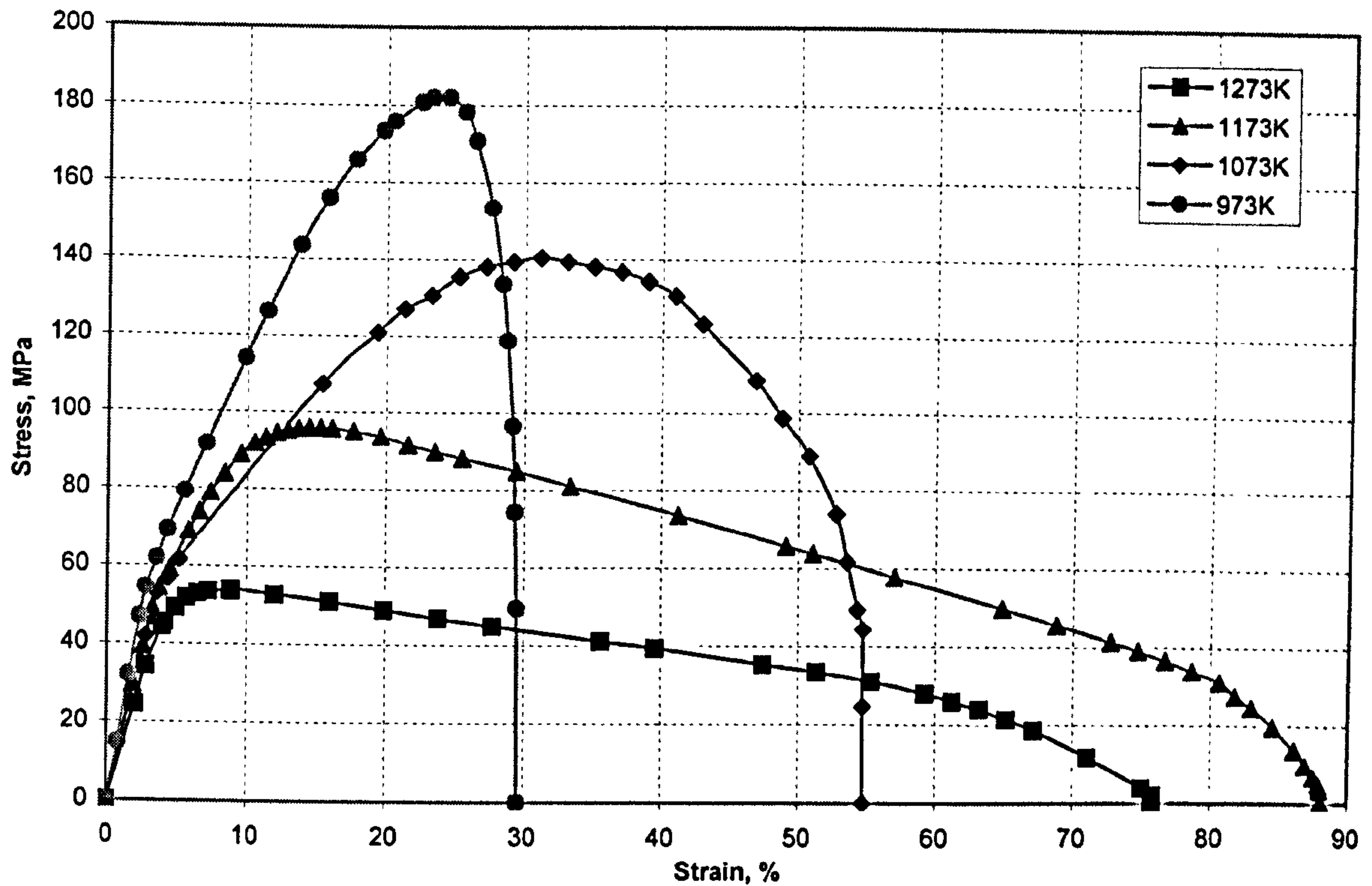


Figure 7.6: Stress – strain curves for samples taken in the through thickness direction (C).

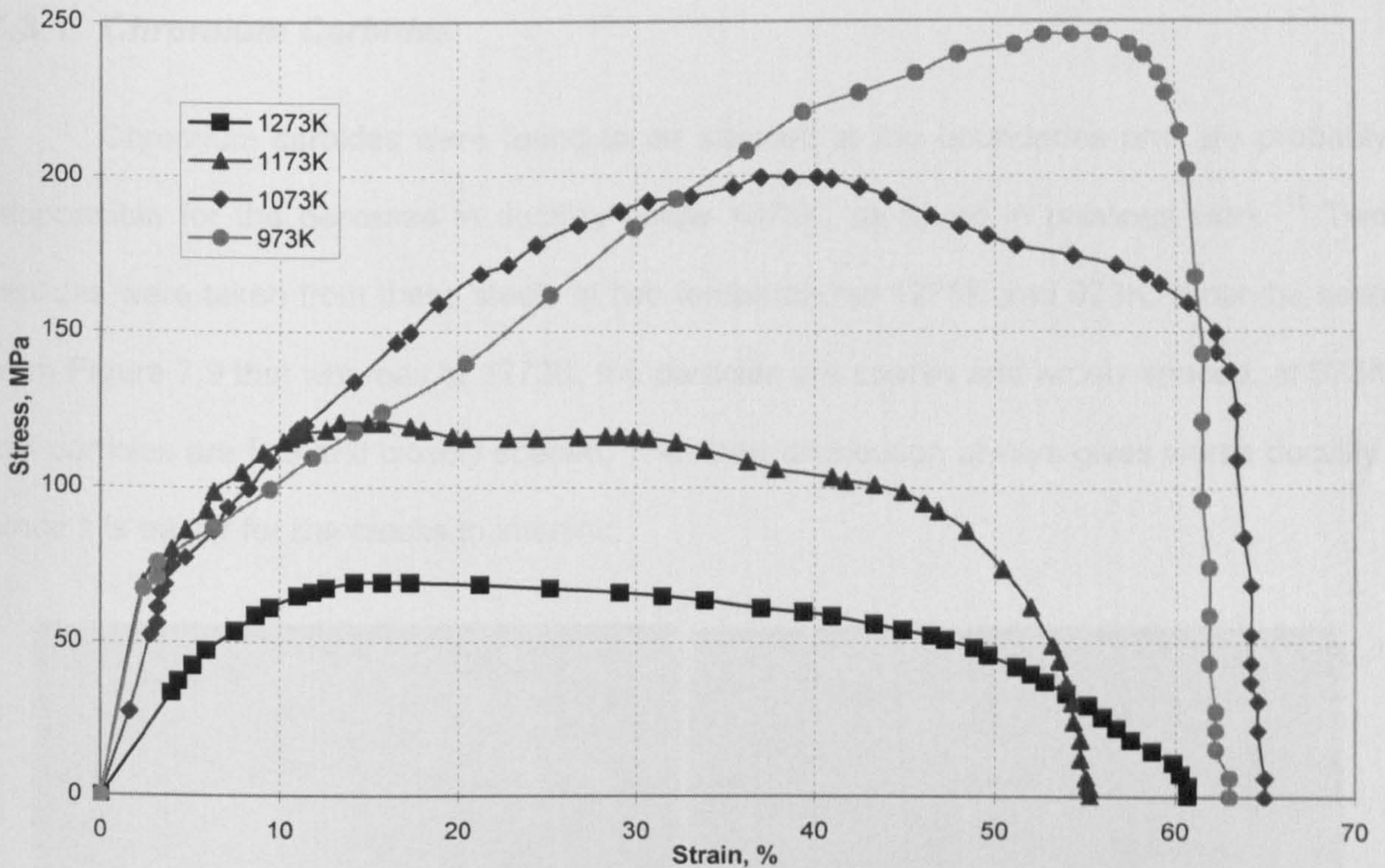


Figure 7.7: Stress – strain curves for samples taken through thickness, 45° to the casting direction (D).

From Figure 7.8(a), it can be seen that the tensile samples for the through-thickness direction, C, have excellent ductility; however, in Figure 7.8(b), samples taken parallel to the casting direction, B, have cracks present at 45° and at right angles to the tensile axis.

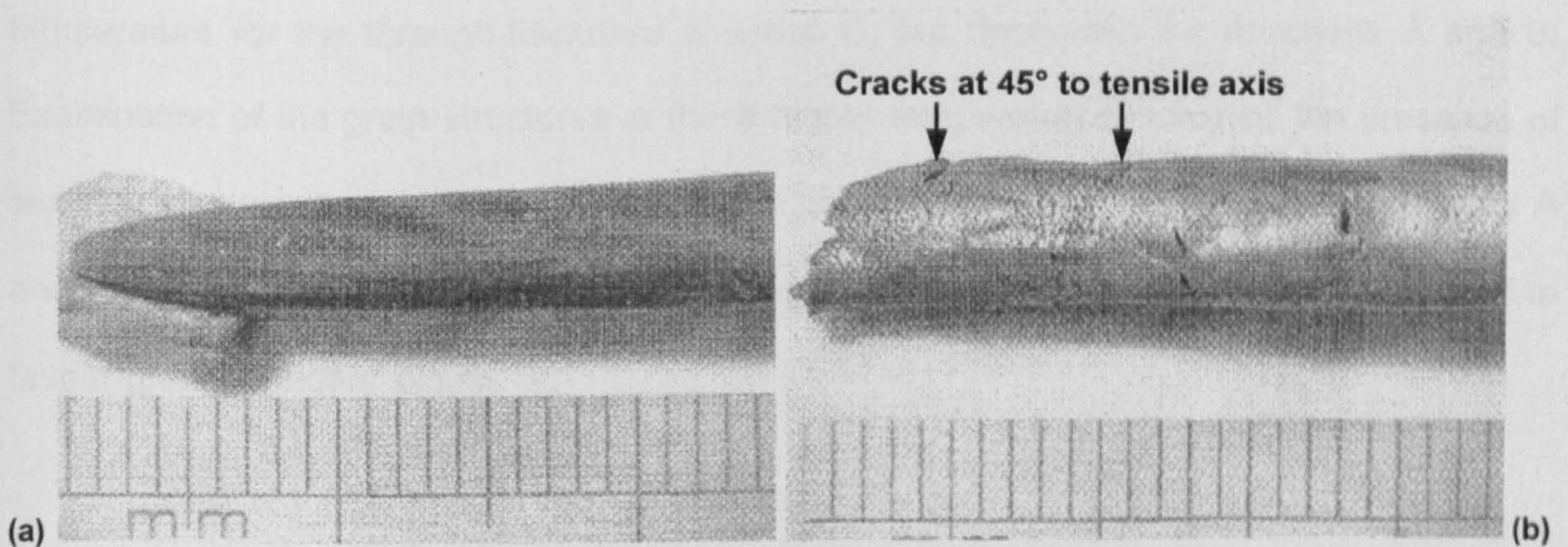


Figure 7.8: Failed samples (a) in the through thickness direction, C, showing excellent ductility and (b) parallel to the casting direction, B, showing poor ductility and numerous cracks.

7.3.1 Chromium Carbides

Chromium carbides were found to be situated at the boundaries and are probably responsible for the decrease in ductility below 1073K, as found in previous work.¹¹² Two replicas were taken from these steels at two temperatures 1273K and 973K. It can be seen from Figure 7.9 that whereas at 1273K, the particles are coarse and widely spaced, at 973K the particles are fine and closely spaced. The latter distribution always gives worse ductility, since it is easier for the cracks to interlink.

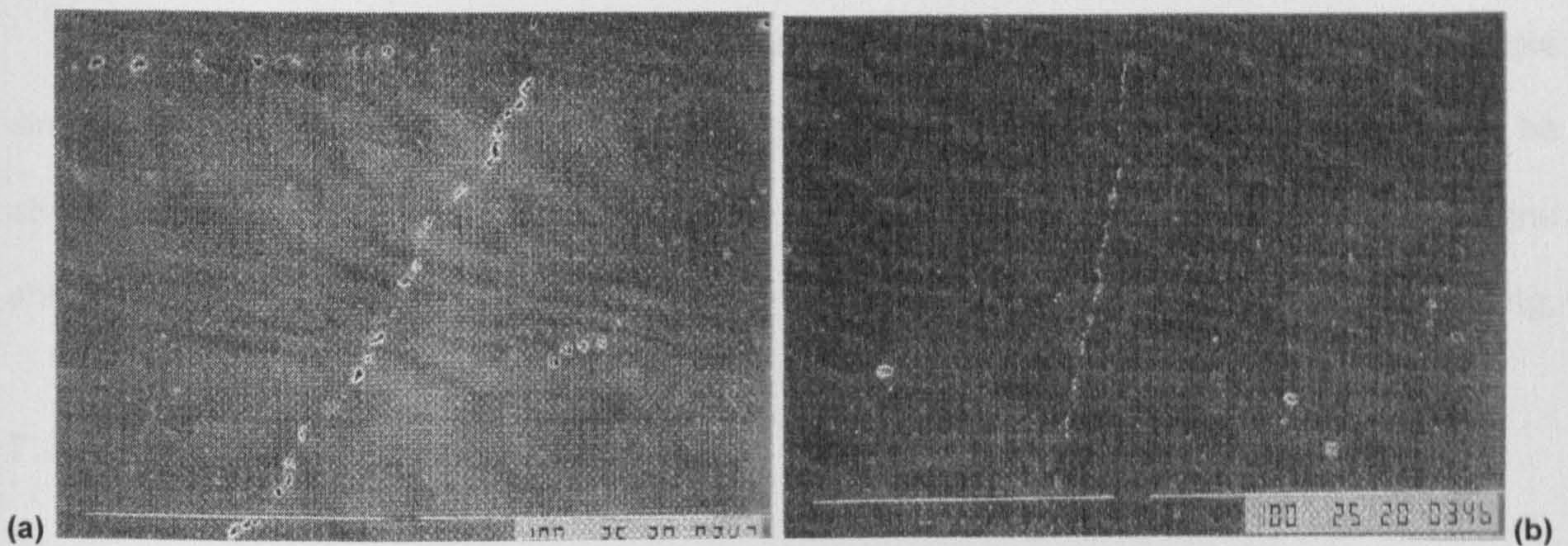


Figure 7.9: Chromium carbides at γ grain boundaries at (a) 1273K and (b) 973K (SEM, mag. x300).

It is interesting to note, that above 1123 K, ductility improves with increase in temperature for the through-thickness direction C, but decreases for directions A and B. Examination of the grain structures at these higher temperatures indicated the presence of serrated boundaries in direction C, but not in direction B, see Figure 7.10. In directions A and B and D, straight boundaries were observed and such boundaries would be expected to favour grain boundary sliding.

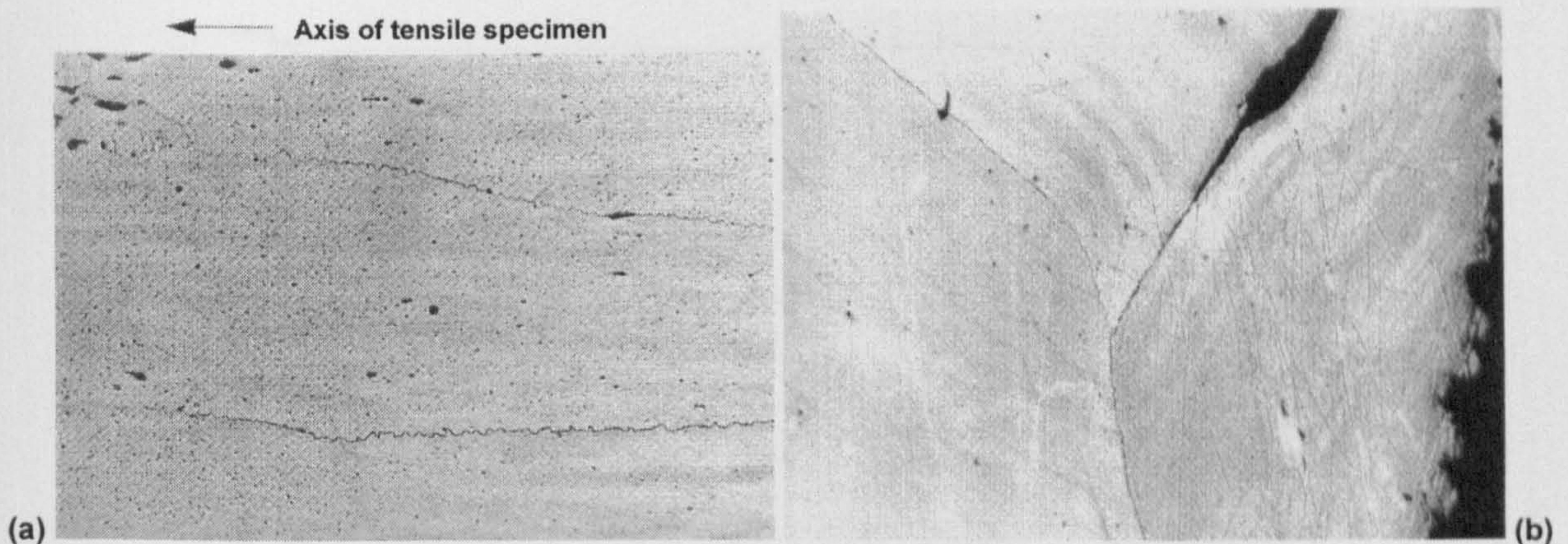


Figure 7.10: Optical micrograph (mag. x60) of (a) serrated boundaries present in through thickness sample, C, tested at >1173K, and (b) absence of serrated boundaries in sample parallel to casting direction, B, at 1173K.

Figure 7.3 shows that ductility decreases at temperatures above 1123K, for sample directions A, B and particularly D. The marked drop in ductility for this latter direction can be attributed to long columnar boundaries being at 45° to the tensile specimen axis so that the shear stress at the boundaries is a maximum, thus greatly enhancing grain boundary sliding.

7.3.2 Analysis of flow curves

The curves of peak stress and the strain to the peak stress are given in Figures 7.11 and 7.12. For the peak stress versus test temperature curves in the lower temperature range 973 to 1173K, the values are similar for directions A and D. Changing the direction of testing to B and then to C results in progressively lower peak stresses. The strain to the peak stress behaviour, Figure 7.12, is again similar for directions A and D in the lower temperature range, but drops significantly for directions B and C.

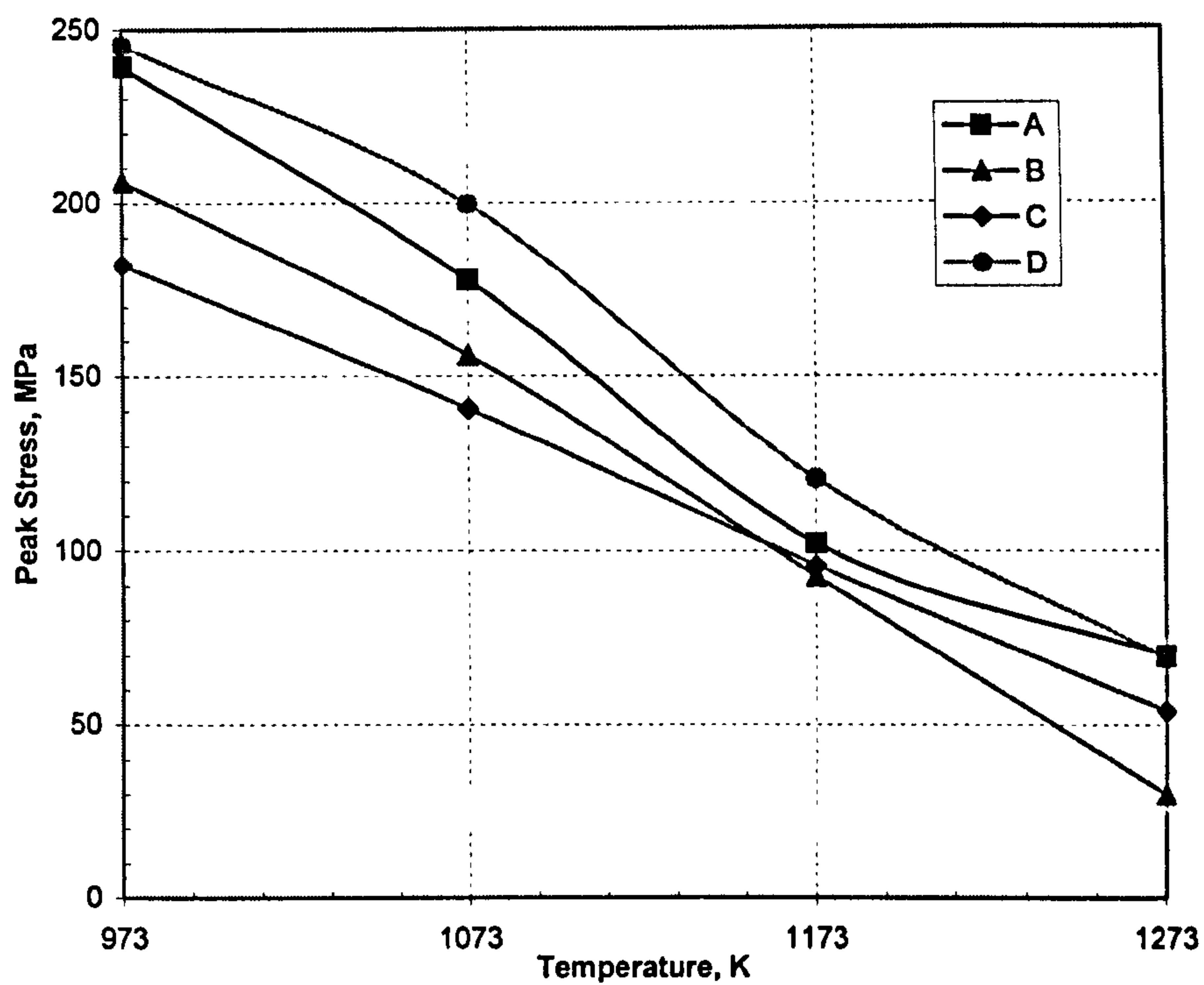


Figure 7.11: Curves showing variation of peak stress with temperature for the four sample directions.

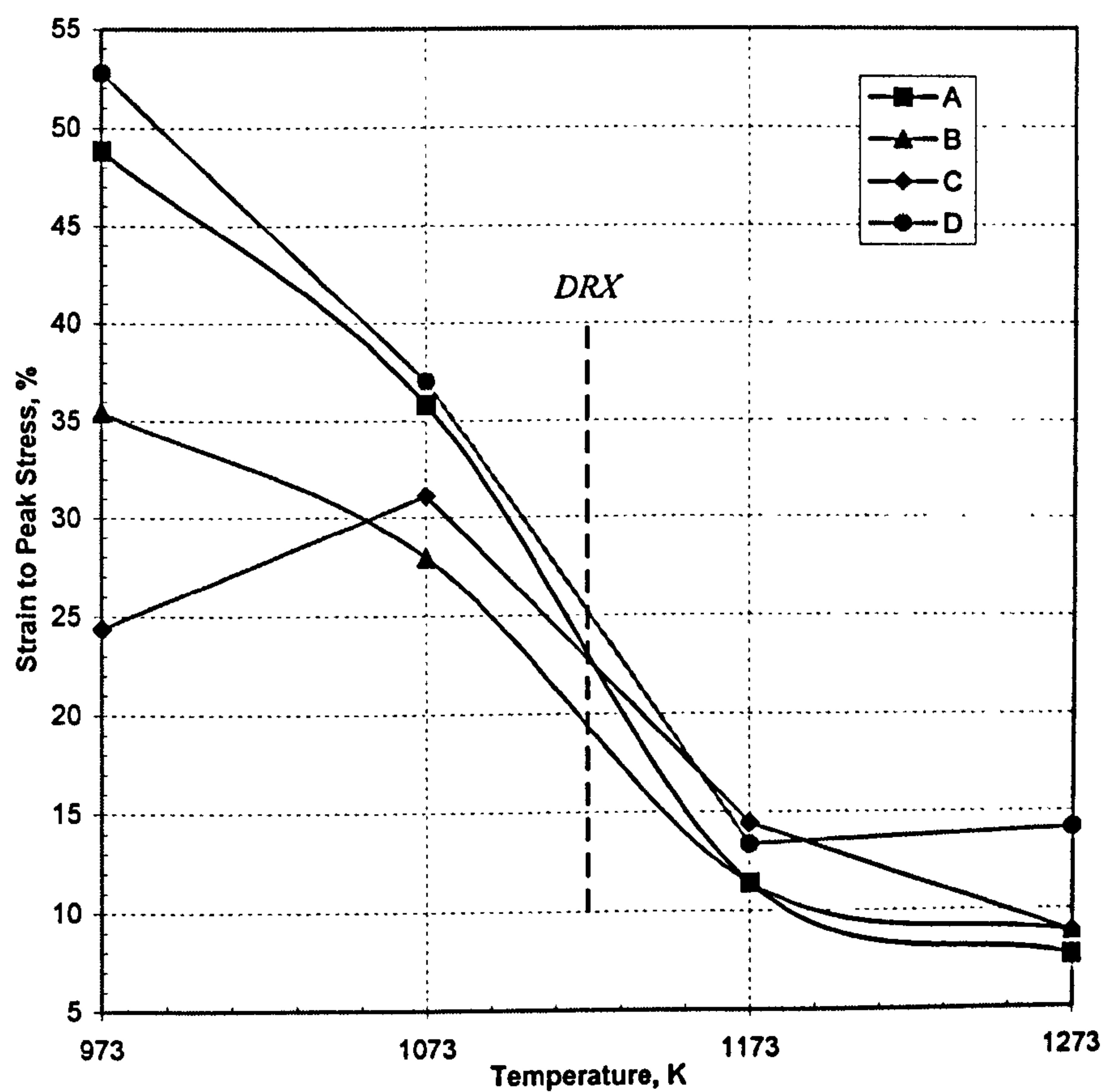


Figure 7.12: Curves of the strain to the peak stress against temperature for the four sample directions.

The smaller stresses required for deformation in direction C are consistent with its good ductility. However, steel B also deforms at low stresses yet has the worst ductility in this lower temperature range. Clearly there are other factors which are influencing behaviour. The most likely of these factors is texture. It has not been possible to determine the texture of the grains, but these are almost certainly highly textured and as such, it would be expected that the peak stress behaviour would also be very directional.

Dynamic Recrystallisation

It can be seen from Figure 7.12, the curve of strain to the peak stress against temperature, that dynamic recrystallisation appears to occur for all directions once a temperature of 1173K is reached. Surprisingly, metallographic examination of the tensile samples taken in direction C gave little evidence for dynamic recrystallisation at 1173K. It is not clear why there is this disparity between the metallographic observations and the flow stress behaviour.

7.3.3 Interpretation of the hot ductility curves

In order to fully understand how the hot ductility behaviour changes with grain orientation relative to the tensile axis, it is necessary to determine the grain shape. The average size of a columnar grain was found to be 8 x 2 x 1 mm and this shape is shown in the schematic diagram in Figure 7.13.

The cigar shaped form of the grains can be deduced from Figures 7.14(a)–(c); Figure 7.14(a) shows the view along the length of the tensile sample in the through-thickness direction, C, Figure 7.14(b) the cross-section of a tensile sample in the through-thickness direction, and Figure 7.14(c) a cross-section of the tensile sample taken in the casting direction, B.

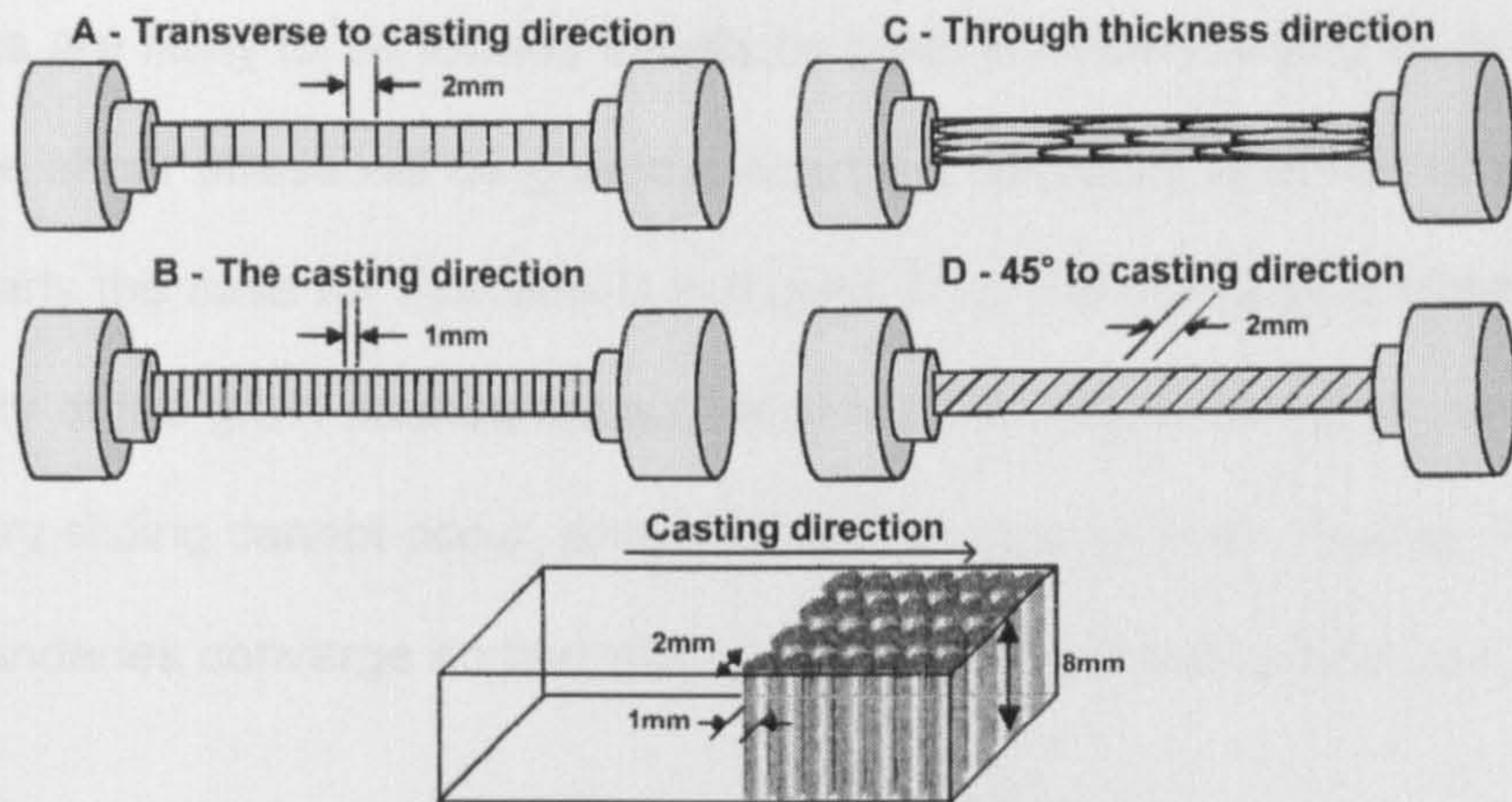


Figure 7.13: Schematic diagram of columnar grain structure in the four sample directions.

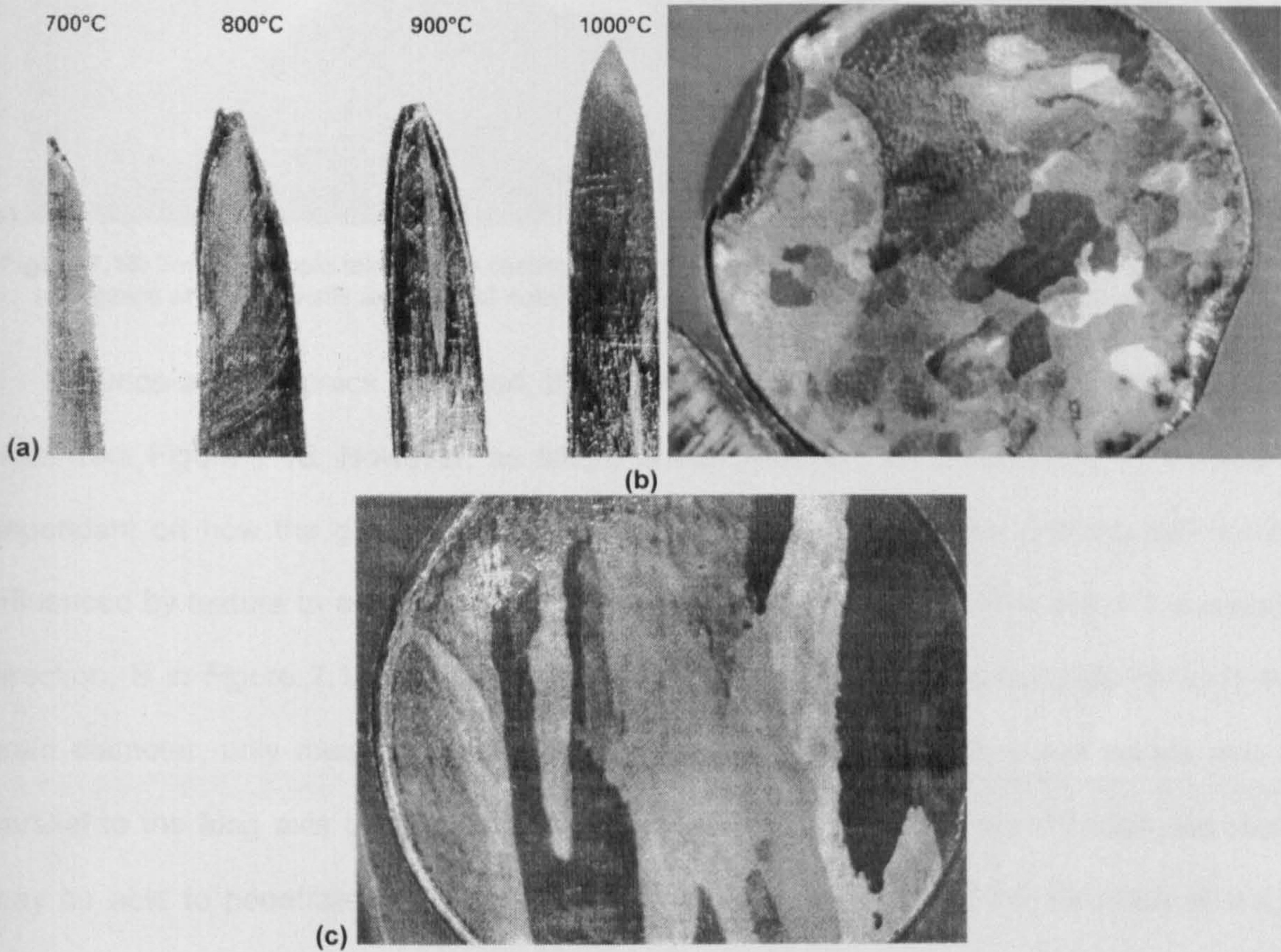


Figure 7.14: Micrographs of sample sections taken in (a) through thickness direction, C, showing long columnar grains (mag. x3), (b) cross-section of through thickness sample, showing cigar shape of columnar grains – the dendritic nature of grains can also be discerned (mag. x6) and (c) cross-section of casting direction sample B, showing presence of very long columnar grains traversing across the entire gauge diameter (mag. x6).

Cracks are likely to be formed initially by grain boundary sliding as in Figures 7.8(b) and 7.15. The shear stress will be greatest when the boundary is at 45° to the stress axis, as is particularly the case for direction D in Figure 7.13. For samples in directions A, B and C, the majority of the grain boundaries will be parallel or perpendicular to the stress axis, so grain boundary sliding cannot occur, except where the grains meet, Figures 7.8(b) and 7.15, when the boundaries converge so that sliding and crack nucleation can occur.

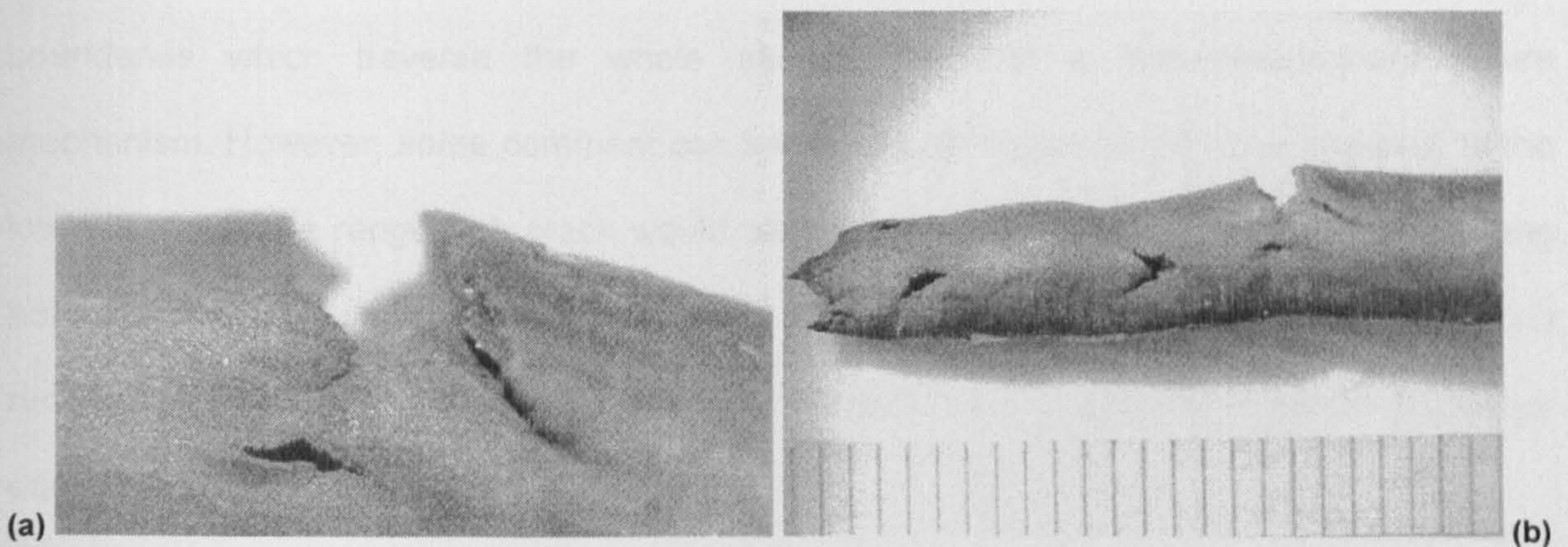


Figure 7.15: Tensile sample taken in the casting direction, B, and strained to failure at 1273K, showing cracks (a) forming at 45° to tensile axis and (b) subsequently being opened by normal stress (scale in b is mm).

Once a shear crack is formed, the normal stresses will also be important as can be seen from Figure 7.15. However, as failure is intergranular, the progression of a crack is dependant on how the grain surfaces are oriented to the tensile axis and this will not be influenced by texture to any great degree. If the grain surfaces are orientated in the casting direction, B in Figure 7.13, then the crack once started can easily propagate through the grain diameter, only meeting a few grains, Figures 7.8(b) and 7.15. If the tensile axis is parallel to the long axis of the columnar grains, C in Figure 7.13, then although the crack may be able to penetrate to $\sim 1\text{mm}$, it then meets a new grain and the direction of crack propagation has to change.

Although the situation is similar in the transverse direction, direction A in Figure 7.13, to that noted for direction B, in that a crack can propagate through the whole of a grain diameter in the through thickness direction before meeting another grain, the width of the crack is narrower leading to better ductility.

The ease of propagation of the cracks is therefore dependant on the average grain boundary surface which lies perpendicular to the tensile axis. Assuming the grain shape is elliptical (Area of ellipse = πab , where $a = \frac{1}{2}$ minor axis and $b = \frac{1}{2}$ major axis), then the respective areas for the A, B and C directions can be calculated as 6.28, 12.5 and 1.57mm^2 in accord with their relative ductilities.

It is more difficult to calculate this value for direction D, but shearing along the grain boundaries which traverse the whole sample diameter is the predominant failure mechanism. However, some comment can be made with regard to the area involved. In the lower temperature range, the crack would be expected to partly propagate along the long boundary of the columnar grain, but would also be able to propagate along the much reduced cross-section of the columnar grains. It would therefore be expected to have better ductility than the B direction.

It is not clear why the ductility should be so poor at 1273K for the D direction, but because the boundaries are oriented at 45° , it may be at this high temperature that grain boundary sliding becomes the dominant method of failure and normal stresses play a lesser role. Certainly, examination of the fracture sample for direction D at 1273K, shows a very different failure to what was normally found – the fracture being completely shear as can be seen from Figure 7.16.

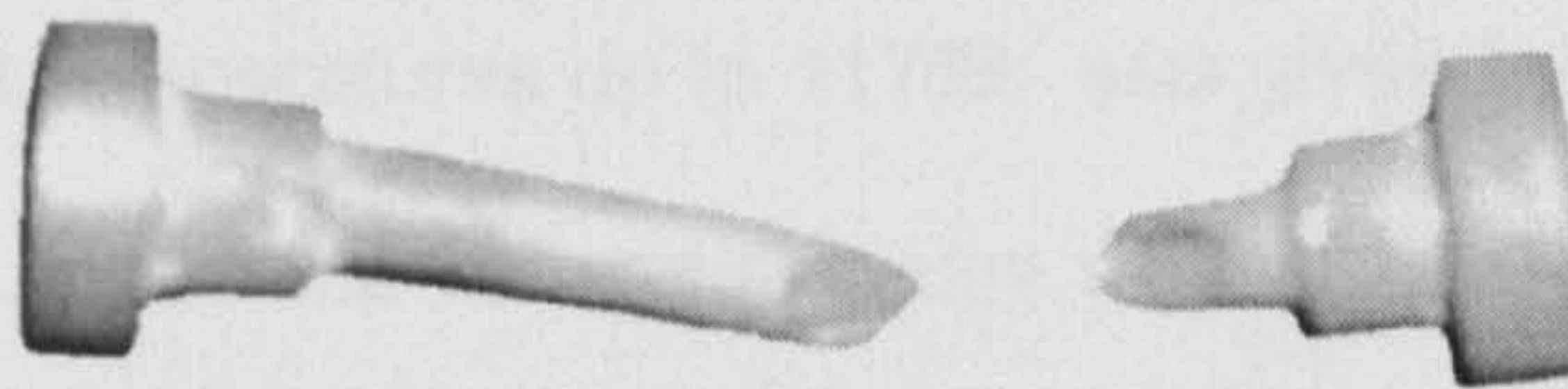


Figure 7.16: Failed sample taken from direction D, showing very poor ductility resulting from enhanced grain boundary sliding due to the long columnar boundaries lying at 45° to the tensile axis.

This work clearly shows that the shape of the grains at the surface of a continuously cast slab is very important. Columnar grains are particularly detrimental, as the straightening stresses are perpendicular to the long axis of the columnar grains and this will encourage crack propagation to the depth of the columnar grains below the surface, which can be up to 15mm. The possibility of magnetic stirring in the mould, in order to break up these columnar grains, should be considered.

7.4 Conclusions

The following observations were made:

1. The R of A values observed in all four sample directions improved as the test temperature was increased from 1023 to 1123K. This improvement was due to a coarsening and reduction in number of Cr carbides situated at the γ boundaries.
2. The R of A values for a given sample direction were found to be related to the amount of grain boundary lying perpendicular to the tensile axis; it was found that the smaller this apparent grain size, the higher the ductility that would be observed.
3. The highest ductility was seen in the samples with the columnar grains parallel to the tensile axis, i.e. taken from the through thickness direction, C, of the continuously cast slab. The propagation of cracks was hindered by the larger number of grain boundaries encountered as the crack attempted to develop through the sample.
4. The worst ductility, at temperatures up to 1173K, was given by samples taken parallel to the casting direction, B, as the columnar grains were then perpendicular to the tensile axis. When a crack formed, it could easily propagate through the sample and in some cases without meeting another grain which would require a change in direction. This is the situation that is experienced in the top surface of the continuously cast slab during the straightening operation, when columnar grains are present.

5. Columnar grains have been shown to contribute to poor ductility and encourage transverse cracking. It is therefore recommended, wherever possible, to avoid developing a columnar structure in the continuously cast slabs.
6. The normal stress was found to control the ductility for temperatures up to 1123K, grain boundary sliding may initiate the cracks but was not principally responsible for the propagation through the sample.
7. At temperatures above 1123K, only samples taken from the through thickness direction of the slab experienced a continued increase in ductility. This continued improvement in ductility is probably due to the higher strains possible in this direction allowing dynamic recrystallisation to occur more readily, thus preventing grain boundary sliding. The start of dynamic recrystallisation being observed as serrated grain boundaries. The deterioration in ductility for the other three sample directions is due to grain boundary sliding dominating the failure process; this was particularly marked for samples taken at 45° to the through thickness direction.

8. Influence of Residual Copper

8.1 Introduction

Only a few investigations have been carried out into the influence of Cu on the hot ductility in the temperature range 1373 to 973K.^{70,87,123} Of these, Hannerz⁸⁷ has examined the influence of Cu most extensively. The steel was a 0.07% C, 1.5% Mn plain C-Mn steel with Cu additions up to 1%, but no significant influence of Cu on hot ductility at temperatures >973K was found, see Figure 8.1. The steels were solution treated at 1623K and cooled at 60Kmin⁻¹.

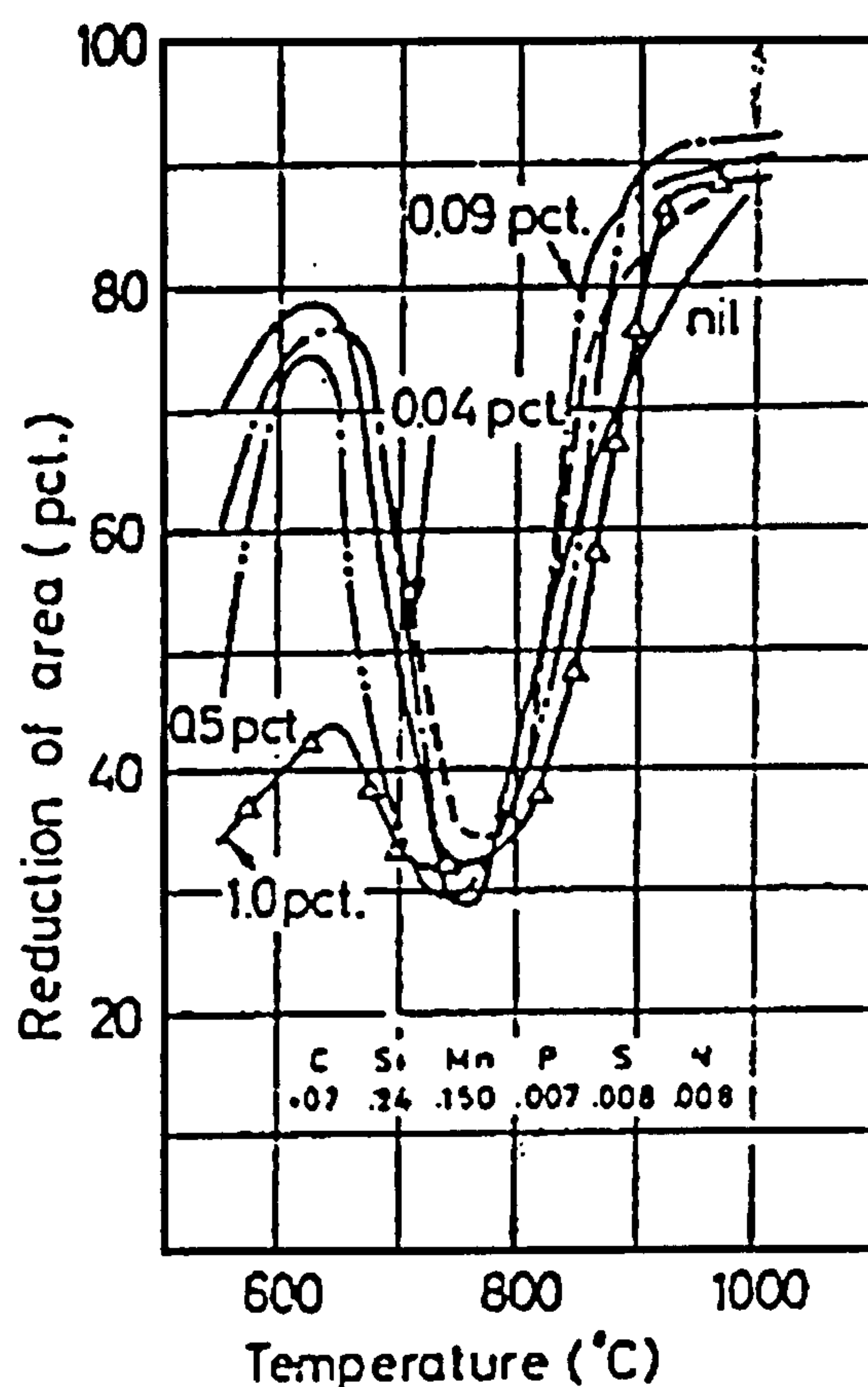


Figure 8.1: Influence of copper on the hot ductility of C-Mn-Al steels.⁸⁷

¹²³ W.T. Nachtrab and Y.T. Chou: Metal. Trans., 1986, 17a, p. 1995.

Hannerz noted in his paper that this insensitivity of ductility to Cu contrasts very much with commercial experience, in which small amounts of Cu cause poor surface quality and cracks. Hannerz suggested that this difference probably arises because of the oxidising atmosphere present during commercial casting. He suggested that the tensile tests should be carried out in an ordinary atmosphere.

Previous work at City University⁷⁰ has examined the influence of both Cu and Ni on the hot ductility of C-Mn-Al and C-Mn-Nb-Al steels; these steels contained Cu or Ni up to 0.5%. As with Hannerz's work, there was no effect of Cu and Ni on hot ductility when the steels were solution treated at 1603K and cooled to the test temperature at 60Kmin⁻¹, see Figure 8.2. However, even when an oxidising atmosphere was used, no influence of Cu could be found, see Figure 8.2.

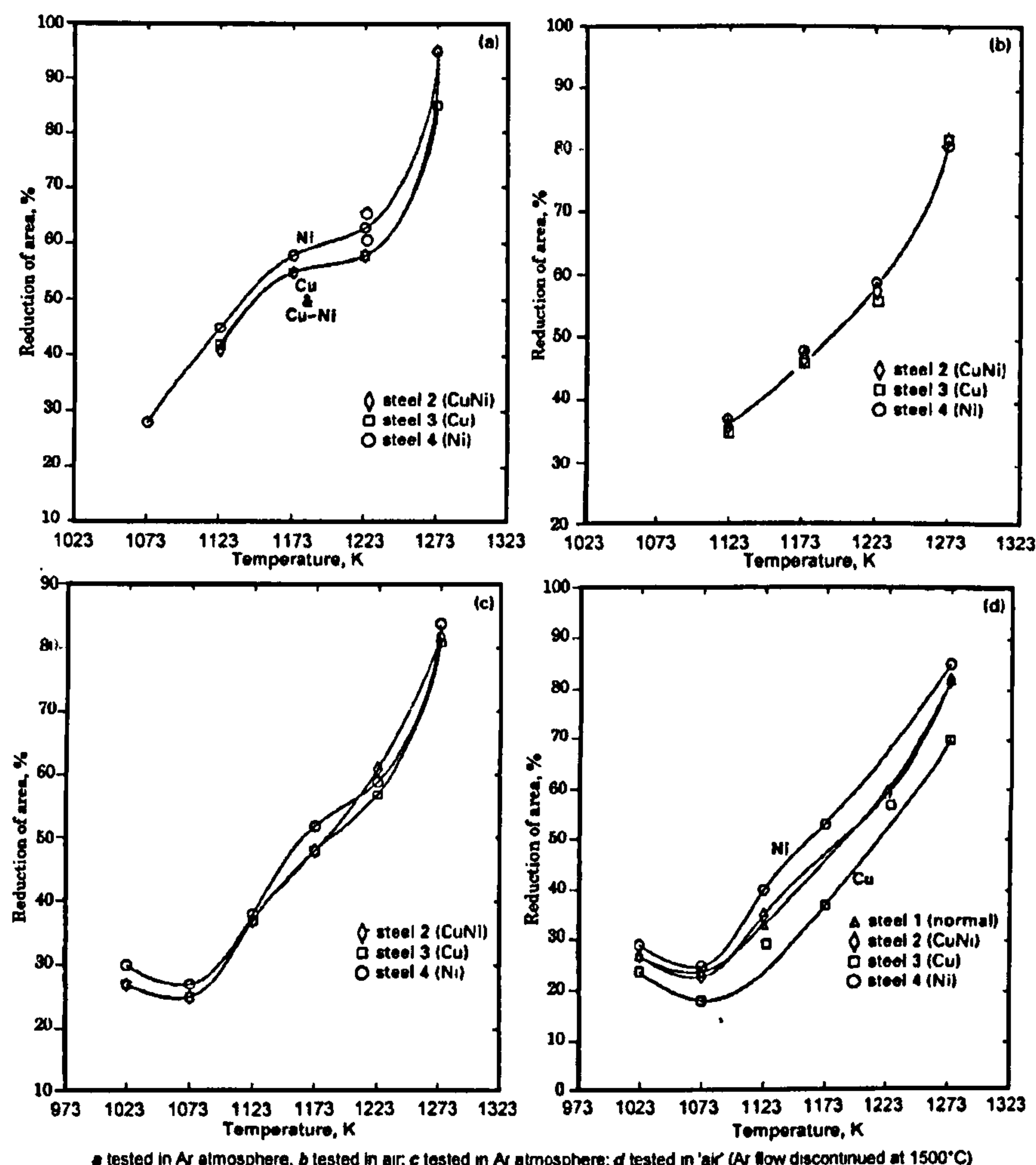


Figure 8.2: Hot ductility curves for a, b solution treated and c, d as cast C-Mn-Al-Nb steels, tested in various atmospheres (steel 1 was only tested as cast in 'air').⁷⁰

The possibility that increased segregation was required was then examined by melting the centre of the tensile samples and cooling directly to the test temperature in an argon atmosphere. Again, no influence of Cu on hot ductility could be found, see Figure 8.2. Only when the tensile samples were cast directly after melting and tested in an oxidising atmosphere was the deleterious influence of Cu obtained. A similar addition of Ni was required to prevent Cu deteriorating the ductility. Hot shortness was found not to be the explanation. The deterioration was due to fine copper sulphides or any sulphide particles at the grain boundaries which had formed on cooling as a result of oxidation and the presence of Cu, according to the reaction:



The present work was designed to examine the effect of Cu at higher cooling rates pertaining to thin slab casting. Unfortunately, due to lack of time it was not possible to use an oxidising atmosphere and only the results for the protective argon atmosphere are given.

8.2 Experimental Details

The compositions of the steels examined in this part of the study are given in Table 8.1, below. Hot ductility results obtained previously at City University ⁷⁰ for steels 15 and 16 have been included in this section for comparison.

Steel	C	Mn	S	P	Si	Nb	Al	N	Cu
13	0.11	1.40	0.007	0.013	0.33	0.029	0.030	0.0065	-
14	0.10	1.57	0.005	0.012	0.42	0.031	0.030	0.0090	0.5
15*	0.10	1.51	0.006	0.010	0.40	0.032	0.034	0.0075	-
16*	0.10	1.57	0.006	0.012	0.42	0.031	0.030	0.0080	0.5

Table 8.1: Analysis of steels studied in this section, wt. %.
* Studied in previous work using oxidising atmosphere.⁷⁰

Induction tensile samples were used. The tensile specimens were melted at 1813K, held for 5 minutes, cooled at 200Kmin⁻¹ to test temperatures in the range 1273K to 1073K, held a further 5 minutes at the test temperature and then strained to failure using a strain rate of 3 x 10⁻³s⁻¹.

8.3 Results and Discussion

It can be seen from the hot ductility curves given in Figure 8.3, that at the faster cooling rate pertaining to thin slab casting, i.e. 200Kmin^{-1} , steel 14 which contains 0.5% Cu gives the worst ductility. Also included in this figure are curves from previous work⁷⁰ on similar as-cast steels (i.e. residual and 0.5% Cu containing steels, 15 and 16 respectively), but in this case tested in an oxidising atmosphere using a slower cooling rate of 60Kmin^{-1} . Again, the ductility can again be seen to be worse in the 0.5% Cu containing steel.

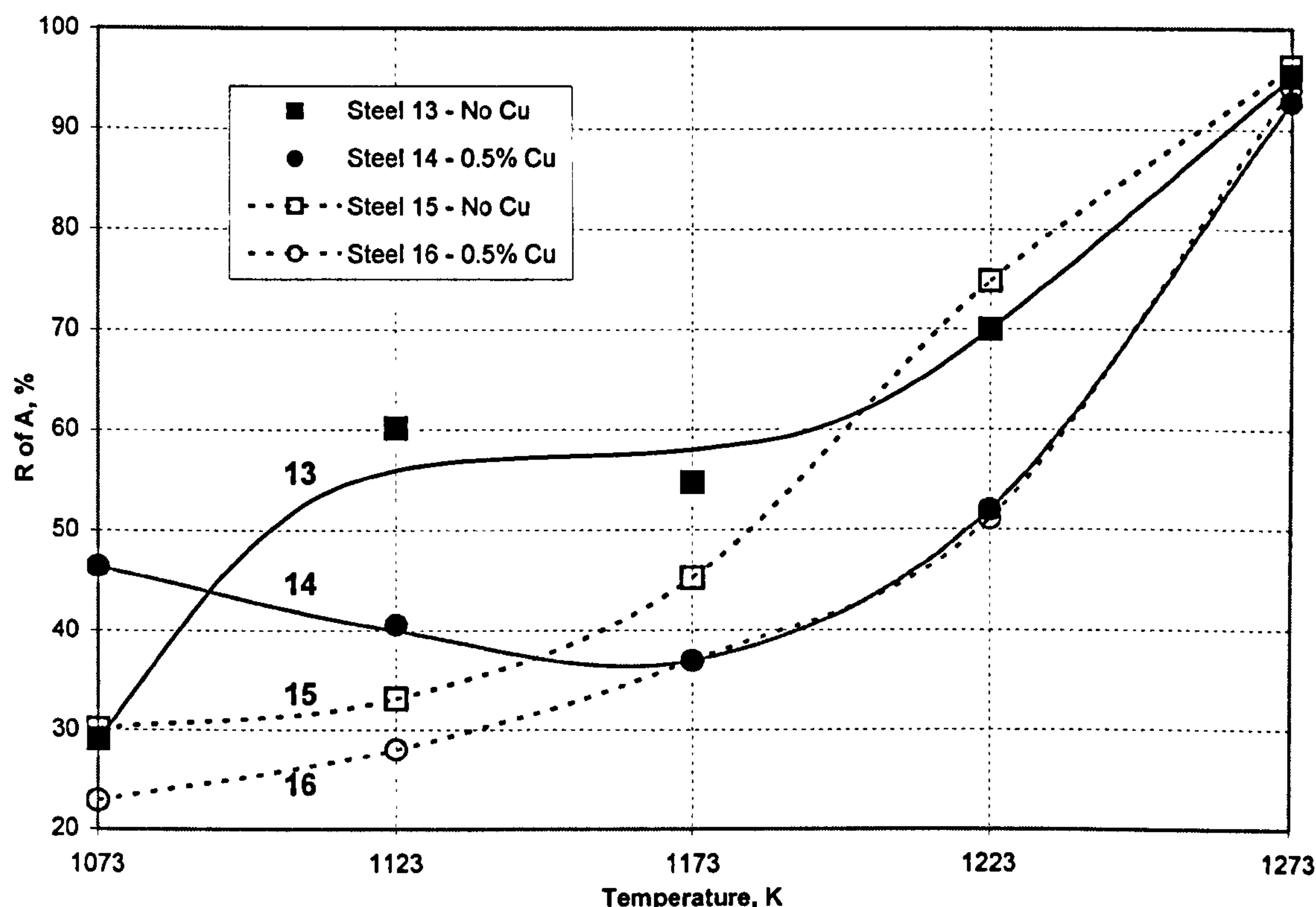


Figure 8.3: Hot ductility curves showing effect of residual copper. Steels 10 and 11 were cooled at 200Kmin^{-1} , 12 and 13 at 60Kmin^{-1} .

Thus, both increasing the cooling rate and oxidation result in Cu additions impairing the ductility. In the present instance, it might be expected that the deleterious influence of Cu would be much more marked in the presence of an oxidising atmosphere. Previous work had ascribed the deterioration in ductility produced by the Cu to be due to the formation of fine CuS particles.⁷⁰ Increasing the cooling rate might be expected to produce a finer sulphide distribution and possibly a greater supersaturation of Cu at the austenite grain boundaries.

8.4 Conclusions

Residual Cu was found to make the hot ductility worse at the faster cooling rate pertaining to thin slab casting, as shown in Figure 8.3. This deterioration would be expected to be much worse in the presence of an oxidising atmosphere as has been found in previous work¹² at slower cooling rates. Insufficient time was available for examining the cause of this deterioration, but previous work has ascribed it to the formation of fine CuS particles. Clearly more work is required to examine the cause of this deterioration seen in the present work.

9. Summary of Results

This chapter collects the results previously given separately in chapters 4 to 8, for a more detailed presentation, please refer to these chapters.

9.1 Low Temperature Straightening

In the four steels examined in chapter 4 (steels 1 to 4), the depth of the troughs were found to be similar, independent of the presence or absence of Nb. This insensitivity to the presence of Nb is believed to be due to the high P level in these steels reducing the amount of Nb(CN) precipitation in the grain boundary region.

Steel 4 (high C and Mn, C-Mn-Al-Nb) had the widest trough which extended for over 200K. In this steel, the trough below the A_{e3} temperature is due to the presence of a thin layer of DIF surrounding the γ grains. Since α is softer than γ , all the strain concentrates in these films; this causes voiding around the MnS inclusions resulting in low ductility intergranular ductile failures. The deformation induced ferrite at the γ boundaries is not able to develop into the matrix as the temperature is reduced and ductility only improves when the temperature has fallen below the A_{r3} (undeformed) and the normal transformation induced ferrite forms in large quantities. Strain is then taken up more homogeneously in the structure and ductility therefore improves. Above the A_{e3} , the trough is extended to higher temperatures by grain boundary sliding in the γ and ductility improves gradually owing to coarsening of the Nb(CN) precipitates and the onset of DRX.

The narrowest trough was given by steel 1 (low C and Mn, C-Mn-Al); in this steel ductility recovered very rapidly on either side of the A_{e3} temperature. Above the A_{e3} , with the absence of Nb(CN) precipitation, DRX occurred easily. Below the A_{e3} , ductility improved rapidly owing to the formation of large amounts of DIF close to equilibrium volume fractions.

Steel 2 (high C and Mn, C-Mn-Al) had a trough which was extended at the low temperature end, below the A_{e3} in the same way as steel 4 (high C and Mn, C-Mn-Al-Nb). DIF only formed as thin films resulting in poor ductility. Above the A_{e3} , ductility again started to recover due to DRX, but this recovery was slower than for steel 1 (low C and Mn, C-Mn-Al), possibly because the A_{e3} temperature is lower reducing the driving force for DRX.

Steel 3 (low C and Mn, C-Mn-Al-Nb) gave a similar curve to steel 4 (high C and Mn, C-Mn-Al-Nb) at the high temperature end of the trough above the A_{e3} , owing to Nb(CN) delaying the onset of DRX. At the low temperature end, ductility still remained poor below the A_{e3} for about 30K, but further reduction in temperature caused ductility to improve and the curve then followed that for steel 1 (low C and Mn, C-Mn-Al) as large amounts of DIF were formed.

It is not entirely clear what is responsible for producing the large amounts of DIF in steels 1 and 3 (low C and Mn) which results in a narrowing of the trough. It is possible that a high transformation temperature may encourage the formation of DIF. This in itself may be enough and the presence of a high Si content in these steels will further raise the transformation temperature. However, another possible explanation is that the high Si content could strengthen the ferrite sufficiently to encourage more of the γ to transform to α under deformation. However, further work is required to clarify these explanations.

When straightening at the low temperature side of the trough, compositional changes which raise the A_{r3} will always enable the straightening operation to be carried out at higher temperatures without risk of cracking. However, it is unclear at the present time whether the necessary requirement of having ~50% ferrite present can be achieved by very low deformation (2 - 4%) or whether much lower temperatures are needed to ensure that the ferrite is present before the straightening operation. Much lower temperatures would require either slower casting speeds, faster heat removal from the strand or a larger

distance between the mould and the straightener. These process changes could result in productivity losses, higher thermal stresses on the solidifying strand or expensive machinery alterations.

9.2 Influence of Cooling Rate and Sulphides on Hot Ductility

The ductility troughs obtained for steels 5 to 8 in chapter 5 can be seen to be grouped as the low Mn (steels 5 and 6) and high Mn (steels 7 and 8) containing steels; the low Mn and high Mn steels giving narrow ductility troughs of approximately 60K centred at ~1135K and ~1060K respectively. There is also a similar displacement in the positions of the observed and calculated curves of percentage ferrite against temperature. This is in agreement with the reduction of transformation temperatures as Mn levels increase; the higher Mn steels have A_e temperatures approximately 40K lower than the lower Mn steels, whereas the A_{r3} temperatures were much lower (~100K). Dilatometry and metallography show that the ductility troughs are caused by the presence of a thin film of deformation induced ferrite.

In the present work it has been shown that sulphur and sulphides do not generally have a major influence on the hot ductility of solution treated C-Mn-Al steels for the compositions examined. This is because for these steels, the temperature range in which a thin band of ferrite forms around the γ grains is very limited. Deformation induced ferrite readily forms in large amounts at temperatures close to the A_{e3} . As such, the trough is governed mainly by the A_{e3} and A_{r3} temperatures, which are little influenced by sulphur levels.

There is some indication that a high volume fraction of elongated MnS inclusions allow recovery in ductility to occur more rapidly on the low temperature side of the trough as has been noted in previous examinations. However, this again is only a small effect. Wider troughs, in which the presence of a thin band of ferrite occurs over a wide range of

temperature, as with the Nb containing steels or higher C or Mn containing plain C-Mn steels might be expected to be more influenced by the level of sulphur, particularly with regards to the depth and this requires further investigation.

In the as-cast steels, large amounts of sulphides are able to precipitate out at the austenite grain boundaries because all the sulphur is in solution. This makes it more difficult for dynamic recrystallisation to occur, thus extending the trough to higher temperatures.

Increasing the cooling rate results in worse ductility, previous work showing this to be due to finer sulphides and precipitation. For the range of cooling rates investigated, 25 to 200 K min^{-1} , the decrease in A_{r3} temperatures as the cooling rate increases is relatively small.

This work has also clearly shown that the width of the trough can be narrowed by reducing the carbon and manganese levels, and to produce a trough $<60\text{K}$ the A_{r3} temperature should be greater than 1103K . Recovery in the ductility at the high temperature end in these hot-rolled and solution treated steels generally corresponds to the onset of dynamic recrystallisation. However, the strains that are required are much greater and the grain sizes too coarse to allow dynamic recrystallisation to occur in the commercial straightening operation during continuous casting.

At the low temperature side of the trough, recovery in ductility corresponds to the formation of a large amount of ferrite ($\sim 40\%$) and therefore any changes in composition that could raise the A_{r3} would be beneficial, e.g. lower C or Mn levels. These changes to the composition would be expected to reduce the width of the trough, thus reducing the risk of transverse cracking.

9.3 Mathematical Modelling

The model used in chapter 6 was found to work reasonably well for very simple plain C-Mn steels, in which no microalloying precipitates were present, provided that the strain rate is about 10^{-3} to 10^{-4} s^{-1} and the cooling rate is in the range 60 to 100 Kmin^{-1} ; these are the conditions pertaining to conventional continuous casting. The model can be used to predict the ductility curve for a simple steel if the A_{e3} and A_{r3} (undeformed) temperatures are known along with the curves of ϵ_c and ϵ_f against temperature. The latter curve requires knowledge of the amount of S able to precipitate out at the γ boundaries and the ferrite volume fraction.

Recovery in ductility at the high temperature end of the trough for the C-Mn steels was found to take place at the point when DRX becomes possible. This occurs either when the curve of the strain to fracture, ϵ_f , either intersects the curve of critical strain for DRX, ϵ_c , or when the A_{e3} temperature is exceeded, whichever is the higher. Recovery at the low temperature end always occurs when substantial amounts of ferrite forms either before or during deformation.

For the austenitic stainless steel with the fine grain size of $40\mu\text{m}$, the model predicted that ductility would be excellent and DRX would occur throughout the entire temperature range; this is in accordance with the experimental and metallographic observations. DRX occurred at tensile strains lower than those causing failure in the coarser grained material throughout the temperatures range studied. For the coarse grained austenitic stainless steel, ductility troughs were obtained with the minimum ductility values for all the strain rates studied occurring at 1123 K. Extensive networks of chromium carbides were found at the γ grain boundaries, which prevented DRX and instead encouraged cracks formed by grain boundary sliding to grow and interlink. Recovery at the low temperature end was found to be due to a reduction in grain boundary sliding even though the carbides were

still present. Whereas the recovery in ductility at the high temperature end was due to DRX occurring, but only at strain rates of $3 \times 10^{-3} \text{s}^{-1}$ as are found in the straightening operation during conventional continuous casting. Increasing the strain rate to $3 \times 10^{-2} \text{s}^{-1}$ resulted in less grain boundary sliding and ductility improved without DRX; whereas at very low strain rates of $3 \times 10^{-4} \text{s}^{-1}$, grain boundary sliding was increased sufficiently such that DRX had little influence on the ductility.

The model used was found to work reasonably well for very simple plain C-Mn steels in which no microalloying precipitates were present. However, for the austenitic stainless steel clearly the model needs to take into account grain boundary sliding and a creep type model of the form given in reference 11 needs to be incorporated.

9.4 Influence of Columnar Grains

Chapter 7 studied the effect of sample orientation on the hot ductility using an austenitic stainless steel slab (steel 12) which would retain its columnar structure down to room temperature. The R of A values observed for all four sample directions improved as the test temperature was increased from 1023 to 1123K. This improvement was due to a coarsening and reduction in number of Cr carbides situated at the γ boundaries. The R of A values for a given sample direction were found to be related to the amount of grain boundary lying perpendicular to the tensile axis; it was found that the smaller this apparent grain size, the higher the ductility that would be observed. The highest ductility was seen in the samples with the columnar grains parallel to the tensile axis, i.e. taken from the through thickness direction, C, of the continuously cast slab. The propagation of cracks was hindered by the larger number of grain boundaries encountered as the crack attempted to develop through the sample.

The worst ductility, at temperatures up to 1173K, was given by samples taken parallel to the casting direction, B, as the columnar grains were then perpendicular to the

tensile axis. When a crack formed, it could easily propagate through the sample and in some cases without meeting another grain which would require a change in direction. This is the situation that is experienced in the top surface of the continuously cast slab during the straightening operation, when columnar grains are present. Columnar grains have been shown to contribute to poor ductility and encourage transverse cracking. It is therefore recommended, wherever possible, to avoid developing a columnar structure in the continuously cast slabs.

The normal stress was found to control the ductility for temperatures up to 1123K, grain boundary sliding may initiate the cracks but was not principally responsible for the propagation through the sample. At temperatures above 1123K, only samples taken from the through thickness direction of the slab experienced a continued increase in ductility. This continued improvement in ductility is probably due to the higher strains possible in this direction allowing dynamic recrystallisation to occur more readily, thus preventing grain boundary sliding. The start of dynamic recrystallisation being observed as serrated grain boundaries. The deterioration in ductility for the other three sample directions is due to grain boundary sliding dominating the failure process; this was particularly marked for samples taken at 45° to the through thickness direction.

9.5 Influence of Residual Copper

In chapter 8, residual Cu was found to make the hot ductility worse at the faster cooling rate pertaining to thin slab casting, as shown in Figure 8.3. This deterioration would be expected to be much worse in the presence of an oxidising atmosphere as has been found in previous work¹² at slower cooling rates. Insufficient time was available for examining the cause of this deterioration, but previous work has ascribed it to the formation of fine CuS particles. Clearly more work is required to examine the cause of this deterioration seen in the present work.

10. Future Work

It is the author's belief that many important findings regarding hot ductility and its relationship to transverse cracking are documented in this thesis, some of which have been published elsewhere, and some being commercially applicable. However, as with any scientific study of this nature, many other questions and avenues for future investigation have presented themselves. Some recommendations for future work are suggested below:

- During this study, new equipment was purchased and many developments were made to the equipment in order to improve accuracy of control and also automate as much of the process as possible. The results obtained are directly comparable to those obtained using other more expensive experimental apparatus. Future improvements could include combining the control of the separate pieces of testing, heating, data logging and monitoring equipment into one system and also improving the methods of quenching failed samples on the two test systems.
- In Chapter 4, it was not entirely clear what was responsible for producing large amounts of DIF in steels 1 and 3, resulting in narrow troughs being formed. It is thought that this may be due to the high transformation temperature and also the high Si content, which strengthens the ferrite encouraging more transformation of γ under deformation. Further work on steels having differing Si contents is required to clarify these explanations.
- It is unclear, from Chapter 4, whether the necessary requirement of having ~50% ferrite present can be achieved by very low deformation (2 - 4%) or whether much lower temperatures are needed to ensure that the ferrite is present before the straightening operation. Much lower temperatures would require either slower casting speeds, faster heat removal from the strand or a larger distance between the mould and the straightener. Repeating the testing, but only straining the samples by 2-4% and varying other test parameters may help in identifying what changes could be made in commercial practice.

- In Chapter 5, a novel approach suggested by Professor Mintz has been used to further study the results obtained from the tensile test. The curves of peak stress and the strain to the peak stress have been plotted against temperature using the results from steels 1 to 8. In some cases, these curves can be seen to highlight where DIF and DRX occur and also T_d , the temperature for the onset of DRX. This method could be applied to previous and future test results to establish how widely applicable it might be.
- As reported in Chapter 6, improvements could be made to the model used if extra parameters, such as one for grain boundary sliding, are built into the equations used. As all of the equations and curves have been plotted separately using Microsoft Excel by supplying values such as grain size and transformation temperatures, it is the authors belief that all of these could be combined into one computer program. Values for all the parameters used can be entered in order to calculate the curves, to which logic is then applied to find the intersections, and automatically produce a 'ductility curve'.
- In Chapter 8, residual Cu was found to make the hot ductility worse at the faster cooling rate pertaining to thin slab casting. This deterioration would be expected to be much worse in the presence of an oxidising atmosphere at slower cooling rates, but insufficient time was available for examining the cause of this deterioration. More work is therefore required to examine the cause of this deterioration and also to complete the testing in an oxidising atmosphere.

11. Publications

A large part of the results presented in this thesis have already been published and the author hopes that further sections of the work may also be submitted for publication in the near future. The papers previously published are listed below under their relevant chapters:

Chapter 4

A. Cowley, R. Abushosha and B. Mintz: 'Influence of A_{r3} and A_{e3} temperatures on hot ductility of steels', Mat. Sci. and Technol., 1998, 14(11), pp. 1145-1153.

Chapter 6

B. Mintz, R. Abushosha, A. Cowley: 'Preliminary analysis of hot ductility curve in simple C-Mn steels', Mat. Sci. and Technol., 1998, 14(3), pp. 222-226.

B. Mintz, A. Cowley, R. Abushosha and D.N. Crowther: 'Hot ductility curve of an austenitic stainless steel and importance of dynamic recrystallisation in determining ductility recovery at high temperatures', Mat. Sci. and Technol., 1999, 15(10), pp. 1179-1185.

Chapter 7

B. Mintz, A. Cowley and R. Abushosha: 'Importance of columnar grains in dictating hot ductility of steels', Mat. Sci. and Technol., 2000, 16(1), pp. 1-5.

12. References

- 1 B. Wilshire, D. Homer and N.L. Cooke: Technological and Economic Trends in the Steel Industries, Pineridge Press, 1983, ISBN 0-906674-21-4.
- 2 B. Mintz, S. Yue and J. J. Jonas: Hot ductility of steels and its relationship to the problem of transverse cracking during continuous casting, *Int. Materials Reviews* 1991, 36(5), pp. 187-217.
- 3 B. Mintz and R. Abushosha: Influence of vanadium on hot ductility of steel, *Ironmaking and Steelmaking*, 1993, 20(6), pp. 445-452.
- 4 R. Abushosha, R. Vipond and B Mintz: Influence of sulphur and niobium on hot ductility of as cast steels, *Mat. Sci. and Technol.*, 1991, 7(12), pp. 1101-1107.
- 5 B. Mintz, Z. Mohamed and R. Abushosha: Influence of calcium on hot ductility of steels, *Mat. Sci. and Technol.*, 1989, 5(7), pp. 682-688.
- 6 R. Abushosha, R. Vipond and B. Mintz: Influence of titanium on hot ductility of as cast steels, *Mat. Sci. and Technol.*, 1991, 7(12), pp. 613-621
- 7 B. Mintz and J. J. Jonas: Influence of strain rate on production of deformation induced ferrite and hot ductility of steels, *Mat. Sci. and Technol.*, 1994, 10, pp. 721-727.
- 8 G. S. I. L. Cardoso, S. Yue and B. Mintz: Hot ductility of Al and Ti containing steels with and without cyclic temperature oscillations, *Ironmaking and Steelmaking*, 1995, 32(5), pp. 367-377
- 9 B. Mintz: Importance of A_{r3} temperature in controlling ductility and width of hot ductility trough in steels, and its relationship to transverse cracking, *Mat. Sci. and Technol.*, 1996, 12(2), pp. 132-138.
- 10 B. Mintz, Z. Mohamed and R. Abushosha: Influence of calcium on hot ductility of steels, *Mat. Sci. and Technol.*, 1989, 5(7), pp. 682-688.
- 11 B. Mintz: The influence of composition on the hot ductility of steels and to the problem of transverse cracking, *ISIJ Int.*, 1999, 39(9), pp. 833-855.
- 12 B. Mintz and J.M. Arrowsmith: The hot ductility behaviour of C-Mn-Nb-Al steels and its relationship to crack propagation during straightening of continuously cast strand, *Met. Technol.*, 1979, 6, pp. 24-32.
- 13 B.G. Thomas: Introduction to Continuous Slab Casting, Continuous Casting Consortium, 2003, <http://bgtsunsparc.me.uiuc.edu/introduction/overview.html>
- 14 B. Kozak and J. Dzierzawski: AISI Learning Center, 2002, <http://www.steel.org/learning/howmade/concast.htm>
- 15 M. Pettifor: 49th Hatfield Lecture, Technology: Driving steel forward, *Steel World*, 2002, Vol. 7, pp. 11-19.
- 16 E.T. Turkdogan: Causes and effects of nitride and carbonitride precipitation in HSLA steels in relation to continuous casting, *AIME Steelmaking Conf. Proc.*, 1987, 70, pp. 399-413
- 17 J.K. Brimacombe and K. Sorimachi: Crack formation in the continuous casting of steel, *Metall. Trans.*, 1977, 8B, p. 489
- 18 D.N. Crowther: The Hot Ductility of Steels, PhD Thesis, 1986, City University London, UK
- 19 L. Schmidt and A. Josefsson: On formation of transverse cracks in continuously cast slabs from curved mould machines, 1974, *Scan. J. Met.*, 3, 193.
- 20 H. Mori: , *Tetsu To Hagane*, 1974, 60, 784.

- 21 R.C. Cochrane: Unpublished work referenced by D.N. Crowther.16,1982.
- 22 B. Mintz: EPSRC Research proposal GR/K61692, 1995, Hot Ductility and its Relationship to Transverse Cracking during continuous casting.
- 23 W.T. Lankford: Some considerations of strength and ductility in the continuous casting process, Metall. Trans., 1972, 3, p. 1331.
- 24 G. Bernard, J.P. Birat, B. Conseil and J.C. Humbert: Etude de la sensibilité a la crique des aciers coulés en continu a l'aide d'essais de ductilité a chaud, Rev. Métall., 1978, 75(7), pp. 467-480.
- 25 H.G. Suzuki et al: , In "100th ISIJ Meeting", October 1980
- 26 A. Cowley, R. Abushosha and B. Mintz: Influence of A_r3 and A_e3 temperatures on hot ductility of steels, Mat. Sci. and Technol., 1998, 14(11), pp. 1145-1153
- 27 R. Abushosha, S. Ayyad and B. Mintz: Influence of cooling rate on hot ductility of C-Mn-Al and C-Mn-Nb-Al steels, Mat. Sci. and Technol., 1998, 14(4), pp. 346-351
- 28 P.J. Wray: Plastic flow and failure of plain carbon steels in ferrite and austenite regions, Met. Technol., 1981, 12, p. 466.
- 29 J. Lewis, J.J. Jonas and B. Mintz: The formation of deformation induced ferrite during mechanical testing, ISIJ Int. 1998, 38(3), pp. 300-309.
- 30 B. Mintz, R. Abushosha and M. Shaker: Influence of deformation induced ferrite, grain boundary sliding, and dynamic recrystallisation on hot ductility of 0.1-0.75%C steels, Mat. Sci. and Technol., 1993, 9(10), pp. 907-914.
- 31 G.I.S.L. Cardoso and S. Yue: Hot ductility of three low carbon steels in continuously cast slabs, 31st Mechanical Working and Steel Processing Conf., ISS of AIME, Chicago, 1989, p. 585.
- 32 A. Sandberg and W. Roberts: , Thermomechanical Processing of Microalloyed Austenite, ed. A.J. DeArdo et. al., TMS-AIME, Warrendale, PA, USA, 1982, p. 405.
- 33 R.K. Amin and F.B. Pickering: , in 'Thermomechanical Processing of Microalloyed Austenite', ed. A.J. DeArdo et. al., TMS-AIME, Warrendale, PA, USA, 1982, p. 377.
- 34 M. Umemoto, H. Ohtsuka, H. Kato and I. Tamura: , Proc. Int. Conf. On Structure and Properties of HSLA Steels, Wollongong, Australia, 1984.
- 35 M. Umemoto and I. Tamura: In ref 28, personal communication, Kyoto University, Japan, 1985.
- 36 T. Maki, T. Nagamichi, N. Be and I. Tamura: Influence of dynamic precipitation of ferrite on the ductility of steels in the $(\alpha + \gamma)$ two phase region, Tetsu To Hagane, 1985, 71, p. 1367.
- 37 D.N. Crowther and B. Mintz: Influence of carbon on hot ductility of steels, Mat. Sci. and Technol., 1986, 2(7), pp. 671-676.
- 38 D.P. Rizio, R.B. Oldland and B.W. Borland: The effect of austenite grain refinement on the hot ductility of steel, In 'Physical Metallurgy of Thermomechanical Processing and other Metals, Thermec 88', 1988, Tokyo, ISIJ, pp. 178-185.
- 39 E. Essadiqi and J.J. Jonas: Effect of deformation on the austenite-to-ferrite transformation in a plain carbon and two microalloyed steels, Metall. Trans., 1988, 19A, pp. 417-426.
- 40 B. Mintz, J. Lewis and J.J. Jonas: Importance of deformation induced ferrite and factors which control its formation, Mat. Sci. and Technol., 1997, 13(5), pp. 379-388.
- 41 Z. Mohammed: Hot Ductility of Steels, PhD Thesis, 1988, City University London, UK.
- 42 B. Mintz, J.R. Wilcox and D.N. Crowther: Hot ductility of directly cast C-Mn-Nb-Al steel, Mat. Sci. and Technol., 1986, 2(6), pp. 589-594.

- 43 Y. Maehara and Y. Ohmori: The precipitation of AlN and NbC and the hot ductility of low carbon steels, *Mat. Sci. Eng.*, 1984, 62(1), pp. 109-119.
- 44 P.J. Wray: , *Metall. Trans.*, 1975, 6A, p. 1379.
- 45 D.N. Crowther and B. Mintz: Influence of grain size and precipitation on hot ductility of microalloyed steels, *Mat. Sci. and Technol.*, 1986, 2(11), pp. 1099-1105.
- 46 J.R. Wilcox and R.W.K. Honeycombe: Hot ductility in Nb-bearing high strength low alloy steels, *Met. Technol.*, 1984, 11, pp. 217-225.
- 47 D.N. Crowther, Z. Mohamed and B. Mintz: Influence of microalloying additions on the hot ductility of steels heated directly to the test temperature, *Trans. ISIJ*, 1987, 27, p. 366-375.
- 48 B. Mintz, S. Yue and J. J. Jonas: , In *Proc. Int. Conf. on 'Recrystallisation in metallic materials'*, Wollongong, NSW, 1990, Warrendale, PA, Met. Soc. AIME, p. 553.
- 49 D.M. Keene, C.M. Sellars and W.J. McG. Tegart: , In *'Deformation under hot working conditions'*, Iron and Steel Institute, London, 1968, 21.
- 50 R.E. Smallman: *Modern Physical Metallurgy*, 1985, Butterworths and Co., ISBN 0750606290
- 51 N.W. Blake: "Hot ductility of simulation castings", Rep. MRL/AMP/87/5, July 1987, BHP, Melbourne.
- 52 J.Y. Fu, C.I. Garcia, S. Pytel and A.J. DeArdo: Hot ductility of continuously cast microalloyed steels, In *"Processing, Microstructure and Properties of HSLA Steels"*, 1988, Warrendale, PA, Met. Soc. Of AIME, pp. 27-38.
- 53 L.E. Cepeda, J.M. Rodriguez-Ibabe, J.J. Urcola and M. Fuentes: Influence of dynamic recrystallisation on hot ductility of aluminium killed mild steel, *Mat. Sci. and Technol.*, 1989, 5(12), pp. 1191-1199.
- 54 B. Mintz and Z. Mohamed: 'Hot Ductility of Directly Cast Microalloyed Steels', In *Int. Symp. On Physical Simulation of Welding, Hot-Forming and Continuous Casting*, CANMET, Canada, 1988.
- 55 P. Deprez, J.P. Bricout and J. Oudin: Tensile test on in-situ solidified notched specimens: effects of temperature history and strain rate on the hot ductility of Nb and Nb-V microalloyed steels, *Mat. Sci. and Eng.*, 1993, A168, pp. 17-22.
- 56 S. Sladik and M. Longauerova: The hot tensile test with direct resistance heating of the specimen, *Metallic Materials*, 1992, 30(4), pp. 210-214.
- 57 J. Oudin, Y. Ravalard, J.C. Gelin, G. Lacombe and T. Labarthe-Vacquier: Determination of the forgeability of metals and alloys, *Matér. Tech.*, 1988, 39, pp. 11-12.
- 58 B. Mintz and R. Abushosha: Effectiveness of hot tensile test in simulating straightening in continuous casting, *Mat. Sci. and Technol.*, 1992, 8, No. 2, pp. 171-177.
- 59 C.M. Sellars and W.J. McG. Tegart: Hot workability, *Int. Met. Rev.*, 1972, 17, pp. 1-24.
- 60 C.M. Sellars and W.J. McG. Tegart: La relation entre la résistance et la structure dans la déformation a chaud, *Mem. Sci. Rev. Met.*, 1972, 23, pp. 731-746.
- 61 J.J. Jonas, C.M. Sellars and W.J. McG. Tegart: , In *"Deformation under Hot Working Conditions"*, Special Report No. 108, London ISI, 1968, p.21.
- 62 R.A. Perkins, R.A. Padgett Jr. and N.K. Tunali: , *Metall. Trans.*, 1973, 4A, pp. 2535-2540.
- 63 W.J. McG. Tegart: , In *"Ductility"*, Metals Park, Ohio, 1968, p. 133.
- 64 J. Sanker, D.N. Hawkins and H.J. McQueen: , *Met. Technol.*, 1979, 6, p. 325.
- 65 Y.V. Prasad, S. Sasidhara, R. Ravi and S. Yellapregada: Indian Institute of Science, 2003, <http://www.processingmaps.com/Graphics/content/Theory/Programs.htm>.

- 66 J.J. Jonas: Dynamic recrystallisation - scientific curiosity or industrial tool?, Mater. Sci and Eng., 1994, A184(2), pp. 155-165.
- 67 D.T. Llewellyn: Metallurgy and Applications, 2nd ed., 1994, Butterworth-Heinemann Ltd, ISBN 0-7506-2086-2.
- 68 B. Mintz, R. Abushosha and J. J. Jonas: Influence of dynamic recrystallisation on the tensile ductility of steels in the temperature range 700-1150 C, ISIJ Int., 1992, 32, pp.241-249.
- 69 B. Mintz, R. Abushosha and D.N. Crowther: Influence of small additions of copper and nickel on hot ductility of steels, Mat. Sci. and Technol., 1995, 11(5), pp. 474-481.
- 70 B. Mintz, J.M. Stewart and D.N. Crowther: The influence of cyclic temperature oscillations on precipitation and hot ductility of a C-Mn-Nb-Al steel, Trans. ISIJ, 1987, 27, pp. 959-964.
- 71 R. Abushosha, S. Ayyad and B. Mintz: Influence of cooling rate and MnS inclusions on hot ductility of steels, Mat. Sci. and Technol., 1998, 14(3), pp. 227-235.
- 72 R. Abushosha, O. Cominelli and B. Mintz: Influence of Ti on hot ductility of C-Mn-Al steels, Mat. Sci. and Technol., 1999, 15(3), pp. 278-286.
- 73 C Ouchi and K. Matsumoto: Hot ductility in Nb-bearing high strength low alloy steels, Trans. ISIJ, 1982, 22(3), pp. 181-189.
- 74 D.N. Crowther and B. Mintz: Influence of grain size on hot ductility of plain C-Mn steels, Mat. Sci. and Technol., 1986, 2(9), pp. 951-955.
- 75 B. Mintz and Z. Mohamed: Influence of manganese and sulphur on hot ductility of steels heated directly to temperature, Mat. Sci. and Technol., 1989, 5(12), pp. 1212-1219.
- 76 A. leBon, J. Rofes-Vernis and C. Rossard: Recrystallisation and precipitation during hot working of Nb-bearing HSLA steel, Met. Sci. J., 1975, 9, pp. 36-40.
- 77 I. Weiss and J.J. Jonas: Interaction between recrystallization and precipitation during the high temperature deformation of HSLA steels, Metall. Trans., 1979, 10A, pp. 831-840.
- 78 M.G. Abken, I. Weiss and J.J Jonas: , Acta Metall., 1981, 29, p. 111.
- 79 W.C. Leslie, R.L. Rickett, C.L. Dotson and C.S. Walton: Solution and precipitation of AlN in relation to the structures of low C steels, Trans. ASM, 1954, 46, pp. 1470-1499.
- 80 D.N. Crowther, Z. Mohamed and B. Mintz: The relative influence of dynamic and static precipitation on the hot ductility of microalloyed steels, Metall. Trans., 1987, 18A, pp. 1929-1939.
- 81 R.A. Higgins: Properties of Engineering Materials, 2nd Rev. Ed, 1994, Publ. Edward Arnold, ISBN 0-340-60033-0.
- 82 E.P. DeGarmo, J. Temple Black and R.A. Kohser: Materials and Processes in Manufacturing, 7th ed, 1990, Macmillan Publ. Co., ISBN 0-02-946140-5.
- 83 B. Mintz: Private communication, 2003.
- 84 Y. Maehara, K. Yasumoto, Y. Sugitani and K. Gunji: Effect of carbon on hot ductility of as cast low alloy steels, Trans. ISIJ, 1985, 25, pp. 1045-1052.
- 85 S.D. Razumov, V.V. Zabilski, V.I. Umanets, V.I. Lebedev and V.A. Oburhov: Influence of chemical composition of steel on quality of continuously cast billet, Steel in the USSR, 1986, 16, pp. 225-228.
- 86 R.E. Mercer and N.A. McPherson: , AIME Steelmaking Conf. Proc., 1979, 62, p. 215.
- 87 N.E. Hannerz: Critical hot plasticity and transverse cracking in continuous slab casting with particular reference to composition, Trans. ISIJ, 1985, 25, pp. 149-158.

- 88 M.H. Burden, G.D. Funnell, A.G. Whitaker and J.M. Young: , In 'Solidification and casting of metals', pp. 229-236; 1979, London, The Metals Society.
- 89 S. Harada, S. Tanaka, H. Misumi, S. Mizoguchi and H. Horiguchi: A formation mechanism of transverse cracks on continuously cast slab surface, *ISIJ Int.*, 1990, 30, pp. 310-316.
- 90 H.G. Suzuki, S. Nishimura, J. Imamnura and Y. Nakumura: Embrittlement of steels occurring in the temperature range 1000-600°C, *Trans. ISIJ*, 1984, 24, pp. 169-177.
- 91 E.P. George, R.L. Kennedy and D.P. Pope: Review of trace element effects on high-temperature fracture of Fe- and Ni-base alloys, *Phys. Status Solids (a)*, 1998, 167, pp. 313-333.
- 92 K. Abico: The evolution of iron, *Phys. Status Solids (a)*, 1997, 160, pp. 285-296.
- 93 T. Revaux, J.P. Bricout and J. Oudin: A new tensile testing procedure for predicting transverse cracking susceptibility of continuous casting slabs, *J. Mat. Eng. And Performance*, 1996, 5(2), pp. 260-268.
- 94 L.P. Karjailen, H. Kinnunen and D. Porter: , in *Microalloying in Steels., Proc. Int. Conf. Microalloying in Steels*, San Sebastian, Spain, Ed. J.M. Rodriguez-lbabe et. al., *Trans. Tech. Publ.*, Switzerland, 1998, pp. 477-483.
- 95 B. Mintz: Private communication from V. Ludlow, Corus, Teeside Technology Centre, 1998.
- 96 G.A.Wilber, R.Batra, W.F.Savage and W.J.Childs: *Metall. Trans.*, 1975, 6A, p.1727.
- 97 B. Mintz: Private communication, 2003.
- 98 B. Sundman, B. Jansson and J.-O. Anderson: The Thermocalc databank system, *Calphad*, 1985, 9, p.153-190.
- 99 R. Abushosha: Unpublished work, 1997.
- 100 K. Yamanaka, F. Terasaki, H. Ohtani, M. Oda and M. Yoshihara: Relation between hot ductility and grain boundary embrittlement of low carbon killed steels, *Trans. ISIJ*, 1980, 20, pp. 810-816.
- 101 E.T. Turkdogan, S. Ignatowicz and J. Pearson: , *J. Iron Steel Inst.*, 1955, 180, p. 349.
- 102 B. Mintz and Z. Mohamed: Intergranular failure in micro-alloyed steels and its relationship to carbon content, In *Proc. 7th Int. Conf. on Fracture*, Houston, TX, 'Advances in fracture research', ed. K. Salama et al., Oxford, Pergamon, 1989, 4, pp. 2545-255
- 103 B. Mintz and J.M. Arrowsmith: The influence of micro-alloying addition on the hot ductility of steels, *Sheffield Int. Conf. 'Hot working and forming processes'*, ed. C.M. Sellars and G.J. Davies, 1979, London, The Metals Society, pp. 99-103.
- 104 H.G. Suzuki, S. Nishimura, J. Imamura and Y. Nakumura: , *Trans. ISIJ*, 1982, 22, p. 48.
- 105 G.D. Funnell and R.J. Davies: , *Met. Technol.*, 1978, 5,150
- 106 B. Mintz: Private communication, 1998.
- 107 B.Mintz, R. Abushosha, S.Y. Ayyad and GISL Cardoso: , *HSLA '95, Proc. Of the Conf. on HSLA steels*, China Science and Technology Press, China, (1995), pp. 342-345.
- 108 B. Mintz, R. Abushosha, A. Cowley: Preliminary analysis of hot ductility curve in simple C-Mn steels, *Mat. Sci. and Technol.*, 1998, 14(3), pp. 222-226.
- 109 B. Mintz, A. Cowley, R. Abushosha and D.N. Crowther: Hot ductility curve of an austenitic stainless steel and importance of dynamic recrystallisation in determining ductility recovery at high temperatures, *Mat. Sci. and Technol.*, 1999, 15(10), pp. 1179-11
- 110 C. Rossard: , in *'Microstructure and Design of Alloys'*, 1973, London, The Institute of Metals, 2, p. 175.

- 111 B. Mintz, R. Abushosha, O.G. Cominelli and M.A. Loyola de Oliveira: , in Proc. Conf. 'Thermec 97' Wollongong, Australia, July 1997, Dept. Materials Engineering, University of Wollongong.
- 112 B. Mintz, M. Shaker and D.N. Crowther: Hot ductility of an austenitic and a ferritic stainless steel, *Mat. Sci. and Technol.*, 1997, 13(3), pp. 243-249.
- 113 K.W. Andrews: , *J. Iron Steel Inst.*, 1965, 203, p. 721.
- 114 H. Kobashi: , *Trans. ISIJ*, 1991, 31, p. 268.
- 115 J. Gurland and J. Plateau: , *ASM Trans.*, 1963, 56, p. 442.
- 116 G.I.S.L. Cardoso: , PhD Thesis, 1986, City University London, UK.
- 117 G. S. I. L. Cardoso, B. Mintz and S. Yue: , *Ironmaking and Steelmaking*, 1995, 22, p. 365.
- 118 A. Cowley: Unpublished work, City University, London, UK, 1997.
- 119 N.J. Grant and A.W. Mullendore: 'Deformation and fracture at elevated temperatures', 1965, Cambridge, MA, MIT Press.
- 120 I. Servi and N.J. Grant: , *Trans. AIME*, 1951, 191, p. 917.
- 121 B. Mintz, A. Cowley and R. Abushosha: Importance of columnar grains in dictating hot ductility of steels, *Mat. Sci. and Technol.*, 2000, 16(1), pp. 1-5.
- 122 F. Vodopivec, M. Torkar, M. Debelak, M. Kmetec, F. Haller and F. Kaucic: Influence of Al on solidification structure and initial deformability of continuously cast C-Mn-Si-N steel, *Mat. Sci. and Technol.*, 1988, 25, pp. 917-925.
- 123 W.T. Nachtrab and Y.T. Chou: High temperature ductility loss in carbon-manganese and niobium-treated steels, *Metal. Trans.*, 1986, 17A, pp. 1995-2006.